Treatment of Dairy Wastewater using *Monoraphidium* sp. KMC4 and Subsequent Thermochemical Conversion of the Biomass to Biofuels

Thesis submitted in partial fulfilment of the requirements for the degree of

DOCTOR OF PHILOSOPHY

By

Pooja Singh

(206107103)

Department of Chemical Engineering

Indian Institute of Technology Guwahati

Assam- 781039, India

May 2026

Treatment of dairy wastewater using Monoraphidium sp. KMC4 and subsequent thermochemical conversion of the biomass to biofuels

Pooja Singh

Department of Chemical Engineering

Indian Institute of Technology Guwahati

Assam- 781039, India

CERTIFICATE

This is to certify that the thesis entitled **"Treatment of dairy wastewater using *Monoraphidium* sp. KMC4 and subsequent thermochemical conversion of the biomass to biofuels"** being submitted by **Ms. Pooja Singh** for the award of the degree of Doctor of Philosophy has been carried out by her at Department of Chemical Engineering, Indian Institute of Technology Guwahati, under my guidance and supervision. This work has not been submitted to any other University or Institute for the award of any degree or diploma.

Date:

Place:

(Signature of Thesis Supervisor)

Prof. Kaustubha Mohanty
Department of Chemical Engineering
Indian Institute of Technology Guwahati

DEDICATION

This thesis is dedicated to my parents, Mr. Kishan Singh

and Mrs. Vijay Rani

Acknowledgement

First and foremost, I express my deepest gratitude to my supervisor, **Prof. Kaustubha Mohanty**, for his invaluable guidance, unwavering support, and constant encouragement throughout my doctoral journey. His expertise, patience, and dedication played an important role in shaping this research and nurturing my intellectual growth. I would like to thank DBT (Department of Biotechnology, Govt of India) under Indo-Danish Research and Innovation Cooperation in the area of 'Water' (Grant no. BT/IN/Denmark/61/KM/2018-19) for funding a few research objectives of my thesis work. I would also like to acknowledge the Purabi treatment plant, Guwahati, Assam for providing dairy sludge samples for conducting the research.

I would like to acknowledge Indian Examiner, **Prof. Ramkrishna Sen** (IIT Kharagpur) and Foreign Examiner, **Prof. Tong Yen Wah** (National University of Singapore) for providing valuable suggestions and comments to enhance the quality of the thesis. I express my sincere gratitude to Viva Voce Committee members, **Prof. Vaibhav V. Goud**, **Prof. V S Mohalkar**, and **Prof. N. Selvaraju**, for their invaluable constructive feedback during the seminar.

I wish to extend my heartfelt appreciation to my doctoral committee members, **Prof. Vaibhav V. Goud**, **Prof. Animes Kumar Golder**, and **Prof. Kannan Pakshirajan**, for their invaluable guidance and constructive feedback provided during my seminars and progress reviews. Their input has been instrumental in the accomplishment of my thesis. I would like to thank **Dr. S Venkata Mohan**, Director, Scientist, CSIR National Environmental Engineering Research Institute, Nagpur, for his guidance and support in my PhD research work. I would also like to thank **Dr Mary Chatterjee**, my Bachelors supervisor for supporting and encouraging throughout my PhD journey.

I express my sincere appreciation to **Prof. Subrata Kumar Majumder**, the current Head of the Department, for his constant administrative support during the later stages of my doctoral research. I sincerely appreciate the guidance and administrative help provided by **Prof. Kaustubha Mohanty and Prof. Anugrah Singh**, former Head of the Department of Chemical Engineering, throughout a significant journey of my Ph.D. work.

I am thankful to the Department of Chemical Engineering, the Central Instruments Facility, Analytical lab facility at IIT Guwahati, for granting access to instrumental facilities. I would like

to acknowledge **Mr Chandan Borgohain**, instrument in charge of TGA-DSC, for his help and support in bio-oil analysis.

I would also like to acknowledge my friend's Ms Suchetna Kushwah, Dr Avinash Anand, Dr Janaki Komandur, Dr Rubeka Idrishi, Dr Jyoti, Mr Aman Chourasia, Ms Chetna Sharma, Mr Amey Shriram Mindewar, Mr Anuj Kumar, Mr Ayush Chouhan, Ms Ritu Sinha, Mr Anchit Saini, Dr Vivek Kumar Nair, Mr Santosh Nambi Yadav, Mr Mashu Bhagat Ratnakar, Dr Somya Madan, Mr Abhishek Kumar, Mr Shantanu Suman, Dr Anuj Rawat, Ms Jyoti Routela, Mr Manikanta Doki, Dr Mahendra Tiwari, Mr Mangal, Ms Anushka Singh, and Ms Mehek for their help and support throughout my journey. Also, I would like to acknowledge Dr Boda Ravi Kiran and Ms Poonam Kumari, CSIR-IICT Hyderabad, for their help and support in my research work.

I am indebted to the selfless help and co-operation of my research group members and seniors, Dr Satya Sundar Mohanty, Dr Sanjeev Mishra, Dr Madonna Roy, Dr Ankit Agarwalla, Dr Anindita Das, Mr Pikesh Kumar, Mr Shanku Borah, Dr Ankita Tadage, Dr Puja Priyadarshini Nayak, Ms Safrin Ahmed, Mr Anand Sagar, Ms Priti Kumari, Mr Saptaswa Biswas, Mr Om Prakash Arya, Mr Nishant Asati, Mr Sharat Chandra, Ms Tripthi Alva, Mr Abhishek Rao, Mr Amal, Mr Manish, Ms Sharon.

My Ph.D. endeavour would not have been successful without the love, trust, support and blessings of my parents and family members. I thank my father Mr Kishan Singh, mother Mrs Vijay Rani, brother Mr Shubham Singh and my sister Ms Anamika Singh for their constant support and love.

I am deeply grateful to God for His unwavering guidance and divine grace throughout the journey of completing this Ph.D. thesis.

Sincerely,

Pooja Singh

Abstract

The depletion of fossil fuel reserves, rising environmental pollution, and accelerating climate change have driven the global search for clean and renewable energy alternatives. Bio-oil offers a promising substitute, and microalgae represent an encouraging third-generation feedstock capable of generating biofuel year-round. However, the high cost of microalgal biomass production limits commercial sustainability. Cultivating microalgae in nutrient-rich wastewater such as dairy wastewater enriched with nitrogen, phosphorus, and organic carbon can substantially reduce production costs while delivering bioremediation benefits, and mixotrophic growth further enhances biomass productivity compared with heterotrophic cultivation. This thesis proposes an integrated microalgae-based biorefinery for the concurrent treatment of simulated synthetic dairy wastewater and bio-oil production.

In the upstream stage, *Monoraphidium* sp. KMC4 was cultivated mixotrophically at varying COD concentrations of dairy wastewater. The strain performed best at 50% wastewater strength, achieving a biomass concentration of 1.47 g L^{-1} and biomass productivity of 122 mg L^{-1} day^{-1}, with carbohydrate (28.73±1.6 wt%), protein (48.50±1.3 wt%), and lipid (20.29±2.3 wt%) accumulation. The biomass exhibited high volatile matter, a significant heating value, and suitable thermal degradation behaviour, confirming its feasibility as a feedstock for thermochemical conversion.

In downstream processing, hydrothermal liquefaction (HTL) and pyrolysis were investigated. Direct HTL yielded 33.50% bio-oil but with high heteroatom content (N/C 0.05, H/C 1.36, O/C 0.11 mol/mol). Furthermore, a two-stage HTL approach employing mild-temperature pretreatment for partial deamination and hydrolysis, followed by higher-temperature conversion and showed improvement in bio-oil quality without compromising yield. Also, nitrogen-based compounds decreased from 13.36% in direct HTL bio-oil to 1.98% in two-stage HTL bio-oil, resulting in a 38% reduction in nitrogen, as confirmed by elemental analysis.

To address waste valorisation, co-hydrothermal liquefaction (co-HTL) of microalgae with dairy sludge was performed at three ratios (75:25, 50:50, 25:75). While HTL of dairy sludge alone produced only 18.16% bio-oil but the 75:25 algae-to-sludge ratio yielded 32.94 wt% bio-oil with the highest heating value of 38.24 MJ kg^{-1}. Co-HTL bio-oil exhibited increased H/C and reduced O/C and N/C ratios due to deoxygenation and dehydration, with fewer N-heterocyclics and

aromatics, more esters, and improved heavy naphtha and kerosene fractions, demonstrating a clear synergistic effect.

Co-pyrolysis of microalgae and dairy sludge in a fixed-bed reactor produced the highest bio-oil yield at 550 °C, 20 °C min^{-1}, and 60 min. Without a catalyst, co-pyrolysis reduced the yields of nitrogenous and aromatic compounds relative to individual feedstocks. Introducing H-ZSM-5 promoted deoxygenation, decarboxylation, and dehydration, increasing hydrocarbons and esters and reduced cyclic nitrogenated compounds, though at the cost of lower bio-oil yield. The catalyst also decreased vacuum residue, indicating fewer heavy fractions.

Overall, HTL and co-HTL produced higher bio-oil yields and energy densities than co-pyrolysis, while two-stage HTL delivered the best bio-oil quality without yield loss. By simultaneously addressing wastewater pollution, waste-to-energy conversion, and sustainable biofuel production, this integrated microalgae-based biorefinery offers a viable pathway toward resource recovery and renewable bioenergy generation.

Thesis Graphical Abstract

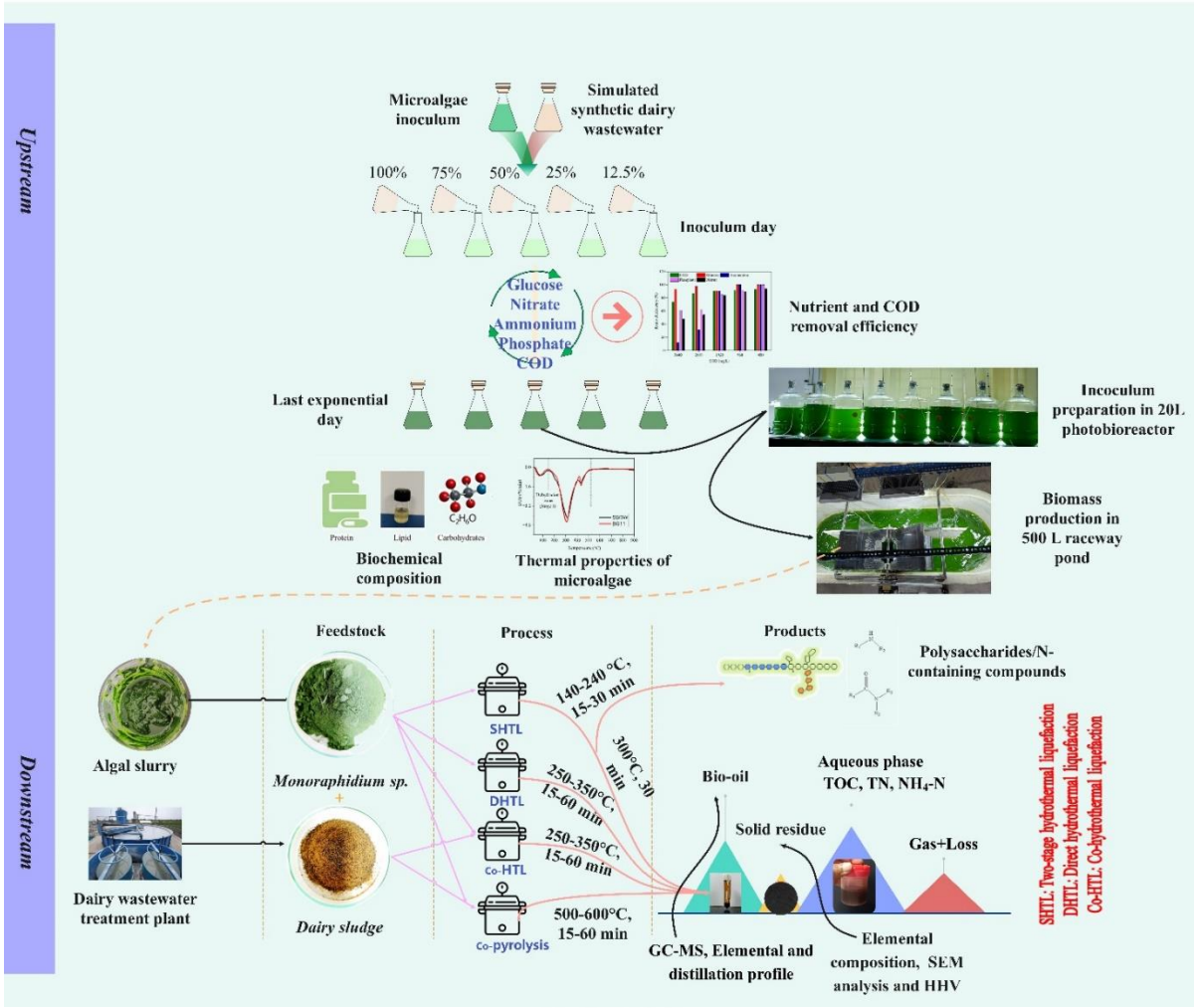

TH-4017_206107103

CONTENTS

List of Tables

List of Figures

NOMENCLATURE

Abbreviations

Acetyl-CoA	Acetyl Coenzyme A
ADW	Anaerobically Digested Wastewater
AE	Antagonistic Effect
APHA	American Public Health Association
ASTM	American Society For Testing And Materials
ATP	Adenosine triphosphate
BET	Brunauer-Emmett-Teller
BG11	Blue-Green 11 medium
BOD	Biological Oxygen Demand
BPD	Boiling Point Distribution
CE	Co-liquefaction Effect
CHNS	Carbon, Hydrogen, Nitrogen, Sulphur
CO_2	Carbon Dioxide
COD	Chemical Oxygen Demand
Co-HTL	Co- Hydrothermal Liquefaction
CP	Critical Point
CPCB	Central Pollution Control Board
DBT	Department of Biotechnology
DCM	Dichloromethane
DHTL	Direct Hydrothermal Liquefaction
DTG	Differential Thermogravimetric
DW	Dairy Wastewater
EPA	Environmental Protection Agency
ERR	Energy Recovery Ratio
FAME	Fatty Acid Methyl Ester
FC	Fixed Carbon
FESEM–EDS	Field Emission Scanning Electron Microscopy-Energy Dispersive Detector
FETEM	Field Emission Transmission Microscopy
FTIR	Fourier Transform Infrared Spectroscopy

GC-MS	Gas Chromatography–Mass Spectrometer
GHG	Greenhouse Gases
H/C	Hydrogen/Carbon
HFM	Hollow Fiber Membrane
HHV	High Heating Value
HR	Heating Rate
HTL	Hydrothermal Liquefaction
HTL-AP	Hydrothermal Liquefaction-Aqueous Phase
JCPDS	Joint Committee on Powder Diffraction Standards
LCA	Life Cycle Assessment
LCFA	Long-chain Fatty Acids
LPG	Liquid Petroleum Gas
N/C	Nitrogen/Carbon
N/O	Nitrogen/Oxygen
NH_4-N	Ammonium-N
NIST	National Institute of Standards and Technology
O/C	Oxygen/Carbon
PBR	Photobioreactors
RIL	Reliance Industries Limited
RuBisCo	Ribulose-1,5-bisphosphate carboxylase oxygenase
SAED	Selected Area Electron Diffraction
SDG	Sustainable Development Goals
SE	Synergistic Effect
SFA	Saturated Fatty Acids
SHTL	Two-Stage Hydrothermal Liquefaction
SPRERI	Sardar Patel Renewable Energy Research Institute
SSDW	Simulated Synthetic Dairy Wastewater
TCA	Tricarboxylic Acid Cycle
TERI	The Energy and Resources Institute
TGA	Thermogravimetric Analyzer
TOC	Total Organic Carbon
TS	Total Solids
TSS	Total Suspended Solids

USFA	Unsaturated Fatty Acids
VM	Volatile Matter
XPS	X-ray Photon Spectroscopy
XRD	X-Ray Diffraction

Notations

P(b)	Biomass Productivity
μ	Specific Growth Rate
ΔX	Change in Cell Concentration
Δt	Number of Days
S_i	Initial Nutrient Concentration
S_f	Final Nutrient Concentration

Chapter 1
Introduction, Literature Survey and Objectives

Chapter 1. Introduction, Literature Survey and Objectives

1.1. Global Scenario

The depletion of fossil fuel resources, coupled with escalating environmental pollution and global climate change, is driving nations worldwide to pursue clean and renewable energy solutions. Fossil fuels are considered the primary source for generating energy worldwide due to their high calorific value. However, the major concern that arises from the combustion of fossil fuels is greenhouse gases from existing production plants. These greenhouse gases are causing detrimental effects on the environment, such as global warming and climate change, which demand the replacement of conventional energy sources by sustainable and renewable technologies. In past few decades, solar, wind, hydro, biomass, hydrogen, and geothermal energies have been introduced to overcome energy and environmental problems. Presently, the global community is striving to shape an energy future that guarantees secure supply, equitable access to resources, and environmental sustainability. Natural processes alone cannot absorb the full extent of greenhouse gas emissions generated by human activities, making alternative solutions essential. This necessitates the integration of high-efficiency technologies with the sustainable use of carbon-neutral resources, particularly renewables. In pursuit of a sustainable industrial transition, the adoption of eco-friendly energy technologies can no longer be postponed. These innovations must operate alongside existing systems, gradually replacing them to achieve long-term environmental and energy goals (Mathimani et al., 2019).

The selection of feedstock is crucial: although first-generation (food-based) and second-generation (lignocellulosic biomass) (Figure 1.1) resources have propelled the biofuel industry, their application is limited by food versus fuel controversies, land-use competition, seasonal availability, and intricate pretreatment demands (Deshavath et al., 2021; Ho et al., 2014). Fourth-generation biofuels are formed from genetically engineered microbial systems. While utilizing microalgae, several benefits occur for biofuel production, like short cultivation duration, carbon dioxide sequestration, and carbon capture, and they can survive in polluted wastewater compared to traditional crops. In view of this, microalgae have come out as a promising third-generation feedstock, with distinct advantages in productivity, resource recovery, and environmental benefits (Mishra and Mohanty, 2019).

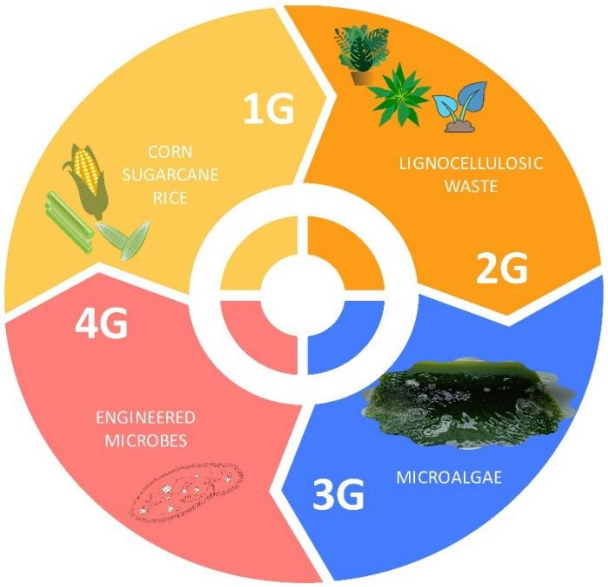

Figure 1.1. Biofuel production feedstocks categories.

In 2015, the United Nations General Assembly adopted the Sustainable Development Goals to accomplish a green future for the earth, with a thriving agenda of sustainable energy by 2030 (Figure 1.2). The Paris Climate Agreement and the 2030 Agenda for Sustainable Development were both centred on energy. Sustainable Development Goal 7 is to provide affordable, reliable, sustainable, and modern energy. On January 26, 2024, the United Nations celebrated its first International Day of Clean Energy, a landmark milestone in the joint commitment to a sustainable future. This meeting served as a forum for addressing climate change and securing a greener environment for future generations (Huck, 2023). India's energy strategy emphasizes renewable energy production to reduce dependency on fossil fuels, enhance supply security, and cut CO_2 emissions and other greenhouse gases.

Renewable energy potential estimated as of March 31, 2022, was 14,90,727 MW, with solar (50.24%) and wind (46.66%) sources dominating. Other contributors include small hydro (1.42%), biomass (1.18%), bagasse cogeneration (0.34%), and waste-to-energy (0.17%). According to geographic distribution, Rajasthan has the highest share of renewable power at about 18.20% followed by Gujarat with 12.10%. Energy consumption patterns revealed that petroleum products grew 36% from 157.06 MTs (2012-13) to 214.13 MTs (2019-20), declined during COVID-19 to 194.30 MTs (2020-21), but rebounded to 204.23 MTs (2021-22). High-speed diesel Oil accounted for 37.55% of total consumption, followed by petrol (15.10%), LPG (13.87%), and pet coke (7.72%) (GOI, 2023). The overconsumption of fossil fuels and non-

renewable energy sources exacerbates the phenomenon of global warming by releasing substantial amounts of greenhouse gases. Effectively managing GHG emissions resulting from energy production is essential in the fight against climate change. To fulfil the objective of the Paris Agreement, which is to restrict the increase in global temperature to a range of 1.5 °C to 2 °C by the year 2100, it is necessary to innovate energy systems and efficiently use renewable energy in all sectors. Research indicates that the use of renewable energy sources within the industrial sector might result in cost savings and provide environmental safeguards against the harmful emissions associated with fossil fuels (Osman et al., 2023). India ranks as the fourth-largest user of petroleum globally, behind China, the United States, and Russia. India's energy consumption will continue to see a strong rise due to modernization and its rapid economic expansion.

Over the previous decade, there has been a significant 38.20% growth in the use of petroleum products in the India (Collard et al., 2023). Two companies in India, namely, Shell Catalysts & Technologies [integrated hydropyrolysis and hydroconversion (IH_2)] and MASH Energy [pyrolysis], involve thermochemical conversion technology for generating gas, jet and diesel fuels, pyrolytic oil from forestry, agricultural and urban waste and waste materials and sewage sludge, respectively (Jamal F, 2023). The Australian company Licella Pty Ltd. has developed the Cat-HTR process, which will be implemented in a commercial plant with a capacity of 125,000 tons per year with non-edible biomass, agricultural, and industrial residues (Castello et al., 2018).

Similarly, the Danish-Canadian company Steeper Energy, in collaboration with the University of Aalborg in Denmark, has developed the HTL process, known as HydroFaction, which is also nearing commercial scale (Jensen et al., 2017). In this context, different biomass can be used for biofuel production, highlighted by many researchers as a potential solution for alternative energy sources to replace fossil-based fuels. The motivation to reduce dependence on petroleum-based fuel mostly comes from its low cost, which might vary based on the type of raw material, the process of conversion, the volume of production, and the geographical location. So, the aim is to generate affordable biomass that may be utilized to produce a range of fuels and chemicals that are economically competitive with traditional commodities.

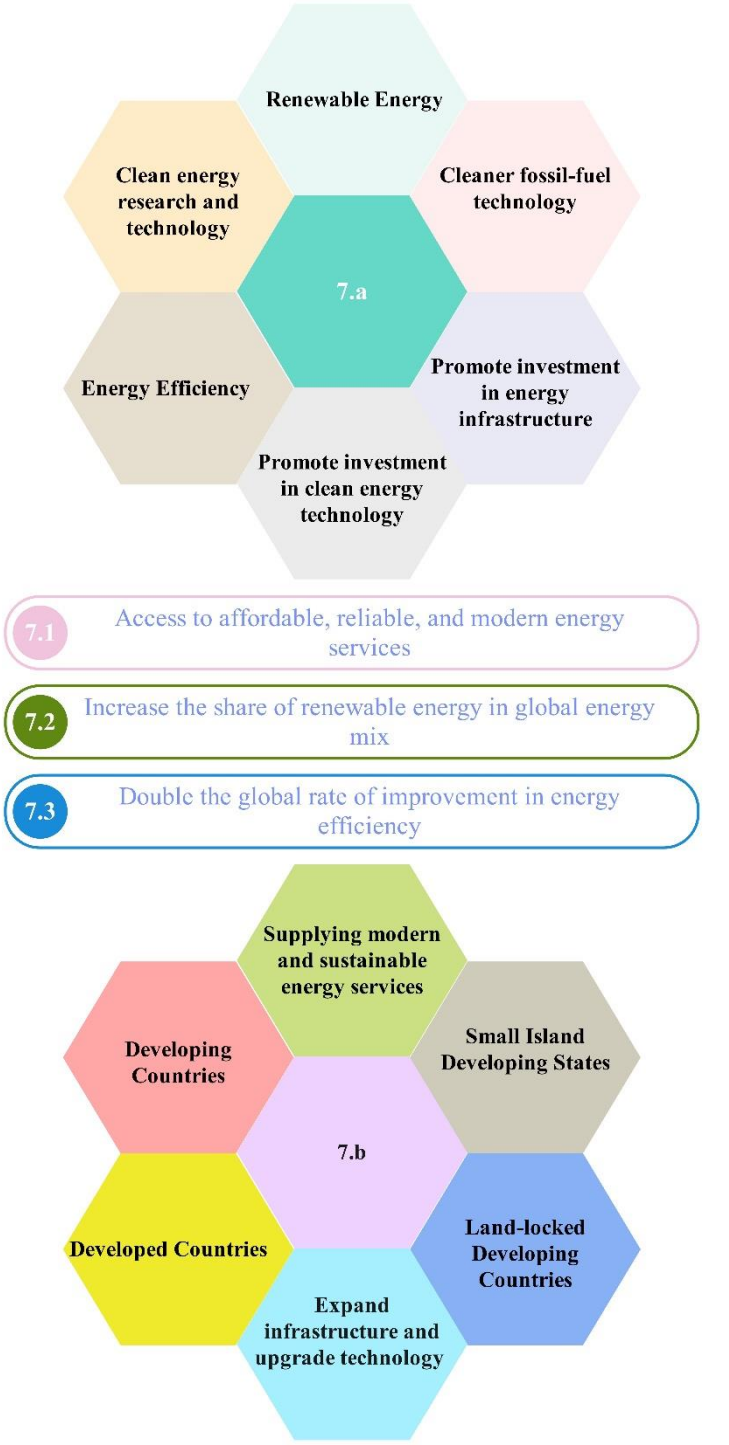

Figure 1.2. The SDG7 targets and the 2030 Agenda for Sustainable Development adopted by the United Nations General Assembly.

1.2. Indian Scenario

After China and the United States, India is the world's third-largest consumer of primary energy and is one of the fastest-growing economies. India's energy security concerning fuel will

continue to be precarious until alternative fuels derived from renewable feedstocks are established. The Indian government aims to decrease the nation's carbon footprint by 30-35% by 2030. The objectives will be attained by a five-pronged plan that encompasses: augmenting domestic production, embracing biofuels and renewables, enforcing energy efficiency standards, enhancing refining processes, and attaining demand substitution. This approach anticipates a pivotal role for biofuels in India's energy portfolio. The availability of feedstock and production costs are the primary factors influencing the sustainable and economic development and adoption of biofuels in India (Ebadian et al., 2019).

Reliance Catalytic Hydrothermal liquefaction - 'RCAT-HTL' is a TRL 8 plant established by Reliance Industries Ltd. (RIL). The plant uses biomass, biowaste and organic waste for producing energy-rich drop-in liquid biofuel and to recover nutrient-rich water and biochar. Research on the RCAT-HTL process at Reliance Industries Limited (RIL) was initiated in 2011 under the "Algae to Oil (A2O)" program, originally aimed at converting algal biomass into renewable biofuels. Over time, the process has proven to possess broad applicability for converting diverse wet organic biomass and bio-wastes into biofuels and value-added products. One of the major advantages of RCAT-HTL over other thermochemical conversion technologies lies in its ability to handle wet feedstocks efficiently. The process utilizes the inherent water content of the feed as a reactant, thereby eliminating the need for energy-intensive drying steps and significantly enhancing overall energy efficiency. This approach not only conserves water but also enables the recovery of valuable nutrients present in the wet biomass. Furthermore, the catalytic hydrothermal liquefaction (RCAT-HTL) process enhances both the yield and the quality of energy-rich bio-oils. Its kinetic tunability allows precise control over reaction conditions, enabling the selective production of desired bio-based products in alignment with market requirements (IEA Bioenergy, 2018).

In India, the scenario for bio-oil production from algae biomass is still very much in the research and development phase. It is considered a key component of the country's long-term strategy for energy security and sustainability, but it has not yet reached commercial scale. The Indian government has recognized the potential of third-generation biofuels, including those from algae, in its National Policy on Biofuels - 2018. The policy explicitly promotes the development of advanced biofuels and acknowledges the need for further research to achieve techno-commercial viability. The Department of Biotechnology (DBT) and The Energy and Resources Institute (TERI) have established a center, "DBT-TERI Centre of Excellence," focused on advanced biofuels. A 100,000 L indigenous sunlight-distributed algal system

(*Dunaliella tertiolecta*) has been installed at Mumbai, which has been successfully grown with the productivity of 15-18 g m^{-2} day^{-1} (Department of Biotechnology, MoS&T GOI, 2021). Another institute that is working on large-scale algal cultivation is the "Sardar Patel Renewable Energy Research Institute" at Anand, Gujarat for aqua feed and bio-diesel production. Given India's diverse climate, there is a focus on identifying and cultivating indigenous algae species that are well-suited to the country's environmental conditions. Researchers are exploring both freshwater and marine algal species, particularly in coastal regions and areas with large bodies of water. The use of wastewater for cultivation is also being researched as a way to address both water management and biofuel production (SPRERI, CENTRE OF EXCELLENCE, 2023).

1.3. Algae Biomass as a potential source for alternative energy

Algal biomass is highly regarded as a favorable raw material for bioenergy production since it possesses numerous advantages. The major advantages include its versatility, higher photoconversion efficiency, and growth efficiency compared to terrestrial plants. Under ideal conditions, several species of algae can double their number of cells within a day, making them produce significant biomass quicker than land-based crops. The rapid rate of growth facilitates a more dependable and steady supply of feedstock for biofuel production. In terms of high productivity per unit area, algal cultivation methods, such as photobioreactors and open ponds, have the potential to produce a greater amount of biomass per unit area as compared to typical agricultural crops, therefore maximizing land utilization. Lastly, algae cultivation gives environmental benefits in terms of the reduction of greenhouse gases from the atmosphere by assimilating carbon dioxide while they grow, thereby compensating for a portion of the emissions produced by the combustion of bio-oil.

Algae can be grown in nutrient-rich wastewater, aiding in the recycling of industrial effluent and the capture of carbon, transforming environmental waste into valuable resources. Also, the non-competition with food crops for arable land makes the algae a sustainable option for green energy. The primary constituents of algae that have the potential to be converted into biofuels are oxygen, hydrogen, carbon, and nitrogen. Algae exhibit significant variation in their biochemical makeup due to factors such as species and growth circumstances. However, they are primarily composed of varying quantities of protein, lipids, and carbohydrates, including starch. The most cultivated microalgae genera used for bio-oil production are *Nannochloropsis*,

Scenedesmus, *Chlorella*, *Spirulina* (Bondurant et al., 2023; Moazezi et al., 2022; Sánchez-Bayo et al., 2021; Zhang et al., 2018).

1.4. Wastewater treatment and biomass production in a sustainable manner

1.4.1. Microalgae cultivation and conditions

Microalgae cultivation and biomass production with the integration of wastewater treatment has garnered significant interest in recent years. Furthermore, the economic viability of the underlying methodology and operational procedures continues to pose challenges. Several investigations were conducted on the screening of potential microalgal strains (Daneshvar et al., 2019; Ravi Kiran et al., 2024), the optimization of culture conditions (Divya Kuravi and Venkata Mohan, 2021; Ravi Kiran and Venkata Mohan, 2022), the design of bioreactors for microalgal cultures (Arora et al., 2021), and other factors to increase the lipid content of microalgae and promote their growth. To reduce overall costs, many studies were conducted on coupling microalgae growth with dairy wastewater treatment (Daneshvar et al., 2019; Kumar et al., 2019; Ravi Kiran et al., 2024). The inorganic and organic nutrients present in the wastewater can be utilized by microalgae during biological treatment (da Silva et al., 2021).

Heterotrophic mode

In heterotrophic mode, the microalgae use the respiration process to obtain energy by organic compound oxidation. Glucose, glycerol, and acetate are the main forms of carbon used for the cultivation of microalgae in heterotrophic mode. The use of glucose as an organic carbon source for microalgae culture has been widely used due to its superior energy in terms of adenosine triphosphate compared to other substrates. Acetate is also a common utilizable carbon source for growing microalgae in heterotrophic mode. Upon entry into the cytoplasm of microalgae cells, the process of acetate metabolism occurs via the acetylation of coenzyme A by acetyl-CoA synthetase. This reaction is a single-step process that utilizes a solitary ATP molecule, resulting in the formation of acetyl coenzyme A (acetyl-CoA). Two major pathways, namely, the glyoxylate cycle and Tricarboxylic Acid Cycle (TCA) further degrade the acetate to malate and citrate, respectively. Nevertheless, large amounts of acetate may exhibit toxicity against several cells, hence impeding their structure (da Silva et al., 2021). Also, bacteria coexisting with microalgae were found to improve the degradation of nitrogen, phosphate, glucose, and chemical oxygen demand, but with a trade-off in lipid productivity (Zhang et al., 2012). *Chlorella* sp. HS2 high-density algal cultures were produced in heterotrophic cultivation

mode using BG11 media with glucose in a fermenter under dark conditions. An increase of the model to a 5-L fermenter revealed that the culture depleted the phosphorus completely, which led to insufficient utilization of the nitrogen and carbon sources (Kim et al., 2019). The respiration of organic carbon during heterotrophic cultivation by microalgae generates CO_2, which contributes to the greenhouse effect.

On the other hand, the coexistence of heterotrophic and autotrophic microalgae in mixed cultures may result in a reduction of carbon dioxide emissions. This is due to the mutually beneficial nutrient requirements of each microorganism, whereby the heterotrophic species consume oxygen and generate carbon dioxide. The high quantities of organic compounds in the growth medium used for cultivating heterotrophic microalgae provide the possibility of invasion by competing bacteria and fungi, which may compromise the quality of the process and products. Heterotrophic growth of microalgae thus demands sterilization of media, which can incur energy costs ranging from 20% to 30% of the overall costs of the production process. This expense might be less if the heterotrophic microalgae produce products with high market value (da Silva et al., 2021). For the generation of high-market-value products, there is a requirement for scale-up technology, namely, raceway pond for microalgae cultivation. It is very difficult to sterilize a huge amount of cultivation media for large ponds in a heterotrophic mode. Also, the risk of bacterial and fungal contamination will increase in such an open system. As far as our knowledge, there are no industrial plants that use a heterotrophic mode of cultivation to treat dairy wastewater.

Mixotrophic mode

In comparison to the heterotrophic mode, mixotrophic cultivation facilitates a higher growth rate and biomass productivity. To produce biochemical compounds and accomplish maximum biomass productivity, a balance between photosynthesis and respiration is important. The utilization of microalgae biomass as a source of renewable energy and its interconnection with numerous biological processes for the production of value-products for their subsequent reuse in a closed-loop biorefinery system facilitates many advantages and makes the process both sustainable and economically feasible (Kuravi and Venkata Mohan, 2022). Many studies have provided evidence for the proliferation of microalgae towards lipid synthesis and the production of high-value products using dairy wastewater (DW) as a nutrient source in a mixotrophic mode. *Monoraphidium* sp. SVMIICT6 was identified and cultured using a mixotrophic approach to treat synthetic dairy effluent. The growth of microalgae was facilitated

by the removal of nutrients, as evidenced by the carbohydrate, protein, and lipid content, in addition to biomass productivity of 0.05 g $L^{-1}day^{-1}$. Heptadecanoic acid and myristoleic acid were found as significant fatty acids which has numerous nutraceutical benefits (Kuravi and Venkata Mohan, 2022). The microalgae cultivation in outdoor open culture using raw DW was also compared with indoor cultivation in some studies. The highest biomass production in indoor bench-scale cultures reached 0.26 g L^{-1} day^{-1}, whereas outdoor conditions only achieved 0.11 g L^{-1} day^{-1}. Also, saturated fatty acids, i.e., C16:0/C18:0 were dominant fatty acids in outdoor biomass, which indicates huge potential for cultivation of *Chlorella* sp. in RDW for biodiesel production (Lu et al., 2015).

Contrastingly, in another outdoor cultivation of *Ascochloris* sp. ADW007 in RDW, the biomass productivity was higher (0.207 ± 0.003 g/L/d) than in the indoor bench scale study (0.102 ± 0.003 g/L/d) (Kumar et al., 2019). In many studies, consortia of microalgae/cyanobacteria and bacteria were used to treat dairy wastewater. One of the primary benefits of microalgae consortia in wastewater treatment is their ability to enhance resilience and compensate for the loss of individual algal species during cultivation. The consortium consisting of *Chlorella* sp. and *C. zofingiensis* had the highest biomass concentration and productivity, with values of 5.41 g L^{-1} and 773.2 mg L^{-1} day^{-1}, respectively. The growth of *Chlorella* sp. alone resulted in the highest total lipid content (21.09%), but the consortium (*Scenedesmus* spp./*C. zofingiensis*) exhibited the best lipid productivity (150.6 mg L^{-1} day^{-1}) (Qin et al., 2016). Hence, the selection of microalgal consortia will depend on the final product requirement. The mixotrophic condition is not restricted to inorganic carbon and sunlight only because of the availability of organic carbon present in dairy wastewater for growth. Still, high concentrations of some compounds in dairy wastewater hinder the growth of microbes.

To overcome this drawback, a strategy is to use extremophilic algae which could tolerate the inhibition and toxicity of high ammonium nitrogen and urea in dairy wastewater. *Chlorella vulgaris* CA1, isolated from dairy effluent, exhibited a remarkable tolerance to a significant concentration of ammonia nitrogen (2.7 g/L), surpassing the tolerance of other *Chlorella* species by more than 20 times. The resilience of the algae to withstand a significant concentration of ammonium nitrogen indicates the possibility of efficiently recycling nutrients from dairy effluent, while simultaneously generating algal biomass and valuable bioproducts (Pang et al., 2020). The incorporation of microalgae with wastewater treatment within a biorefinery framework entails the formation of bio-based products together with bioremediation of waste towards solving the environmental issues.

1.4.2. Bioremediation potential of microalgae to treat dairy wastewater

1.4.2.1. Characteristics of Dairy wastewater

Dairy industry wastewater is considered as one of the most polluted effluents in terms of BOD (Biological Oxygen Demand), COD (Chemical Oxygen Demand), and total suspended solids (TSS). However, the volume of wastewater and pollution load is dependent on the type of products produced and the production process. The sterilized packaging unit of the Saras dairy factory processes a total of 1,00,000 L of milk/day, whereas the facility's processing capacity is 5,00,000 L per day. Brar et al. (2019) reported that wastewater generated from the Saras dairy plant, Jaipur, has a COD of 1,280 ± 226.47 mg L^{-1} and BOD of 245.95 ± 8.48 mg L^{-1}. The total phosphate and nitrogen content of the dairy wastewater also have significant values of 19,583 ± 424 mg L^{-1} and 363.97 ± 23.93 mg L^{-1}, respectively (Brar et al., 2019). Comparatively, the dairy wastewater at Jelgava, Latvia, has a COD of 1,680 ± 20 mg L^{-1} and BOD of 1,196 ± 50 mg L^{-1}, which is higher than the permissible limits. The wastewater contains nitrogen and phosphate of 115 ± 30 mg L^{-1} and 22 ± 05 mg L^{-1}, respectively. Additionally, lipids in the wastewater were confirmed by Nuclear Magnetic Resonance (NMR) spectroscopy (Ekka et al., 2022).

Qasim and Mane (2013) characterized the dairy wastewater of Pune City, Maharashtra, with a COD of 8,960 ± 716.4 mg L^{-1} and BOD of 442 ± 3.1 mg L^{-1} (Qasim and Mane, 2013). In another work, wastewater generated from yogurt and buttermilk dairy wastewater in Erbil City has less pollution load in terms of COD and BOD, generates 40–50 tons of yogurt and buttermilk every day. The COD value ranges from 0.986 to 1.132 g L^{-1} and the BOD ranges from 0.6 to 0.8 g L^{-1} (Aziz and Ali, 2017). When the DW is released into lakes and rivers without treatment leads to eutrophication, increases the growth of microorganisms that may deplete the dissolved oxygen in the water bodies. Hence, dairy sector becomes one of the most notable contributors to the pollution of water bodies.

pH is a crucial parameter in evaluating wastewater quality, as microbial growth depends on the pH level of the wastewater. White wastewater produced after the cleaning of pasteurizers at both two Canadian dairy plants has an alkaline pH ranging from 8.23 to 12.45. However, the total solid from plant A (0.50 ± 0.04 g/L) was comparatively less than those from plant B (3.12 ± 0.24 g/L), which signifies less dilution of second plant. Additionally, the alkaline and acidic wastewater were collected after the second and fourth steps of the cleaning-in-place protocol and characterized for their chemical properties. The acidic wastewater generated from both

plants A and B has very acidic pH (1.82 ± 0.06-plant A and 1.17 ± 0.01-plant B) with comparative electrical conductivity (5.35 ± 0.10 µS/cm -plant A and 14.25 ± 0.13 µS/cm -plant B). The comparative conductivity was observed due to significant presence of calcium ions (177.04 ± 0.43 mg/L) in plant B acidic wastewater (Alalam et al., 2021). While the pH of Yoruksut dairy wastewater has a slight acid-to-neutral range (6.75–7.71), the total solid was lower (1,200 mg/L) in March compared to May month (3,900 mg/L), exceeding the EPA limit (Aziz and Ali, 2017).

Sawalha et al. (2022) characterized the dairy industry wastewater in Palestine. Three samples were collected after pasteurization, cheese making, and the washing process (soda washing and acid washing). The wastewater from different places was massively concentrated in terms of organics, chloride ions, pH, and TSS. However, the organics and TSS of cheese production wastewater were higher than those from the yogurt production process (Sawalha et al., 2022). TSS are a crucial polluting indicator that is used for evaluating DW pollution and for measuring the effectiveness of the wastewater treatment plant. The suspended matter in wastewater comes from viscous milk and small fragments of curd or flavorings (Garcha et al., 2016). The higher values of TSS and COD in cheese wastewater may be attributed to the presence of whey protein, lactose, and fats (Sawalha et al., 2022). Whey wastewater has a high level of organic matter and nutrients, which can be utilized by microorganisms for their growth and metabolism.

In another investigation, de Andrade et al. (2023) collected and analyzed the curd cheese whey for microalgal bioremediation. The whey has a COD of 52,886 ± 269.25 mg L^{-1} with total nitrogen and phosphate of 1.56 ± 0.035 g L^{-1} and 0.66 ± 0.012 g L^{-1}, respectively (de Andrade et al., 2023). In a study conducted by Bharadwaj et al. (2018), 52 microbes which include both bacteria and fungi have been identified and subjected to a screening process to determine their efficiency in degrading dairy wastewater. The genera *Serratia*, *Stenotrophomonas*, *Brachybacterium*, and *Cunninghamella* were reported for their activity in degrading dairy wastewater. The COD level of wastewater was reduced to 58%–72% using these three native genera (Bhardwaj et al., 2018). Overall, in both developed and developing nations, compliance with stringent environmental regulations has become obligatory for the discharge of effluents beyond the allowable limit. The initial physicochemical characteristics of different dairy wastewater collected in previous studies are given in Table 1.1.

Table 1.1. Initial physico-chemical characteristics of different collected and synthetic dairy wastewater.

Collection location	Initial COD (mg/L)	Initial Nitrogen (different forms) (mg/L)	Initial phosphate/phosphorous (different forms) (mg/L)	pH	Solids (mg/L)	TOC (mg/L)	Reference
Sarvottam Dairy Effluent (Gujarat, India)	2593.33 ± 277.37	277.40 ± 10.75	5.96 ± 0.04	7.8	2800 ± 20	116.23 ± 4.38	(Chokshi et al., 2016)
Aochun Dairy Co., Ltd. (Foshan, Guangdong, China)	2128 ± 12	121.0 ± 1.4	39.6 ± 3.2	9.31 ± 0.10	560 ± 6	-	(Qin et al., 2016)
Local dairy industry (Saharanpur city, Uttar Pradesh)	2843 ± 13	105 ± 3	36 ± 3	9.15 ± 0.2	1586 ± 18	-	(Chandra et al., 2021)
Wastewater from dairy products from Agro industries (Parana, Brazil)	190± 20	18.04 ±0.50	2.63 ± 0.06	10.26 ± 0.25	60	7.42 ± 0.12	(Melo et al., 2022)
DW (Amul dairy,	7110	46.5	74.1	3.69	3720	-	(Kumar et al., 2019)

Gujarat, India)							
DW, Pune City	8960 ± 16.4	120.1± 2.5	-	7.10 ± 0.12	543.4 ±5.2	-	(Qasim and Mane, 2013)
Synthetic Dairy wastewater	3840	247.8	401.3	7	-	-	(Singh et al., 2023)
Synthetic Dairy wastewater	3600	160 ± 3 mg/L;	180 ± 2.1	-	-	-	(Mohanty and Mohanty, 2023a)
Synthetic Dairy wastewater	3600	158.69 ± 2.40	175.97 ± 1.81	7.0 ± 0.5	-	-	(Kiran and Venkata Mohan, 2022)
Synthetic Dairy wastewater	1164	16.51	12.9	7	-	-	(Divya Kuravi and Venkata Mohan, 2021)
CPCB (1986)	250	50 (NH_4-N) 10 (Nitrate)	-	5.5 to 9.0	100 (suspended)	-	(Central Pollution Control Board, 1986)

1.4.2.2. Metals and organic matter present in the dairy wastewater

The presence of organic matter, such as urea, carbohydrates, and fats also affects the quality of the wastewater. Various fatty acids were analyzed in wastewater from a dairy industry located at Jelgava, Latvia. The wastewater comprises 65% hexadecanoic acid followed by 21%

octadecanoic acid. Tetradecanoic acid was also present in wastewater in major amounts, but oleic acid, linolenic acid, lauric acid, and linoleic acids were present in smaller concentrations. It was found that milk fatty acids consist mainly of saturated fatty acids. The presence of fatty acids in dairy wastewater offers a viable and cheap option for biodiesel production (Ekka et al., 2022). The quality and treatment efficiency of dairy wastewater also depend on the types of organic matter present, as these compounds can attach to particulates and cause abrasion, deposition, and clogging of membranes and filters during operations. The examination of trace organic chemicals found in the effluent of a dairy plant revealed the presence of common milk degradation products as well as compounds that may be linked to their synthetic or agricultural origins. The compounds found to be highest in the effluent were 1-methyl-5-oxo-L-proline methyl ester (Verheyen et al., 2011).

Zinc (Zn), cobalt (Co), copper (Cu), chromium (Cr), iron (Fe), and lead (Pb) were among the prevalent heavy metal pollutants detected in DW, and considered among the most critical global environmental problems (Table 1.2). Metals present in water bodies can persist for a prolonged period or undergo biological transformations. Eventually, they accumulate throughout the food chain, presenting a significant threat to the ecology if not adequately removed. Removing heavy metals from wastewater is challenging due to their resistance to chemical or biological treatment. The chloride, iron, and fluoride concentrations of 199 mg L^{-1}, 5.17 mg L^{-1}, and 4.833 mg L^{-1} were observed by Kumar et al. (2019) in raw dairy wastewater collected from Amul Dairy, Gujarat, India (Kumar et al., 2019). Also, the dairy eluent collected from Pune City has a chloride level of 186.4 ± 3.4 mg L^{-1} (Qasim and Mane, 2013), which is lower than EPA regulations (Qasim and Mane, 2013).

However, the DW obtained from Sarvottam Dairy effluent contained a high amount of sodium (345.65 mg/L). While little amount of nickel, copper, cobalt, iron, and chromium was observed in DW (Chokshi et al., 2016). The elevated levels of sodium and chloride were attributed to the extensive use of alkaline cleaning agents in dairy facilities. Aluminum can come from aluminum sulfate which is frequently employed in water treatment facilities for the purpose of clarifying the water (Qasim and Mane, 2013). Trace elements such as copper and zinc, as well as other heavy metals including cadmium, arsenic, chromium, and mercury, may be found in dairy wastewater. These elements enter the wastewater via therapeutic substances and organic molecules from pesticides (Qasim and Mane, 2013).

Table 1.2. Comparison of metals present in the different dairy industry-generated wastewater.

Wastewater collection points	K	Na	Cl	Cr	Zn	Ca	Cd	Mg	Al	Mn	Ni	Cu	Co	Fe	Pb	Reference
Mean of 15 plants	46.6	544	-	-	-	48.9	-	20.9	139	163	36	8	2	725	-	(Danalewich et al., 1998)
Yoruksut dairy factory wastewater (Jan 2016)	-	-	53.98	-	-	-	-	-	-	12.5	-	-	-	-	-	(Aziz and Ali, 2017)
Yoruksut dairy factory wastewater (March 2016)	-	-	70	-	-	-	-	-	-	10.2	-	-	-	-	-	(Aziz and Ali, 2017)
Yoruksut dairy factory	-	-	94.97	-	-	-	-	-	-	26.6	-	-	-	-	-	(Aziz and Ali, 2017)

wastewater (May 2016)																
Dairy products	4.39 ± 1.91	0.067 ± $9e^{-5}$	-	-	-	29.86 ± 0.13	-	2.72 ± 0.01	22.53 ± 0.82	-	-	-	-	-	(Melo et al., 2022)
Sarvottam DW	0.30	345.65	-	0.50	0.30	38.10	-	28.45	0.30	1.25	0.80	0.30	0.65	0.30	0.65	(Chokshi et al., 2016)
DW (Amul)	-	-	-	-	-	-	-	-	-	-	-	-	-	5.17	-	(Kumar et al., 2019)
Acid cleaning wastewater Plant A	0.76 ± 0.09	155 ± 13	-	-	-	12.22 ± 1.45	-	1.89 ± 0.17	-	-	-	-	-	-	-	(Alalam et al., 2021)
Acid cleaning wastewater Plant B	1.57 ± 0.06	23 ± 4	-	-	-	177.04 ± 0.43	-	7.07 ± 0.05	-	-	-	-	-	-	-	(Alalam et al., 2021)

Alkaline cleaning wastewater Plant A	9.41 ± 0.26	10,665 ±191	-	-	-	45.15 ± 1.76	-	0.82 ± 0.10	-	-	-	-	-	-	-	(Alalam et al., 2021)
Alkaline cleaning wastewater Plant B	6.48 ± 0.07	4033 ± 46	-	-	-	18.81 ± 1.98	-	0.23 ± 0.03	-	-	-	-	-	-	-	(Alalam et al., 2021)
DW	5.26	-	186.4 ±3.4	0.061	-	-	0.065	-	-	0.32	-	0.061	-	0.065	0.040	(Qasim and Mane, 2013)
CPCB (1986)	-	-	-	-	5.0	-	2.0	-	-	2	3.0	3.0	-	3	0.1	(Central Pollution Control Board, 1986)

1.4.3. Nutrient removal capabilities of microalgae

1.4.3.1. Removal of Nitrogen, Phosphate, and COD

The organic matter present in dairy wastewater is the primary contaminant that needs to be treated in any wastewater treatment facility (Vieira Costa et al., 2021). Several researchers have studied the ability of microalgae to treat DW. COD quantifies the concentration of organic compounds in the DW. A huge amount of COD increases the eutrophication in water bodies if discharged without treatment. Previously, *Acutodesmus dimorphus* decreased the COD of dairy effluent by more than 90% (2,593.33 ± 277.37 to 215 ± 7.07 mg/L) when cultivated for 4 days. The observed reduction in COD indicates that microalgal cells possess the ability to effectively use an organic form of carbon as a building block for their metabolism. Extending the treatment time did not have a substantial impact on decreasing the COD level (Chokshi et al., 2016). Kuravi and Venkata Mohan (2022) reported a maximum removal efficiency of 75.5% of the organic content from synthetic dairy wastewater by microalgae, which contributed to their growth and photosynthetic activity (Divya Kuravi and Venkata Mohan, 2022). Acetate present in DW undergoes metabolism via the glyoxylate route to produce malate inside the cells, which serves as a precursor for the production of fatty acids (da Silva et al., 2021).

On the other hand, algae convert carbon dioxide present in the air into organic matter by harnessing ATP and NADPH via the Calvin cycle (Mohsenpour et al., 2021). Microalgae utilise carbon dioxide as their primary source of carbon during the photoautotrophic mode. The dissociation of gaseous CO_2 into bicarbonate and carbonate ions in water is dependent upon the pH level of a medium. The specific equilibrium between these ions is also influenced by factors such as temperature, cation amount, and salinity. Carbon dioxide can pass through the plasma membrane of cells due to its non-polar nature, while bicarbonate requires an active transport system to diffuse. Through the enzymatic activity of carbonic anhydrase, bicarbonate is rapidly catalysed to CO_2 in the chloroplast, facilitating the fixation of inorganic carbon. Most microalgae have developed carbon concentration mechanisms to mitigate the decline in photosynthetic performance, hence enhancing the rate of carbon dioxide accumulation. The low CO_2 concentration in water mainly drives this adaptation.

The Calvin cycle converts an inorganic form of carbon to an organic form of carbon via CO_2 fixing to the acceptor molecule (Ribulose-1,5-bisphosphate) in the presence of RuBisCo (Ribulose-1,5-bisphosphate carboxylase oxygenase) enzyme to yield 2 molecules of 3-phosphoglycerate and subsequently forms Glyceraldehyde-3-phosphate. During this process,

the production of four molecules of Ribulose-1,5-bisphosphate for every three molecules of carbon dioxide that are fixed, leaving just three molecules left in the cycle. One molecule of Glyceraldehyde-3-phosphate is either stored or further converted into pyruvate, which is then incorporated into the tricarboxylic acid cycle (Mohsenpour et al., 2021).

Also, microalgae are capable of removing a substantial amount nitrogen and phosphate. Nitrogen is available in the form of ammonium, which can be toxic to microalgae. Therefore, strains that are tolerant to high concentrations of ammonium should be used to treat such effluent. Nitrogen is supplied as an essential source of growth for microalgae during cultivation. Nitrate is used as a supplement in synthetic culture media, while the ammonium form of nitrogen is present in effluents for microalgae (Vieira Costa et al., 2021). According to reports, ammoniacal nitrogen is the preferred nitrogen source for microalgae due to its direct metabolism and low energy requirements due to absence of reduction step (Pritchard et al., 2015; Sanz-Luque et al., 2015). After 6 days of cultivation, all ammoniacal nitrogen was consumed by *A. dimorphus* from RDW (277.4 ± 10.75 mg/L) (Chokshi et al., 2016).

Kuravi and Venkata Mohan (2022) reported that the nitrogen was reduced from 165 mg L^{-1} to 27.1 mg L^{-1} using *Monoraphidium* sp. in dairy wastewater, achieving a maximum treatment efficiency of 83.5% (Divya Kuravi and Venkata Mohan, 2022). A prior investigation has also shown that an elevated concentration of ammonium-N has the potential to impede the proliferation of microalgae (Lin et al., 2021). In the mechanism of nitrogen absorption, the cellular uptake of nitrate occurs, followed by its reduction to nitrite by the action of the cytosolic-NADH-dependent nitrate reductase enzyme. Following this, the nitrite is transported to the chloroplast, where it undergoes reduction to ammonium through the catalytic action of NADPH-linked nitrite reductase (Mohsenpour et al., 2021).

Hemalatha et al. (2019) reported a nitrate removal efficiency of 65.5% by cultivating mixed microalgae in DW (Hemalatha et al., 2019). In contrast, Kothari et al. (2012) observed a 90% nitrate removal from 75% DW using *Chlamydomonas polypyrenoideum* after 10 days (Kothari et al., 2012). Phosphate is also an essential nutrient for the growth of microalgae. Phosphate is found in wastewater in the form of phosphate and inorganic salts (Vieira Costa et al., 2021). According to Kothari et al. (2012), *C. polypyrenoideum* demonstrated a phosphate removal efficiency of 70% after cultivation in 75% DW. The assimilation of phosphorus by microalgae has been classified as a component that limits their growth. The polyphosphate reserves are used to store surplus phosphorus for synthesizing phosphatides, proteins, and nucleic acids.

Furthermore, phosphorus may facilitate the augmentation of cellular division and the production of ATP, requiring more phosphate for energy transfer and subsequent protein synthesis (Magyar et al., 2024). As seen through the removal efficiency of microalgae towards contaminants from wastewater, the DW industry has the potential to prevail over the high expense of biomass production. It is recommended to conduct dairy wastewater treatment along with biomass production using toxicity-tolerant microalgal strains in a biorefinery approach. Table 1.3 presents previous literatures on microalgae for dairy wastewater treatment and potential product formation.

Table 1.3. Literature covering studies conducted on dairy wastewater treatment using microalgae.

Microalgal species	Conditions	Biomass concentration or productivity	Potential Product	Remarks	References
Chlorella variabilis Scenedesmus obliquus	Diluted synthetic DW	673 mg L^{-1}	Lutein	The consortia exhibited phosphate removal of 70.19%, ammoniacal nitrogen removal of 86.22%, COD removal of 54.72%.	(Gatamaneni Loganathan et al., 2020)
C. minutissima N. muscorum Spirulina sp.	70% DW + 10 g/L of glucose at 18:6 h photoperiod	5.76 ± 0.06 g/L	Biodiesel feedstock	Polyculture removed about 58.76% of nitrogen. Removal of phosphate was observed in the range of 83–84%.	(Chandra et al., 2021)
Ascochloris sp. ADW007	Indoor bench-scale in DW	0.102 ± 0.003 g/L/d	Biodiesel	Over 95.1% of COD was reduced	(Kumar et al., 2019)

				in both indoor and outdoor cultivation	
Ascochloris sp. ADW007	Outdoor pilot-scale in DW	0.207 ± 0.003 g/L/d	Biodiesel	Over 95.1% of COD was reduced in both indoor and outdoor cultivation	(Kumar et al., 2019)
Chlorella sp.	5% DW outdoor	47.50 mg L^{-1} day^{-1}	Biodiesel	Total COD removal efficiency%: 21.99 ± 0.66 Total N removal efficiency%: 85.12 ± 3.37 Total P removal efficiency%: 88.47 ± 3.90	(Lu et al., 2015)
Chlorella sp.	10% DW outdoor	160.0 mg L^{-1} day^{-1}	Biodiesel	Total COD removal efficiency%: 38.88 ± 4.09 Total N removal efficiency%: 85.17 ± 0.35 Total P removal efficiency%: 66.68 ± 1.29	(Lu et al., 2015)
Chlorella sp.	25% DW outdoor	110.0 mg L^{-1} day^{-1}	Biodiesel	Total COD removal efficiency%: 54.82 ± 0.91 Total N removal efficiency%: 83.83 ± 1.19	(Lu et al., 2015)

				Total P removal efficiency%: 65.33 ± 2.05	
Chlorella sp./*C. zofingiensis*	Autoclaved DW	5.41 g L^{-1}	Biodiesel	The highest COD removal of appx 50% was achieved.	(Qin et al., 2016)
Scenedesmus spp./*C. zofingiensis*	Autoclaved DW	5.11 g L^{-1}	Biodiesel	The highest COD removal of 62.87 % was achieved.	(Qin et al., 2016)
A. dimorphus	DW	840.67 ± 11.11 mg/L	Biodiesel and Bioethanol	Maximum removal of COD i.e. 91.71% was observed. Total (100%) removal of nitrite and ammoniacal nitrogen was observed.	(Chokshi et al., 2016)
Monoraphidium sp.	Synthetic DW	50 mg L^{-1} d^{-1}	Biofertilizers and nutraceutical	COD, nitrates, and phosphates removal efficiencies were 75%, 85%, and 60% respectively.	(Divya Kuravi and Venkata Mohan, 2022)
Tetradesmus sp. SVMIICT4	Synthetic DW	2.38 g L^{-1}	Biodiesel	The removal efficiency of 95.5% COD was observed. Nitrates/phosphates removal efficiency of 65.2/ 57.35% was observed.	(Kiran and Venkata Mohan, 2022)

Monoraphidium sp. KMC4	Synthetic DW	1.9 g L^{-1}	Wide spectrum biopesticide	The reduction efficiency was reported to be 96% when the initial COD of the medium was 500 mg/L, it is reduced to 78% when the initial COD of the medium was maintained at 2000 mg/L.	(Mohanty and Mohanty, 2023b)

1.4.4. Algal Biomass Production

Microalgae biomass derived from dairy effluents holds potential for energy applications, offering a CO_2-neutral alternative to fossil fuels. These microalgae exhibit versatility in various growth modes, including autotrophic, heterotrophic, and mixotrophic, thereby enhancing their suitability for biofuel production (Pandey et al., 2019). Microalgae cultivation can be conducted through both open and closed systems (Figure 1.3). Open systems, naturally occurring in environments such as ponds, lagoons, seas, and oceans, provide a habitat for the growth of microalgae. Conversely, closed systems such as photobioreactors offer controlled conditions of temperature, pH, and nutrient availability to optimise biomass yield. Microalgae can be grown in the industrial effluents, which is interesting since it makes them more useful for wastewater bioremediation (Posadas et al., 2017).

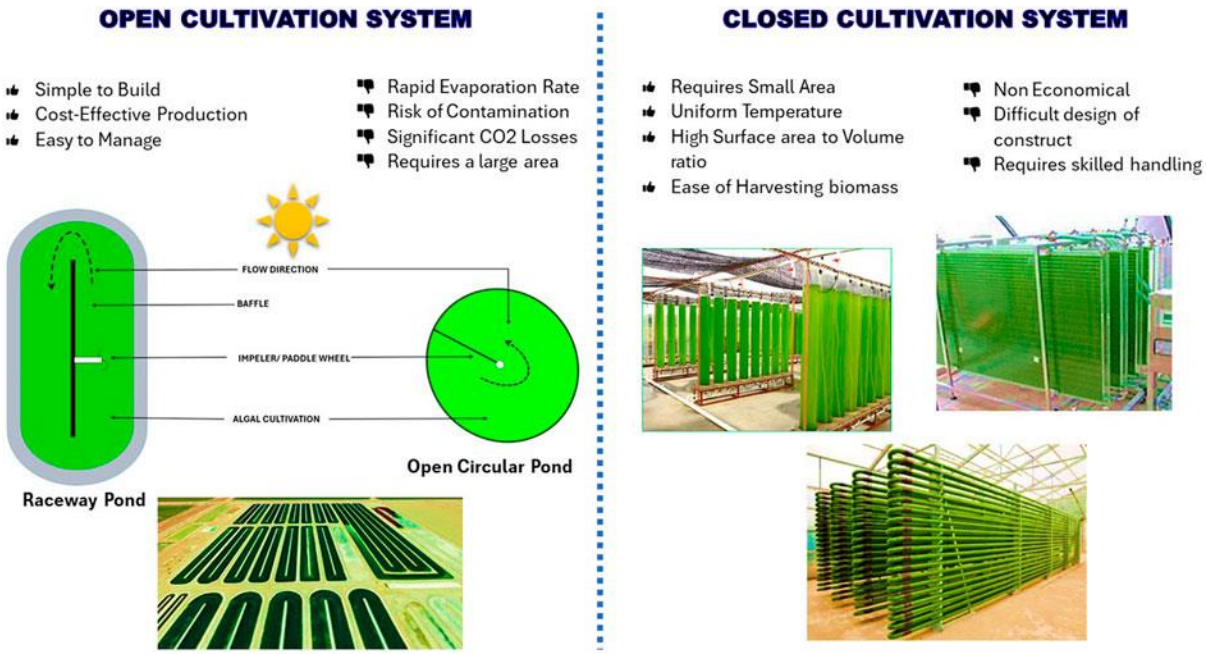

Figure 1.3. Open and closed pond system for algae cultivation.

1.4.4.1. Open systems

Open ponds represent the simplest and most convenient method for large-scale microalgae cultivation. They encompass natural bodies of water like lakes and ponds, as well as human-made structures such as circular and raceway systems. In this method, shallow ponds or raceways are utilized as the cultivation environments for microalgae, harnessing the nutrient-rich nature of dairy wastewater to promote algal growth. The process begins by introducing dairy wastewater into the open ponds, providing essential nutrients such as nitrogen and phosphorus required for microalgae growth (Arora et al., 2021). Under natural sunlight, microalgae photosynthesize and utilize these nutrients, effectively removing pollutants from the wastewater. This bioremediation process helps in reducing the organic load, nitrogen, and phosphorus content in the wastewater, thereby mitigating environmental pollution. In raceway ponds, mixing is typically facilitated by paddle wheels, while in circular ponds, rotating arms serve a similar purpose. Additionally, in larger ponds, mixing can be achieved in specific areas using impeller blades (Yen et al., 2019). These mixing mechanisms play a crucial role in maintaining homogeneity within the pond environment, ensuring adequate nutrient distribution, and promoting optimal conditions for the growth of microalgae.

Open pond cultivation offers a viable and sustainable solution for treating dairy wastewater, providing economic, operational, and environmental advantages over other treatment methods. Its simplicity, scalability, and efficiency make it an attractive option for dairy facilities seeking

cost-effective and environmental friendly wastewater management solutions. Open pond systems are typically less expensive to construct and operate compared to closed systems such as photobioreactors. They require minimal infrastructure and maintenance, making them a cost-effective option for dairy wastewater treatment. Open ponds can be easily scaled up or down to accommodate varying wastewater volumes (Gupta et al., 2019). This scalability makes them suitable for both small-scale dairy operations and large-scale industrial facilities. Open ponds utilize natural sunlight for photosynthesis, eliminating the need for artificial lighting. This reduces energy consumption and operational costs associated with providing light in closed systems. Dairy wastewater is rich in nutrients such as nitrogen and phosphorus, which are essential for microalgae growth. Open pond systems leverage these nutrients, promoting robust algal biomass production. Open pond cultivation is relatively simple and requires minimal technical expertise. Operators can easily monitor and manage the system without the need for sophisticated equipment or complex control systems. Open ponds can be adapted to cultivate various species of microalgae, offering flexibility in biomass production.

However, open systems come with certain limitations. They are susceptible to contamination by various microorganisms, including protozoa and bacteria, present in the surrounding environment (Lam et al., 2018). These contaminants can compete with the desired microorganisms for nutrients and space, affecting the overall productivity and purity of the culture. Unlike closed or controlled systems, open systems lack precise control over growth parameters such as temperature, pH, light intensity, and nutrient availability (Faried et al., 2017). As a result, fluctuations in environmental conditions can occur, leading to inconsistent growth and productivity of the microorganisms. Open systems are exposed to environmental factors including weather conditions, seasonal changes, and fluctuations in water quality. These external factors can negatively impact the stability and reliability of the cultivation process, making it challenging to maintain optimal growth conditions. Scaling up open systems for large-scale production can be impractical due to space limitations and the need for extensive infrastructure (Tan et al., 2018). Additionally, achieving uniform mixing and distribution of nutrients in large open systems can be challenging, resulting in uneven growth and productivity throughout the system. Open systems are susceptible to pest infestations and predation by insects, birds, and other wildlife (Vieira Costa et al., 2021). These pests can damage the microorganism culture or consume the biomass, resulting in reduced yields and economic losses. The discharge of effluents from open systems into natural water bodies can have

environmental consequences, such as nutrient runoff and eutrophication, which can disrupt aquatic ecosystems and degrade water quality.

1.4.4.2. Closed system (photo-bioreactors)

Given the limitations associated with pond systems, there is a common preference to cultivate algae strains in photobioreactors. These systems enables precise control and monitoring of operating conditions and nutrient levels through automated control systems, significantly reducing the risk of contamination (Suparmaniam et al., 2019). An ideal PBR model should incorporate the following features: 1) efficient light-harvesting capabilities to facilitate the transport, channelling, and distribution of light among microalgal species for optimal biomass production; 2) the ability to maintain operational parameters feasibly to promote high utilization of light energy by the cells; 3) minimized investment and operational costs; and 4) reduced energy consumption (Xiaogang et al., 2022). Two prevalent types of photobioreactors include straight tubes, which are either arranged horizontally on the ground or vertically in long rows called tubular bioreactors, and helical bioreactors, consisting of spirally wound tubes around a central support. These bioreactors commonly employ tubes made of glass or perpex.

Tubular bioreactors are predominantly utilized outdoors and can be oriented vertically, horizontally, inclined, or helically to optimize sunlight exposure, thereby enhancing photosynthesis and maximizing algal biomass production (Ting et al., 2017). Photobioreactors (PBRs) should be designed to be straightforward, cost-effective, and capable of achieving high volumetric productivity while remaining energy-efficient and scalable to industrial levels. Tubular bioreactors exhibit a specific limitation in their photosynthetic efficiency, resulting in higher energy consumption. A significant drawback of these photobioreactors is the uneven concentration gradient along the lengthy tubes, leading to inadequate mass transfer (Tan et al., 2018).

Additionally, closed systems like tubular bioreactors are prone to the uncontrolled proliferation of pathogenic microorganisms on inner surfaces, forming biofilms that impede reagent mass transfer due to external resistance at the biofilm interface (Skoneczny and Tabiś, 2015). Plastic bag photobioreactors are gaining popularity for their cost-effectiveness and varying volumes, typically constructed from polythene (Wang et al., 2012). However, challenges arise from difficulties in mixing components and the bags susceptibility to damage, potentially reducing the system longevity. Despite their benefits, closed systems incur high operational and construction expenses.

One major hurdle associated with photobioreactors (PBRs) in microalgal biomass production is the substantial expense incurred in their construction and maintenance. While these high costs may render PBRs impractical for biofuels production, they hold promise for producing high-value compounds with greater commercial potential. Researchers such as Nugroho and Zhu (2019) have suggested strategies to mitigate operational expenses, including the utilization of cost-effective materials like wastewater as a feedstock and the adoption of energy-efficient pumps for resource recovery (Nugroho and Zhu, 2019).

Another significant challenge faced by PBRs is the gradual limitation of light penetration on the surface where algal biofilms develop. However, advancements in bioengineered PBR designs offer solutions to operational issues while maintaining high efficiency and minimizing maintenance costs. For instance, Wu et al. (2019) developed an innovative algal biofilm photobioreactor using hog manure wastewater, resulting in significant *C. vulgaris* growth and easy harvesting via a scraping method (Wu et al., 2019). Additionally, in response to the light attenuation problem arising from suspended solids and contaminants in anaerobically digested wastewater (ADW), Chen et al. (2018) implemented a hollow fiber membrane (HFM) system within the photobioreactor. This setup enables nutrients to permeate from the inner chamber containing ADW to the outer chamber housing the algal culture medium via the HFM. Consequently, this configuration effectively controls pollutants, mitigating the inhibition caused by suspended particles (Chen et al., 2018).

One more disadvantage of using photobioreactors for treating dairy industry wastewater is the potential for fouling and clogging. Dairy wastewater contains organic compounds, nutrients, and suspended solids, which can accumulate and form biofilms on the surfaces of the photobioreactor, obstructing light penetration and inhibiting algal growth. This fouling can decrease the efficiency of the photobioreactor, leading to reduced wastewater treatment performance and increased maintenance requirements. Additionally, the presence of fats, oils, and proteins in dairy wastewater may further increases fouling issues, requiring frequent cleaning and maintenance to prevent culture system failure. Therefore, managing fouling and clogging challenges is a crucial consideration when implementing photobioreactors for dairy wastewater treatment.

1.5. Biorefinery Approach of Algal Biomass

Biorefinery is the sustainable conversion of biomass into a range of commercial products and energy. It is necessary to elucidate several particular components of this definition.

'Biorefining' might be regarded as a concept, facilities, methods, or clusters of industries. The term 'sustainable' signifies that the biorefinery provides economic, environmental, and social advantages. A 'spectrum' denotes a range of energy and non-energy products. 'Marketable' signifies the necessity for an existing or projected market volume at a viable price. Ultimately, 'products' may encompass food/feed ingredients, chemicals, materials, and bioenergy. The foundation of the initial IEA Bioenergy Task 42 biorefinery classification system is predicated on four principal elements or category groups: *feedstock, conversion process, platforms, and products* (Annavelink et al., 2022). Different forms of biofuel can be formed from microalgae like bio-diesel, biohydrogen, methane, and bioelectricity (Figure 1.4). These biofuels can be produced using thermal or biological methods.

Microalgal growth is dependent on various environmental factors. Also, the composition of lipid, carbohydrate, and protein inside cells is dependent of different nutrient component ratios in the cultivating medium. The integration of wastewater treatment with microalgal cultures presents an attractive path for concurrently addressing wastewater management and energy generation. Microalgae absorb nutrients from wastewater and recycle CO_2, eliminating the need for fertilizers and herbicides, while the resultant biomass can be converted into diverse energy resources. This combination between wastewater treatment and microalgal cultivation significantly reduces processing costs, hence benefiting both sectors (Bhatia et al., 2021).

Biomass is the main key starting point for establishing a successful biorefinery system. However, for a successful biorefinery system, infrastructure facilities must be incorporated to facilitate efficient production of biofuels and bioenergy. The microalgal biorefinery approach utilises all upstream and downstream processes to form value-added products from algae. The use of less-expensive wastewater as a substrate medium for cultivating microalgae for bio-oil generation reduces the overall process cost. This step also reduces environmental hazards associated with wastewater discharge. This study suggests simultaneous dairy wastewater treatment and utilization of wastewater for microalgae growth for bio-oil production. Other product from thermochemical conversion technology can be reused for various applications. The approach demonstrates a cascade flow strategy for wastewater treatment with a path for product recovery and an alternative strategy for wastewater disposal.

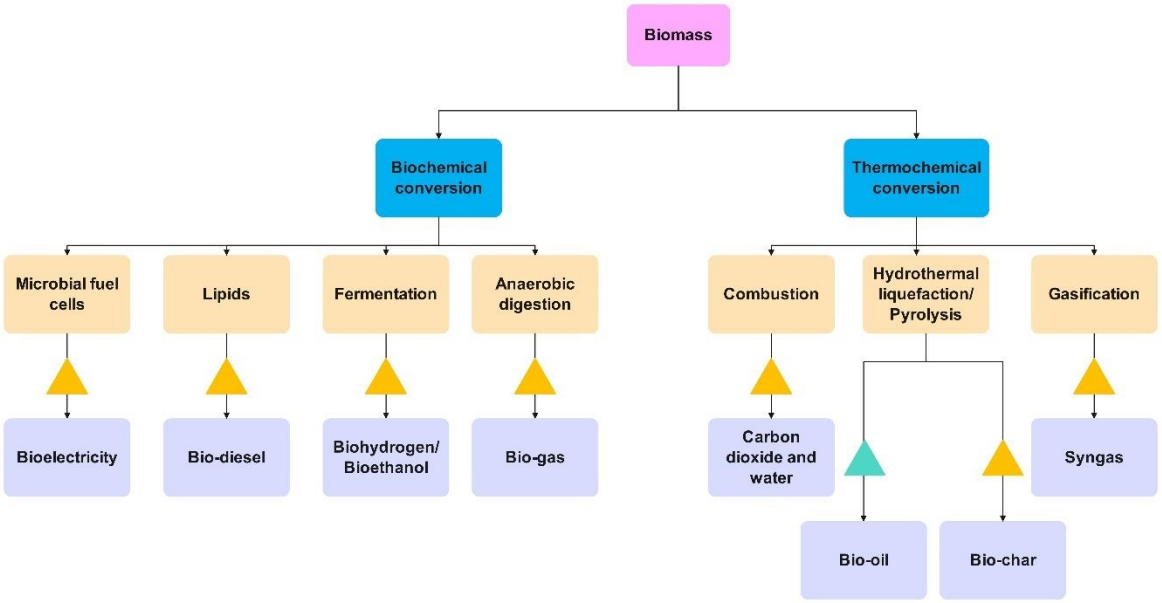

Figure 1.4. Biomass conversion for production of different value-added products.

1.6. Thermochemical conversion pathway

The thermochemical conversion process is a promising option for transforming feedstocks into energy-dense, transportable liquid fuels that can be upgraded into petroleum replacements. Thermochemical conversion technologies like pyrolysis (Kumar et al., 2024), gasification (Moser et al., 2021), and hydrothermal liquefaction (He et al., 2018), have been widely used for biomass conversion. Compared to all, hydrothermal liquefaction and pyrolysis have been observed to be two of the most used processes for liquid fuel production. Direct combustion, although widely practiced, is often regarded as inefficient due to the emission of harmful particulate matter and fly ash, which pose serious environmental and health concerns. Therefore, the development of advanced thermochemical methods for sustainable biomass valorization has become a key research priority.

Two thermochemical methods exist for converting biomass into bio-oil: hydrothermal liquefaction and pyrolysis. Both have been extensively utilized to transform wet and dry biomass. Hydrothermal liquefaction (HTL) stands out as a particularly effective technique for converting wet or liquid biomass feedstocks into high-quality bio-oil. A major advantage of HTL lies in its ability to directly process wet biomass, thereby eliminating the need for energy-intensive drying steps. However, the process requires high-pressure operation, often under an inert atmosphere, which presents engineering and operational challenges. Pyrolysis, another prominent thermochemical process, involves the thermal decomposition of biomass in the

absence of oxygen to yield bio-oil, biochar, and non-condensable gases. The composition and yield of these products depend strongly on operating temperature and heating rate. Typically, pyrolysis is conducted at temperatures between 250 °C and 700 °C. At temperatures below 300 °C, biochar is the dominant product, whereas at 400 °C–600 °C, the formation of liquid bio-oil is favored. Beyond 700 °C, the process increasingly produces gaseous products due to extensive cracking and deoxygenation reactions. Bio-oil is the liquid product derived from thermochemical conversion process, identified as an eco-friendly resource due to its carbon-neutral characteristics. Bio-oil comprises numerous organic molecules, including hydrocarbon, esters, N and O based compounds, aldehydes, acids, ketones, and phenols. Consequently, bio-oil is considered a promising feedstock for the production of high-quality biofuels and value-added chemicals.

1.6.1. Fundamentals of Hydrothermal Liquefaction

Water plays a key role as a reactant and catalyst at high temperature and high pressure (Yabalak et al., 2023). A phase diagram is a graph that illustrates the regions where different phases coexist in a system at equilibrium, based on the state variables (Figure 1.5). The specific shape of this graph can vary depending on the function being plotted and the variables involved (pressure vs temperature). Thermodynamically, the triple point of a substance occurs when all gas, liquid, and solid phases exist together in equilibrium, at a specific temperature and pressure. At this point, the sublimation, fusion, and vaporization curves meet. The critical point marks the termination of a phase equilibrium curve. An example is the liquid-vapor critical point, which marks the point where a liquid and its vapor can coexist under particular pressure and temperature conditions.

At elevated temperatures, the gas cannot be condensed solely through pressure, while at reduced pressures, temperature alone is insufficient for its liquefaction. At the critical point (CP), characterized by a critical temperature T_c and a critical pressure p_c, phase boundaries disappear (Keszei, 2012). The CP of H_2O occurs at 373.94 °C and 22.06 MPa (Brunner, 2014). As the temperature increases beyond a critical point of H_2O, gasification turns into governed process.

Subcritical water exhibits varying physical characteristics compared to H_2O in its normal state, including the dielectric constant (κ), which is commonly employed to measure polarity and can be readily adjusted by altering temperature and pressure (Yabalak et al., 2023). When water reaches near a critical point, there is a change in viscosity (low) and solubility of organic

compounds (high), which makes the subcritical process efficient for bio-oil production (Toor et al., 2011). At the subcritical conditions, there is a decrease in the interphase mass transfer resistance (Peterson et al., 2008). The enthalpy of water decreased when undergoing a phase transition at higher pressure, i.e. hot compressed state rather than vapor. This results in a reduction of latent heat loss and an improvement in the energy efficiency of HTL (Kruse and Dinjus, 2007). Pure water at 25 °C acts as a polar solvent, but it transforms to more like a non-polar solvent when it reaches above the critical temperature of 374 °C (Peterson et al., 2008). Also, the important property of water, the κ reduced from 78 Fm^{-1} at room temperature (0.10 MPa) to 14.07 Fm^{-1} at 350 °C (20 MPa) (Uematsu and Frank, 1980), increases the solubility of fatty acids in water with the increased temperature and pressure (Huang et al., 2013).

The ionic product changed from 10^{-14} to 10^{-11} just below 350 °C and then decreased by five orders of magnitude or more above 500 °C (Brunner, 2014; Peterson et al., 2008). An increase in ionic value indicates that reactions involving the H_2O ions as catalysts are mostly increased. As the thermal energy rises, there is a tendency for the electron shared by O and H atoms to circulate more evenly, resulting in a reduction of the oxygen electronegativity (making it less polar). Furthermore, the dissociation of H_2O exhibits a significant increase as the temperature rises. Water, similar to other aqueous solutions, undergoes hydrolysis or dissociation, resulting in the formation of H^+ and OH^- ions. This process can be reversed and the rate is fast enough to be considered in equilibrium at any given moment (Möller et al., 2011). With the abundant hydronium and hydroxide ions, it is possible for certain reactions to occur in subcritical water without the need for an additional catalyst. Also, the introduction of acids and bases in HTL with H_2O results in an increased concentration of H^+/OH^- ions and a higher ionic strength (Asghari and Yoshida, 2006; Möller et al., 2011; Watanabe et al., 2005).

The process of separating or extracting products into distinct phases can be done in highly compressible near-critical regions. By manipulating temperature or pressure in a near-critical area, one compound or solvent can quickly modify its solubility and selectively, cause them to separate into different phases, either by precipitating or dissolving certain components (Peterson et al., 2008). For producing biofuel such as jet fuels from biomass, one major concern is to reduce oxygen when the raw feedstock consists of 40-60 wt%. And, the commercial petroleum fuel consists of minimal oxygen. The removal of oxygen is most achieved through dehydration and decarboxylation reactions which eliminates oxygen in the form of water and CO_2. Decarboxylation is important because it not only reduces the amount of oxygen in the raw biomass but also raises the H:C ratio, resulting in the production of more desirable fuels.

From a thermodynamic perspective, water is oxidized and does not possess any residual heating value. Therefore, they can be considered as an excellent component for eliminating oxygen without losing the calorific value of the O-containing compounds being eliminated. The dehydration process fastened up by the catalytic effect of an Arrhenius acid. In a mixture comprising numerous functional groups, the chemical pathways can be altered via reactions and interactions, both intermolecular and intramolecular (Peterson et al., 2008).

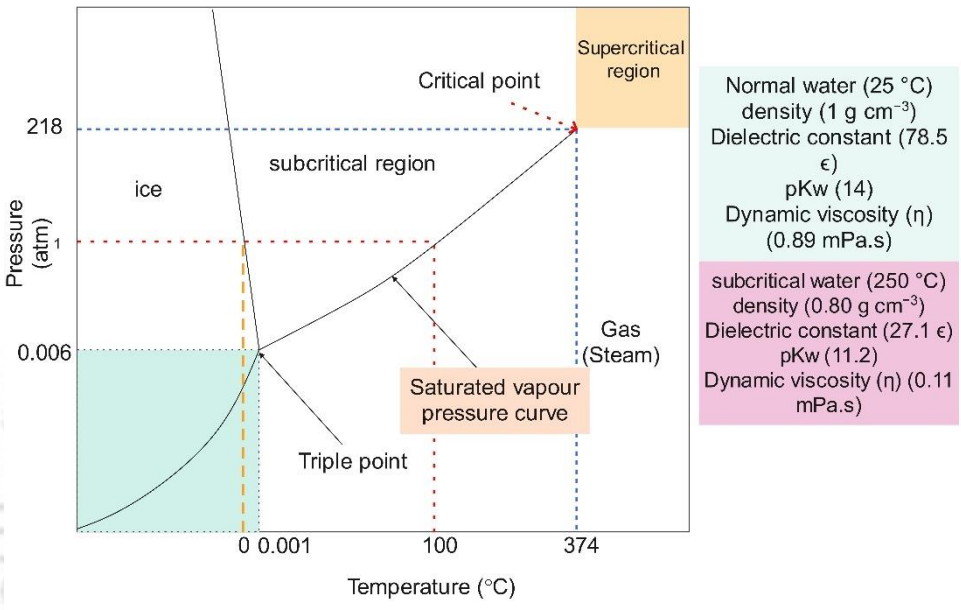

Figure 1.5. Properties of water at normal and subcritical conditions.

1.6.2. Significant Process Parameters

1.6.2.1. Effect of temperature and pressure

It is considered that 200 °C to 380 °C is optimum for the production of bio-oil from biomass. Several investigations were performed to analyze the influence of temperature on the product distribution by different microalgal species (Sahoo et al., 2021). There is a direct relationship between temperature and pressure. When the temperature increases, the pressure also increases. The bio-oil yield from microalgae increased from 14 % to 29.60% as the reaction temperature rose from 275 to 325 °C (Ravi Kiran et al., 2024). Similarly, a lower temperature of around 250 °C gives a lower bio-oil quantity compared to a higher temperature of 375 °C. It is also evident that the nitrogen and sulfur content is higher in the case of bio-oil derived at 375 °C than at 250 °C, due to the significant protein degradation at former temperature (López Barreiro

et al., 2013). At 310 °C for 60 min, the differences between light bio-oil yields are quite broad from one microalga to another, which differ in low lipid and high protein or vice-versa. The high lipid, low protein species produced the highest light bio-oil at 350 °C for 60 min. Two different mechanisms worked for different microalgal species for maximum bio-oil production (Cheng et al., 2017). At lower temperatures, the peptide bond in proteins is stronger compared to the glycosidic bond found in carbohydrates and requires more energy to break the former one (Ravichandran et al., 2022). As the temperature rises, the formation of low-polarity heterocyclic compounds increases through Maillard and rearrangement reactions from proteins and carbohydrates. This leads to an enhancement in bio-oil yield. Beyond optimum temperature, compounds in bio-oil break down into gaseous CO_2 and NH_3 or combine to form solid residue (Cheng et al., 2017). Lastly, a strong heat source is required to sustain the temperature in the two-phase system.

In this process, pressure plays an important role in keeping the single medium phase. By implementing this approach, it is possible to regulate the rate at which biomass dissolves and undergoes hydrolysis. An increase in solvent density leads to a corresponding rise in pressure. The involvement of high-density molecules in the biomass components leads to enhanced extraction and breakdown (Ravichandran et al., 2022). By obtaining subcritical conditions, the pressure impact on the bio-oil, liquid, or gas yield becomes extremely small. The pressure has an insignificant impact on the bio-oil and gas production (Sangon et al., 2006). Using higher initial pressure, the bio-oil transformed into solids by self-condensation reactions. The self-condensation of bio-oil to solids is classified as a free radical reaction in terms of reaction mechanism and increased initial pressure can lower the activation energies for free radical reactions in the liquid phase. Therefore, the high initial pressure exerts a negligible influence on the overall bio-oil output (Yin et al., 2010). It has a crucial impact on the energy usage of the HTL process (Ravichandran et al., 2022).

1.6.2.2. Effect of biomass loading

The amount of feedstock in a reactor has an influence on bio-oil yield. The water content in the feedstock ranges from 70% to 80% when algal slurry is used. Moazezi et al. (2018), studied the effect of algae-to-solvent ratio with respect to temperature and time using the RSM methodology. The optimum point was achieved at 302 °C and 35 min with 0.09 wt% biomass loading. However, the critical point is observed at 320 °C with 0.13 wt% loading. The decrease in intermolecular interactions with increasing concentration is responsible for this

phenomenon. This is because the lower kinetic energy required to activate molecular interactions at low temperatures leads to a lower bio-oil.

Conversely, increasing intermolecular interactions at higher temperatures enhances the bio-oil. It is important to observe that when temperature rises and water evaporates, its mass drops and the suspended solids concentration in the liquid increases. With the reactor low volume, the evaporation process results in a minimal amount of mass loss, causing the solid in the solvent to increase by less than 1% (Moazezi et al., 2022). Conversely, the gaseous products and solid residue increased due to a higher biomass-to-solvent ratio. Increasing the quantity of feedstock lowers the molecular interactions and solubility of the compounds, resulting in a reduction in bio-oil yield (Yin et al., 2010). At higher loading concentrations, the HTL process exhibits pyrolytic behavior (Moazezi et al., 2022). From an economic standpoint, it is more desirable to have a slurry that is more concentrated with solids for the process of liquefaction (Yin et al., 2010).

1.6.2.3. Effect of residence time

The residence time is considered one of the important parameters for determining product distribution. The 30 and 60 min were found to be optimum in many studies (Cheng et al., 2019; Lavanya et al., 2016). It was noticed that bio-oil yield is high in the case of high temperature with less reaction time. While the solid yield is high with long residence time (60 min) and high temperature (350 °C) (Audu et al., 2021). Bio-oil yield of 50.60%, 54.30% and 58.10% was observed from *Scenedesmus obliquus*, *Nannochloropsis gaditana*, and *Scenedesmus almeriensis* at 375 °C for 5 min (López Barreiro et al., 2013).

The water-soluble phase yield is affected by the residence time. In one case, if the reaction time was raised from 5 to 30 min, the light bio-oil increased from 9.80 ± 0.40 wt% to 10.80 ± 0.60 wt%, and the bio-char increased from 28.70 ± 1.20 wt% to 29.80 ± 0.10 wt% with an expense of aqueous phase (reduced from 16.50 ± 0.60 wt% to 14.30 ± 0.40 wt%). Increasing the time from 30 min to 60 min reduced the light bio-oil fraction (7.60 ± 0.40 wt%) with an increase in solid fraction (35.60 ± 1.00 wt%) and a decrease in the more aqueous phase (11.60 ± 0.30 wt%). At short residence time, light and heavy bio-oil have low nitrogen and sulfur content (Cheng et al., 2019). This suggests that bio-oil yield & quality are affected by reaction time during HTL. Previous literatures on the HTL/DHTL process are provided in Table 1.4.

Table 1.4. Bio-oil production from different microalgae species through HTL.

Feedstock	Reaction conditions	Bio-oil yield (%)	C (%)	H (%)	N (%)	HHV (MJ/Kg)	References
Chlorella vulgaris	350 °C for 10 min	30.50	73.20	9.50	7.40	-	(Jazrawi et al., 2015)
Chlorella	350 °C for 30 min	31.70	72.59	8.88	6.91	35.30	(He et al., 2018)
Chlorella	300 °C for 30 min	27.56	72.59	10.26	7.20	41.17	(Chen et al., 2022)
Chlorella sorokiniana	300 °C for 60 min	27.80	72.00	15.00	1.14	43.70	(Chakraborty et al., 2012)
Chlorella sorokiniana	300 °C for 60 min	31.00	75.33	10.60	1.50	37.92	(Miao et al., 2012)
Spirulina	340 °C for 120 min	33.52	65.58	8.96	6.65	31.58	(Huang et al., 2018a)
Galdieria sulphuraria	350 °C for 60 min	27.50 (LBO)	-	-	-	-	(Cheng et al., 2017)
Nannochloropsis salina	310 °C for 60 min	54.30 (LBO)	-	-	-	-	(Cheng et al., 2017)
Chlorella sorokiniana	350 °C for 30 min	31.00	74.1	9.33	5.94	36.60	(Mahata et al., 2023)
Nannochloropsis gaditana	320 °C for 10 min	42.30	73.71	9.18	6.12	35.70	(Sánchez-Bayo et al., 2021)
Monoraphidium sp. KMC4	350 °C for 30 min	33.00	73.82	9.01	5.80	35.84	(Mishra and Mohanty, 2019)

1.6.3. Reactor Design and Configuration

The design and configuration of the reactor are critical for optimizing the process efficiency and bio-oil yield and quality. Batch Reactors are used for small-scale and optimization experimental studies. These reactors are simple, allowing for precise control of reaction parameters but may not be efficient for continuous production. Continuous flow reactors are

suitable for large-scale operations, offering consistent throughput and better scalability. The products formed from both batch and continuous process of sludge feedstock were compared. A lower amount of bio-oil was obtained in a continuous process compared with batch processing, likely due to reduced repolymerization of water-soluble products into bio-oil. However, continuous process produced bio-oil with a lower nitrogen content compared to the batch process under similar conditions. The higher nitrogen content in the batch process may be attributed to Maillard reactions and amidation during the heating phase and the formation of nitrogen-containing unstable intermediates during the cooling phase (Fan et al., 2022).

Additionally, a recent pilot-scale continuous HTL system has processed algae and household sludge for bio-oil production. The investigation revealed a bio-oil yield of 33 wt% from *Spirulina* feedstock in a continuous HTL. The study employs the use of a heat exchanger for heat recovery and the incorporation of a hydraulic oscillation system to increase the turbulence in the tubular reactor, showing promising results from batch and continuous HTL studies in terms of energy efficiency. The bio-oil consisted mainly of majorly palmitic acid, glycerol, heptadecane, and linolelaidic acid (Anastasakis et al., 2018). Also, the comparison of batch and continuous HTL processes is complex due to the challenges in accounting for the effects of heating and cooling periods, despite using the same separation procedures (Fan et al., 2022).

1.6.4. Influence of Feedstock Composition

The composition of algae significantly affects bio-oil quantity in the HTL process. The efficiency of bio-oil production highly depends on macromolecule composition, ash content, and heteroatoms present in biomass. Previous studies have demonstrated the influence of biomass composition on bio-oil yield and quality (Aljabri et al., 2022; He et al., 2020). Also, to improve the yield and quality of bio-oil, single algae biomass is mixed with other carbonaceous feedstock (Obeid et al., 2021).

Lipids and protein are the precursors for bio-oil, while carbohydrate products primarily transfer into an aqueous phase and solid residue and contribute minimally to bio-oil yield (Vo et al., 2017). Lipids directly contribute to higher bio-oil yields due to their high energy density and suitability for conversion into hydrocarbon chains (Gai et al., 2015b). The principal component analysis revealed that the lipid content of freshwater microalgae is positively correlated with carbon content, yield, energy recovery, and HHV value of the bio-oil. Also, protein content is highly correlated with the negative characteristics of bio-oil like nitrogen and nitrogen/carbon ratio (Ratha et al., 2022).

López Barreiro et al. (2013) evaluated the impact of macromolecular composition of different microalgae on bio-oil yield at 250 °C and 375 °C. The bio-oil yields were varied with different species at 250 °C. The yield was highest (44.80 wt%) for *D. tertiolecta* and lowest (17.60 wt%) for *S. obliquus*. The difference is related to the biochemical composition and cell wall strength. Contrastingly, the bio-oil yields were not that much different at 375 °C from all the species, varying from 45.60 wt% for *T. suecica* to 58.10 wt% only for *S. almeriensis*. The results suggested that at low temperatures, the type of strain parameter affects the bio-oil yield (López Barreiro et al., 2013).

Cheng et al. (2017) performed the hydrothermal liquefaction of microalgae with different compositions (high lipid and low lipid microalgae). The high lipid *N. salina* requires moderate conditions for bio-oil production and contains C_{14}-C_{18} fatty acid amides. While severe temperatures were required for high protein-containing *G. sulphuraria* for biocrude production and contain majorly $N_{1\text{-}3}O_{0\text{-}2}$ compounds (Cheng et al., 2017). The bio-oil yield showed a positive effect from lipid compared to protein, followed by carbohydrate (Biller and Ross, 2011; Shakya et al., 2017). Majorly, the protein and lipids of microalgae contribute to the bio-oil fraction without any additional catalysts. While the carbohydrates can be processed using sodium carbonate catalyst towards bio-oil, selectively enhancing the decarboxylation reaction process, forming fewer products that are water-soluble. Protein fraction majorly forms nitrogen heterocycles, pyrroles, indoles, and some alkanes in the bio-oil. The result also showed that solid residue was increased with the addition of Na_2CO_3 during the liquefaction of biomass. The use of Na_2CO_3 increased phenolic compounds and enhanced the alkane production from lipids. While the use of water and formic acid formed majorly aliphatic amides. Interestingly, the high-carbohydrate *Porphyridium* does not exhibited compounds associated with carbohydrates, likely because the carbohydrate fraction contributed only about 7% to the bio-oil yield (Biller and Ross, 2011).

Another study revealed that the bio-oil yield was higher from high lipid algae (82.90%) compared to low lipid algae (55%). The study suggested that the biochemical composition affected the conditions required for liquefaction of different algae. The low-lipid algae achieved a better yield of light bio-oil compared to high-lipid algae, suggesting the insignificant correlation of lipid content to the light bio-oil yield. The results stated that alkanes in light bio-oil from low-lipid algae were produced via protein degradation. Hence, the high-protein and low-lipid algae form more light-bio-oil due to the formation of short-chain hydrocarbons. The energy recovery was better from algae *Chlorella* compared to low-lipid *Nannochloropsis*

because hexadecenoic acid (32.90% of total) in bio-oil, contributing to higher HHV. The results suggested that the conditions required for the highest bio-oil yield and better quality are not similar. The higher bio-oil yield was obtained from high-lipid algae, but the quality is better from low-lipid algae (Li et al., 2014).

Shakya et al. (2017) also confirmed through a predictive model that lipid contributed to a major proportion in bio-oil formation compared to protein fraction. Carbohydrates contributed a lesser proportion to the bio-oil formation (Shakya et al., 2017). The high ash in biomass can bring limitations in heat transfer during the reaction due to slagging and fouling, diminishing the efficiency of HTL operation. Also, high ash quantity in the biomass increased the concentration of inorganics partitioning into the oil phase (Audu et al., 2021). The reduction of ash quantity from feedstock reduces the solid residue after liquefaction and increases the aqueous and gas phase yields. Also, the HHV and light fraction compounds in bio-oil will be increased by reducing the ash quantity. Also, this process facilitates denitrogenation and hydrocarbon formation reactions. The investigation demonstrated that feedstock ash content level below 40% can be effectively converted to bio-oil phase with better quality (Chen et al., 2017).

1.7. Two-stage HTL

Another finely tuned process, namely, two-stage hydrothermal liquefaction, has received attention for improving the bio-oil quality together with the formation of high-value coproducts from microalgae (Chakraborty et al., 2012). The two-stage HTL is a two-step reaction in which algae are solvolyzed initially at the moderate temperature range of 120–240 °C, resulting in a stage-I solid residue. The solids from the first step are subjected to severe temperatures of 275–350 °C for bio-oil formation.

The hydrothermal treatment of microalgae has led to a decrease in the N/C with an increase in the C content of pretreated microalgae biomass, i.e., the H/C ratio (Bondurant et al., 2023). During the hydrolysis step (mild temperature), carbohydrates are partially broken down into disaccharides and monosaccharides, while soluble proteins and amino acids from microalgae are extracted during the first step (Gu et al., 2020a; Usami et al., 2020). The water-soluble aqueous phase produced from the first step of the two-stage HTL includes carbohydrate and protein-derived compounds (Usami et al., 2020; Vadlamudi et al., 2024), while carbon is retained in solid residue I. The elemental properties and calorific value of bio-oil are enhanced after higher temperature reaction in two-stage HTL, decreasing the hydrogen requirement for

the hydrotreatment step (Vadlamudi et al., 2024). Additionally, the partial removal of nitrogenous compounds enhances the mass transfer between H_2O and lipid molecules during step II of two-stage HTL, enhancing the overall conversion efficiency (Gu et al., 2020a).

Bondurant et al. (2023) performed a two-step HTL using *Scenedesmus*/*Desmodesmus* microalgae. The conditions of 260 °C for 0.5 h effectively reduced the N and O amounts in pretreated algae for bio-oil production (Bondurant et al., 2023). In another similar investigation, the nitrogen concentration of bio-oil was lowered from 7.40 (by direct hydrothermal liquefaction) to 4.50% (two-stage HTL), while the yield significantly reduced from 30.50 wt% to 13.60 wt% (Jazrawi et al., 2015). During the two-stage HTL, the ammonium ions were eluted from the aqueous phase by enhancing the amino acid deamination during the first pretreatment stage. This process will reduce the nitrogen content by restraining the generation of amides and N- and O-heterocyclic compounds at higher temperature conditions (Bondurant et al., 2023; Huang et al., 2018a). Furthermore, in this process, the carbohydrates and proteins are hydrolyzed and fragmented into an aqueous phase at a lower temperature, which reduces the N and O in bio-oil under severe temperature conditions (Huang et al., 2018a). Suppressing the production by amides and heterocyclic compounds via deamination of amino acids at initial pretreatment stages and elution in the stage I aqueous phase is the one of the ways to decrease the nitrogen in bio-oil. Studies described above observed improved bio-oil yields and quality with low-N content by emphasizing a two-stage HTL. Previous literatures on two-stage HTL process are provided in Table 1.5.

Table 1.5. Bio-oil production from different microalgae from two-stage HTL process.

Feedstock	Pretreatment conditions	Bio-oil production conditions	Bio-oil Yield (%)	C (%)	H (%)	N (%)	HHV (MJ/ Kg)	References
Scenedesmus/ Desmodesmus spp.	260 °C for 30 min	360 °C for 72 h	-	-	-	(1.3 ± 0.0	-	(Bondurant et al., 2023)
Chlorella vulgaris	150 °C for 15 min	350 °C for 10 min	32.0	70.70	9.10	6.40		(Jazrawi et al., 2015)
Chlorella	250 °C for 20 min	350 °C for 10 min	~31.8	71.04	9.00	8.11	34.90	(He et al., 2018)
Chlorella	300 °C for 10 min	350 °C for 10 min	33.90	72.61	8.86	7.42	35.40	(He et al., 2018)

Chlorella sorokiniana	160 °C for 30 min	300 °C for 60 min	23.40	76.00	12.00	0.78	40.80	(Chakraborty et al., 2012)
Chlorella sorokiniana	160 °C, 20 min	240 °C for 20 min	30.40	70.34	11.09	0.87	37.30	(Miao et al., 2012)
Spirulina	225 °C for 10 min	340 °C for 120 min	34.34	70.01	9.71	5.71	34.90	(Huang et al., 2018a)
Spirulina	225 °C for 50 min	340 °C for 120 min	26.55	73.62	10.09	4.18	37.10	(Huang et al., 2018a)

1.8. Co-Hydrothermal liquefaction of algal biomass with other feedstocks

In today's scenario, India represents the 2nd largest populated country, where a huge amount of waste is generated over time. Thus, research should be focussed on energy conversion and utilization from waste feed by HTL and co-HTL process to address the issues related to landfill and segregation. The co-feeding system in hydrothermal liquefaction enhances the quality of the product along with an increase in the yield of bio-oil. The process makes an advantage of the utilization of all types of waste, which provides the pathway towards a waste valorization approach. For economic feasibility, two or more feeds are blended in such a ratio that the maximum yield and better quality of bio-oil can be obtained. Before understanding the chemical interaction between blended feeds, it is important to go through the HTL of individual chemical compounds to understand the resultant bio-oil formation (Sahoo et al., 2021). Based on previous literature, the co-liquefaction process can improve quality of bio-oil by decreasing N-content and improving heating value derived from protein-rich feedstock (Figure 1.6). Many studies reported the HTL of blending feedstock like swine manure, sewage sludge, pharmaceutical plant treated sludge, and microalgae (Mishra and Mohanty, 2020; Prestigiacomo et al., 2019; Xu et al., 2019; X. Zhang et al., 2022).

Due to correlated interaction between degraded and unstable compounds from feedstock blend, a synergistic impact was evaluated (Dandamudi et al., 2021). Also, the co-HTL process gives the benefit of increasing the high heating value of bio-oil. However, in a few studies, the co-HTL of blended biomass had shown a negative trend on bio-oil quality, maybe because co-liquefaction suppressed the deoxygenation reaction and increased the carbon and hydrogen loss in the gaseous product. Co-HTL of algae with other biomass could affect the bio-oil production efficiency. Co-HTL of *Chlorella* and sewage sludge with three different ratios was studied by

Xu et al. (2019) who observed a positive trend of bio-oil yield because of conversion of organic compounds in the raw feedstock to produce more biocrude (Xu et al., 2019). Co-liquefaction of swine manure and mixed algae has reported a 35.70% of bio-oil (Chen et al., 2014). Bio-oil yield from a single feedstock and a mixture of feedstock (domestic sewage sludge and microalgae biomass grown on wastewater) were compared by Mishra and Mohanty (2020). The co-HTL of biomass mixture resulted in high bio-oil yield in comparison to individual single feedstock liquefaction (Mishra and Mohanty, 2020).

Also, the dairy sludge approximately contains 40-70% organic matter and 60-80% volatile matter, which can be used as key starting components for bio-oil production in our work. The presence of a good amount of volatile matter signifies high targeted product formation during the thermal degradation process (Balasubramanian et al., 2018). Therefore, valorisation of algal biomass with dairy sludge for bio-oil will be a cost-feasible and sustainable process. Previous literatures on co-HTL process of microalgae with other feedstocks are provided in Table 1.6.

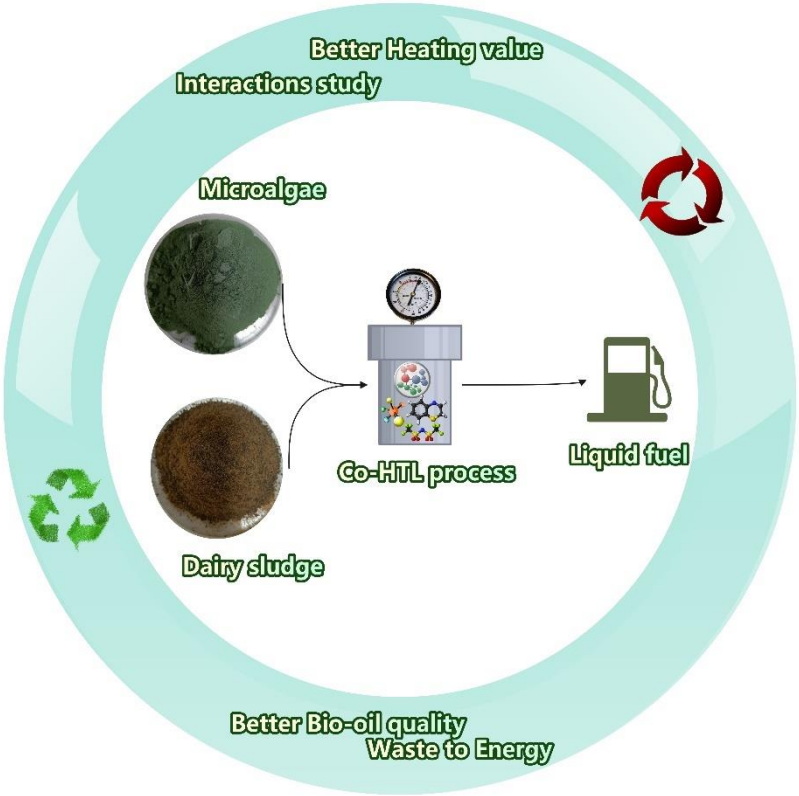

Figure 1.6. Co-Hydrothermal liquefaction of algal biomass with dairy sludge.

Table 1.6. Bio-oil production from microalgae with other waste feedstock from co-HTL process.

Feedstock	Feedstock ratio	Bio-oil production conditions	Bio-oil Yield (%)	C (%)	H (%)	N (%)	O (%)	HHV (MJ/Kg)	References
Microalgae with faecal sludge	25% microalgae: 75% faecal sludge	300 °C for 60 min	38	69.19	9.63	2.81	18.37	33.83	(Islam et al., 2022)
Microalgae and peat	50:50 ratios	300 °C for 60 min	36.6	66.91	9.42	2.75	20.23	32	(Hossain et al., 2022)
Chlorella and sewage sludge	50:50 ratios	350 °C for 15 min	16.4	72.1	4.4	8.4	14.1	32.9	(Ellersdorfer, 2020)
Chlorella and food waste	50:50 ratios	350 °C for 15 min	17.1	71.2	3.9	8.7	15.8	32.4	(Ellersdorfer, 2020)
Chlorella and pharmaceutical sludge	1:1	320 °C for 60 min	40.58	73.82	8.80	5.79	9.61	35.99	(X. Zhang et al., 2022)
Galdieria sulphuraria and crude glycerol	12.5 wt% GS+ Crude glycerol	350 °C for 30 min	65.5	-	-	-	-	-	(Cui et al., 2020)
Microalgae and sewage sludge	1:1	340 °C for 30 min	~26	70.88	8.09	6.52	12.61	33.44	(Xu et al., 2019)

1.9. Pyrolysis and Co-pyrolysis Process

Among the numerous conversion pathways for microalgal valorization, such as transesterification for biodiesel (Kothari et al., 2013), anaerobic digestion for biogas (Kusmayadi et al., 2023), and hydrothermal liquefaction for bio-oil (Singh and Mohanty,

2025), pyrolysis is distinguished as an another thermochemical technology that can transform the entire feedstock into liquid, solid, and gaseous products (Mustapha and Isa, 2024). Fast pyrolysis has been extensively researched for its ability to optimize bio-oil yield, whereas slow pyrolysis promotes biochar synthesis, which is utilized for soil enhancement and carbon sequestration (Yu et al., 2017).

Pyrolysis provides microalgae with the additional advantage of transforming protein and carbohydrate fractions, in addition to lipids, into viable energy carriers, thus improving overall carbon usage efficiency. Notwithstanding the obstacles posed by the elevated nitrogen content of microalgae, which may result in unwanted nitrogenous compounds in bio-oil, progress in process optimization and catalytic interventions persistently enhances product quality and process feasibility. Non-catalytic pyrolysis serves as an essential baseline for understanding thermal decomposition pathways and product distribution, though it typically produces bio-oils with poor stability and elevated oxygen and nitrogen contents. In contrast, catalytic pyrolysis employs solid catalysts such as zeolites and metal oxides to facilitate deoxygenation, denitrogenation, and cracking reactions, thereby enhancing the calorific value, stability, and chemical selectivity of the resulting bio-oils.

1.9.1. Fundamentals of Microalgal Pyrolysis

Microalgae are becoming acknowledged as a viable fuel for renewable energy due to their varied biochemical constitution and high growth rates. Microalgae growing in water are usually present in very low cell concentrations when outdoor conditions are maintained. The lower biomass productivity presents a major obstacle in microalgal technology, creating a bottleneck for upstream and downstream algal processes. Figure 1.7 shows a process flow for bio-oil production from microalgae pyrolysis, which includes grinding, sieving, size reduction, pyrolysis, and product separation.

Several studies have been conducted on pyrolysis studies using microalgae such as *Scenedesmus almeriensis* (Niu et al., 2024), *Scenedesmus obliquus* (Mustapha et al., 2021; Mustapha and Isa, 2024), *Chlorella* sp. (Shirazi et al., 2020), and *Isochrysis* sp. (Wang et al., 2016). Microalgal cellular composition (

Table 1.7) typically comprises lipids (20–50%), proteins (30–60%), carbohydrates (10–40%), pigments including chlorophylls and carotenoids, and minerals such as phosphorus, potassium, calcium, and trace elements (C. Yang et al., 2019). The nitrogen proportion in microalgal cells is observed due to major protein components. Also, inorganic nitrogen (10-15%) is present in microalgae as nitrites, nitrates, and ammonia. When these species undergo pyrolysis, the ash is formed as metal oxides. Some minor nitrogen comes from nucleic acids, which consist of nitrogenous bases. Glucose, cellulose, and hemicellulose are the major carbohydrates in microalgae (Debiagi et al., 2017). Thermogravimetry analysis (TGA) and analytical pyrolysis revealed the different degradation behaviour of distinct forms of carbohydrates in microalgae (Anastasakis et al., 2011). Lipids consist of a fatty acid chain of 14-20 carbon atoms with variations in unsaturation degree. Other inorganic and ash minerals present in microalgae as carbonates, sulphates, phosphates, and chlorides other than N-form. These inorganics converted to oxides, releasing a volatile fraction (Debiagi et al., 2017).

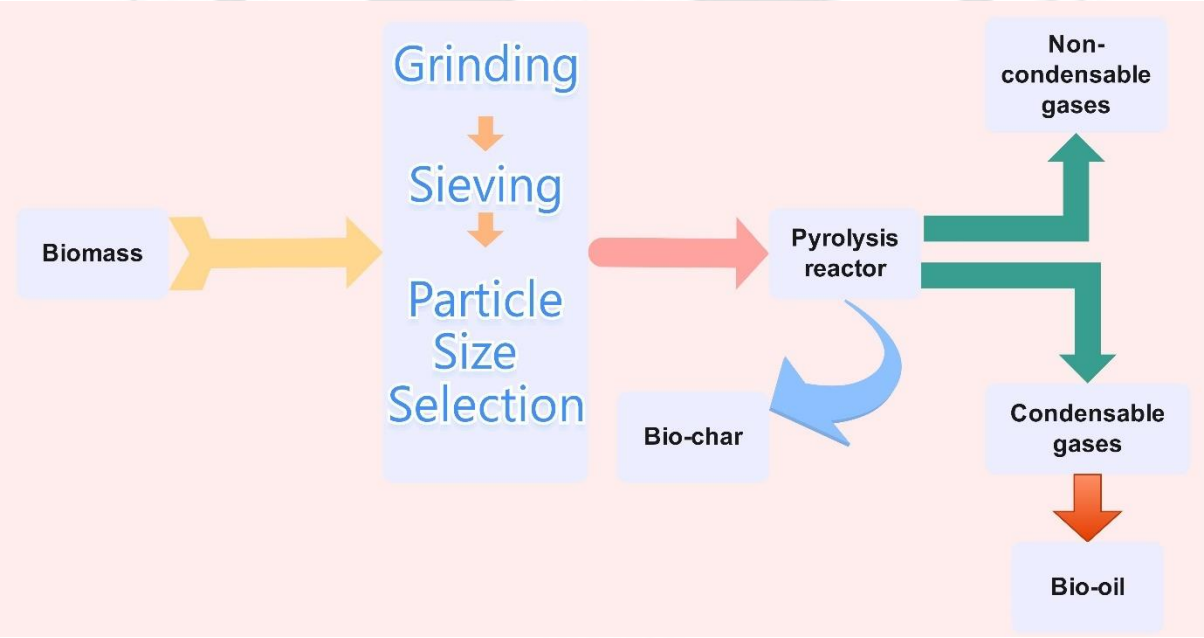

Figure 1.7. Process flow of microalgae pyrolysis.

Table 1.7. The composition of microalgae was provided in previous literature for the pyrolysis study.

Unit (wt%)	*Chlorella* sp. (Borges et al., 2014)	*Chlorella vulgaris* (Thangalazhy-Gopakumar et al., 2012)	*Nannochloropsis* sp. (Borges et al., 2014)	*Scenedesmus obliquus* (Mustapha et al., 2021)	*Isochrysis* sp. (Wang et al., 2016)
Ultimate					
C	41.21	44.5 ± 0.3	49.07	45.03	49.26
H	6.21	6.2 ± 0.0	7.59	7.50	7.50
N	7.04	9.6 ± 0.2	6.29	3.59	6.24
S		0	1.42	0.98	0.96
0	34.06	29.3 ± 0.5	35.63	42.90	31.74
Proximate					
Moisture	7.28	8.4 ± 0.2	5	-	1.69
Volatile matter	81.15	-	79.69	81.77	79.79
Fixed carbon	-	-	10.64	-	11.63
Ash	11.57	10.3 ± 0.2	5.03	10.17	6.89
Biochemical					
Protein		58.13	44	22.08	35.9
Carbohydrate		-	21	42.55	15.2
Lipid		-	30	21.62	42.9

The main purpose of pyrolysis studies of microalgae is:

1. To investigate the viability and practicality of pyrolysis process for processing microalgae.
2. To produce maximum yield of one of the 3 process products: bio-oil, biochar, or syngas.
3. To explore the influence of a catalyst on increasing required product from this process.

As of now, the microalgae-based pyrolysis process has not been commercialised and performed at laboratory and pilot level studies. However, previously, TGA was implemented to replicate slow pyrolysis process and show the effect of temperature on biomass degradation kinetics. Two different modes of pyrolysis process can be performed (Table 1.8).

Slow pyrolysis is achieved by slow heating rates, while fast pyrolysis process happens at a high heating rate in a fixed bed reactor. Only some investigations are reported on fast pyrolysis of microalgae; however, Py-GC/MS (Pyrolysis-Gas Chromatography/Mass Spectrometry) can be used to analyse volatile products of fast pyrolysis without any secondary reaction products. During slow pyrolysis, a sweeping gas at a constant flow rate was incorporated in the fixed bed reactor to keep an inert atmosphere and remove volatiles from the reactor. The reactor was heated at 10 °C s^{-1} to a required temperature (C. Yang et al., 2019). Briefly, with slow pyrolysis, the highest bio-oil obtained from *Chlorella Vulgaris*, *Isochrysis* sp., *Isochrysis* sp., and *Scenedesmus almeriensis* were 45.62% at 520 °C (Khodaparasti et al., 2023), 49.36% at 450 °C (Wang et al., 2016), 37% at 500 °C (Rahman et al., 2018), and 42.4% at 500 °C (Niu et al., 2024), respectively. Due to inexpensive and easy operation advantages, slow pyrolysis refers the most investigated conversion process. However, this process forms high solid biochar and gas product (C. Yang et al., 2019).

Pyrolytic bio-oil from *Scenedesmus obliquus* was 29.2 wt% at 500 °C with a major proportion of aliphatic and acids (Mustapha and Isa, 2024). Also, in one of the study the temperature difference of 25 °C is not enough to make a significant change in the bio-oil yield. *Isochrysis* sp., when subjected to 450 °C, 49.36% of bio-oil was recovered while almost similar yield was noticed at 475 °C. A major change in the decrease of bio-oil was noticed when the temperature was increased to 500 °C (Wang et al., 2016). The pyrolysis carried out at 500 °C with *Isochrysis* sp. in another study with volatile matter content of 76.90% and high N content (4%) formed bio-oil with a major proportion of aliphatic, alcohols and nitrogen-based compounds. The microalgae and acid pretreated microalgae constitute of ash with 16.80% and 4.50%, respectively, were pyrolyzed. The bio-oil yield with a difference of 42.40% and 43.30% was reported from microalgae and acid-pretreated microalgae, respectively (Niu et al., 2024).

The preferred mode of pyrolysis is fast pyrolysis due to minimization of intermediates secondary cracking, condensation, and polymerization (C. Yang et al., 2019). Another form of fast pyrolysis reactor, i.e. falling solid reactor, showing better liquid yield than slow pyrolysis (Campanella and Harold, 2012). Previous work has been conducted on *Chlorella* (Campanella and Harold, 2012) and *Scenedesmus almeriensis* (CCAP-276/24) (Niu et al., 2024) for fast pyrolysis. Maximum bio-oil from *Chlorella* and *Scenedesmus almeriensis* was found to be 35.50% (500 °C) and 42.20% (500 °C), respectively. It was also observed in one of the studies that steam as a carrier gas in pyrolysis reaction, showed a milder effect on product yield but had a major influence on the bio-oil composition. The steam reduced oxygenated species and

increased hydrocarbons in the bio-oil due to steam reforming and deoxygenation (Campanella and Harold, 2012). Pyrolysis with *Chlorella sorokiniana* str. SLA-04 produced 62% bio-oil at 550 °C compared to 450 °C and 500 °C. Bio-oil constitutes of oxygen-based compounds like acetic acid, ketones, aldehydes, and furans generated from carbohydrate degradation; nitrogen-based compounds, namely pyrroles, indole, pyrazoles, oleoamides, and fatty nitriles from protein fragmentation; fatty ester, aliphatic, and fatty acids from lipid decomposition. The increase in temperature increases the carboxylic acid and aliphatic content and decreases the glyceride formation because of glyceride degradation at higher temperatures (Shirazi et al., 2020). It was also reviewed that bio-oil yield was affected if cells were manipulated during growth stage in terms of the autotrophic or heterotrophic mode of cultivation. The heterotrophic *C. protothecoides* showed 3 times more bio-oil by fast pyrolysis. Also, the HHV and carbon content of bio-oil from heterotrophic *C. protothecoides* were comparatively higher than autotrophic process-grown microalgae bio-oil (Miao and Wu, 2004).

Table 1.8. Previous studies on slow and fast pyrolysis.

Microalgae	Catalyst	Experimental details	References
Chlorella sp.	H-ZSM-5	450 °C, 500 °C, 500 °C in two modes: ex-situ and in-situ catalytic and catalyst-free pyrolysis.	(Shirazi et al., 2020)
Chlorella vulgaris	None	500 °C with a heating rate of 48.0 ± 0.3 °C/min.	(Gong et al., 2014)
D. salina	None	500 °C with a heating rate of 48.0 ± 0.3 °C/min.	(Gong et al., 2014)
Chlorella sp.	None	450 °C and 550 °C	(Borges et al., 2014)
Nannochloropsis sp.	None	450 °C and 550 °C	(Borges et al., 2014)
Chlorella sp.	H-ZSM-5	450 °C and 550 °C with catalyst to biomass ratio of 1:1 and 1:2.	(Borges et al., 2014)
Nannochloropsis sp.	H-ZSM-5	450 °C and 550 °C with catalyst to biomass ratio of 1:1 and 1:2.	(Borges et al., 2014)
Chlorella vulgaris	None	30 to 800 °C at different heating rates of 10, 20, 30, and 40 °C/min.	(Thangalazhy-Gopakumar et al., 2012)

Scenedesmus obliquus	None	1g microalgae sample at heating rate of 10°C/min and performed at 500 °C.	(Mustapha et al., 2021)
Scenedesmus obliquus	M/Fe_3O_4-H-ZSM-5	microalgae:catalyst =1:1g/g at temperature between 400 °C and 700 °C.	(Mustapha et al., 2021)
Isochrysis sp.	Li-LSX-zeolite	500 °C and catalyst to microalgae ratio 1:1	(Wang et al., 2016)

1.9.2. Co-pyrolysis with another waste feedstock

Nowadays, researchers are investigating co-pyrolysis of microalgae with other wastes to enhance bio-oil production and economic viability (Khodaparasti et al., 2023). Also, researchers are focusing on understanding the synergistic interaction between two feedstocks that enhance and weaken the quality and yield of required product (Abnisa and Wan Daud, 2014). A major factor that affects the synergistic effect is the mixing of two feedstocks. The synergistic effect relies on feed type, contact, reaction time, temperature, heating rate, removal or equilibrium of volatiles formed, catalyst, and hydrogen donors (Abnisa and Wan Daud, 2014).

Co-pyrolysis of two feedstocks has favourably enhanced the oil quantity and quality in previous work. An important advantage of using co-pyrolysis process is the reduction of waste in terms of consumption as a feedstock, reducing the environmental problems and enhancing energy security. Additionally, the co-pyrolysis is considered as one of the favourable routes for a thermal conversion technology to generate pyrolytic bio-oil. It was reported that the economic consequences of the synergistic effects found to be more profitable compared to a single feedstock conversion process (Kuppens et al., 2010). According to their findings given by Khodaparasti et al. (2023), higher gas yield was observed due to more deoxygenation reactions (Khodaparasti et al., 2023).

Presence of metals in feed might have enhanced secondary reactions due to catalytic activity, resulting in more gas formation and reduction in solid residue (Wu et al., 2018). Co-pyrolysis of microalgae and sewage sludge synergistically improved the hydrocarbon content in bio-oil, while reduced nitrogenous and oxygenous compounds (Kumar et al., 2024). In another investigation, co-pyrolysis process of bio-oil of microalgae and sewage sludge increased the C4 and C7 but decreased C9 in carbon distribution. While N-heterocyclic compounds was found to be highest in bio-oil (Wang et al., 2016).

Other studies on co-pyrolysis of microalgae with swine manure and textile dyeing sludge were reported to understand their interaction within the process (Peng et al., 2015; Vuppaladadiyam et al., 2019). The synergy between blended feedstock was noticed in the gas fraction, as the total gaseous products were increased with an increase in the ratio of microalgae in the blends with swine manure digestate (Vuppaladadiyam et al., 2019). On the other hand, the yield of gas was not altered by blending microalgae with textile dyeing sludge for co-pyrolysis. However, the synergy was observed between microalgae and textile dyeing sludge in a 80:20 ratio (Peng et al., 2015). A 28.20% bio-oil with high solid yield was recovered from pyrolysis of *S. platensis* at 500 °C with reactor dimensions of 0.20 x 0.20 x 0.20 m. The lower length to diameter allows more trapping and condensation of vapours, giving more bio-oil yield, even though the biomass constituent has more protein compared to lipids. Nearly 50% bio-oil (~50%) was achieved from *Chlorella* sp. in catalyst-free pyrolysis (Shirazi et al., 2020). The co-pyrolysis technique offers several advantages, including reduced reliance on fossil fuels, mitigation of environmental issues, enhancement of energy security, and improvements in waste management. Additionally, co-pyrolysis is considered a relatively economically feasible process.

Achieving high-quality liquid products requires careful selection and optimization of feedstock types and mixing ratios. Not all feedstock is suitable for this process, like plastic material and coal, which require higher temperature for pyrolysis process if other feedstock requires lower temperature compared to another (Abnisa and Wan Daud, 2014).

1.9.3. Catalytic co-pyrolysis

Catalytic pyrolysis is essential because the direct thermal degradation of microalgal biomass often yields bio-oil with high oxygen, nitrogen, and moisture content, resulting in poor stability, low heating value, and corrosiveness. The use of catalysts helps to upgrade the vapors during pyrolysis by promoting cracking reactions, thereby producing higher-quality hydrocarbon-rich bio-oil that is more compatible with conventional fuels (Li et al., 2019). The major challenge arises in designing a catalyst that enhances the bio-oil quality through performing denitrogenation and deoxygenation reactions and increasing the hydrocarbon amount. Also, the catalyst helps in reducing the cracking temperature and reaction time and thus lowering the energy investment during process (Li et al., 2019, 2017; Rahman et al., 2018). It was also observed that catalyst addition increases the gas formation and lowers the bio-oil generation (Tang et al., 2021).

Zeolites, highly porous structure, are widely used in chemical engineering with cracking and dehydration as major reaction routes. H-ZSM-5 is the most widely used zeolite, as its acidic sites facilitate catalytic activity through the carbonium ion mechanism. Also, zeolite helps in enhancing decarboxylation, decarbonylation, and deoxygenation reactions. The catalytic performance of H-ZSM-5 is closely linked to its acidity, which is governed by the Si/Al ratio. A lower Si/Al ratio corresponds to higher acidity, thereby promoting greater carbon incorporation into bio-oil in the form of aromatic hydrocarbons (Pan et al., 2010; Thangalazhy-Gopakumar et al., 2012; Wang and Brown, 2013). The strong acidity of H-ZSM-5 facilitates the breakdown of high-molecular-weight compounds into smaller intermediates, which subsequently diffuse through the zeolite pores and undergo further catalytic reactions, ultimately forming light hydrocarbons. This catalytic property makes zeolites particularly effective in microalgae pyrolysis, as they significantly enhance the production of aromatic hydrocarbons.

Zeolites are also highly advantageous due to their deoxygenation capability, which reduces oxygenated compounds like phenols, aldehydes, and furans, thereby improving bio-oil quality. Zeolites are relatively cheap and can easily be regenerated to extract the deposited coke. Zeolites operate without the need for hydrogen or other reactive agents and are effective under atmospheric pressure. This makes them highly suitable for both in-situ and ex-situ catalytic conversion of pyrolysis vapors into partially or fully deoxygenated products, which can serve as blendstocks for upgrading into transportation fuels (Wang et al., 2015). Among three different zeolites, like HY, H-ZSM-5, and Hβ, different effect was observed in product distribution during catalytic pyrolysis. The stimulative effect followed the order: HY > Hβ > HZSM-5. This catalytic activity trend was consistent with surface area and micropore volume, suggesting that gas formation is closely linked to the pore structure of the zeolite. The abundant pore network likely enhanced secondary reactions of volatiles, thereby facilitating demethylation, decarbonization, and hydrogen condensation, which in turn promoted the release of methane, hydrogen, and carbon dioxide (Tang et al., 2021).

Many investigations have reported that catalytic upgrading of microalgal bio-oil not only increases hydrocarbon yield but also decreases oxygen and nitrogen-containing compounds. For instance, *Chlorella vulgaris* with H-ZSM-5 improved the aromatic hydrocarbon from 0.9% to 25.8% (Thangalazhy-Gopakumar et al., 2012). Du et al. (2013) further demonstrated that increasing the catalyst-to-biomass ratio from 1:1 to 5:1 significantly enhanced aromatic

hydrocarbon production. In a comparative study involving three zeolites (H-Y, H-ZSM-5, and H-B), H-ZSM-5 exhibited the highest aromatic compounds (18.13%). Moreover, metal-modified catalysts showed additional benefits; for example, copper-impregnated H-ZSM-5 enhanced the aromatic to 21.16%. These catalysts were also effective in reducing oxygen- and nitrogen-containing compounds (Du et al., 2013). However, nitriles were more difficult to hydrodenitrogenate even if zeolite catalyst is used, due to the strong stability of C≡N bonds (Tang et al., 2021).

Two main catalytic approaches are employed: **in-situ** and **ex-situ** catalytic pyrolysis. In in-situ catalytic pyrolysis, the catalyst is blended directly with the microalgae, allowing intimate contact between the feedstock and catalyst during thermal decomposition. This often improves reaction efficiency and enhances deoxygenation at the early stage (Li et al., 2019), but it can lead to catalyst deactivation due to coke deposition (Wang et al., 2015) and difficulties in catalyst recovery due to solid microalgae-biochar-catalyst mixing. On the other hand, in an ex-situ catalytic pyrolysis, the pyrolysis vapors are first generated in a reactor and then passed through a separate catalyst bed (Li et al., 2019). This configuration provides better control over vapor–catalyst contact, reduces catalyst contamination from ash and minerals, and facilitates easier catalyst regeneration and separation. However, ex-situ processes may require additional reactor design for a catalytic process and bring higher operational costs if catalyst is added in second reactor (Wang et al., 2015).

Overall, in-situ catalytic pyrolysis is relatively simpler and more cost-effective but suffers from faster catalyst deactivation and biomass-catalyst-biochar separation bottleneck, while ex-situ offers higher product quality and longer catalyst life due to separate catalyst placement onto wool at the expense of added complexity (Li et al., 2019). Previous studies observed that an ex-situ process gives more carbon yield on comparison to in-situ. The ex-situ process with *C. pyrenoidosa* and modified ZSM-5 zeolite resulted in 31.90% of light olefins at 650 °C in presence of steam (Dong et al., 2013).

The incorporation of an integrated vapor phase upgrading catalyst can be inexpensive if it removes the multi-reactor setups and bio-oil handling issues. As bio-oil from microalgae constitutes a complex class of mixtures that distinctly react with catalyst, two catalytic reactors will be essential to acquire required product composition (Li et al., 2019). An increment in gaseous product (major carbon monoxide) was observed together with highest olefins after catalyst addition to microalgae in the 1:1 ratio at 700 °C. The increase in temperature

transformed the aliphatic and nitrogeneous compounds in bio-oil into carbon monoxide, carbon dioxide, methane, hydrogen and small molecular weight olefins. Olefins (C_2H_4, C_2H_3, C_3H_6, C_4H_8) were increased from 29.17 wt% to 38.23 wt% when the temperature was raised from 400 °C to 700 °C. These outcomes suggested that Li-LSX-zeolite can be used as a catalyst for better microalgae bio-oil quality with enhanced aliphatics and aromatics which can be blend in gasoline and diesel. However, this catalyst positively increases gas formation at the cost of the bio-oil yield (Rahman et al., 2018).

In another study, the Co/Fe_3O_4-H-ZSM-5 resulted in the lowest biochar formation, indicating the highest conversion efficiency compared to other supported metal catalysts. This represented approximately a 30% reduction in biochar formation, compared to non-catalytic reactions. In addition, Co/Fe_3O_4-HZSM-5 achieved the highest bio-oil yield, whereas W/Fe_3O_4-H-ZSM-5 produced the lowest. With respect to gaseous products, the maximum gas yield was obtained using Zr/Fe_3O_4-H-ZSM-5, while Mo/Fe_3O_4-H-ZSM-5 produced the minimum. Based on bio-oil yield, the catalysts can be ranked as Co/Fe_3O_4-H-ZSM-5 > Zr/Fe_3O_4-H-ZSM-5 > Mo/Fe_3O_4-H-ZSM-5 > W/Fe_3O_4-H-ZSM-5. Furthermore, the bio-oils derived from nutrient-stressed *S. obliquus* exhibited substantially lower oxygen contents (11.84 wt% for non-catalytic and 6.57–10.37 wt% for catalytic pyrolysis) (Mustapha et al., 2021). Table 1.9 shows previous literature on bio-oil yield from non-catalytic and catalytic co-pyrolysis.

Table 1.9. Literature showing pyrolysis and catalytic pyrolysis of feedstocks.

Feedstock	Feedstock ratio	Conditions	Bio-oil Yield (%)	C (%)	H (%)	N (%)	O (%)	HHV (MJ/Kg)	References
Sewage Sludge and Microalgae *Chlorella Vulgaris*	Microalgae /sludge= 0.82)	520 °C for 30 min	32.93	52.35	7.81	7.14	32.16	23.14	(Khodaparasti et al., 2023)
Chlorella vulgaris residue (CVR) and Sewage	80:20-microalgae residue:SS	539.33 °C for 23 min	47	-	-	-	-	-	(Kumar et al., 2024)

Sludge (SS)									
Isochrysis sp. and Sewage Sludge	Sludge: *Isochrysis* - 1:2	500 °C	34.90	-	-	-	-	36.908	(Wang et al., 2016)
Chlorella sp.	-	550 °C with HZSM-5	41.9	-	-	-	-	-	(Shirazi et al., 2020)
Chlorella sp.	-	550 °C	62	-	-	-	-	-	(Shirazi et al., 2020)
Nannochloropsis sp. residue	-	HZSM-5 catalyst- to-material of 1/1 at 400 °C	19.7	65.21	9.83	5.43	19.53	32.2	(Pan et al., 2010)
Nannochloropsis sp. residue	-	400 °C	47.6	56.13	7.13	5.34	30.09	24.4	(Pan et al., 2010)
Chlorella vulgaris	-	500 °C for 30 min	52.7	51.4	10.4	12.4	24.8	18.6	(Thangalazhy-Gopakumar et al., 2012)
Microalgae and Sewage Sludge	Biomass blend ratio of 1:1	500 °C, biomass to HZSM-5 catalyst ratio of 2:1	24	74.81	9.77	7.11	6.57	36.46	(Mustapha and Isa, 2024)
Microalgae and Sewage Sludge	Biomass blend ratio of 1:1	500 °C	22	71.53	9.42	7.48	11.57	34.82	(Mustapha and Isa, 2024)

1.10. Products of HTL and pyrolysis

Bio-oil is the main liquid product recovered from HTL and pyrolysis process, representing 30-50% of feedstock, depending on the operating parameters (Figure 1.8). The HTL bio-oil is a

complex viscous, and energy-dense liquid with a higher heating value (HHV) generally ranging from 30 MJ/kg to 36 MJ/kg, higher than that of raw biomass. The HTL bio-oil constitutes of major esters, hydrocarbons, nitrogenous compounds (amines, amides), and oxygenated species. Bio-oil can be separated into light and heavy fractions, and is rich in Carbon, hydrogen, nitrogen and oxygen (Krishnan et al., 2022).

The major advantage of HTL is the applicability of process to consider wet biomass and less heat energy consumption compared to other thermochemical conversion process (Ayub et al., 2022). The bio-oil formed from pyrolysis consists of nitrogenated and oxygenated compounds and hydrocarbons. The major nitrogen-based compounds are amides, amines, pyrroles, indoles, pyridines, pyrazines, imidazoles, and their derivatives. The oxygen-based compounds are carboxylic acids, ketones, aldehydes, cyclic aromatics, and phenols. Also, esters and ethers are present in pyrolytic bio-oil (Gong et al., 2014; Razzak et al., 2024; C. Yang et al., 2019). The pyrolytic bio-oil has a major proportion of carbon in the range between 46–77 wt%. The H-content can vary from 7 wt% to 12 wt%. Significant amount of N-content (found up to 12.4 wt%) creates a substantial difference in bio-oil quality (Table 1.10). The molar atomic ratios of H/C, O/C, and N/C give an accurate assessment of microalgal bio-oil quality.

The higher HHV of bio-oil ranges from 26.8 to 42 MJ kg^{-1}, which exceeds that of cellulosic biomass bio-oil (15–21 MJ/kg). Its density is approximately 0.98–1.2 kg L^{-1}, while the viscosity varies depending on the water content and chemical composition (C. Yang et al., 2019). Oxygen-based compounds result in acidity, corrosion, and high viscosity of bio-oil (Lee et al., 2020; Li et al., 2019). The increase in nitrogen content substantially affects bio-oil quality, resulting in elevated viscosity, acidity, and a greater boiling point range, which brings inhibitory effects during the refining process (Gu et al., 2020b). Compared to fossil fuels, bio-oil from both processes has a high amount of oxygen, which results in lower heating values, increased acidity, and instability over time due to polymerization.

Another important product produced from pyrolysis process is solid biochar. The biochar generated from pyrolysis process is receiving attention for several applications due to its inexpensive and abundant advantages (C. Yang et al., 2019). Slow pyrolysis is the preferred route for biochar generation because long reaction time helps in more condensation and polymerization of unstable intermediates and enhances solid product yield (Ronsse et al., 2013; Song and Guo, 2012). The process can generate more biochar between 15-43 wt% from microalgal biomass. The carbon content of biochar is around is comparable to lignocellulosic

biomass. The nitrogen in microalgal biochar is higher than that present in lignocellulosic material-based biochar. Also, the metals and nonmetals are more in microalgal-based biochar than in lignocellulosic material biochar (Borges et al., 2014). Additionally, the surface area of microalgal biochar is comparatively less than lignocellulosic material biochar (Gong et al., 2014; C. Yang et al., 2019).

Biochar has a porous structure with a high amount of carbon and has a large surface area. However, these properties vary according to operating conditions and feedstocks. Biochar consists of carboxyl, phenol, carbonyl, and lactone groups, which play a role in chemical properties and biochar reactivity. Because of its high carbon content, biochar can act as an excellent candidate for carbon sequestration. The solid residue or biochar can be also used in other applications such as adsorption (Ponnusamy et al., 2020), wastewater treatment (Law et al., 2022; Ponnusamy et al., 2020), catalyst for energy generation (Wang et al., 2021), and in anaerobic digestion as a carbon supplement and buffer (Chen et al., 2018; Ponnusamy et al., 2020).

Another waste by-product from HTL process is the aqueous phase (AP). The chemical oxygen demand of the aqueous phase reveals a huge number of organic compounds, which are a source of valuable platform chemicals. Also, this by-product consists of N, P, and K, which can serve as important nutrients for algal growth (Swetha et al., 2021). It was observed that HTL-AP has potential to support algal productivity (Ramírez-Romero et al., 2023; Swetha et al., 2021). It was noted that HTL-AP was blended with fresh water for algae cultivation. Also, this HTL-AP can be utilised for cultivating bacteria for value-added product accumulation (Nelson et al., 2013).

Gasification is another route for converting AP wastewater to syngas (Swetha et al., 2021). During high-temperature reaction in pyrolysis of microalgae, gases are also formed. The gaseous products/syngas formed from HTL and pyrolysis can be converted to hydrocarbons via Fisher-Tropsch synthesis using a CO and H_2 gas mixture (Demirbas, 2009). Water-gas, water-gas-shift, and the Boudouard reactions play an important role in gas formation. The major gases formed are hydrogen, methane, carbon dioxide, carbon monoxide, acetylene, ethylene, ethane, propylene, and butane (Dong et al., 2013). Microalgal species *Lyngbya* sp. produced 46.5 wt% of gases with a major proportion of H_2 and CO_2 after pyrolysis at 600 °C. However, gases produced from *Cladophora* sp. formed highest amount of carbon dioxide, followed by H_2 and CO at 600 °C (Maddi et al., 2011). Microalgae *C. vulgaris* and *D. salina,*

when pyrolyzed at 700 °C, formed C_2H_4 and C_2H_6 in major proportions along with hydrogen, methane, carbon dioxide, and carbon monoxide (Gong et al., 2014).

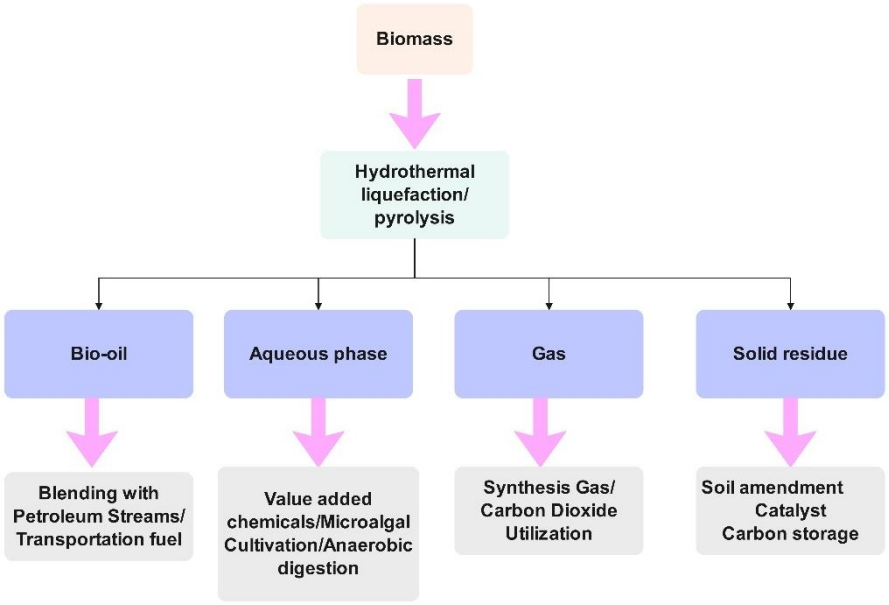

Figure 1.8. Products obtained from HTL/pyrolysis process and their applications.

Table 1.10. Elemental analysis of bio-oil recovered from non-catalytic and catalytic pyrolysis.

	Microalgae	Catalyst	C (wt%)	H (wt%)	O (wt%)	N (wt%)	HHV (MJ/kg)	Reference
Bio-oil	*C.protothecoides* (autotrophic cultivation)	None	62.07	8.76	19.43	9.74	30	(Miao and Wu, 2004)
	C.protothecoides (heterotrophic cultivation)	None	76.22	11.61	11.24	0.93	41	(Miao and Wu, 2004)
	Spirulina	None	74.66	10.57	6.81	7.13	33.62	(Jena and Das, 2011)

Spirulina sp.	None	46.05	7.97	36.28	9.7	21.68	(Chaiwong et al., 2013)
Chlorella	None	54.52	9.06	25.69	11.51	25.5	(Campanella and Harold, 2012)
Chlorella	H-ZSM5	63.64	8.49	19.41	9.18	29.1	(Campanella and Harold, 2012)
Chlorella	Fe-ZSM-5	59.67	8.44	23.58	10.96	26.8	(Campanella and Harold, 2012)
Chlorella	Cu-ZSM5	60.54	8.60	23.07	10.06	27.5	(Campanella and Harold, 2012)
Chlorella	Ni-ZSM-5	58.54	8.99	21.39	10.57	28.22	(Campanella and Harold, 2012)
C. vulgaris	ZSM-5 (SiO_2/Al_2O_3 = 50)	51.4	10.4	24.8	12.4	18.6	(Thangalazhy-Gopakumar et al., 2012)
C. vulgaris	None	55.1	7.5	27.7	9.3	-	(Gong et al., 2014)
D. salina	None	56.3	7.8	24.8	10.8	-	(Gong et al., 2014)
Scenedesmus obliquus	None	70.77	11.50	11.84	5.46	36.99	(Mustapha et al., 2021)

	Scenedesmus obliquus	W/Fe_3O_4-HZSM-5	75.98	10.89	6.57	5.89	38.65	(Mustapha et al., 2021)
	Scenedesmus obliquus	Zr/Fe_3O_4-HZSM-5	71.99	12.03	10.37	5.19	38.20	(Mustapha et al., 2021)
	Scenedesmus obliquus	Co/Fe_3O_4-HZSM-5	73.00	12.42	9.38	5.25	39.12	(Mustapha et al., 2021)
	Scenedesmus obliquus	Mo/Fe_3O_4-HZSM-5	71.47	12.61	10.33	5.25	38.69	(Mustapha et al., 2021)
Commercial crude	-	-	85–90	10-14	1-1.5	<0.1–2.0	42	(Chaudhuri, 2016)

1.11. Limitations and advantages of HTL and pyrolysis process

The important difference between liquefaction and pyrolysis process is their operating conditions: liquefaction happens at 5-20 MPa (725-2900 psi) pressure and low temperature (250-350 °C), whereas pyrolysis occurs at near atmospheric pressure (0.1-0.5 MPa, i.e.14.5-72.5 psi) and high temperature of 400-600 °C. The pyrolysis process requires dry feedstock while HTL can process high moisture biomass. Dewatering process for pyrolysis consumes additional energy. An important point to note is that HTL results in higher bio-oil whereas pyrolysis, in most cases (except fast pyrolysis), gives higher amount of solid char. On comparison of slow and fast pyrolysis, the former produces higher gas yields (30–45%) than the latter (13–20%) (Hu et al., 2019) (Figure 1.9).

The comparison (Figure 1.10) highlights the different products derived from pyrolysis and hydrothermal liquefaction (HTL) processes, emphasizing their respective energy requirements. An energy balance analysis between the two techniques revealed that processing 1 ton of algal biomass with 20% total solids (TS) requires approximately 1.6 times more energy for pyrolysis than for HTL. This elevated energy demand in pyrolysis primarily occurs from the drying step, as it is inherently a dry thermochemical process, accounting for nearly 50% of the total energy input (Yang et al., 2017).

The Energy Recovery Ratio (ERR), defined as the proportion of useful energy recovered relative to the total energy content of the feedstock, was found to be 78.7% for fast pyrolysis, while HTL exhibited the highest efficiency with an ERR of 89.8% (Table 1.11). To mitigate the excessive energy consumption associated with pyrolysis, the integration of a solar-assisted drying system has been suggested, which could significantly lower the overall energy demand of the process (Xia et al., 2022).

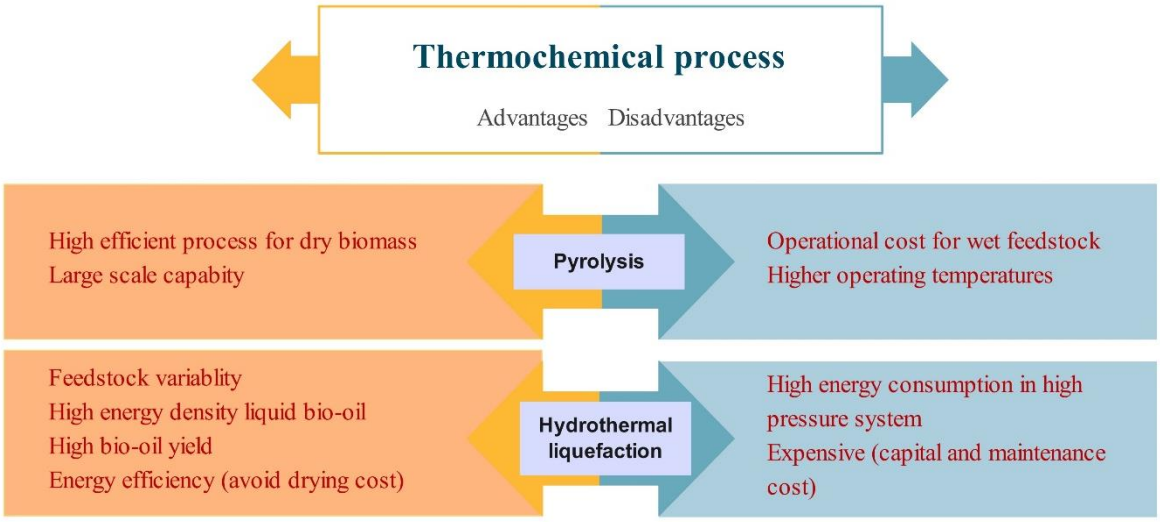

Figure 1.9. Benefits and drawbacks of HTL and pyrolysis process.

In contrast to pyrolysis, which has been established for several decades, hydrothermal liquefaction (HTL) is still primarily limited to the pilot-scale stage, with significant progress yet to be made toward full industrial implementation. The major barriers hindering large-scale commercialization include the need for specialized reactor and separator designs, as well as the substantial capital investment required for high-pressure systems. Additionally, achieving continuous HTL operation poses a considerable engineering challenge, as feeding biomass into a high-pressure reactor remains technically complex and energy-intensive, representing a key limitation in scaling up to industrial capacities. Despite these challenges, HTL holds tremendous promise as a sustainable technology for converting wet biomass into high-value chemicals and biofuels. With advancements in process design, material engineering, and cost optimization, HTL could emerge as a viable and efficient pathway for large-scale bioenergy production in the near future.

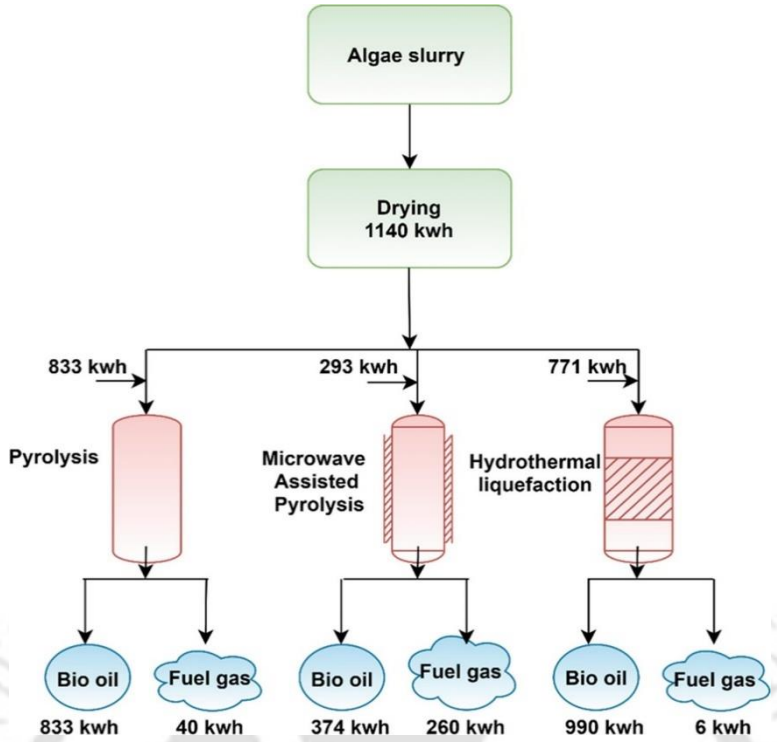

Figure 1.10. Comparison of various process in terms of energy content. (procured via copyright from (Xia et al., 2022)).

Table 1.11. Comparison of Pyrolysis and HTL (procured via copyright from (Xia et al., 2022)).

Factors	Pyrolysis	HTL
Type of biomass	Dry biomass	Wet biomass
Temperature	300 to 700 °C	200 to 400 °C
Pressure	Atmospheric pressure	5 to 25 MPa
Drying needed	Yes	No
Main products	Bio-oil, fuel gases	Bio-crude or bio-oil
Co-products	Biochar	Mixture of gas
Heating value of bio-oil	30–42 MJ/kg	30–50 MJ/kg

Energy input	504 MJ	2776 MJ
Energy recovery ratio (ERR)	78.70%	89.80%
Energy cost *	High energy cost (80% of the energy used for drying, gas compression and size reduction)	Less energy cost (not needed drying process but includes catalyst)
Capital cost (M $)	358	244.3
Fixed operating cost (M$/a)	21.9	22.1

1.12. Thesis motivation and objectives

The rapid development of the dairy sector has produced substantial quantities of nutrients-rich wastewater, that if untreated, may cause significant environmental issues, including eutrophication, odor nuisances, and degradation of water quality. Traditional wastewater treatment techniques, while efficient in eliminating pollutants, can incur substantial operational expenses and generate considerable sludge that necessitate additional management. In this context, the advancement of a sustainable, cost-effective, and resource-recovering treatment system is essential. Microalgae-based treatment systems have emerged as a viable option due to their dual benefits: efficient nutrient removal and concurrent production of biomass abundant in lipids, proteins, and carbohydrates appropriate for biofuel generation.

Monoraphidium sp. KMC4, a freshwater microalga, demonstrates excellent adaptability to nutrient-rich wastewaters such as dairy effluent. Its rapid growth rate, high nutrient uptake efficiency, and balanced biochemical composition make it an attractive candidate for both wastewater remediation and subsequent bioenergy conversion. Employing *Monoraphidium* sp. KMC4 for dairy wastewater treatment thus not only provides an eco-friendly solution for waste management but also enhances the circular bioeconomy by converting biomass into valuable bioenergy precursors.

A significant problem in the algal biorefinery method lies in the effective conversion of high-moisture, protein-rich feedstock into energy-dense fuels. Hydrothermal liquefaction (HTL),

working under subcritical water conditions, has proven to be an effective thermochemical method for the direct processing of wet algal biomass, eliminating the necessity for energy-intensive drying. The generation of bio-oil using both direct and two-stage hydrothermal liquefaction presents an opportunity to enhance conversion processes, augment energy recovery, and tailor product composition to achieve preferred fuel characteristics. Examining the conversion behavior of *Monoraphidium* sp. KMC4 under these conditions can yield significant insights into reaction mechanisms and process optimization strategies. Moreover, the integration of microalgae cultivated in simulated synthetic dairy wastewater with dairy sludge by co-liquefaction strategy is an interesting and sustainable approach for waste valorization approach. This synergistic processing can augment carbon and nitrogen utilization efficiency, enhance bio-oil yield and quality, and reduce the environmental impact of dairy waste. The examination of synergistic effects in co-liquefaction is crucial in developing adaptable, economical bioenergy systems that adhere to the circular economy and sustainable principles.

Catalytic and non-catalytic co-pyrolysis provides a complementary approach to hydrothermal liquefaction for the advancement of sustainable biofuel production. The use of catalysts such as HZSM-5 facilitates selective deoxygenation, dehydration, and the reduction of nitrogenous chemicals, resulting in better fuel fractions. Examining these catalytic pathways in an ex-situ fed-batch configuration enhances comprehension of product distribution and catalyst–biomass interactions which is important for the design of efficient thermochemical processes.

In summary, the motivation behind this research is rooted in addressing three interlinked global challenges: wastewater pollution, waste-to-energy conversion, and sustainable biofuel production. By integrating microalgal wastewater treatment with thermochemical valorization processes such as HTL, co-HTL and catalytic co-pyrolysis, this work aims to develop an environmental friendly system that not only mitigates waste but also contributes to renewable energy generation. The findings of this research will provide significant insights into the scalability, efficiency, and environmental benefits of an integrated microalgae-based biorefinery approach, paving the way toward sustainable resource recovery and green energy technologies.

Research Gaps

Based on the literature review, the following research gaps has been identified:

a) There is a significant gap in research regarding the two-stage HTL, specifically how mild-temperature pretreatment (Stage I) for protein/carbohydrate extraction fundamentally alters the chemical pathway and nitrogen-partitioning in the subsequent high-temperature liquefaction (Stage II) to produce a better-quality bio-oil.

b) There is a lack of comparative data on how the same co-feedstock (algae and dairy sludge) behaves under different thermochemical environments, specifically regarding how process-specific parameters affect the final fuel properties with influence on comparative bio-oil yield and heteroatom distribution.

c) There are less literatures reported on how the interaction between these specific biomass components promotes specific pathways, or how these interactions differ when subjected to high-pressure aqueous environments (HTL) versus atmospheric thermal degradation (Pyrolysis).

1.13. Thesis Objectives

Based on the gaps in the literature for addressing the interlinked global issues, the objectives of this thesis are as follows:

1. Dairy wastewater treatment using *Monoraphidium* sp. KMC4 and its potential as hydrothermal liquefaction and pyrolysis feedstock.

2. Bio-oil production via two-stage and direct hydrothermal liquefaction process from high-protein *Monoraphidium* sp. KMC4.

3. Bio-oil as a promising product from co-liquefaction of dairy wastewater grown microalgae with dairy sludge: Study on synergistic effect and sustainable energy generation.

4. Non-catalytic and catalytic co-pyrolysis of microalgae and dairy sludge: An ex-situ fed batch process using HZSM-5 towards sustainable biofuel production.

1.14. Thesis Outline

Chapter 1: *Introduction, Literature Review and Objectives*

The chapter presents a concise overview of upstream and downstream processing of microalgae, with particular emphasis on hydrothermal liquefaction (HTL) and pyrolysis as effective routes for converting microalgae, along with other industrial waste into biofuels. Recent advancements in the use of wastewater-grown microalgae and sludge as sustainable

feedstocks are discussed in detail, highlighting their dual role in environmental remediation and bioenergy generation. Special attention is given to the cultivation of *Monoraphidium* sp. KMC4 in dairy wastewater, demonstrating its ability to remove nutrients while producing biomass, which can be suitable feedstock for subsequent thermochemical processing. The fundamentals of both direct and two-stage hydrothermal liquefaction from high-protein microalgal biomass are detailed, focusing on reaction mechanisms, product distribution, and bio-oil characteristics.

Furthermore, the concept of co-liquefaction of microalgae with dairy sludge is overviewed to exploit synergistic interactions between these feedstocks, thereby enhancing bio-oil yield, improving energy recovery, and supporting sustainable waste management. In addition, the chapter reviews non-catalytic and catalytic co-pyrolysis approaches, particularly the use of H-ZSM-5 in an ex-situ fed-batch system to upgrade vapors towards higher-quality fuel products. The main aim of all the processes was to understand the effect of different systems on the differentiation in yield and quality of bio-oil. The comprehensive literature review identifies existing challenges, research gaps, and future research opportunities, which directly shape the objectives of this thesis. Finally, the chapter outlines the overall structure of the dissertation.

Chapter 2: *Experimental Methodology and Characterization Techniques.*

This chapter outlines the experimental methodologies employed in both the upstream wastewater treatment process and the downstream thermochemical conversion of microalgal biomass, including HTL, SHTL, Co-HTL, pyrolysis and co-pyrolysis. It also presents a summary of the preliminary characterization of dairy sludge used in co-hydrothermal liquefaction and co-pyrolysis experiments. The fundamental characterization techniques applied to all feedstocks are briefly described, along with the catalyst activation procedures and the methods used for catalyst characterization. In addition, the essential analytical techniques required for the characterization of the liquid products are summarized in this section.

Chapter 3: *Dairy wastewater treatment using Monoraphidium sp. KMC4 and its potential as hydrothermal liquefaction and pyrolysis feedstock.*

Monoraphidium sp. KMC4 demonstrated strong adaptability to simulated synthetic dairy wastewater, generating substantial biomass while simultaneously achieving efficient reductions in chemical oxygen demand. Among the tested conditions, the 50% dilution of synthetic dairy wastewater supported the highest biomass productivity (122 mg L^{-1} day^{-1}) with

biomass concentration of 1.47 g L^{-1} and exhibited superior nutrient removal efficiency (~90%). Biomass cultivated under mixotrophic conditions possessed a biochemical composition with high protein content due to high nitrogen in the wastewater. The proximate, elemental, and thermogravimetric analyses further confirmed that the harvested biomass possesses desirable characteristics for thermochemical conversion. These findings collectively highlighted the dual functionality of *Monoraphidium* sp. KMC4 for dairy wastewater remediation and as a feedstock for bio-oil production, reinforcing its potential integration into a microalgae-based biorefinery framework.

Chapter 4: *Bio-oil production via two-stage and direct hydrothermal liquefaction process from high-protein Monoraphidium sp. KMC4.*

A two-stage hydrothermal liquefaction (HTL) strategy was employed to improve the quality of the algal bio-oil. In the first stage, low-temperature solvolysis and hydrolysis promoted the extraction of protein- and carbohydrate-derived fractions into the aqueous phase, while enriching the remaining solid residue in energy-dense components. Pretreatments conducted at 220 °C and 240 °C for 30 min, resulted in a noticeable reduction in nitrogen and oxygen contents in the solid residue, with only negligible differences observed in the H/C and N/C ratios between the two temperatures. The ammonium and total nitrogen of first stage aqueous phase confirmed the extraction of nitrogen-based compounds from microalgae. Given the lower energy requirement, 220 °C was identified as the more suitable pretreatment condition.

The pretreated microalgae at 220 °C produced the highest bio-oil yield during subsequent liquefaction at 300 °C. The bio-oil from direct HTL had a significant number of nitrogen-based compounds (13.36%), i.e., amides, amines, and heterocyclic forms, while it was reduced to 1.98% in the two-stage hydrothermal liquefaction process, confirmed by GC-MS. Also, a reduction of 38% nitrogen in bio-oil was observed from direct HTL compared to two-stage HTL.

The total bio-oil yield from two-stage HTL of KMC4 microalgae was 36.67 wt% (combining first- and second-stage bio-oil) under stage I conditions of 220 °C & 30 min, and stage II conditions of 300 °C & 30 min. A plausible reaction pathway suggested that the initial pretreatment step suppresses Maillard reactions and limits amine formation, thereby reducing nitrogen incorporation into the bio-oil. Overall, the two-stage HTL approach effectively enhanced bio-oil quality without compromising yield.

Chapter 5: *Bio-oil as a promising product from co-liquefaction of dairy wastewater grown microalgae with dairy sludge: Study on synergistic effect and sustainable energy generation.*

Microalgae, as a renewable feedstock, have attracted considerable interest for bio-oil production through hydrothermal liquefaction (HTL). However, ensuring a continuous and year-round supply of microalgal biomass remains a significant challenge. To address this issue and support a waste-to-energy strategy, this study investigated the feasibility of co-HTL using microalgae and sludge derived from dairy wastewater treatment as combined feedstocks for bio-oil generation. It was found that the combination of microalgae and dairy sludge in a ratio of 75:25 produced bio-oil with 32.94 wt% yield compared to other combinations with a calorific value of 38.24 MJ kg^{-1}.

Individually, microalgae produced a higher yield (33.50 wt%) than dairy sludge (18.16 wt%) at 350 °C and a residence time of 30 minutes. The co-HTL bio-oil exhibited the highest H/C ratio (1.5 mol/mol) and the lowest N/C ratio (0.03 mol/mol), indicating increased hydrogen content and reduced nitrogen content, which contributed to an elevated heating value. Additionally, the co-HTL bio-oil demonstrated improved quality, as evidenced by a higher H/C ratio and a lower O/C ratio (0.11 mol/mol), confirmed effective deoxygenation and dehydration reactions. Compared to individual feedstocks, bio-oil obtained from the co-liquefaction process showed reduced concentrations of nitrogen-heterocyclic compounds and aromatics, along with an increased ester content, resulted in a better calorific value. Furthermore, the thermal degradation profile indicated a better boiling-point distribution for the co-HTL bio-oil, particularly for the 25:75 dairy sludge-to-microalgae blend, with higher fractions of heavy naphtha and kerosene-range compounds. This bio-oil can be further refined through an upgradation system for its utilization as a substitute for blending purposes. Overall, the bio-oil characterization confirmed that the co-HTL of dairy sludge and microalgae is a promising and sustainable route for renewable bioenergy production, reflecting a clear synergistic effect in both yield and quality.

Chapter 6: *Non-catalytic and catalytic co-pyrolysis of microalgae and dairy sludge: An ex-situ fed batch process using HZSM-5 towards sustainable biofuel production.*

The bio-oil produced through co-pyrolysis demonstrates significant potential as an alternative to conventional fossil fuels. In this study, a fed-batch co-pyrolysis process using microalgae and dairy sludge was carried out for liquid fuel production. The maximum yield of co-pyrolysis oil was obtained from algae and dairy sludge at 550 °C and 60 min. Results indicated a

synergistic interaction between the two feedstocks, enhanced both the yield and quality of the bio-oil. The effect of the H-ZSM-5 catalyst on hydrocarbon formation and the increase in nitrile compounds through catalytic cracking was also examined. The presence of the catalyst improved the bio-oil yield while reduced the concentration of nitrogen-containing compounds and aromatics, which were originally dominated in microalgae and dairy sludge-derived oils. A decrease in the O/C and N/C ratios, along with a slight increase in the H/C ratio, confirmed the effective deoxygenation, denitrogenation, and dehydration, leading to a higher heating value.

The reaction pathways suggested that H-ZSM-5 increased the nitriles from the dehydration of amides and followed the denitrogenation reaction to reduce the formation of lower cyclic compounds. The Boiling Point Distribution profile of the catalytic bio-oil showed increased fractions of heavy naphtha and gas oil, which can be due to a higher presence of hydrocarbons, fatty acids, and esters. Characterization of the fresh catalyst revealed a well-defined crystalline structure, while analysis of the spent catalyst showed coke deposition and partial structural changes as confirmed by XPS, TGA, elemental mapping, and BET analyses. Overall, the result suggested that the addition of a catalyst helped in enhancing the quality of bio-oil, which can be further upgraded for blending purposes.

Chapter 7: *Conclusions, Social Impact and Future Prospect*

This section presents the key conclusions drawn from the research undertaken in this thesis and offers recommendations for future investigations that can further expand upon the findings and framework established in this study. In this research work, research gaps present in the co-processing of waste dairy sludge with microalgae towards bio-oil production together with the aim of reducing nitrogen content in bio-oil via a two-stage HTL process. Identifying important feedstocks for producing value-added products is crucial in thermochemical conversion processes.

This study investigated the potential of *Monoraphidium* sp. KMC4 towards bioremediation potential for simulated synthetic dairy wastewater. The microalgae was processed for the thermochemical conversion processes. In two-stage HTL, microalgae was pretreated at a lower temperature for bio-oil production with lower heteroatom content, increasing the H/C and decreasing the N/C of solid I from the first stage. The nitrogen, organic carbon, and inorganic carbon were recovered in the aqueous phase of stage I. The effect of the first stage on the bio-oil composition in the second stage is of much interest to thermochemical conversion processes

due to the achieved better quality. Together with microalgae, another waste derived from the dairy industry, i.e., dairy sludge, was co-processed for bio-oil production from two widely used technologies, hydrothermal liquefaction and pyrolysis for liquid fuel production.

From co-processing, the purpose is to understand the synergistic interaction between two feedstocks along with their change in compound composition. Boiling point distribution profile revealed better boiling point compounds in bio-oil from co-HTL of dairy sludge and microalgae (25:75) with enhanced heavy naphtha and kerosene fractions. In catalytic co-pyrolysis of dairy sludge and microalgae, the aim is to reduce the nitrogen of bio-oil by incorporating H-ZSM-5.

Future Perspective

The identification and cultivation of diverse microalgal strains with optimized biochemical compositions, rapid growth rates, and strong environmental resilience are critical for effective feedstock development. This requires systematic investigation of genetic modifications and advanced cultivation strategies to improve both biomass yield and quality. In parallel, the design and optimization of continuous-flow reactors, particularly for two-stage hydrothermal liquefaction (HTL) systems are essential for increasing process. Ensuring consistent performance across different algal species and operating conditions is equally important, as is the development of continuous HTL reactor systems capable of flexible recovery of high-value co-products. Furthermore, the valorization of the aqueous phase through its reuse in microalgae cultivation represents a promising pathway for maximizing resource efficiency and minimizing waste. Future efforts should concentrate on addressing key challenges associated with reactor design, heat and mass transfer limitations, and catalytic upgrading processes. Finally, conducting a comprehensive comparative life cycle assessment (LCA) and carbon footprint analysis of the proposed thermochemical conversion pathways will be essential to ensure the long-term environmental sustainability and viability of the integrated system.

Chapter 2

Experimental Methodology and Characterization Techniques

Chapter 2. Experimental Methodology and Characterization Techniques

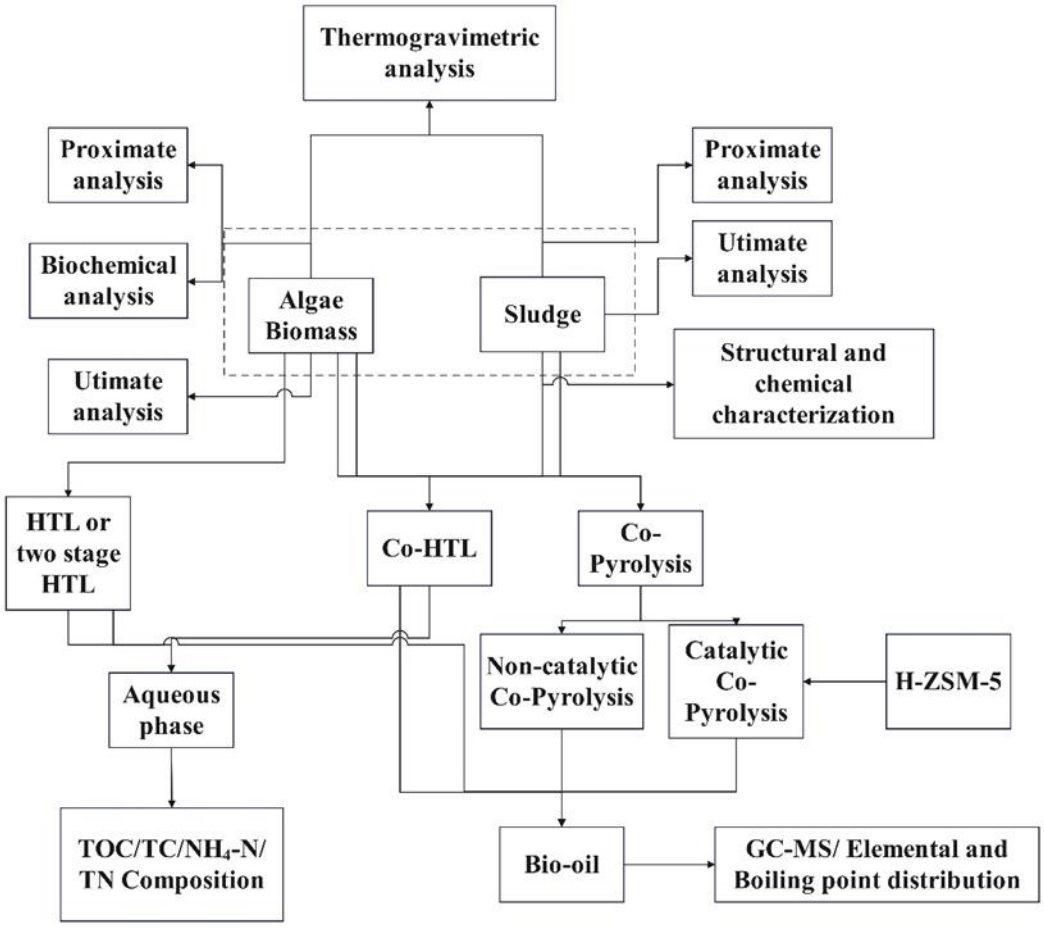

Figure 2.1. Overall Methodology of thesis work.

2.1 Background

This chapter describes the experimental methodologies adopted for both upstream and downstream processing of microalgae biomass production and conversion (Figure 2.1). This chapter also describes the initial characterization of dairy sludge used in co-hydrothermal liquefaction and co-pyrolysis experiments. The fundamental characterization method used for feedstocks are also briefly summarized in this chapter. Similarly, the catalyst activation procedure and characterization techniques are listed and described in this chapter. The basic characteristics techniques required for liquid and solid product analysis are also summarized in this section.

2.1.1 Experiment for Microalgal based wastewater treatment

2.1.1.1 Microalgal strain and growth medium

The *Monoraphidium* sp. KMC4 was considered for this study due to its superior biomass and lipid accumulation with enhanced bioremediation capability (Mishra and Mohanty, 2019). The simulated synthetic dairy wastewater (SSDW) was prepared according to the composition suggested by Kiran and Venkata Mohan, 2022 (Ravi Kiran and Venkata Mohan, 2022): glucose (2.4 g/L); milk powder (1.44 g/L); ammonium chloride (0.54 g/L); manganese sulfate monohydrate (0.024 g/L); sodium phosphate dibasic dihydrate (0.90 g/L); ferric sulfate (0.024 g/L); calcium chloride monohydrate (0.036 g/L); sodium bicarbonate (1.56 g/L) and magnesium sulfate heptahydrate (0.60 g/L) and urea (0.27 g/L).

2.1.2. Experimental design

The chemical oxygen demand was taken as a parameter for diluting the simulated synthetic dairy wastewater for the growth study. The SSDW initial COD was determined and found to be 3840 mg L^{-1}. The *Monoraphidium* sp. KMC4 was cultivated in varying strengths of SSDW (100%: 3840 mg/L, 75%: 2880 mg/L, 50%: 1920 mg/L, 25%: 960 mg/L, 12.5%: 480 mg/L) in a 500 mL Erlenmeyer flask with 250 mL of SSDW. The initial concentration of algal biomass was 0.134 g L^{-1} as inoculum for the growth study at 25±2 °C in shaking conditions. The initial pH of the SSDW was 7 and was not maintained during the treatment study. The 16:08 h of light and dark period was provided using fluorescent tubes of 100 µmol $m^{-2}s^{-1}$ light (Agarwalla et al., 2022; Mishra and Mohanty, 2019).

2.1.3 Analytical methods

2.1.3.1 Biomass growth

The algal cell density was evaluated by measuring optical density at 680 nm using a UV–Vis Spectrophotometer (Thermo Fisher Scientific, USA) every day till the culture attained the stationary phase. After reaching the stationary phase, cell culture was centrifuged at 5000 rpm for 10 min and was further dried at 80 °C until invariant weight reached for dry cell weight estimation. The following equations were used for calculating overall biomass productivity (P(b), mg L^{-1} day^{-1}) and specific growth rate (µ, day^{-1}) [Eqs. (2.1) and (2.2)] (Mishra and Mohanty, 2019).

$$P(b) = \frac{\Delta X}{\Delta t} \quad [2.1]$$

$$\mu = \ln\left(\frac{Xf}{Xi}\right)/\Delta t \quad [2.2]$$

where "*ΔX*" is the change in cell concentration (g/L) in time of "*Δt*" (days). X_f and X_i are cell concentrations (g/L) at the end and the start of the experiment and *t* is time in days.

The consumption of ammonium, nitrate, phosphate and glucose in the culture was analyzed every alternate day till the end of the experiment by standard protocols as reported earlier (APHA, 1998; Dubois et al., 1956; Gebremedhin et al., 2018; Swain et al., 2020). The initial and change in the chemical oxygen demand of simulated synthetic dairy wastewater were calculated using standard methods given by APHA (APHA, 1998). The overall chemical oxygen demand removal efficiency (%) was determined using the following equation

$$\text{Removal efficiency (\%)} = [(S_i - S_f)/(S_i)] * 100 \quad [2.3]$$

S_i = Initial chemical oxygen demand (mg/L), S_f = Final chemical oxygen demand (mg/L)

The overall nutrient removal efficiency in the simulated synthetic dairy wastewater was estimated using the equation given below:

$$\text{Removal efficiency (\%)} = [(S_i - S_f)/(S_i)] * 100 \quad [2.4]$$

S_i = Initial nutrient concentration (mg/L), S_f = Final nutrient concentration (mg/L)

2.1.3.2 Biochemical analysis

Algal dried biomass was analyzed for carbohydrate estimation using the Phenol Sulphuric acid method (Dubois et al., 1956). Lowry method was adopted for protein estimation (Lowry et al., 1951). Briefly, the KMC4 dried cells were hydrolyzed in NaOH (0.2 N) at 80 °C for 20 min. The mixture was then neutralized to pH 7.5 for protein estimation. The Lipid was extracted from biomass according to the protocol performed by Najafabadi et al. (Najafabadi et al., 2015). The biomass (1 g) was mixed with chloroform/methanol (1:2 v/v) and was sonicated for 30 min (LABMAN LMUC6). The mixture was further vortexed and the chloroform layer was separated from methanol after layer separation. The collected solvent was dried using a rotary evaporator at 60 °C (Rotavapor® R-300, Buchi, Switzerland) and the gravimetric method was used for the quantification of extracted lipids.

2.1.3.3 Fatty acid methyl ester analysis

The FAME preparation was carried out by transesterification reaction using neutral lipids with protocol as earlier reported (Najafabadi et al., 2015). Briefly, methanol was added to 250 mg of previously extracted neutral lipid followed by the addition of concentrated sulphuric acid as an acid catalyst. The reaction was performed in a water bath at 65 °C. After 2 h, the FAMEs were separated using hexane at room temperature and analyzed by Gas chromatography (PerkinElmer Clarus680 GC/600C MS) equipped with an FID detector. The GC–MS was equipped with a column Elite- 5MS (length- 60 m, ID- 0.25 mm, and film thickness- 0.25 µm). Dimethyl polysiloxane (95%) - diphenyl (5%) and helium gas were used as stationary phase and mobile phase (flow rate 1 mL/min), respectively. A volume of 2 µL was injected and the temperature of injector was set at 280 °C. The temperature of column was programmed at 60 °C for 1 min, with an increment of 7 °C min^{-1} to 200 °C and then ramped at 10 °C min^{-1} to 300 °C and was held for 5 min. An EI(+ve) mode at 70 eV was used for mass spectral analysis within a range of 50 to 600 m/z. The interpretation of peaks was obtained by searching the library of the National Institute Standard and Technology which reveals molecular weight and relevant details about them.

2.1.4 Collection of dairy sludge

Three dairy wastewater treated sludge from different points were collected from Purabi Milk dairy treatment plant, Assam, India (26.13'N, 91.81'E) in April month of the year 2023 (Figure 2.2). In the treatment plant, the raw dairy wastewater is incorporated in an anaerobic digester for bio-gas production and further transferred to the flash mixer, flocculation and sludger thickener (Figure 2.3). The remaining generated wastewater goes to aeration tank and clarifier. The sludge samples were collected after flocculation (Dairy sludge I) at sludge thickener, after aeration tank (Dairy sludge II), and after clarifier (Dairy sludge III). The collected sludge samples were mixed and kept undisturbed for 15 h for settlement of ash and minerals present in them. The upper lower-density sludge was used as feedstock for liquefaction studies. The sludge and microalgal biomass were oven dried at 65 °C for two days and stored at 4 °C for future HTL and co-HTL experiments.

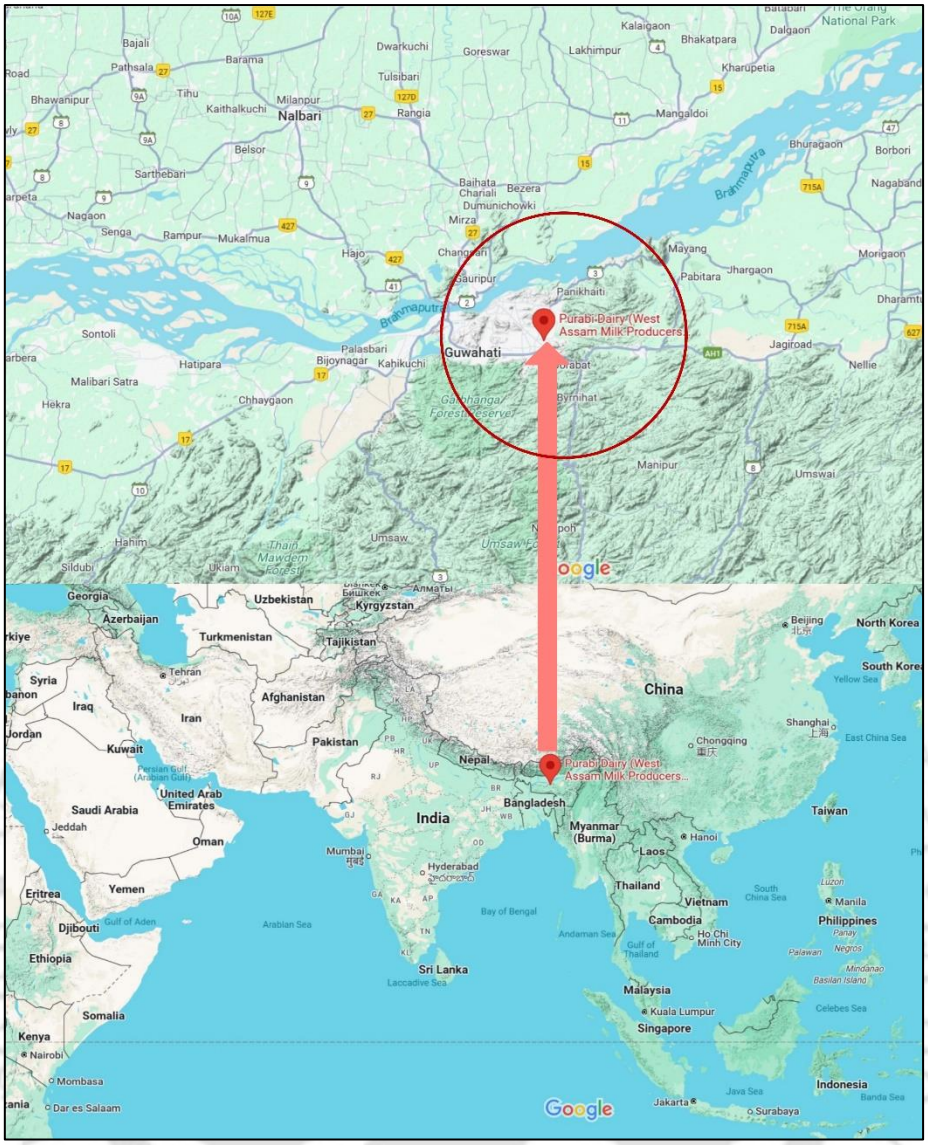

Figure 2.2. Location of collected samples from Purabi Milk dairy treatment plant, Assam, India (26.13'N, 91.81'E).

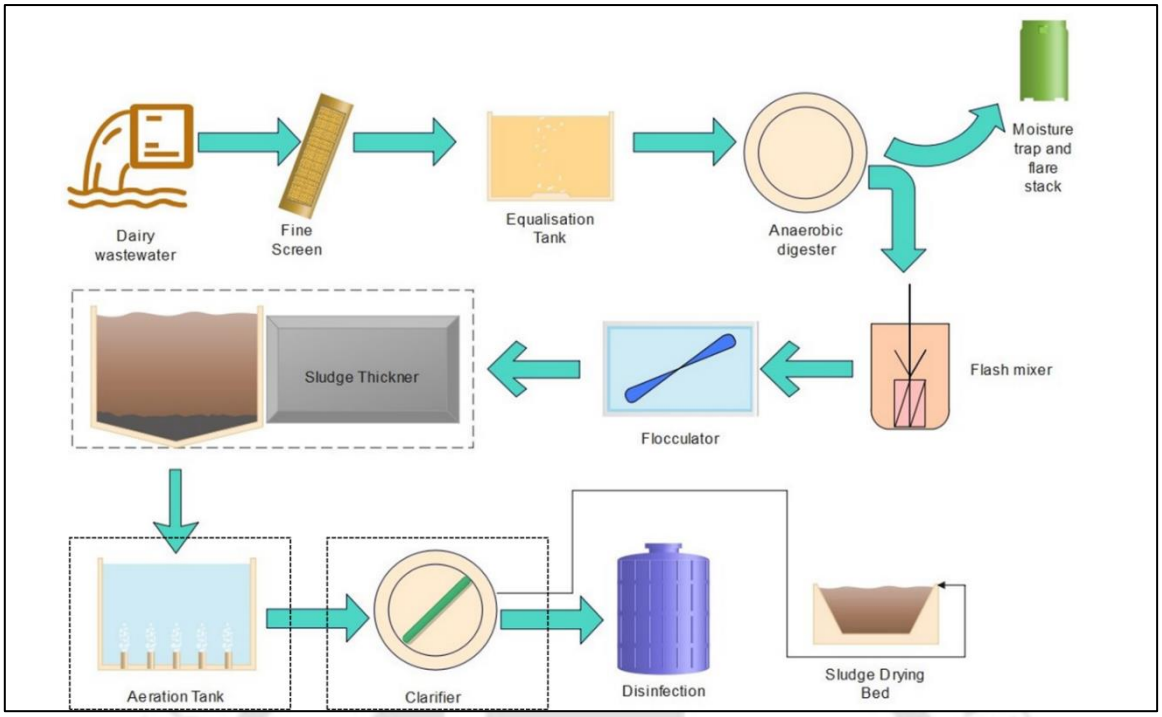

Figure 2.3. Schematic representation of collection points (doted box) at dairy wastewater treatment plant.

2.2 Preliminary Characterization

2.2.1. Physico-chemical characterization of feedstocks for HTL and pyrolysis

The proximate analysis of *Monoraphidium* sp. KMC4 and dairy sludge dry feedstock were estimated according to ASTM standards (E-871, D1102-84). The moisture content in the feedstock was measured by heating the sample at 105 °C for 24 h. The volatile content was measured by placing the sample at 925±10 °C for 7 mins. Further, the ash content in feedstock was estimated at 575±10 °C for 4 h followed by placing it in the desiccator. Also, the percentage of fixed carbon was determined by weighing the residue. CHNS Elemental Analyzer (Flash EA 1112 series, Thermo Finnigan, Italy) was employed for the analysis of elemental composition of the dried feedstock. Oxygen was calculated by difference.

The thermal degradation of individual and co-feedstock was conducted in a thermogravimetric analyzer (NETZSCH TG 209) instrument in the presence of N_2 gas. A sample of 8-10 mg was considered for analysis and the program was computed from 25 °C to 900 °C with a 20 mL min^{-1} gas flow rate and heating rate of 10 °C min^{-1}.

2.2.2 Characterization of microalgae and dairy sludge

A FESEM–EDS (Field Emission Scanning Electron Microscopy-Energy Dispersive Detector) instrument (Make: Zeiss, Model: Sigma 300) was used to estimate the minerals of microalgae and dairy sludge. Also, the surface functional bonds in dairy sludge were confirmed by XPS (PHI 5000 Versa probe III (Make: Physical Electronics, USA)), respectively. The X-ray photon spectroscopy (XPS) data was analyzed with a micro-focused (< 10 to 300 µm), monochromatic K-Alpha X-ray source, and at 1486.7 eV. During spectral acquisition, the instrument applied charge compensation with low-energy electrons and positive ions. The 9KW Powder X-Ray Diffraction System (XRD) (Make: Rigaku Technologies, JAPAN, Model: Smartlab) was used to analyse the dairy sludge for crystalline phases in the sludge, which can help to understand its composition and properties. The FTIR spectrometer (PerkinElmer, Spectrum Two) was employed to identify functional groups present in feedstocks. The range of 400 cm^{-1} – 4000 cm^{-1} was chosen for scanning the bands with step size and scan rate of 4 cm^{-1} and 20, respectively.

2.3 Two-stage, direct hydrothermal liquefaction and co-HTL experiments

All the experiments were conducted using a 100 mL high-temperature high-pressure stirred autoclave reactor (4598 Micro Bench Top Reactor, Parr, USA). In all experiments of HTL (direct HTL, two-stage HTL and co-HTL), 50 mL of a water slurry with a dry solid content (raw biomass or pretreated biomass and co-feed) of 10 wt% was used.

2.3.1 Direct hydrothermal liquefaction (DHTL) experiments

In direct HTL, the experiments were performed at four high temperatures at their respective pressures: 6 MPa (275 °C), 8.5 MPa (300 °C), 12.5 MPa (325 °C), and 17 MPa (350 °C). The heating rate was 5 °C per min and the experiments were performed for 30 min at 300 rpm At optimum temperature, the effect of three retention times (15 min, 30 min, and 45 min) on the products distribution was analyzed.

2.3.2 Two-stage hydrothermal liquefaction (SHTL) experiments

For the first stage, six mild temperatures, namely 140 °C, 160 °C, 180 °C, 200 °C, 220 °C, and 240 °C at different retention times (10-30 min) were used for solvolysis and pretreatment of microalgal biomass. The solid residue I obtained after the first step of two-stage HTL was used as feedstock for bio-oil production in the second stage at three temperatures (275 °C, 300 °C,

and 325 °C). The first series of pretreatment reactions were performed to decrease the N/C and increase the H/C ratio of feedstock for bio-oil production i.e. solid residue I.

2.3.3 Co-hydrothermal experiment details

The single dairy sludge reactions were performed at four temperatures ranging from 275-350 °C with agitation speed of 300 rpm. The autogenous pressure was reached at their respective temperature: 60 bar, 87 bar, 125 bar, and 17 bar at 275 °C, 300 °C, 325 °C, and 350 °C, respectively. The effect of reaction time was also studied at 15 min, 30 min, and 45 min. The direct HTL experiments in previous section is considered as HTL reactions for microalgal feedstock. For co-hydrothermal liquefaction studies, the sludge having better volatile matter and lower ash was considered. The above-mentioned four temperatures and reaction times were used to see their effect on product distribution for the co-HTL studies. Feedstock ratio of 25:75, 50:50, and 75:25 wt%-microalgae: dairy sludge, was used to optimize conditions for high bio-oil yield and better quality.

2.4 Equations used in DHTL, SHTL and co-HTL

The investigation was conducted in triplicate, and the following equations were used to determine product yield and energy values (Mahata et al., 2023). Others* in Eq. 2.7 include the aqueous phase, gaseous product, and losses during the process. The total bio-oil yield was calculated according to Eq. 2.10 as given below.

$$Bio-oil\ yield\ (wt\%) = \frac{m_{bio-oil}}{m_{feedstock}} * 100\% \quad [2.5]$$

$$Solid\ residue\ yield\ (wt\%) = \frac{m_{solid}}{m_{feedstock}} * 100\% \quad [2.6]$$

$$Others*\ (wt\%) = 100\% - [Bio-oil + Solid]\% \quad [2.7]$$

$$Conversion\ (\%) = 100\% - Y_{solid}\ \% \quad [2.8]$$

$$Energy\ yield\ (\%) = (HHV_{Bio-oil} \times Y_{bio-oil}/HHV_{feedstock}) \times 100 \quad [2.9]$$

$$Total\ bio-oil\ yield\ (wt\%) = (Bio-oil_{stage\ I} + Bio-oil_{stage\ II})\% \quad [2.10]$$

2.5 Product separation in HTL and co-HTL process

2.5.1 Direct HTL (DHTL) or HTL

After reaction completion, the reactor was cooled down to ambient temperature using cooling jacket and the gas was released by depressurizing the reactor. The solvent, dichloromethane (DCM) was added to the reactor and the product mixture (combination of bio-oil, solid residue, and aqueous phase) was collected in tubes. The bio-oil was extracted via liquid-liquid extraction methodology. The solid residue was rinsed thrice with DCM to extract any residual bio-oil components. The liquid mixture was filtered using Whatman® filter paper 42 and separated into a separating funnel. The solvent was removed from bio-oil using a rotary evaporator (Rotavapor® R-210, Buchi, Switzerland) and was quantified gravimetrically.

2.5.2 Two-stage HTL (SHTL)

After stage I, the mixture was centrifugation at 4000 rpm to segregate the liquid layer and solid fraction. The solid residue I was washed out by DCM to withdraw any bio-oil component and dried at 65 °C for stage II bio-oil production (Bisht et al., 2022). After stage II, the DCM was added to the reactor, and the product mixture was collected in tubes. The liquid mixture was filtered and quantified with the same abovementioned method in stage I.

2.5.3 Co-HTL studies

The product separation in co-HTL studies was performed like DHTL studies.

2.6 Catalyst characterization, and coked catalyst characterization

Ammonium-ZSM-5 powder with SiO_2:Al_2O_3 of 23:1 mole ratio was procured from Alfa Aesar (India) for catalytic studies. H-ZSM-5 was prepared by calcining ammonium ZSM-5 in a furnace at 550 °C for 5 h (Rahman et al., 2018). The catalyst was sealed to avoid moisture before any characterization and catalytic co-pyrolysis experiments. The thermal stability of fresh and coked H-ZSM-5 catalyst was examined by the thermogravimetric analysis (NETZSCH STA 449F3). The analysis was performed in the presence of argon gas at a heating rate of 10 °C min^{-1} from 25 °C to 1000 °C. The physical characteristics of calcined and coked catalyst were measured in Brunauer-Emmett-Teller (BET) analyser (TriStar II 3020, micromeritics). The surface area, pore size, and pore volume of fresh and coked catalyst and absorption and desorption isotherms were also measured. The catalyst was weighed around

400-500 mg and degassed for 8 h under inert conditions at 180 °C. The amount of nitrogen adsorbed per gram of sample was plotted against the relative vapor pressure (P/P_0) of nitrogen, and the resulting data were analyzed using the Brunauer-Emmett-Teller (BET) equation to determine the surface area. The phase composition of a fresh and spent catalyst was determined using 9KW Powder X-Ray Diffraction System (Make: Rigaku Technologies, JAPAN, Model: Smartlab). CuKa radiation source with a wavelength of 0.154 nm was used in XRD analysis, and the plot was taken in the 2θ range of 5° to 60°. The structure, morphology and elemental composition of fresh and coked H-ZSM-5 were examined using high-resolution field emission transmission microscopy connected with energy-dispersive spectroscopy (Make: JEOL, Model :2100F). A small amount of sample was dissolved in ethanol and then dispersed over carbon film supported copper grid and kept at 60 °C in a vacuum oven before analysis. The scanning electron microscopy was also used to record the topography of catalyst (FESEM, Sigma 300). The functional bonds of fresh and coked H-ZSM-5 were studied using XPS (PHI 5000 Versa probe III (Make: Physical Electronics, USA). XPS data were acquired according to above mentioned methodology in section 2.2.2.

To understand the combustion behaviour of coke in spent and recycled catalyst, thermal degradation analysis was performed in the presence of air. The temperature profile was set from ambient temperature to 800 °C at a heating rate of 10 °C min^{-1}. Also, the thermal degradation of spent and recycled catalyst was performed in the presence of argon gas as an inert environment to see if mass loss is related to the thermal decomposition, volatilization, and coking of a catalyst. In that case, mass loss is due only to thermal decomposition, desorption of volatiles, or physical changes. While in the presence of air, coke burns off as CO_2 or CO during heating. And, the mass loss corresponds to the amount of coke deposited on the catalyst surface.

2.7 Non-Catalytic and Catalytic pyrolysis experiments

All the experiments related to pyrolysis/co-pyrolysis were performed in fixed-bed reactor. Individual feedstocks (microalgae and dairy sludge) as well as co-feedstock mixtures of *Monoraphidum* sp. KMC4 and dairy sludge (75:25 by wt%) were subjected to pyrolysis (40 g per run) in a reactor constructed from Inconel 800. The reactor had an outer diameter of 73 mm, an inner diameter of 62.62 mm, and a length of 438 mm, and was operated in semi-batch mode. The reactor was heated by a split tubular furnace with temperature measured using a

thermocouple placed inside the reactor. The temperature was precisely controlled by a PID controller.

Nitrogen gas, serving as both fluidizing and carrier gas, was preheated to 250 °C and introduced at the base of the reactor at a flow rate of 200 mL min^{-1}. The resulting hot vapors were transferred through a well-insulated line to a straight, single-pass condenser made of SS316 stainless steel. The condensed vapors were collected in a beaker and designated as bio-oil. Slow pyrolysis of feedstocks was carried out at a heating rate of 20 and 40 °C min^{-1}, with final temperatures set at 500 °C, 550 °C, and 600 °C for 60 min and 120 min. The yield of liquid products was determined based on the mass of condensable vapours collected, while the yield of non-condensable gases was calculated using an overall mass balance, as shown in Equation 2.11. A temperature of 550 °C was identified as optimal and was subsequently used to evaluate the impact of sludge addition during co-pyrolysis on the quantity and quality of the resulting bio-oil. All experiments were performed in duplicate and the average values are reported.

The pyrolysis reaction with H-ZSM-5 was also conducted in the same fixed-bed reactor. The catalytic experiments were conducted in ex-situ form within the reactor. High-temperature insulation wool was used as a basket for placing the catalyst within the reactor, which can be separated from the feedstock and biochar after the reaction. The wool was placed at a distance from the feedstock bed or in the middle of the reactor. The influence of the catalyst was studied at optimum co-pyrolysis conditions (550 °C, 20 °C/min, and 60 min) at two different feedstocks to catalyst ratios (1:1 and 1:0.5 g/g). A schematic of the experimental setup used in this study is presented in Figure 2.4.

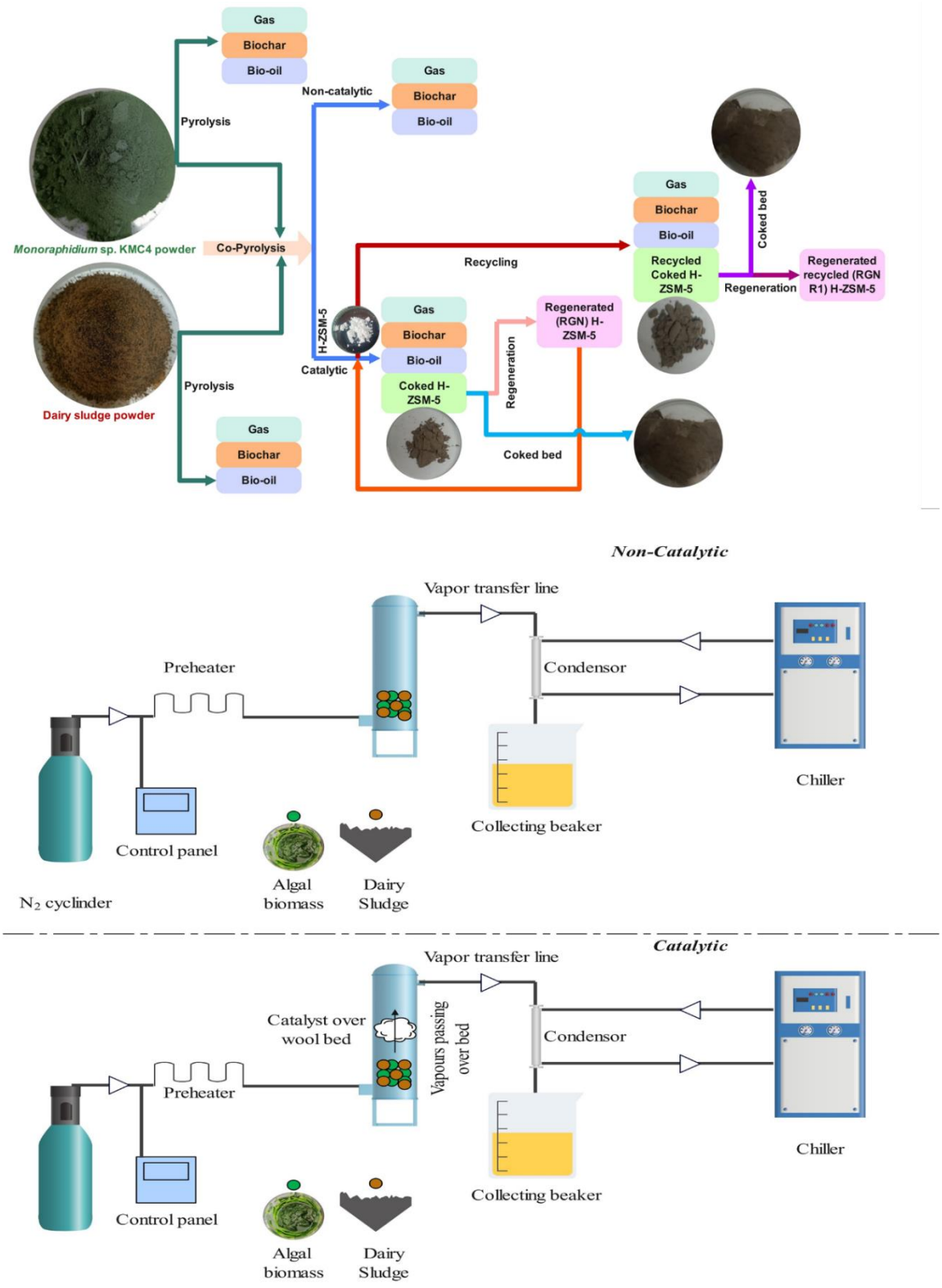

Figure 2.4. Schematic of the pyrolysis experimental setup.

2.7.1 Product separation

In both catalytic and non-catalytic reactions, the solid biochar remains in the reactor. The solid biochar was retrieved after quenching with a chiller by opening the down flange of the reactor. The wool bed+catalyst was fixed properly in the middle of the reactor; both were recovered after biochar collection by pushing downward with a pipe, weighed, cooled to room temperature and then sealed for further characterization. In both cases, the pipelines were washed with acetone to collect the remaining fraction of bio-oil and separated by filtration for any particle removal. The acetone soluble phase was rota-evaporated (Rotavapor® R-210, Buchi, Switzerland) at 60 °C and weighed gravimetrically. The overall yield of bio-oil was calculated by adding both condensable vapours and acetone-soluble phase after rota evaporation. The non-condensable gases yield with losses were estimated according to equation given below.

$$[\text{Gas yield} + \text{Losses}](\%) = 100\% - (\text{bio} - \text{oil yield}\ (\%) + \text{biochar yield}\ (\%)) \quad [2.11]$$

2.8 Products characterization

The major elements present in the bio-oil from HTL, DHTL, co-HTL, and pyrolysis reactions were measured using elemental analyser (Flash smart V CHNS/O). The CHNS analysis of solid residue and biochar from all thermochemical experiments was performed in an CHNS analyzer (Eurovector EA3000). The oxygen content was estimated by difference given in equation 2.12.

$$\text{O}\ (\text{wt}\%) = 100\% - [\text{C}\ (\%) + \text{H}(\%) + \text{N}(\%) + \text{S}(\%)] \quad [2.12]$$

The chemical composition of the bio-oils was analyzed using an GCMS-TQ8030 (Make: Shimadzu) gas chromatography–mass spectrometer (GC-MS) under the following conditions: helium was used as the carrier gas and a 1 µL injection volume was used. The GC oven temperature was initially set at 80 °C for 2 min, then ramped to 300 °C at a rate of 5 °C min^{-1} and held for 10 minutes. The analysis was conducted in scan mode over a mass range of 50–600 m/z. The injector and detector temperatures were maintained at 250 °C and 300 °C, respectively. Compound identification was performed using the National Institute of Standards and Technology (NIST) mass spectral library. The boiling point distribution of the bio-oils was determined using a thermogravimetric analyzer (TGA) (Netzsch STA449F3) under an argon atmosphere. The temperature was ramped from 25 °C to 600 °C at a heating rate of 10 °C min^{-1}, with an argon flow rate of 40 mL min^{-1}.

The surface morphology of the used catalyst wool bed was also examined with a SEM instrument (Sigma 300). FTIR spectroscopy was conducted using an IRAffinity-1 instrument (PerkinElmer, Spectrum Two) to identify the functional groups present in the bio-oil. Spectral data were collected over the range of 4000–400 cm^{-1}, with a step size of 8 cm^{-1}. The total organic carbon, inorganic and organic carbon concentration in aqueous phase from DHTL, SHTL, and co-HTL were estimated from TOC analyser (Make: Shimadzu, Model: TOC-L CPH).

Chapter 3

Dairy wastewater treatment using *Monoraphidium* sp. KMC4 and its potential as hydrothermal liquefaction and pyrolysis feedstock

Chapter 3. Dairy wastewater treatment using *Monoraphidium* sp. KMC4 and its potential as hydrothermal liquefaction and pyrolysis feedstock.

Graphical abstract of Chapter 3

3.1 Background

Production of co-products in a loop biorefinery model can be used as an approach to give numerous advantages and improve the process's sustainability and economic viability. The mixotrophic strategy for wastewater treatment, biomass productivity, and biochemical compound accumulation gives a valuable option for green energy production. This work aims to explore the potential of KMC4 in reducing the nutrient load from wastewater during a remediation study. Also, the influence of different strengths of wastewater on the growth rate of KMC4 was investigated.

As people's awareness of nutrition and health increasing in the last 45 years, the dairy industry has grown into an organized industry of large magnitude. India produced 155.2 million tonnes of milk in 2016–17 and now stands first in the milk production. Approximately, the amount of wastewater generated in terms of volume is 2–10 times higher than that of the milk processed. Dairy wastewater which has high chemical oxygen demand and ammonia content needs proper pre-treatment or dilution before using for microalgal cultivation (Hemalatha et al., 2019; Kuravi and Venkata Mohan, 2022). Previously, several efforts have been conducted utilizing dairy wastewater for biomass production, lipid biosynthesis, biodiesel production, and value-added product accumulation under a mixotrophic regime (Chokshi et al., 2016; Patel et al., 2020).

Monoraphidium sp. KMC4 is considered a potential strain with significant biomass and lipid accumulation along with high remediation capability. The objective of this investigation is to: (1) assess the bioremediation potential of *Monoraphidium* sp. KMC4 to treat simulated synthetic dairy wastewater by noticing the variation in COD, glucose, ammonium, phosphate, and nitrate under different strengths; (2) analyze the effect of different strengths of SSDW in growth and biomass productivity; (3) validate the potential of biomass as feedstock towards bio-oil production.

3.2 Methodology

The *Monoraphidium* sp. KMC4 was cultivated in varying strengths of SSDW and the biomass concentration was analysed every alternate day till exponential phase along with nutrient removal efficiency. Further, the biomass collected was analysed for its thermochemical conversion potential.

3.3 Results and discussion

3.3.1 Cultivation of Monoraphidium sp. KMC4

3.3.1.1 Growth study of *Monoraphidium* sp. KMC4

Monoraphidium sp. KMC4 was cultivated in varying strengths (3840 mg/L, 2880 mg/L, 1920 mg/L, 960 mg/L, 480 mg/L) of simulated synthetic dairy wastewater (SSDW), and the change of biomass concentration during the cultivation period is represented in Figure 3.1. This species has adapted to all the selected wastewater strengths. Comparing these selected strengths, it was noticed that *Monoraphidium* sp. KMC4 outperformed in 50% diluted (1920 mg/L) wastewater with a biomass concentration of 1.47 g L^{-1}. The exponential phase in 50% diluted SSDW (1920 mg/L COD) was sustained until the 11th day and achieved biomass productivity and a specific growth rate of 122 mg L^{-1} day^{-1} and 0.22 day^{-1}, respectively. The biomass concentration in 100%, 75%, 25%, and 12.5% SSDW reached 1.12, 1.17, 0.97, and 0.86 g L^{-1}, respectively. The minimum biomass concentration obtained in the 12.5% SSDW treatment was a consequence of nutrient exhaustion.

After maintaining the pH of the 50% strength algal culture (7–7.5), a significant biomass concentration and biomass productivity of 3.69 g L^{-1} and 223 mg L^{-1} day^{-1} were observed on the 16th day of the late exponential phase. The *Monoraphidium* sp. KMC4 has exhibited superior biomass concentration in SSDW as compared to the control Blue green medium (BG11) (1.53 g L^{-1}). The *Monoraphidium* sp. KMC4 achieved 1.47 g L^{-1} with biomass

productivity and a specific growth rate of 122.5 mg L^{-1} day^{-1} and 0.27 day^{-1} respectively, in raw domestic sewage wastewater (Mishra and Mohanty, 2019). The 75% diluted simulated dairy wastewater was found to have sufficient strength for the growth of *Tetraselmis* sp. with 95% COD reduction efficiency and achieved a biomass concentration of 3.004 g L^{-1} (Swain et al., 2020). Kuravi and Venkata Mohan (2022), reported that mixotrophic cultivation has improved nutrient removal efficiency and reached productivity of 50.9 mg L^{-1} day^{-1} in synthetic dairy wastewater (Kuravi and Venkata Mohan, 2022).

During the treatment period, organic carbon and light energy were consumed simultaneously to produce energy molecules via photosynthesis and respiration. The ratio of energy carriers is directly linked to the rate of carbon fixation resulting in the formation of secondary metabolites. The mixotrophic regime can significantly enhance biomass productivity which in turn increases lipid productivity to make the mixotrophic mode of cultivation a promising pathway toward biomass production (Penhaul Smith et al., 2020).

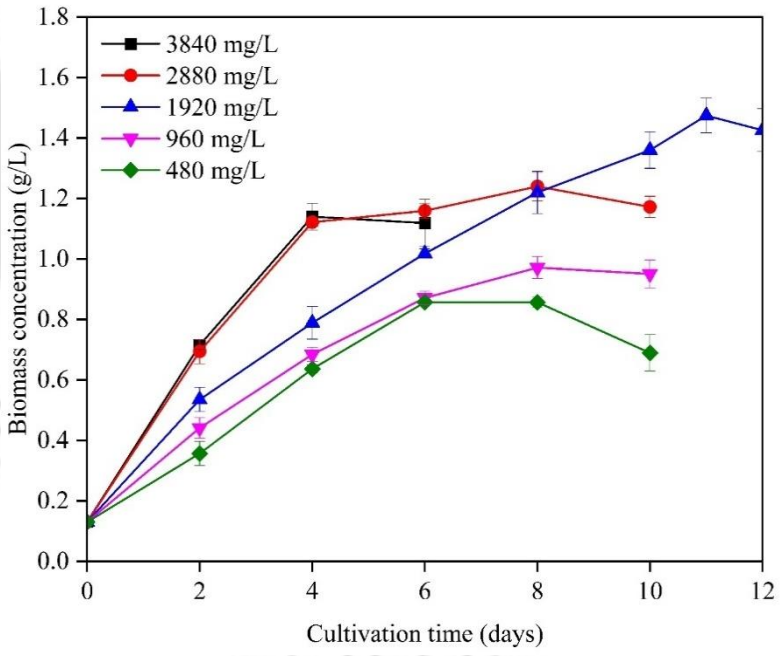

Figure 3.1. Growth study of *Monoraphidium* sp. KMC4 in varying strength of simulated synthetic dairy wastewater without maintaining pH.

3.3.2. Change in pH during bioremediation study

The pH was measured every alternate day and an upsurge increase from neutral to alkaline was observed (Figure 3.2). The pH value in 100% and 75% SSDW were not raised beyond 9.5 due to the release of CO_2 caused by the heterotrophic component of mixotrophic metabolism. While

the pH in 25% and 12.5% dilution rises to 11.3 due to a predominant shift in autotrophic conditions and increased photosynthesis after exhaustion of organic carbon source from the medium. The pH value will increase where photosynthetic activity during autotrophic metabolism is higher which suggests that autotrophic mode was performed after the utilization of organic carbon by *Monoraphidium* sp. KMC4 in 25% and 12.5% SSDW within 4 and 2 days, respectively (de Morais and Costa, 2007; Markou and Georgakakis, 2011).

During the CO_2 concentrating mechanism, the rise in pH was due to accumulation of hydroxide ions outside the cell, increasing the pH of the water, which corresponds to higher photosynthetic activity. The pH level of the system affects the dissolution of CO_2 in water and further sequestration of nutrient will affect the growth and metabolism of microalgae. Previous studies also reported an increase in the pH from 7 to 11 due to an increase in photosynthetic activity and carbon fixation by reducing CO_2 during the autotrophic growth mode of cultivation (de Morais and Costa, 2007; Gao, 2021; Markou and Georgakakis, 2011).

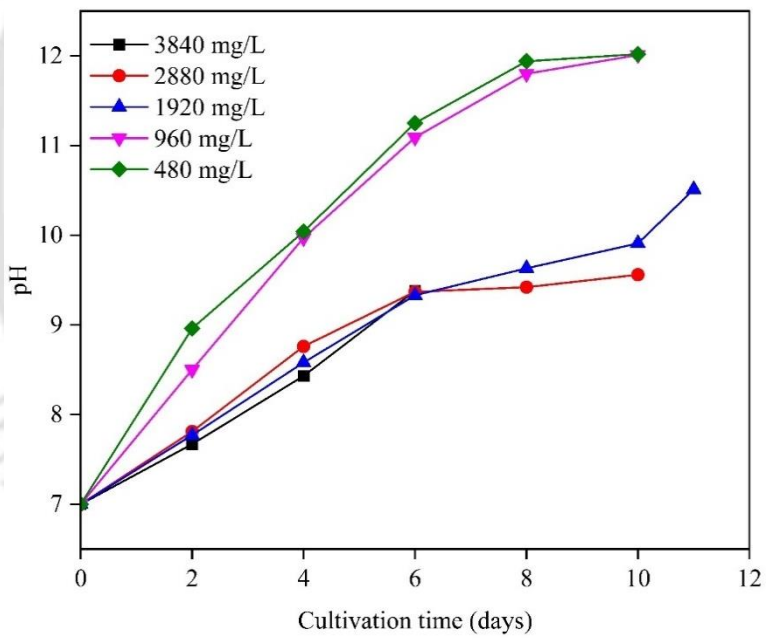

Figure 3.2. Change in pH during growth study of *Monoraphidium* sp. KMC4 in varying strength of simulated synthetic dairy wastewater.

3.3.3. Nutrient removal profile during bioremediation study

Microalgae utilize carbon, nitrogen, and phosphorous as essential growth factors during cultivation for their growth. The nutrient removal by *Monoraphidium* sp. KMC4 during the treatment study was exhibited in Figure 3.3. The microalgae have utilized majorly glucose with

93.36% and 98.13% of removal efficiency in 100% and 75% SSDW respectively (Figure 3.3a and e), which shows that the carbon source was consumed by microalgae for their growth. Within 11 days, the microalgae utilized almost 90.93% of glucose in 50% SSDW whereas complete removal was observed in 25% and 12.5% SSDW within 4 and 2 days, respectively. Smith et al. (2015) reported that *Micractinium inermum* utilized glucose as a carbon source and shown maximum biomass productivity of 373.37 mg L^{-1} day^{-1} during mixotrophic growth mode (Smith et al., 2015). In another investigation, a total sugar reduction of 39.68% (15.76% total inorganic carbon and 39.91% total organic carbon) was observed by *A. dimorphous* in dairy wastewater after 4 days (Chokshi et al., 2016). The supplementation of organic carbon in wastewater during the mixotrophic mode of cultivation is a promising approach to increase biomass productivity (Cheng et al., 2022; Smith et al., 2015).

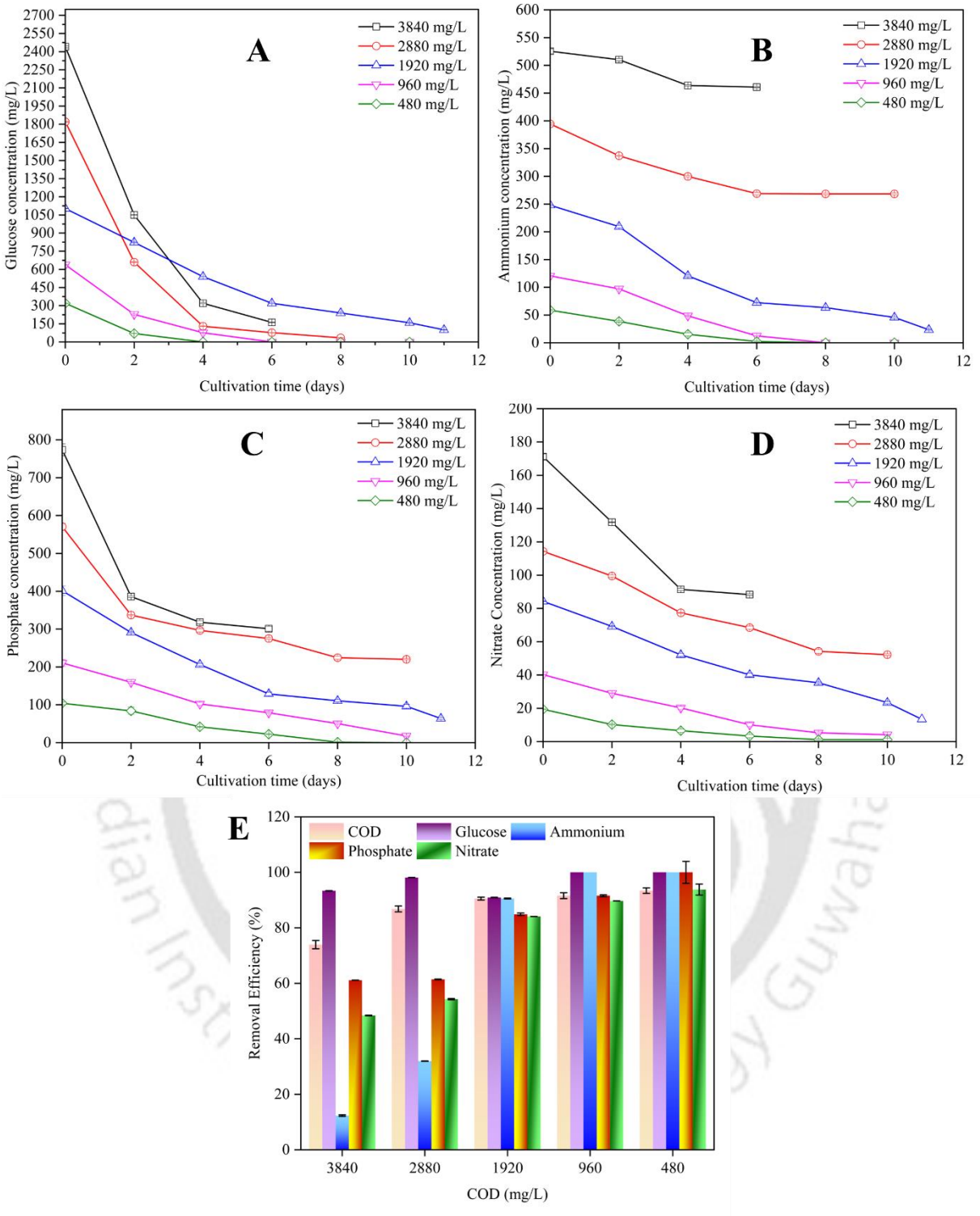

Figure 3.3. Nutrient removal profile during bioremediation study a) change in glucose concentration; b) change in ammonium concentration; c) change in phosphate concentration; d) change in nitrate concentration; e) chemical oxygen demand and nutrient removal efficiency.

From Figure 3.3b, it is evident that ammonium-N was reduced from 247.8 mg L^{-1} to 23.39 mg L^{-1} in 50% SSDW with a removal efficiency of 90.56% in 11 days (Figure 3.3e). By end of the 8th day, ammonium-N could not be observed in 25% and 12.5% SSDW, which is similar to the results reported by Lu et al. (2015) for 5% raw dairy wastewater (Lu et al., 2015). While a removal efficiency of only 12.33% and 31.98 % was achieved in 100% and 75% SSDW (Figure 3.3e). Choksi et al. (2016) reported a complete reduction of ammonium-N after 6 days in dairy wastewater (Chokshi et al., 2016). In a similar investigation, Kothari et al. (2013) observed a 90% removal of ammonia after 10 days of treatment from 75% dairy wastewater by *Chlamydomonas polypyrenoideum* (Kothari et al., 2013).

Therefore, it can be inferred that the KMC4 had consumed glucose as an organic nutrient source till the 6th and 8th day of cultivation in 100% and 75% SSDW without insignificant utilization of ammonium-N (removal efficiency of 12.33% and 31.98% respectively) which conferred that a high concentration of ammonium-N might have inhibited the viability of KMC4 after significant consumption of glucose (Figure 3.4). While the ammonium-N of ~ 247 mg L^{-1} was not found to be inhibitory for KMC4. This result suggested that *Monoraphidium* sp. KMC4 has strong tolerance in high ammonium conditions. A previous study also reported that a high concentration of ammonium-N can inhibit the growth of microalgae (Markou and Georgakakis, 2011). This result was found to be similar with previous study where the ammonium concentration above 14 mM was found to be inhibitory for *Monoraphidium* HDMA-01 (Lin et al., 2021). The nitrate was removed above 80% in 50%, 25%, and 12.5% SSDW while below 55% was eliminated in 100% and 75% SSDW (Figure 3.3d). Microalgae first utilize all ammonium source before using other nitrogen sources because of low energy utilization for uptake and accelerating amino-acid biosynthesis and forming proteins. The presence of ammonium in SSDW redirects microalgae to proceed with the pathway toward protein synthesis (Lin et al., 2021; Markou and Georgakakis, 2011).

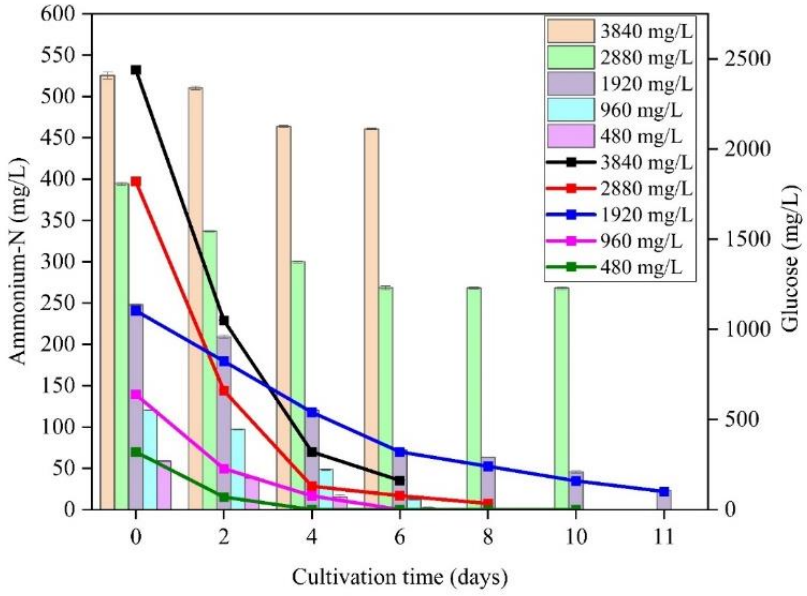

Figure 3.4. Consumption of glucose and ammonium by KMC4 during treatment of SSDW.

As shown in Figure 3.3c and e, the phosphate removal efficiency of 84.13% was achieved with a reduction from 401.3 mg L^{-1} to 63.67 mg L^{-1} in 50% SSDW during the treatment study. The phosphate removal efficiency of above 90% was observed in 25% and 12.5%, compared to only 61.1% and 61.42% achieved in 100% and 75% SSDW, respectively (Figure 3.3e). *Chlamydomonas polypyrenoideum* exhibited 70% phosphate removal efficiency from 75% dairy wastewater after 10 days (Kothari et al., 2013). In similar studies, phosphate removal efficiency above 70% was observed after the remediation of dairy wastewater (Chokshi et al., 2016; Hemalatha et al., 2019). Phosphorus was assimilated by microalgae and considered a growth limiting factor. The excess phosphorous is stored as polyphosphate reserves for phosphatides, proteins, and nucleic acids synthesis. In addition, phosphorous can help in enhancing the cell division and synthesis of ATP (Kiran and Venkata Mohan, 2021).

The *Monoraphidium* sp. KMC4 in 50% SSDW, showed a COD removal efficiency of 90.54% (Figure 3.3e). The highest COD removal efficiency of 93.4% was achieved in 12.5% SSDW while the lowest (73.95%) was observed in 100% SSDW. *Tetradesmus* sp. SVMIICT4 in a mixotrophic mode had shown 95.5% COD removal efficiency by the end of cultivation with 65.20% and 57.35% nitrates and phosphates removal efficiency (Ravi Kiran and Venkata Mohan, 2022). *C. sorokiniana* achieved 90% COD reduction after treating dairy wastewater with a concomitant decrease of nitrate (65.5%) and phosphate (73%) (Hemalatha et al., 2019). The treatment study during the mixotrophic mode of operation resulted in good nutrient removal efficiency and biomass growth. Hence, the present investigation provides the evidence

for the significant removal of nutrients from dairy wastewater by *Monoraphidium* sp. KMC4 without an adverse effect on the growth rate.

3.3.4. Characterization of KMC4 biomass

3.3.4.1. FTIR analysis

The FTIR analysis of the microalgal biomass was performed to provide information about the alcohol, carboxyl, amino group, and others primarily present in the organic compounds (Figure 3.5). The –OH stretching at peak 3281.6 cm^{-1} corresponded to the presence of carbohydrates, proteins, lipids, and nucleic acids. The –CH stretching at a peak between 3040 cm^{-1} and 3060 cm^{-1} represented the unsaturated lipid structures. Further, the peaks at 2950 cm^{-1} and 2850 cm^{-1} represented CH_3 and CH_2 stretching, respectively, of aliphatic groups of lipids and proteins. The presence of lipid was also validated from bands between 1710 cm^{-1} and 1800 cm^{-1} for C=C stretching. Furthermore, the confirmation of protein in algal biomass was marked by stretching peaks at 1633.2 cm^{-1} and 1534.3 cm^{-1} for C=C and C-N, respectively. Moreover, the band at 1426.45 cm^{-1} is related to the presence of C=O stretching of carbonate ion. Furthermore, the peak at 1233.68 cm^{-1}, 1149.65 cm^{-1}, and 1036.79 cm^{-1} represented phospholipids of nucleic acids & proteins: amide III band (P=O and C–N bending), polysaccharides (C-O-C) and phospholipids & carbohydrates of nucleic acid (P=O), respectively (Mishra and Mohanty, 2019; Patel et al., 2020).

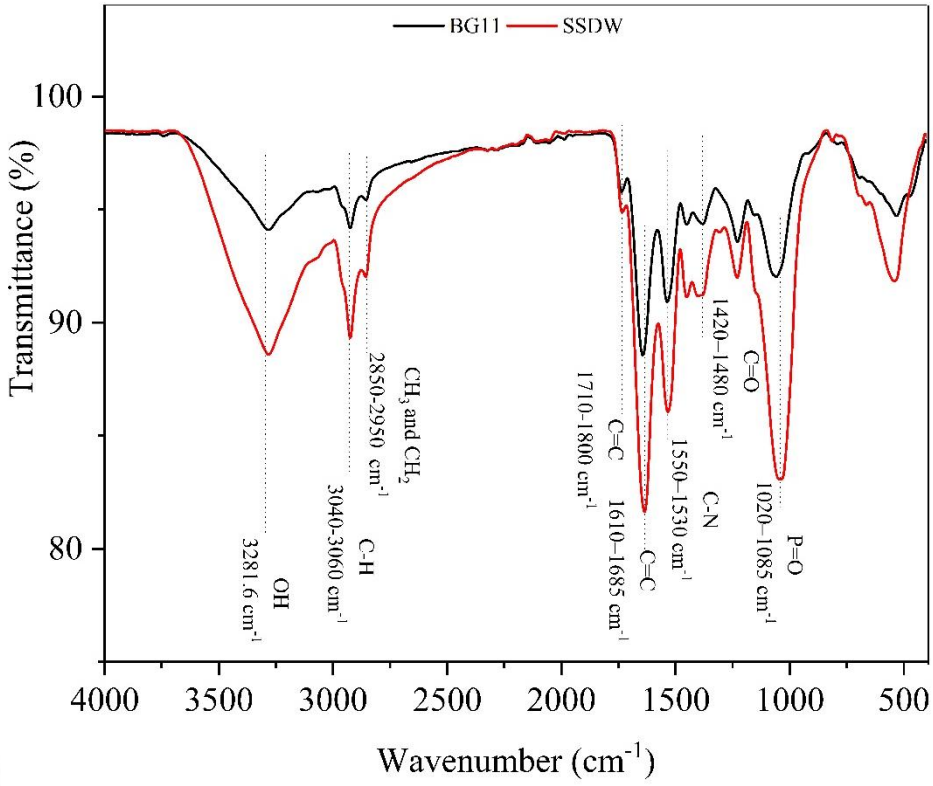

Figure 3.5. FTIR spectrum of KMC4 biomass from simulated synthetic dairy wastewater and BG11.

3.3.4.2. Physico-chemical analysis of biomass

The proximate, elemental, and bio-chemical composition of algal feedstock in this study was compared with previous studies and are presented in Table 3.1. It was observed that algal biomass has a volatile content of 71.54% and low ash content (~of 8.4%). Furthermore, the lower ash content in biomass could effectively increase bio-oil quality in terms of high heating values and light fraction compounds with lower boiling points. This considerably improved the thermochemical conversion towards bio-oil production and reduces the operating cost (Brindhadevi et al., 2021). The lipids and protein content in algal biomass are 20.29±2.3 and 48.5±1.3, respectively. The evaluation of C, H, N, and S in biomass revealed a greater fraction of carbon (43.58%), followed by 6.73% hydrogen, 8.7% nitrogen, and 0% sulfur. The elemental contents of algal biomass using Dulong's equation (Arif et al., 2021) were utilized to determine the higher heating value (HHV) and achieved 18.5 MJ kg^{-1} of energy. The biomass grown from SSDW can be exploited as a feedstock for efficient thermochemical conversion to produce bio-oil.

Table 3.1. Comparison of physico-chemical properties of *Monoraphidium* sp. KMC4 grown on SSDW with previous studies.

Properties	*Monoraphidium* sp. KMC4 (This study)	*Tetraselmis* sp. (Vo et al., 2017)	*Chlorella* sp. (Xu et al., 2019)	*Monoraphidium* sp. KMC4 (Mishra and Mohanty, 2019)
Proximate analysis				
Moisture content (%)	6.30 ± 0.36	-	-	4 ± 0.50
Volatile matter (%)	71.50± 0.18	-	-	74 ± 0.80
Ash (%)	8.40 ± 0.12	-	16.06	6.74 ± 0.10
Fixed carbon[$] (%)	13.80± 0.30	-	-	15.26 ± 0.20
Ultimate analysis				
C (%)	43.58 ± 1	40.49	40.31	47.91 ± 0.11
H (%)	6.73 ± 0.01	8.67	5.99	7.83 ± 0.05
N (%)	8.70± 0.40	47.13	9.14	6.80 ± 0.10
S (%)	0	-	0.76	0.17 ± 0.01
O[*] (%)	32.59± 0.20	3.71	27.74	30.55 ± 0.13
Biochemical analysis				
Carbohydrates (%)	28.73±1.60	18.50	-	27.4 ± 2.20
Protein (%)	48.50±1.30	37.50	-	39.7 ± 1.07
Lipid (%)	20.29±2.30	14	-	28.86 ± 2.90
HHV (MJ/Kg)	18.50	18.10	17.31	21.38

*The oxygen content (%) is obtained from the equation: (100-%(C-H-N-S-ash));

[$]The fixed carbon is obtained from the equation: (100-% (moisture content +ash +volatile matter))

3.3.4.3. Elemental and TGA analysis

The pyrolytic study of KMC4 biomass from SSDW and BG11 was evaluated for its thermal decomposition behavior and is represented in Figure 3.6. It was observed that both biomass represented three phases of decomposition. The initial decrease in weight loss of appx. 5 wt% corresponded to the moisture content removal and exclusion of volatile matter from biomass

up to a temperature of 140 °C. The second stage represented the devolatilization phase at a temperature of 140–500 °C, which accounted for a maximum mass loss of ~ 62–65 wt% due to the decomposition of major organic compounds from biomass. Lastly, the third stage (above 500 °C) signified the char formation zone or decomposition of high-temperature stable compounds. Also, the differential thermogravimetric (DTG) spectra represented the decomposition profile of algal biomass. The temperature up to 150 °C corresponded to the moisture removal from biomass. The two others main DTG peaks are also observed at a temperature between 150 and 350 °C and 350–500 °C. The prior temperature is related to the decomposition of carbohydrates and proteins which started from 150 °C & 160 °C and is followed by a temperature of 350 °C while the latter temperature is associated with lipid devolatilization from biomass. The thermal decomposition profile observed was found to be comparable to prior results on algal biomass feedstocks (Agarwalla et al., 2022; Mishra and Mohanty, 2019).

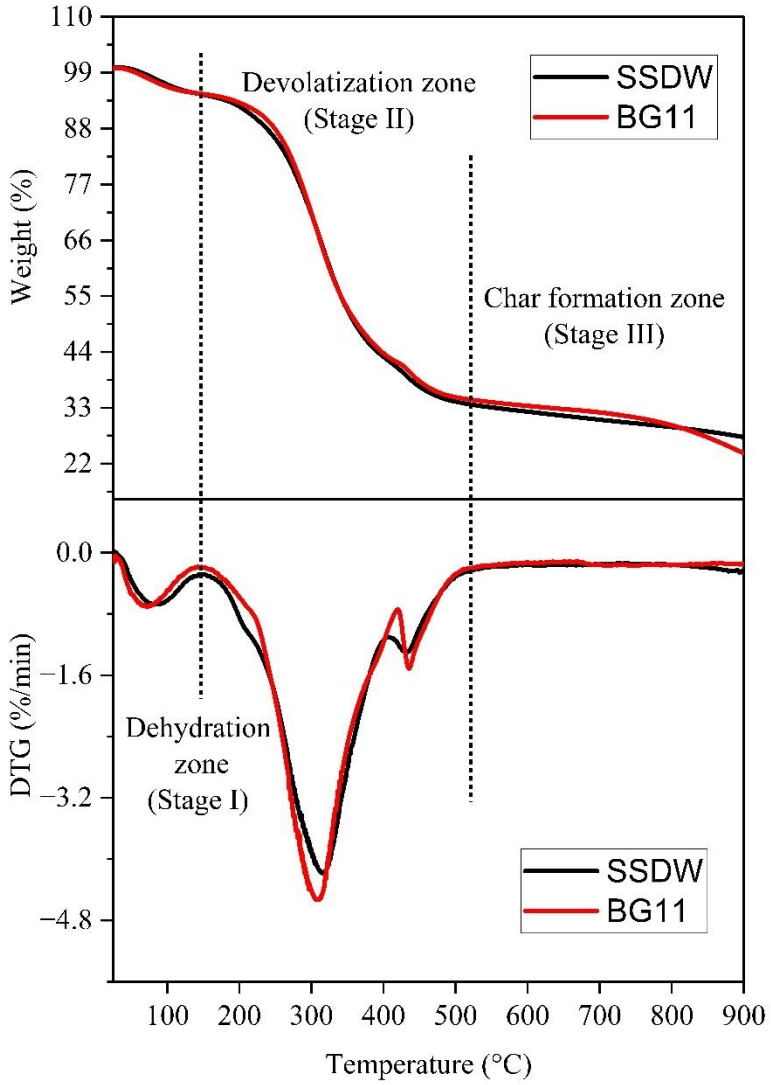

Figure 3.6. Thermogravimetric curve (TGA-DTG) for dry microalgae biomass (SSDW and BG11) at 10 °C/min.

To obtain the distribution of elemental composition in microalgal biomass, an energy-dispersive X-ray system was used to show the presence of macroconstituents and microconstituents (Figure 3.7 and Figure 3.8). The KMC4 obtained from SSDW contains a high amount of phosphorous, manganese, and sulfur while zinc, copper, iron, phosphorous, and sulfur were found in major proportion in BG11 biomass. A very small percentage of chlorine, potassium, calcium, and magnesium was observed on KMC4 biomass from SSDW. This change in the cell surface elemental percentage of biomass from SSDW and BG11 can be due to the variation in growth medium.

The insignificant amount of less water-soluble elements like calcium and magnesium suggested its minor availability in char after liquefaction (Table 3.2). Also, the sodium and potassium tended to blend into the aqueous phase after the liquefaction process. The absence or minor availability of these elements (Na, K, Ca, Mg, P) will be an advantage during the downstream processing of aqueous, bio-oil, and char fractions after hydrothermal liquefaction (Cheng et al., 2018).

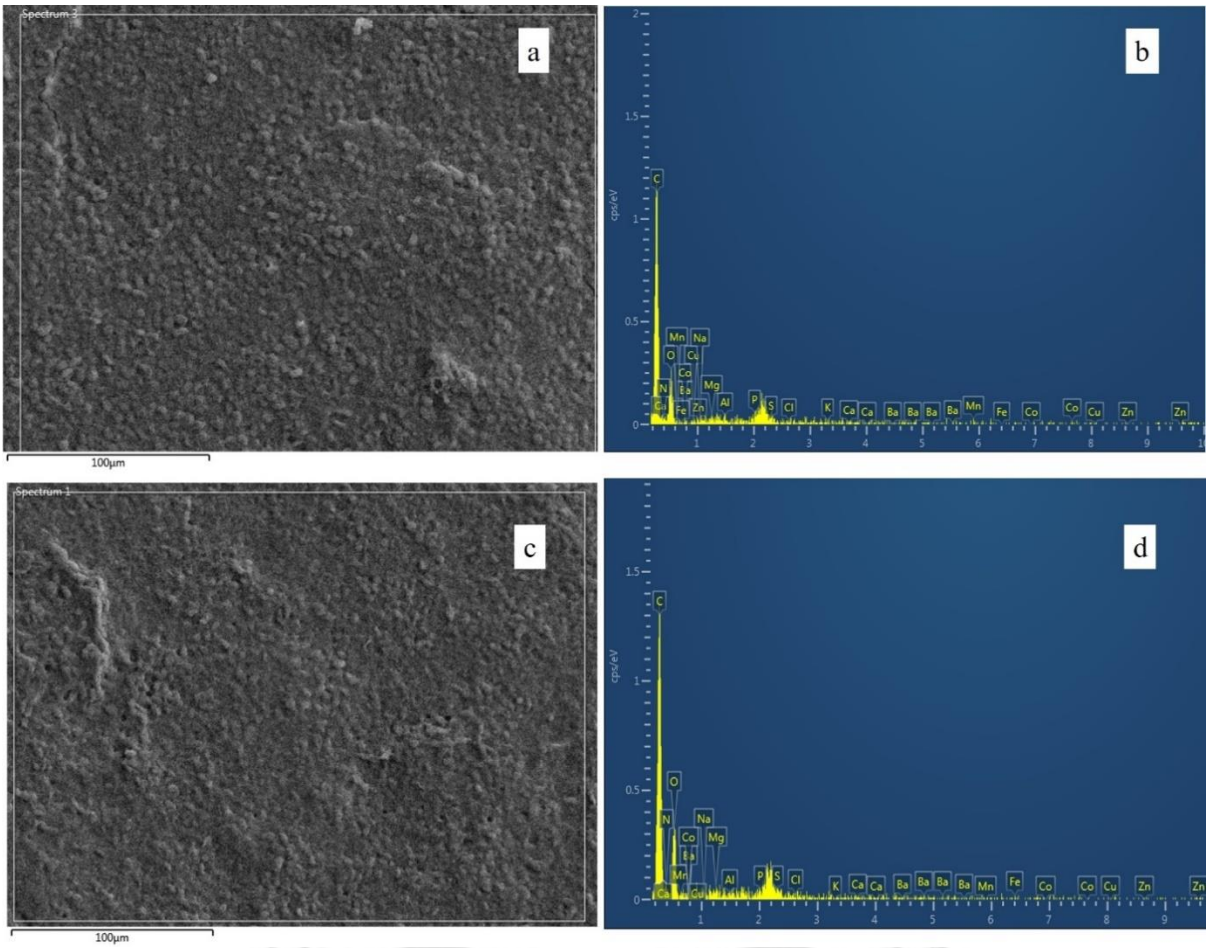

Figure 3.7. A picture of the surface of microalgae biomass by scanning electron micrographs and elemental analysis of microalgae cultivated on a) and b) SSDW; c) and d) BG11.

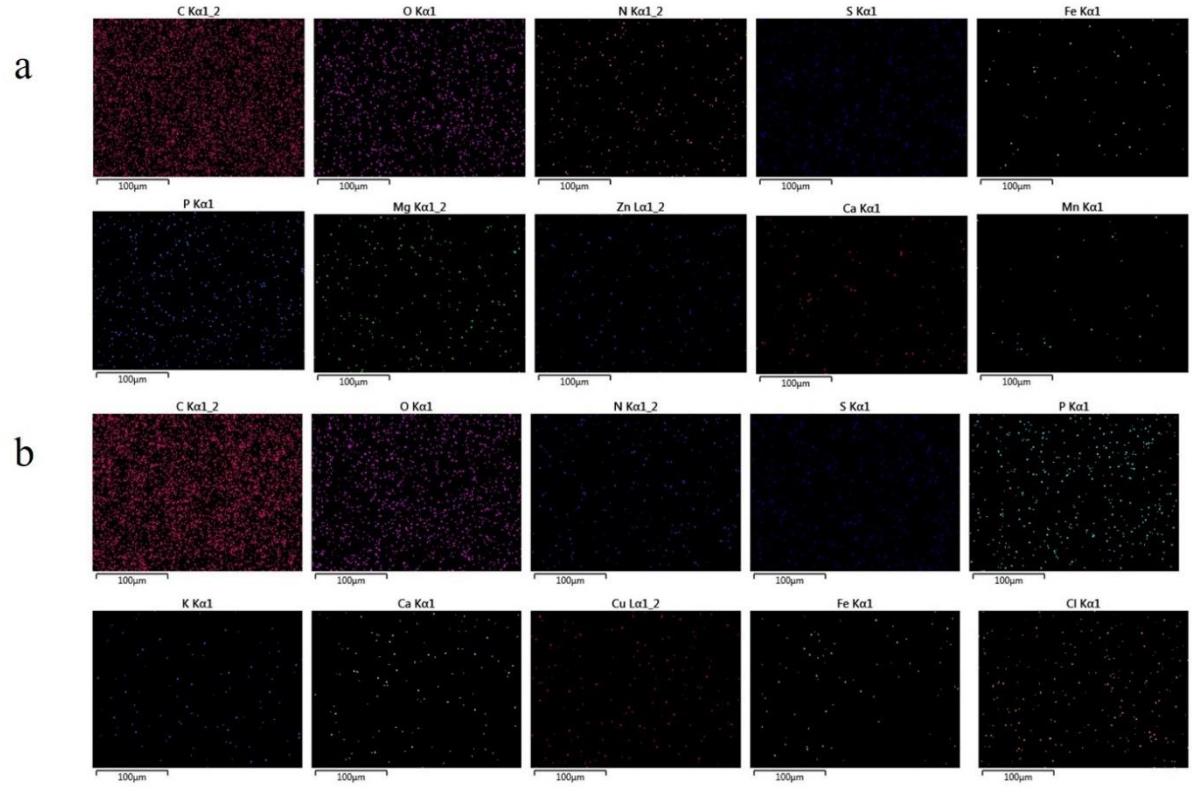

Figure 3.8. Elemental map of microalgae cultivated on a) SSDW and b) BG11.

Table 3.2. Elemental Analysis of microalgae cultivated on SSDW and BG11 on the dry basis by SEM-EDS.

Elements	SDDW (wt%)	BG11 (wt%)	Elements	SDDW (wt%)	BG11 (wt%)
C	71.0	65.7	Cu	0.2	0.8
O	20.0	22.7	Cl	0.1	0.0
N	6.1	7.7	K	0.1	0.0
S	0.6	0.4	Ca	0.1	0.2
P	0.6	0.5	Mg	0.1	0.1
Mn	0.8	0.0	Co	0.0	0.0
Al	0.3	0.0	Na	0.0	0.0
Zn	0.2	1.0	Fe	0.0	0.7

3.3.4.4. FAME profiling of KMC4 biomass

The wastewater offers a good amount of micronutrients and macronutrients for the growth of microalgae. The FAME spectra constituents varied amounts of saturated (4SFA) and unsaturated fatty acids (3USFA). The majority of the fatty acids were found to be C-16:0, C-16:1, C-18:0, C-18:1, C-18:2, and C-18:3 (Table 3.3). The results showed a relatively higher amount of palmitic acid followed by stearic acid and myristic acid in SFA class. Linolenic acid (C18:3) which constituted the major proportion of polyunsaturated fatty acid, is a vital dietary source for the human system. Oleic acid (C18:1) and Linolenic acid (C18:2) were also found in larger proportion compared to palmitoleic acid (C16:1). The oleic acid (C18:1) was reported to be good for controlling body weight and reducing the risk of coronary heart disease. Also, the intake of linoleic acid lowers the risk of cardiovascular disease and diabetes. The highest proportion of palmitic acid of saturated fatty acid was found similar to the previous study reported (Swain et al., 2020).

According to previous investigations, the presence of long-chain fatty acids (LCFA) from the different group can provide better stability during the storage of biodiesel because saturated fatty acids have poor low-temperature operation tendency. The high amount of LCFA can improve biodiesel quality under low-temperature conditions and the high cetane number obtained by long-chain SFA is related to the release of lesser NO_X emission. The fatty acids indicated for good biodiesel properties include myristic acid, palmitic acid, palmitoleic acid, stearic acid, oleic acid, and linoleic acid. The quality of biodiesel cannot be satisfied by including single fatty acid methyl ester class. The lipid derived from KMC4 contains a good amount of LCFA with a diverse class of LCFA which is promising for biodiesel stability (Patel et al., 2020).

Table 3.3. Fatty acid methyl ester profile of *Monoraphidium* sp. KMC4 cultivated in SSDW.

S.no.	Fatty acid type	Fatty acids	Peak Area (%)
1	SFA, C14:0	Myristic acid	0.18
2	SFA, C16:0	Palmitic acid	26.00
3	USFA, C16:1	Palmitoleic acid	0.16
4	SFA, C18:0	Stearic acid	1.34
5	USFA, C18:1	Oleic acid	12.93
6	USFA, C18:2	Linoleic acid	5.52
7	USFA, C18:3	Linolenic acid	17.13

3.4 Summary

Monoraphidium sp. KMC4 was cultivated in simulated synthetic dairy wastewater and a significant amount of biomass was obtained along with efficient removal of chemical oxygen demand. The maximum biomass was produced in 50% diluted SSDW and showed notable nutrient removal efficiency. Biomass derived from mixotrophic cultivation displayed a good lipid profile which offers KMC4 a promising choice for biofuel production. The proximate, elemental, biochemical, and thermal decomposition behavior of KMC4 biomass revealed its suitability as a feedstock for bio-oil production. The current study demonstrated the potential of KMC4 in treating dairy wastewater with high-value biomass production which can be utilized for biofuel production.

Chapter 4

Bio-oil Production via two-stage and direct hydrothermal liquefaction process from high-protein *Monoraphidium* sp. KMC4.

Chapter 4. Bio-oil Production via two-stage and direct hydrothermal liquefaction process from high-protein *Monoraphidium* sp. KMC4.

Graphical abstract of Chapter 4

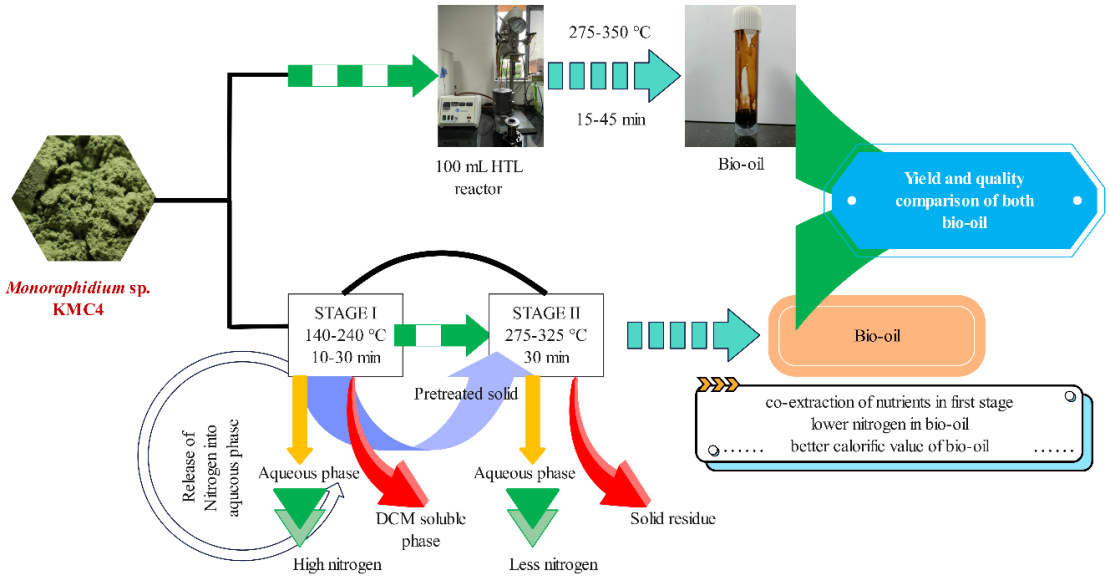

4.1 Background

Over the last several decades, the increasing use of fossil fuels, urban growth, and activities associated with modernization have led to elevated levels of greenhouse gases in the atmosphere. Researchers have turned their attention toward exploring alternative carbon-neutral renewable biomass over conventional oil reserves for the generation of green energy for the transportation industry. Given that the transportation sector was accountable for 14% of GHGs by 2010, the Intergovernmental Panel on Climate Change reported that microalgae-based drop-in fuels could replace petroleum-derived fuels (Denton et al., 2022). High temperature and high pressure in HTL are used for the conversion of biomass to generate bio-oil in HTL/DHTL (direct HTL) (Yue et al., 2018). But, the higher amount of nitrogen present in the bio-oil fraction via direct HTL is still a significant obstacle to its upgrading (Yin et al., 2023). The increase in nitrogen content substantially affects bio-oil quality, resulting in elevated viscosity, acidity, and a greater boiling point range, which brings inhibitory effects during the refining process (Gu et al., 2020b). Therefore, there is a need to lower the nitrogen in bio-oil by extracting the protein as ammonium ions into the aqueous phase (Cheng et al., 2017; Shia and Yu, 2023).

The N-based compounds in bio-oil from high-protein algae are a concern during the upgrading process; however, the removal of carbohydrates is recommended instead of protein, since the carbohydrate-derived compounds from microalgae form aromatic heterocompounds, which are more challenging to reduce during refining (Cheng et al., 2017). Also, carbohydrates contribute to the production of char precursors, which are highly aromatic compounds, irrespective of the algal species used in the reaction (Cheng et al., 2017; Shia and Yu, 2023). Also, some compounds converted from carbohydrates and proteins, such as furfural and N-based aromatic compounds in the aqueous phase, cannot be utilized by biological organisms during cultivation, limiting their potential applications (Gu et al., 2020b). Therefore, the extraction of carbohydrates and proteins species from algal feedstock is beneficial to enhance the quality of bio-oil via SHTL process (Cheng et al., 2017; Huang et al., 2018a).

The relationship between the better bio-oil quality in stage II of two-stage HTL and the effect of a varying set of pretreatment temperature/retention time in the initial stage is poorly understood. Moreover, it is necessary to understand the trade-off through mild treatment studies to generate optimized conditions between reducing nitrogen in solid residue I and its elution in aqueous phase I and maximizing the bio-oil yield when biomass is subjected to two-stage HTL. The aqueous phase obtained in the stage I process with respect to ammonium nitrogen and total nitrogen concentration will elucidate the severity of pretreatment temperature and reaction time, indicating the efficiency of algal component (protein and carbohydrate) hydrolysis.

The chapter presents a comprehensive investigation that is conducted to examine the impact of varying reaction times on the hydrolysis/pretreatment of wastewater-grown microalgae during the first stage of two-stage HTL, and its influence on the H/C ratio of the pretreated algae through a Van Krevelen diagram. Initially, different temperatures and retention time values were optimized for the partial extraction of carbohydrates and proteins, obtaining solid residue I as a feedstock for the second stage. The solid residue I obtained from stage I was continued for stage II at a higher temperature for bio-oil production (Figure 4.1). The comparison of direct and two-stage HTL was performed in this work to determine the change in elemental properties, calorific value, and compound differentiation in bio-oil.

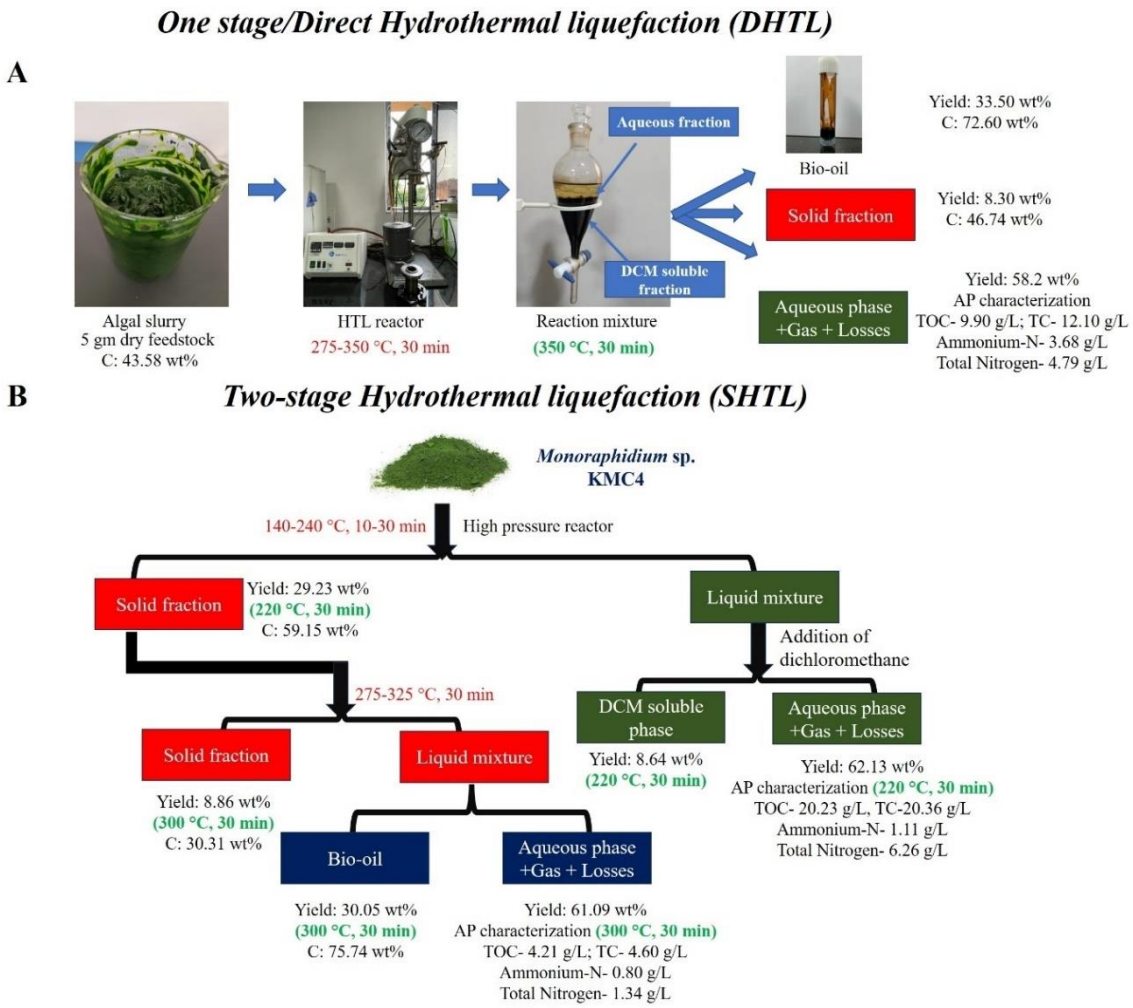

Figure 4.1. Schematic diagram of direct and two-stage hydrothermal liquefaction process.

4.2 Methodology

For direct HTL experiments, the feedstocks were used directly for high temperature reactions. For two-stage reactions, the microalgae were pretreated or hydrolyzed at lower temperature to reduce the nitrogen from feedstock, then, the dried stage I solid was used for high temperature hydrothermal reactions. The pretreated solid was characterized at optimal conditions with better H/C and low N/C ratio before proceeding for bio-oil formation at high temperature and high-pressure conditions. The bio-oil quality was assessed through GC-MS, elemental and boiling point distribution.

4.3 Results and discussion

4.3.1 Direct Hydrothermal Liquefaction

4.3.1.1 Effect of Temperature and Retention Time on HTL Product Yield

The process exhibited varying desirable temperatures, which affect the overall conversion rate, bio-oil, and solid char yield. Figure 4.2A shows the impact of the temperature on the distribution of products from the hydrothermal liquefaction of *Monoraphidium* sp. KMC4. It was evident that when the temperature increased from 275 °C to 350 °C, the bio-oil yield increased from 20.31% to 33.50%. However, the bio-oil yield started to decrease when the reaction temperature was raised above 350 °C. The decrease in bio-oil yield after an optimum temperature can be a result of the cracking of compounds present in the reaction mixture towards gas formation or the repolymerization of unstable intermediates into the water-soluble phase and solid residue. The difference in the bio-oil yield is correlated with the biochemical complexity and the composition of microalgae.

In a previous investigation, a lower temperature (230 °C) for bio-oil production (43 ± 2.0%) was found to be optimum from an algal consortium (Naaz et al., 2019). In our investigation, the solid residue yield declined progressively as the temperature was increased. During the reaction, the given temperature provided enough activation energy to break the bond of raw components, present in algae biomass, which promoted the fragmentation and degradation pathway. The endothermic process during the HTL was facilitated by the initial increase in temperature, which provided the requisite activation energy for bond breaking. Several unstable intermediates, including unstable radicals and fragmented compounds, are generated during the bond-breaking process. The exothermic characteristics of HTL is the result of the energized or unstable radicals undergoing repolymerization, which involves the creation of new bonds and the release of energy as the temperature rises (Mathanker et al., 2021).

Thus, the increasing temperature results in a change in the chemistry and yield of bio-oil. Many strains lead to better bio-oil yield with reduced or no cell wall; these characteristics enhance the accessibility of compounds present in the microalgae at milder conditions. Meanwhile, species with resistant and thick cell walls show lower bio-oil yield at milder conditions and therefore require more harsh conditions. In addition, the nitrogen content increased as the temperature was raised from 250 °C to 375 °C, which is indicative of the substantial

degradation of proteins at elevated temperatures. Also, higher temperature promotes the content of sulfur in oil, although the concentration remains less (López Barreiro et al., 2013).

The product yields and compositions are also considerably affected by the reaction time. The effect of time on the product yield at a temperature of 350 °C was also studied (Figure 4.2B). The bio-oil yield showed an increasing trend when the retention time increased from 15 min to 30 min. However, above 30 min, the yield started to decline. From this observation, it was noted that 30 min was found to be sufficient for the conversion of biomass and achieved the highest bio-oil. A remarkable increase in bio-oil yield to 33.50 wt % with an energy value of 34.14 MJ kg^{-1} was obtained at 350 °C and 30 min. This optimal condition resulted in a decreased yield of solid residue (8.30%) at a maximum conversion rate of 91.70 wt%. Longer residence times result in higher yields, but they also encourage the production of gases and heavy components that degrade the quality of bio-oil (Ocampo et al., 2023).

Sánchez-Bayo et al. (2021) discovered that 10 min was optimal for achieving the highest bio-oil yield (42.30 ± 0.80 wt %) at 320 °C (Sánchez-Bayo et al., 2021). In another study, only 5 min of duration at 375 °C led to the highest bio-oil from 8 microalgal species (López Barreiro et al., 2013). The breaking of carbon–carbon bonds of major fraction components in algal biomass results in degradation, hydrolysis, and recombination of intermediate fragments corresponding to an increase in bio-oil yield. However, prolonged duration of reaction time decreases the bio-oil yield due to the cracking of components, resulting in the formation of low molecular weight gases or repolymerization of some unstable intermediates into solid residue or water-soluble phase (Mathanker et al., 2021).

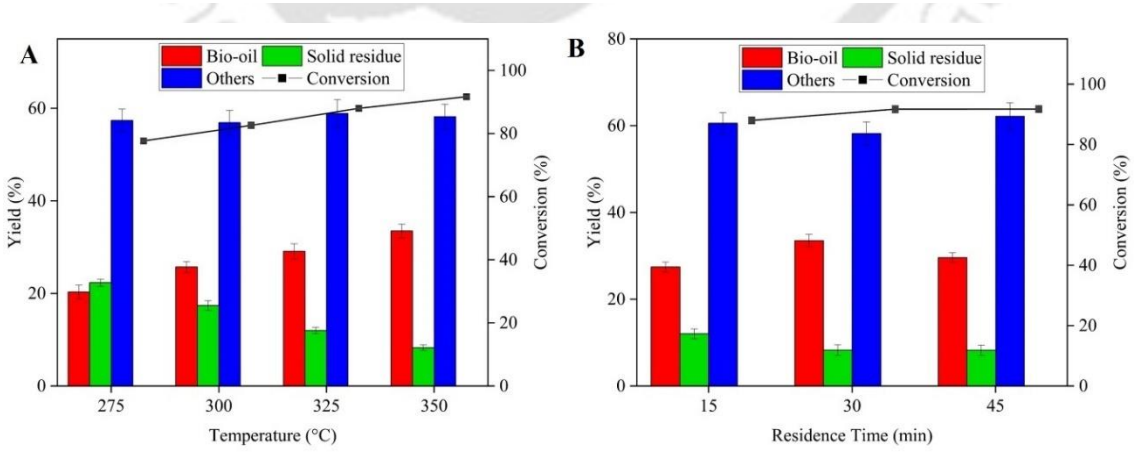

Figure 4.2. (A) Products yield profile at different reaction temperatures, (B) Products yield profile at different residence times at optimum temperature of 350 °C (direct HTL).

4.3.2 Two-Stage HTL

4.3.2.1 Product Characterization of Stage I of Two-Stage HTL

A) Characterization of Pretreated Microalgae

The stage I of the two-stage HTL process is specifically designed to separate polysaccharides and protein-based compounds from microalgae. Therefore, the selection of temperature and residence time is aimed at finding the optimal combination of temperature and time for the pretreatment of microalgae. The elemental characterization of solid yield I after stage I is given in Table 4.1. This optimal pretreatment combination initiates the hydrolysis of the complex and strong algal cell wall. The hydrothermal pretreatment performance was evaluated by varying the temperature and retention time during the reaction, and the findings are shown in Figure 4.3A and 4.3B.

Prolonging the retention time to 30 min significantly influenced the yield of pretreated algae (solid residue I), resulted in 29.23% and 27.02% at pretreatment temperatures of 220 °C and 240 °C, respectively. A reduction of only 7–10% in solid yield I was noticed when retention times were increased within the lower temperature range of 140 °C – 200 °C. However, using the range of higher temperatures (220 °C – 240 °C), the solid yield I steadily decreased. The use of rigorous pretreatment conditions resulted in a significant decrease in the solid yield I. The change in reduction efficiency of solid yield might probably be due to the heating rate or the biochemical complexity of microalgae species. There is an apparent relation between the reduction in nitrogen from algal biomass to the liquid phase and the increase in temperature from 140 °C to 240 °C.

The energy density of pretreated algae can be depicted using the Van Krevelen illustration (Figure 4.4). The carbon content increased when the temperature increased from 140 °C to 240 °C. The decrease in the N/C atomic ratio, determined by elemental investigation, suggested reduced nitrogen-based components from microalgae feedstock. The ratio of H/C was increased by increasing the pretreatment temperature. Increasing the severity of the pretreatment conditions leads to a greater reduction in the N/C ratio. The decrease in the high heating value of pretreated microalgae was due to the release of carbohydrate and protein-based components from them compared to raw algae feedstock biomass. The hydrothermal treatment of dry algal feedstock leads to an increase in C content with decreasing N and O content on increasing temperature or reaction time, due to the selective removal of carbohydrates and proteins (Bondurant et al., 2023).

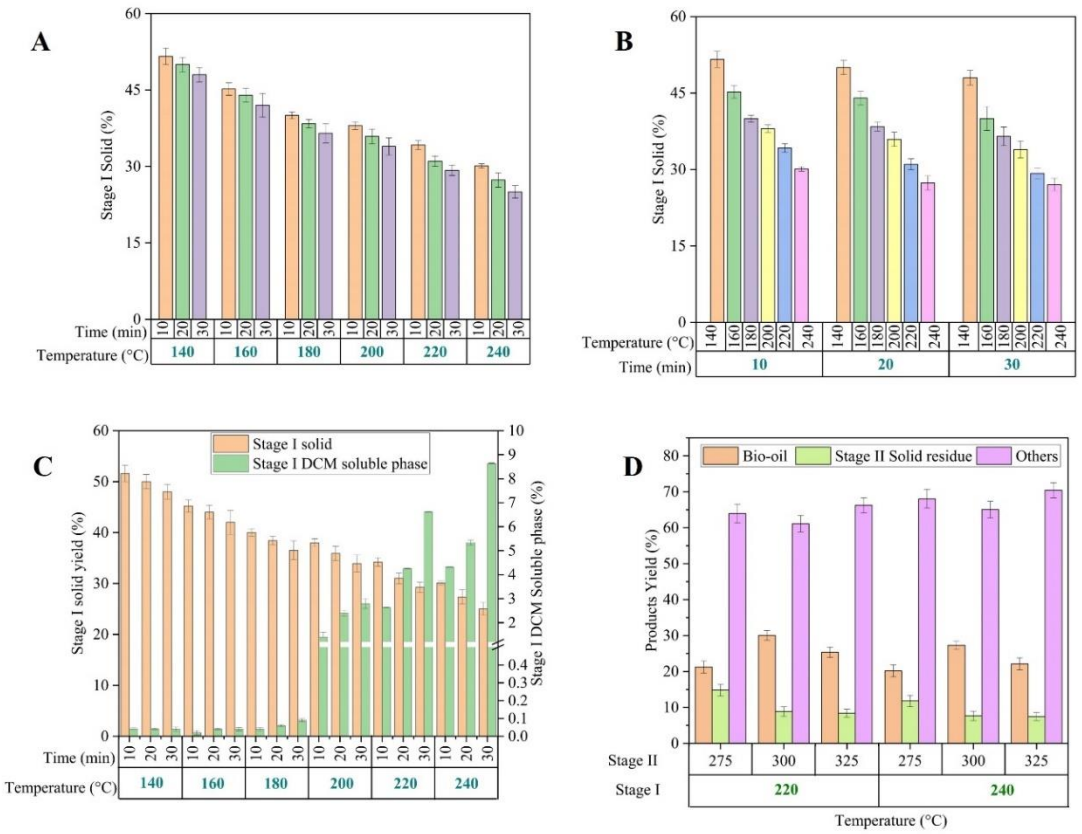

Figure 4.3. Products profile from hydrothermal liquefaction of microalgae (A) and (B) Solid yield after stage I of two-stage HTL, (C) Production of DCM soluble phase after stage I of two-stage HTL, (D) Bio-oil yield from pretreated microalgae at higher temperature.

Table 4.1. Elemental composition of Stage I solids.

Residence time (min)	Temperature (°C)	C%	H%	N%	H/C (mol/mol)	N/C (mol/mol)
30	140	50.42	5.42	7.43	1.28	0.12
30	160	53.02	5.01	6.31	1.13	0.10
30	180	53.98	6.12	5.32	1.36	0.08
30	200	56.24	7.32	4.10	1.56	0.06
30	220	59.15	8.02	3.64	1.62	0.05
30	240	64.56	8.70	3.41	1.61	0.04
Raw KMC4	NA	43.58	6.73	8.70	1.86	0.17

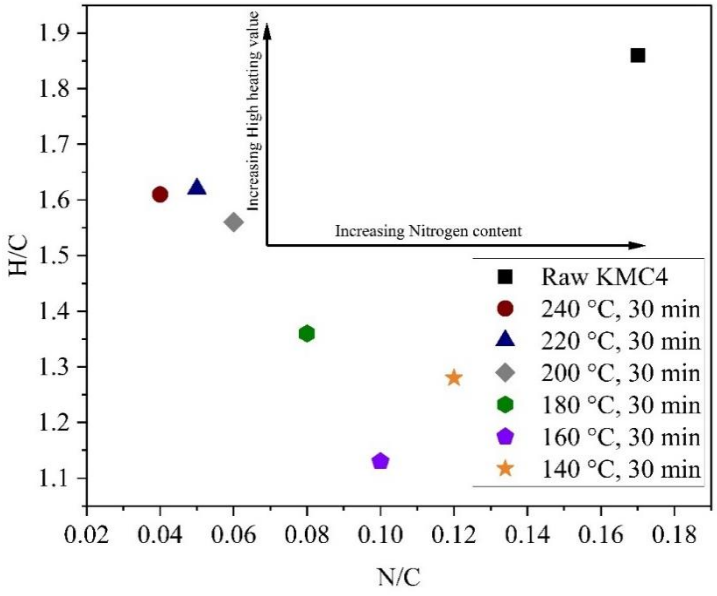

Figure 4.4. Van Krevelen diagram of solid residue I from the first stage of two-stage HTL.

Initially, at a lower temperature (140 °C), a nominal decrease in the nitrogen content during pretreatment from microalgae feedstock was noted, while a significant reduction in nitrogen amount was observed at higher pretreatment temperatures (>200 °C). There was a 76.47% decrease in the N/C ratio from algae feedstock to solid residue I at 240 °C, which was almost 2.5 times higher than that at a lower pretreatment temperature (calculated from Table). The decrease in solid yield I was majorly due to the removal of some component fraction from algal biomass into the aqueous phase during the reaction. The lower pretreatment temperature was found to be insufficient to break the bond in proteins to promote the breakdown of amino acids from biomass.

But, at higher temperatures, the breakage of peptides was enhanced due to the attainment of the same bond energy to break N≡C bonds, which resulted in the reduction of solid yield I. The temperature should be high enough to break carbon–nitrogen and carbon–oxygen bonds during hydrolysis (Bondurant et al., 2023). As a result, the pretreated algae showed a drop in the solid yield as the pretreatment temperature increased. The increment in carbon content in solid residue I was achieved at a higher pretreatment temperature as a result of the carbonization of feedstock biomass (Huang et al., 2018a). Also, the pretreatment temperature above 200 °C produced a dichloromethane-soluble phase, which corresponded to the formation of oil-based compounds. The reaction was not conducted above 240 °C, as the bio-oil formation increased significantly at this pretreatment temperature, resulting in a lower solid yield and lower nitrogen extraction in aqueous phase.

The decline in the pretreated algal yield in the first stage was mostly caused by the rupture of the algal cells, which resulted in the hydrolysis of extracted proteins and carbohydrates from the biomass into the water phase. A lower temperature (below 200 °C) was insufficient to disrupt the cells for nitrogen removal, which can be correlated with the total nitrogen in the aqueous phase at a corresponding pretreatment temperature. At higher temperatures, the acid-catalyzed hydrolysis of the peptides improves. As a result, the pretreated algal yield dropped as the temperature of the pretreatment increased.

B) Characterization of First-Stage Aqueous Phase

The total organic carbon (TOC) of the first stage aqueous phase was analyzed by using a TOC analyzer to estimate and correlate the extraction of organic compounds (Table 4.2). The aqueous phase TOC exhibited an upward trend with rising pretreatment temperatures. At 140 °C, the TOC of the aqueous phase was 1.6 g L^{-1}, while it increased to 22.21 g L^{-1} at 240 °C. The significant TOC concentration of the higher temperature aqueous phase was due to the major extraction of water-soluble compounds from microalgae. The rise in the value was due to the release of major components from microalgae into the water-soluble phase.

The pH of the aqueous phase ranged from neutral to slightly alkaline (7.51 to 8.03). The color of the aqueous phase was initially green at lower pretreatment temperatures, but it changed to dark brown on increasing the temperature to 240 °C. This might be because of reactions that took place between the sugar and amino acids to form compounds like melanoidins in the water phase (Minowa et al., 2004).

The total nitrogen also increased from 1.15 g L^{-1} to 6.81 g L^{-1} when the temperature was increased from 140 °C to 240 °C due to more hydrolysis of algae biomass at extreme temperatures (Figure 4.5). The insignificant difference of total nitrogen in the aqueous phase obtained between 220 °C and 240 °C could be due to the formation of a small amount of dichloromethane soluble phase (which can be called bio-oil after solvent evaporation) at pretreatment temperatures, which can be related to the passing of some N-based compounds to the DCM soluble phase at the first stage. The high carbon content of the aqueous phase after stage I results in high energy density, which expands the application toward microalgae cultivation.

Table 4.2. Characterization of aqueous phase from hydrothermal liquefaction of microalgae.

Temperature (°C)	Retention time (min)	TOC (g/L)	pH
140	30	1.6	8.03
160	30	2.91	7.51
180	30	17.06	7.75
200	30	18.74	7.95
220	30	20.23	8.02
240	30	22.21	8.01

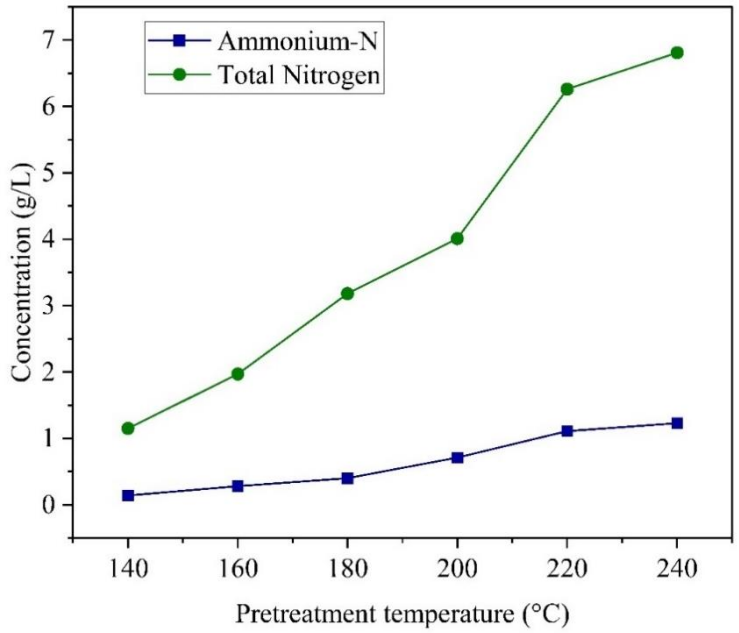

Figure 4.5. Total nitrogen and ammonium nitrogen of aqueous phase from the first stage of two-stage HTL.

4.3.3. Bio-Oil from Pretreated Microalgae from Stage I

The pretreated algae were hydrothermally treated at high temperatures and pressures for bio-oil production. Figure 4.3D shows the impact of the pretreatment parameters on the yield of bio-oil or other products. The change in the pretreatment temperature has a clear correlation with the reformation of biomass to bio-oil. The 180 °C pretreated microalgae resulted in the highest bio-oil (32.56 wt%) at 350 °C than at 325 °C (29.01 wt%). While the biomass pretreated at 200 °C recorded a decline in bio-oil yield at 350 °C (26.41 wt%) and a maximum at 325 °C (31.05 wt%) (Figure 4.6). The decrease in some valuable compounds during the pretreatment

at 200 °C resulted in a reduction of protein and carbohydrate fractions from algal biomass, which might have decreased the bio-oil yield at 350 °C.

A maximum temperature of 350 °C is required to produce bio-oil from pretreated microalgae (temperature <200 °C). The requirement of higher temperatures for bio-oil production from lower temperatures pretreated microalgae (solid residue I) could be due to the demand for high activation energy for breaking the N≡C bond. The mild hydrothermal pretreatment conditions partially solubilize the biomass, resulting in the formation of a solid that generates bio-oil under more severe conditions (Jazrawi et al., 2015). The protein present in the algae pretreated at lower temperatures requires higher temperatures for generating the N-based compounds, which increases the yield of bio-oil overall (Cheng et al., 2017). Also, the bio-oil yield from pretreated algae at 220 °C showed an increasing trend from 275 °C to 300 °C for 30 min, with the maximum yield at 300 °C (30.05 wt%). At 325 °C, the algae pretreated at 220 °C exhibited a declining profile in bio-oil yield (25.36 wt%) (Figure 4.3D).

The lower temperature used in the bio-oil formation process promotes the degradation of components present in the pretreated algae to form bio-oil, but a further increment beyond the optimum temperature causes an increase in secondary cracking of some compounds present in the bio-oil, which leads to the formation of more gaseous products. The bio-oil yield at 300 °C was lower (27.30 wt%) from pretreated microalgae at 240 °C compared with pretreated microalgae at 220 °C (30.05 wt%). This can be due to the significant dichloromethane soluble phase (8.64 wt%) recovered at higher pretreatment temperature (240 °C) in stage I of two-stage HTL, which gives low bio-oil yield at higher temperature 300 °C (Figure 4.3 C and D).

Huang et al. (2018) noticed that the production of bio-oil was enhanced at lower pretreatment temperature conditions but reduced with rigid pretreatment conditions (higher temperature). The observed response may be attributed to the difference in the algal composition at lower pretreatment temperatures, leading to an increased internal surface area of the algae. Consequently, this facilitates more water accessibility during the hydrothermal liquefaction process (Huang et al., 2018a). The total bio-oil yield from two-stage HTL of KMC4 microalgae was 36.67 wt% (combining first- and second-stage bio-oil) under stage I conditions of 220 °C and 30 min, and stage II conditions of 300 °C and 30 min. Moreover, when stage I conditions were raised to 240 °C (while keeping stage II at 300 °C for 30 min), the total bio-oil yield was lowered to 35.94 wt%. These results confirmed that higher pretreatment conditions do not reduce the bio-oil yield when considering the combined yield from both stages.

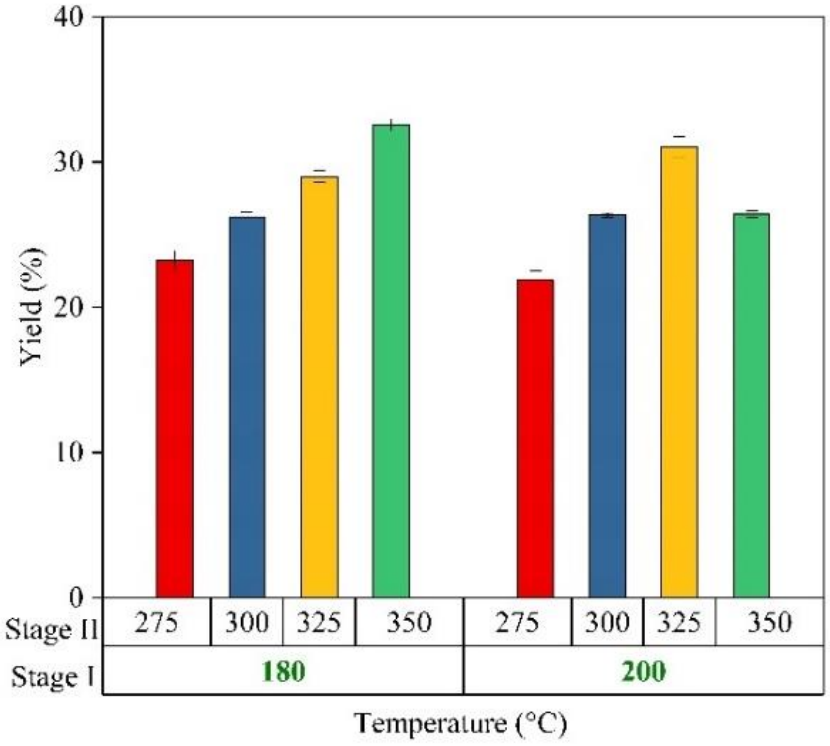

Figure 4.6. Bio-oil yield from lower pretreated microalgae solid at a higher temperature.

4.3.4. Bio-Oil Characterization

4.3.4.1. GC–MS Analysis

The bio-oil composition was characterized by GC-MS, and the compounds were confirmed using the NIST library (Table A.1 in Appendix). The bio-oil obtained from direct hydrothermal liquefaction contained a complex mixture of compounds with different classes, which majorly include hydrocarbons (48.07%), esters (16.50%), N and O-based compounds (13.36%), phenols and their derivatives (6.48%), other alcohols (2.55%), and a few other compounds (Figure 4.7). The compounds in bio-oil from DHTL comprised the range of C10–C28. The lipids in microalgae under hydrothermal conditions are hydrolyzed at lower temperatures (~200 °C) to glycerol and fatty acids. The major fractions in bio-oil were hydrocarbons obtained from the decarboxylation of fatty acids (Gai et al., 2015b; Liu et al., 2022). The hydrocarbons obtained in these reactions consist of compounds ranging from carbon number 9 to 20, which include both light and heavy compounds. The major hydrocarbons (>1%) include eicosane, 1-nonadecene, hexadecane, 9-octadecene,(*E*)-, dodecane, 2,6,11-trimethyl-, 1-dodecene, and heptadecane (Gai et al., 2015b). Briefly, the fatty acids react with alcohols to

generate esters (Gai et al., 2015b) (>1%), with hexadecanoic acid, methyl ester, butyl(2,4-dichlorophenoxy)acetate, dibutyl phthalate, and dimethyl phthalate.

Besides all the above reactions, the hydroxyl group in fatty acid can react with ammonium ions to produce aliphatic amine compounds via deamination of amino acids, namely, hexadecanamide, (2*RS*)-*N*,*N*-diethyl-2-(1-naphthyloxy)propanamide, arachidamide, *N*-ethyl-, arachidamide, *N*-3-methylbutyl-. Hexadecanamide is formed when hexadecenoic acid reacts with ammonia under high temperature and pressure conditions (Gai et al., 2015b; Liu et al., 2022). A similar type of amide was reported by Liu et al. (2022) from HTL of *Spirulina*, which is the product of cyclodimerization of amino acids and fatty acids (Liu et al., 2022). The degradation pathway of protein in microalgae biomass is difficult to predict. Generally, the amino acids follow decarboxylation and deamination reactions simultaneously under hydrothermal treatment. The dominating reaction of protein degradation will depend on the type of amino acid present in the biomass. Compounds such as asparagine and glutamine can deaminate easily.

Also, the amino acid reacts with cyclic oxygenates to form pyrazines, pyrroles, indoles, and quinolines derivatives compounds via thermal decomposition of proteins, (Garcia Alba et al., 2012; Liu et al., 2022) such as methyl *N*-[2-[[1-(4-chlorophenyl)pyrazol-3-yl]oxymethyl]phenyl]-*N*-methoxycarbamate, 4-piperidinone, 2,2,6,6-tetramethyl-, oxime and 4-piperidinone, 2,2,6,6-tetramethyl-, observed in our work. The amides, amines, nitriles, and N and O cyclic compounds, i.e., C═O and C–N functional group compounds, were categorized as N- and O-based compounds.

The bio-oil from direct HTL had a significant number of nitrogen-based compounds (13.36%), which are formed due to the intermediate repolymerization of lipid–protein or carbohydrate–protein breakdown products. The high concentration of N and O in the bio-oil is unsuitable for mixing with crude oil during refining. The reduction of nitrogen from bio-oil requires catalytic upgrading to achieve fuel quality (Shakya et al., 2017). The bio-oil produced from a two-stage HTL resulted in decreased hydrocarbons (43.56%) and increased esters (29.38%). The nitrogen-based compounds, i.e., amides, amines, and heterocyclic forms, were significantly reduced in this process. The area percentage declined from 13.36% in direct hydrothermal liquefaction to 1.98% in two-stage hydrothermal liquefaction. The formation of nitrogenous heterocyclic compounds resulted from the Maillard reaction between amino acids (from protein) and sugars (from carbohydrates) (Aljabri et al., 2022; He et al., 2020). The Maillard

reaction enhanced the production of bio-oil and led to a higher nitrogen content. Additionally, elevated temperatures promote the progression of this reaction.

Simultaneously, the proteins amino acids undergo cyclodimerization by hydrolysis, resulting in the formation of cyclodipeptides. The cyclodipeptides mostly consist of piperazinediones and pyrrolo-pyrazinediones (Liu et al., 2022). In the current investigation, the decrease in nitrogen content during two-stage HTL was attributed to the release of nitrogen-based components into the aqueous phase during pretreatment, which might have decreased the formation of pyrrole- and indole-based compounds.

Interestingly, the proportion of ketone, ether, and aldehyde classes were increased in two-stage HTL compared to direct HTL. It has been previously noted that glycerol, when separated from fatty acids during the process, can be transformed into aldehydes, ketones, and long-chain hydrocarbons (He et al., 2020). In the direct HTL process, the high temperature reactions can crack long-chain fatty acids into hydrocarbons. While in two-stage HTL, partial lipid breakdown in stage I and recombination in stage II may have promoted ester formation instead of cracking to hydrocarbon. This can also be confirmed by the presence of higher alcohols in stage II bio-oil compared to the direct HTL process.

Bio-oil was also found to be composed of phenol and its derivatives in small amounts, which is derived from the degradation of carbohydrate-based compounds, suggesting a less toxic nature (acidity) of bio-oil. The glucose and fructose sugars in microalgae are initially converted to furan-based intermediates and then to phenol through rearrangement (Gai et al., 2015b; Obeid et al., 2020).

Overall, the bio-oil derived by HTL from pretreated algae, i.e., two-stage HTL, exhibited improved quality, characterized by decreased levels of N- and O-heterocyclic compounds and higher hydrocarbon content. The practical implementation of bio-oil in the biofuel industry can be ascribed to the availability of these valuable compounds. This indicates that the hydrothermal pretreatment of algae is viable for improving the quality of bio-oil. Therefore, it can be inferred that using hydrothermal pretreatment in a hydrothermal reaction process is a better strategy for enhancing the bio-oil quality from low-lipid microalgae.

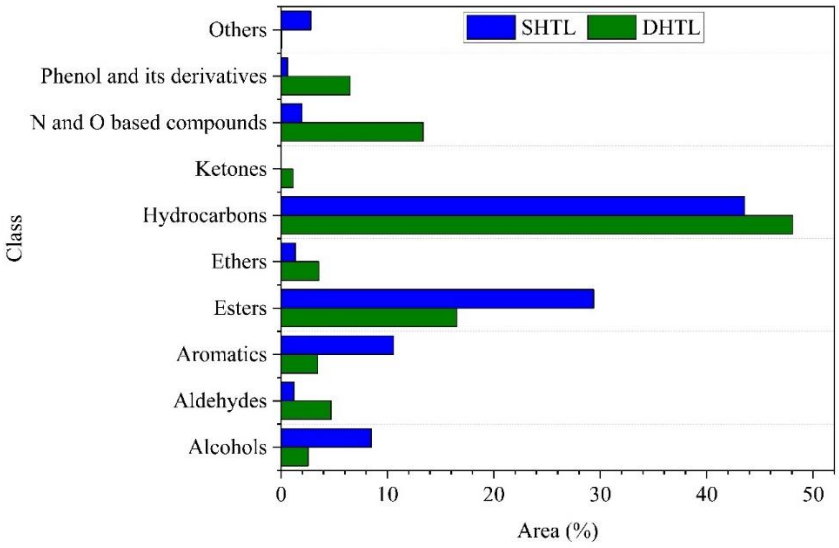

Figure 4.7. GC–MS analysis of the bio-oils obtained from direct HTL (untreated) and two stage HTL (pretreated algae).

4.3.4.2 Boiling point distribution

Boiling point distribution of bio-oils was employed to ascertain the fractions of bio-oil obtained from both processes. By incrementally heating the sample and quantifying the residual mass as the temperature rises in an inert condition, it can be determined the proportions of bio-oil corresponding to various petroleum-like fraction, heavy naphtha, kerosene, gas oil, vacuum gas oil, and vacuum residue. The distillation curves for bio-oils generated by direct hydrothermal liquefaction (DHTL) and two-stage hydrothermal liquefaction (SHTL) exhibited distinct variations in volatility and content (Figure 4.8).

The bio-oil from SHTL exhibits a significantly more pronounced mass reduction at lower temperatures, suggesting a greater concentration of light, low-boiling components. This indicates that a greater portion of the sample evaporates at lower temperature, resulting in enhanced yields of heavy naphtha, kerosene, and lighter gas-oil fractions. Hydrocarbons are predominant components of heavy naphtha and kerosene found in both bio-oil. Esters are not classified as petroleum-derived naphtha or kerosene fractions. Esters are found in SHTL bio-oil, resembling molecules in naphtha-range fuels due to their volatility and moderate boiling points.

Conversely, the DHTL bio-oil thermal stability curve has a more gradual decline, indicating that its constituents vaporize over a wide temperature range. This behaviour is characteristic of denser bio-oils that comprise a wide range of compounds which having large range of boiling

points or thermally stable compounds, can be due to more nitrogenous heterocyclic compounds. However, a large vac residue remains in SHTL bio-oil compared to DHTL illustrates that bio-oil from former one also constitutes compounds which are thermally stable or having high boiling points. Still, highest amount of lower boiling points compounds in SHTL bio-oil suggests that it has better fuel properties and can be feasible for biofuel applications.

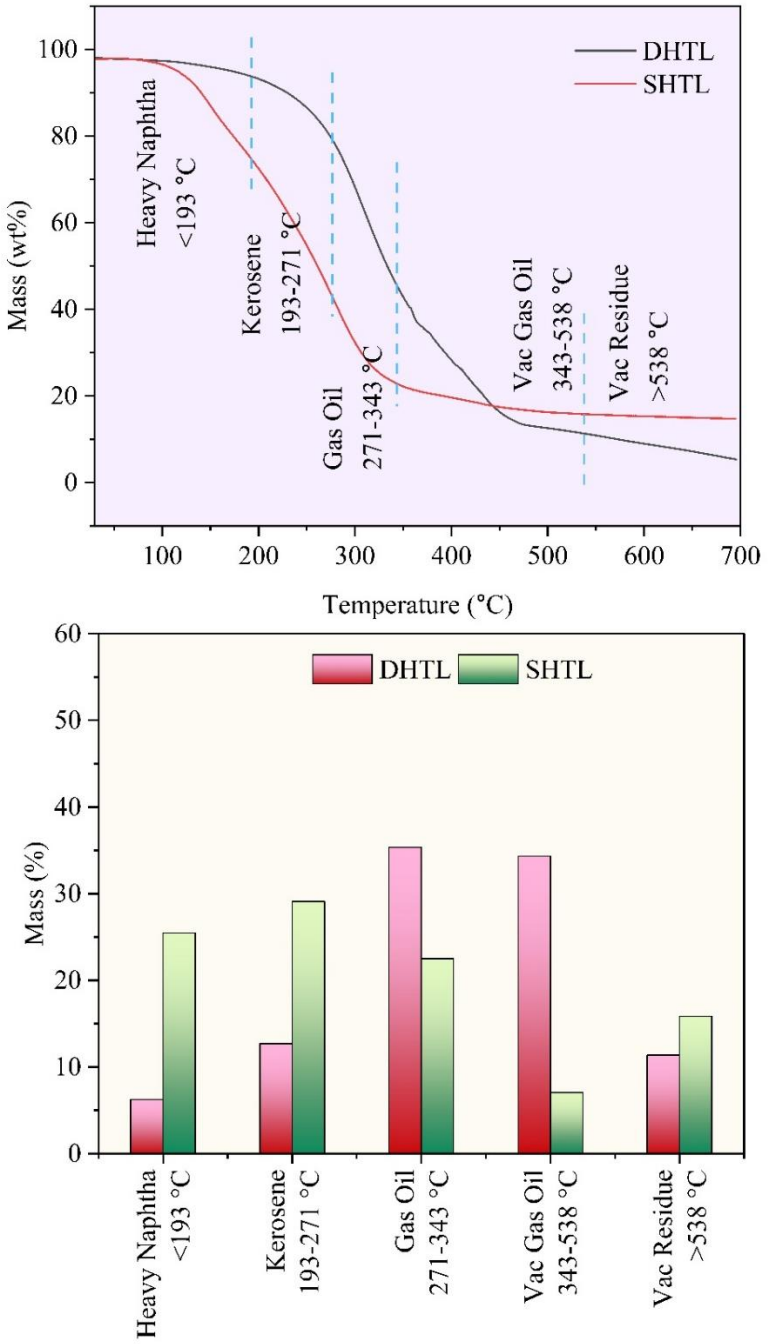

Figure 4.8. Thermal degradation curve and boiling point distribution of the bio-oils obtained by DHTL and SHTL.

4.3.4.3. Elemental Composition

The elemental compositions of bio-oils produced via both direct and two-stage HTL are given in Table 4.3. The direct HTL bio-oil consisted of 72.60% carbon, 8.24% hydrogen, 4.60% nitrogen, 13.69% oxygen, and 0.87% sulfur. However, the nitrogen in bio-oil generated from stage II via two-stage HTL using pretreated microalgae (200 °C) was lower. This can be due to a notable decrease in the nitrogen content during pretreatment from biomass to the aqueous phase. These pretreated microalgae were used for bio-oil production in the second stage of two-stage HTL. The bio-oil obtained from two-stage HTL with stage II conditions of 300 °C and 30 min reaction time was composed of lower nitrogen content (2.88%) and high carbon (75.74%) and hydrogen content (9.17%).

A reduction of 37.39% in nitrogen was observed from direct HTL bio-oil when compared to two-stage HTL bio-oil (pretreated solid 220 °C, 30 min and bio-oil conditions: 300 °C, 30 min). Due to the significant amount of protein fraction that is extracted from the microalgae during the various pretreatment conditions, the heteroatom concentration in bio-oil from two-stage HTL is reduced (Huang et al., 2018a). In conclusion, the hydrothermal pretreatment is advantageous in reducing nitrogen from the bio-oil.

The atomic composition of bio-oil produced from both processes can be depicted using the Van Krevelen illustration (Figure 4.9). The H/C of bio-oil derived via two-stage HTL was higher than that of DHTL bio-oil. Meanwhile, the N/C of both bio-oils from two-stage HTL was comparably lower than DHTL bio-oil. Deamination, dehydration, and decarboxylation processes enhanced the C and H amounts of the bio-oil while decreasing the nitrogen level, giving high-HHV bio-oils. The decrement of N/O in two-stage HTL bio-oil reflects the lower abundance of nitrogen- and oxygen-containing compounds. This gives insights into fewer nitrogenous aromatics and heterocyclic compounds, which require less denitrogenation in further upgradation processing. However, the O and N levels were still higher than those of petroleum-based products (Huang et al., 2018a).

The bio-oil generated through DHTL showed a calorific value of 34.14 MJ kg^{-1} with a 61.82% energy yield. Meanwhile, the SHTL process remarkably increased the energy yield (69.59 wt %) and HHV value of bio-oil (37.34 MJ kg^{-1}). Table 4.4 presents a structured benchmarking of two-stage hydrothermal liquefaction (HTL) process against previous literature.

Table 4.3. Elemental composition of bio-oils obtained from direct and two-stage HTL.

Residence time (min)	DHTL	SHTL	SHTL
Pretreatment conditions	NA	220 °C, 30 min	240 °C, 30 min
Bio-oil production conditions	350 °C, 30 min	300 °C, 30 min	300 °C, 30 min
C %	72.6	75.74	75.72
H%	8.24	9.17	9.14
N %	4.6	2.88	2.85
O%	13.69	11.98	11.08
S%	0.87	0.23	0.21
N/C (mol/mol)	0.05	0.03	0.03
H/C (mol/mol)	1.36	1.45	1.44
O/C (mol/mol)	0.14	0.13	0.13
N/O (mol/mol)	0.37	0.26	0.28
HHV (MJ/Kg)	34.14	37.34	-

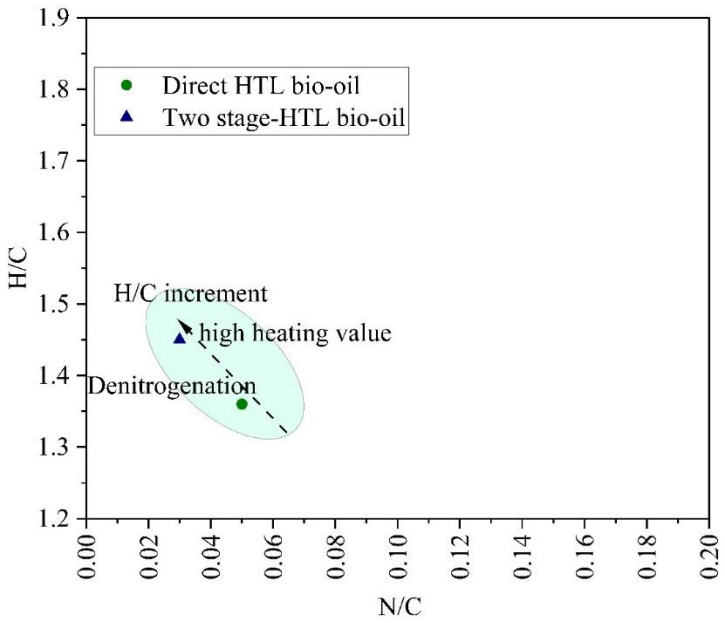

Figure 4.9. Van krevelen diagram of bio-oil obtained from DHTL and two-stage HTL.

Table 4.4. Literature comparison of the microalgae two-stage HTL process.

Feedstock	Pretreatment conditions	Bio-oil production conditions	Bio-oil Yield (%)	C (%)	H (%)	N (%)	HHV (MJ/ Kg)	References
Scenedesmus/ Desmodesmus spp.	260 °C for 30 min	360 °C for 72 h	-	-	-	(1.3 ± 0.0	-	(Bondurant et al., 2023)
Chlorella vulgaris	150 °C for 15 min	350 °C for 10 min	32.0	70.70	9.10	6.40		(Jazrawi et al., 2015)
Spirulina	225 °C for 10 min	340 °C for 120 min	34.34	70.01	9.71	5.71	34.90	(Huang et al., 2018a)
Spirulina	225 °C for 50 min	340 °C for 120 min	26.55	73.62	10.09	4.18	37.10	(Huang et al., 2018a)
Monoraphidium sp. KMC4	220 °C for 30 min	300 °C for 30 min	36.67	75.74	9.17	2.88	37.34	Present work

4.3.4.4. FTIR Analysis

The Fourier transform infrared spectra were studied to analyze the functional groups in the bio-oils (Figure 4.10). The wide absorption band seen between 3300 cm^{-1} and 3100 cm^{-1} was assigned to the O–H/N–H stretching. The reduced intensity of bands in bio-oil from pretreated algae was in agreement with the N and O content. The bio-oil obtained from pretreated algae exhibited intensified absorption bands ranging from 2971 to 2800 cm^{-1}. These bands can be related to the symmetrical and asymmetrical aliphatic C–H stretching, which are common in fatty acids and hydrocarbons. The C═O stretching presence confirmed the presence of esters, ketones, aldehydes, and acids between 1700 cm^{-1} and 1650 cm^{-1} (Gai et al., 2014). Furthermore, peaks at 1467 cm^{-1} and 1370 cm^{-1} were evident in the spectra and ascribed to the methyl and methylene groups, respectively.

The observation of an absorption peak between 800 cm^{-1} and 600 cm^{-1} validated the availability of aromatics with C–H bending. The complementary absorption regions observed in the spectrum of both bio-oils indicated the presence of similar functional groups. The decrease in heteroatom content has resulted in improved bio-oil quality, and similar findings have been documented in the present investigation. Results from Huang et al. (2018) work on

hydrothermal liquefaction of pretreated microalgae also support this finding (Huang et al., 2018a). Therefore, a two-stage HTL can be utilized to enhance the bio-oil quality.

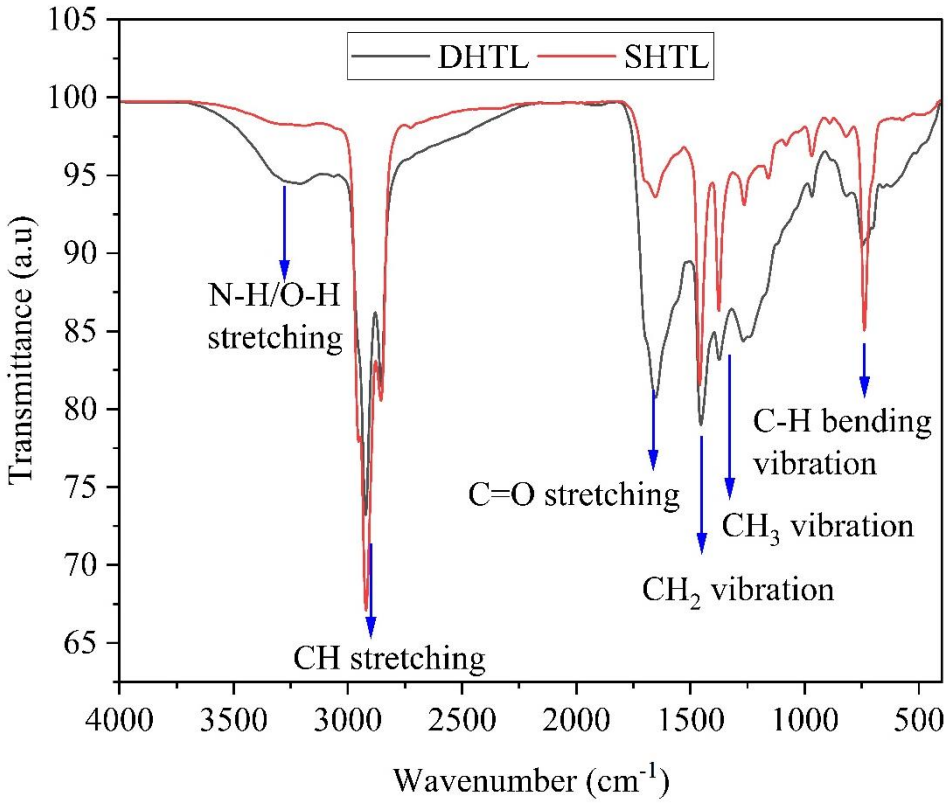

Figure 4.10. FT-IR spectra of the bio-oils produced by direct and two-stage HTL.

4.3.5 Comparison of Other Products Obtained from Direct HTL and the Second Stage of Two-Stage HTL

The aqueous phase derived from both processes was characterized to understand the reaction mechanism and its future applicability. The aqueous phase from direct hydrothermal liquefaction has an alkaline pH of 8.97, which can be due to phosphate and ammonium-N from hydrolysis and deamination reactions under high temperature and pressure conditions. The total nitrogen (4.79 g/L) and ammonium-N (3.68 g/L) were extremely high in the DHTL aqueous phase.

The aqueous phase obtained from the HTL reaction at 300 °C of pretreated microalgae (220 °C) was determined to have a low alkaline pH of 8.04, attributed to the reduced N content of pretreated microalgae biomass and fewer deamination reactions. The validation can be confirmed by examining the nitrogen levels present in the sample, specifically the amounts of

ammonium nitrogen (0.80 g/L) and total nitrogen (1.34 g/L), which were significantly less than the level found in the DHTL aqueous phase (Figure 4.11).

The concentration of phosphate in the stage II aqueous phase of two-stage HTL was 0.11 g L^{-1}, attributed to the transfer of organophosphates to the aqueous phase. Concentrations of TOC (9.90 g/L) and total carbon (12.10 g/L) of the DHTL aqueous phase were higher than those from stage II of two-stage HTL (300 °C with pretreated microalgae of 220 °C) (4.21 g/L TOC and 4.60 g/L total carbon). The removal of protein extractives during the initial pretreatment stage of two-stage HTL reduced the amount of total nitrogen and ammonium nitrogen in the second stage aqueous phase.

The solid residue obtained from DHTL consisted of carbon (46.74 wt%), hydrogen (6.34 wt%), nitrogen (3.12 wt%), and sulfur (0.17 wt%). Meanwhile, the solid residue obtained from the stage II via two-stage HTL has a comparative amount of carbon (30.31 wt%), hydrogen (6.03 wt%), nitrogen (2.06 wt%), and sulfur (0.02 wt%). Also, the HHV value of solid residue obtained from the second stage of two-stage HTL (13.33 MJ/kg) is less compared to DHTL biochar (17.64 MJ/kg). The solid residue or biochar can be also used in other applications such as adsorption (Ponnusamy et al., 2020), wastewater treatment (Law et al., 2022; Ponnusamy et al., 2020), catalyst for energy generation (Wang et al., 2021), and in anaerobic digestion as a carbon supplement and buffer (Chen et al., 2018; Ponnusamy et al., 2020).

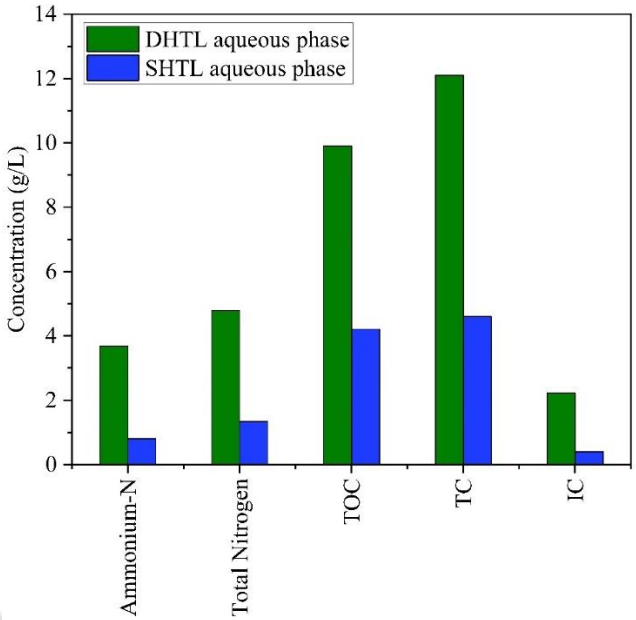

Figure 4.11. Aqueous phase characterisation obtained from both DHTL and SHTL processes. TOC represents total organic carbon, TC represents total carbon and IC represents inorganic carbon of aqueous phase.

4.3.6 Basic Hypothetical Pathway Involved in Direct and Two-Stage HTL

The reaction in hydrothermal liquefaction is a superimposition of many decomposition and recombination reactions (Figure 4.12A). The three macroconstituents of microalgae, carbohydrates, protein, and lipids, are involved in the formation of bio-oil compounds. Initially, the polysaccharides and polypeptides of carbohydrates and protein, respectively, are formed after reacting with water at higher temperatures and pressures. The carbohydrate component of microalgae breaks down into monosaccharide sugars, including glucose and xylose, the 6-carbon sugar, in major amounts. Further, the 5-Hydroxymethylfurfural, acetic acid, fructose, gases, and char are produced as a result of the sequential breakdown of glucose (Hietala and Savage, 2021; Shia and Yu, 2023). The smaller polysaccharides can polymerize into insoluble biochar or can be further broken down into other small saccharides. Also, these reactions are reversible, and the insoluble biochar can be hydrolyzed back to small polysaccharides. Saccharides undergo retro-aldol condensation reactions to form aldehydes, ketones, and some furan derivatives, which can be partitioned in the aqueous phase and bio-oil.

During lower temperature conditions, proteins are also hydrolyzed into polypeptides, followed by decomposition to peptides, which are further degraded to amino acids. The amino acids further undergo deamination and decarboxylation reactions (Hietala and Savage, 2021). For

proteins, amino acid peptide cyclodehydration, and Maillard reaction are responsible for the formation of piperazine, pyrroles, and indole-based products in bio-oil (Hietala and Savage, 2021; Liu et al., 2022; Shia and Yu, 2023). Piperidines are synthesized above 300 °C, and higher temperatures facilitate the generation of piperidines. These were mostly formed by the process of lysine undergoing deamination and decarboxylation. A 7.44% to 8.17% of indoles or quinolines were formed between 300 °C – 340 °C from *Spirulina* (Liu et al., 2022).

The formation of pyrrolidine is achieved by the decarboxylation of a proteinogenic amino acid and proline. The amino acids, glycine, aspartic acids, and serine undergo a deamination reaction to form various forms of acids (Hietala and Savage, 2021; Sato et al., 2004). The phenylalanine is transformed to phenylethylamine and then to the aromatic compound styrene following a decarboxylation step. The serine and methionine amino acids are transformed into glycine, while the arginine is converted to proline (Shia and Yu, 2023).

The Maillard reaction, which takes place between amino acids and reducing sugars, is a significant reaction pathway that has an impact on the spatial dispersion of intermediate products, particularly in the bio-oil and aqueous phase, carbon recovery, and nitrogen recovery. It is also demonstrated that the Maillard reaction most likely increased the bio-oil yield (Ratha et al., 2022), along with the enhancement in the recovery of carbon and nitrogen (Hietala et al., 2019). Additionally, these effects resulted in a reduced recovery of ammonium-N in the aqueous phase. Furthermore, this impact was more evident for the slurries with high concentrations (Hietala and Savage, 2021).

Concomitantly, the amino acids undergo a deamination reaction to form ammonia and aqueous phase soluble products (mainly ammonium-based compounds). The liberation of ammonium nitrogen from amino acids to the aqueous phase can be a bioavailable source of nitrogen for microorganisms cultivation. It is reported that a major proportion of the gas that is produced during the hydrothermal liquefaction of microalgae at higher temperatures is carbon dioxide. Other gases are also formed at higher temperatures due to the decarbonylation of carbohydrates. The triglycerides react with water to release fatty acids from the lipids. The formation of amides is a result of consecutive reactions that are characterized by the interaction of ammonia with fatty acids. The gaseous product, carbon dioxide, is also formed via the decarboxylation of fatty acids successively (Hietala and Savage, 2021).

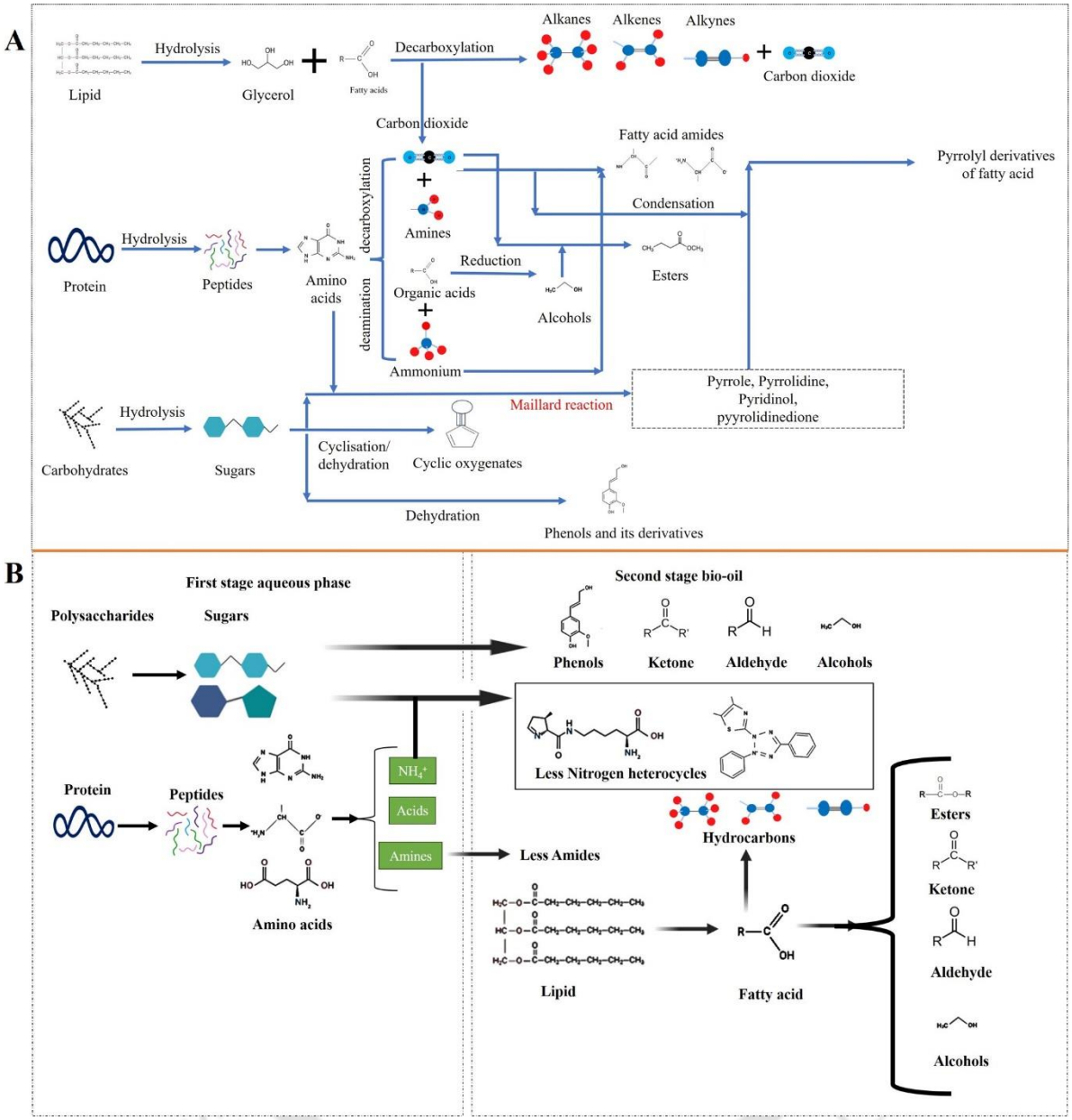

Figure 4.12. Proposed hypothetical reaction pathway in direct and two-stage hydrothermal liquefaction of microalgae.

A two-stage HTL approach for the extraction of carbohydrates and protein during pretreatment followed by high-temperature bio-oil production, was performed using *Monoraphidium* sp. KMC4 grown on simulated synthetic dairy wastewater. The product of the two-stage HTL (Figure 4.12B) is the extractive phase from stage I (aqueous phase), bio-oil, aqueous phase from stage II, solid residue II, and gas from the second stage. In the initial lower temperature stage, the heat and temperature are sufficient for solvolysis and hydrolysis to remove carbohydrate and protein components from disrupted microalgae biomass. It is possible that by improving the initial stage conditions during two-stage HTL, possible reaction pathways could

be likely enhanced for selectively extracting substances such as polysaccharides, proteins, amino acids, pigments, and inorganic nutrients. The reaction mixture was filtered and separated from the DCM soluble phase, and the dried solid residue was loaded with a 10 wt% loading into the reactor for bio-oil production.

Removal of carbohydrate and protein extractives to a major extent will reduce the formation of fatty acid amides and N- and O-based compounds from the Maillard reaction and acylation reaction between fatty acids and amines. Thus, this strategy was found to be better for enhancing the quality of bio-oil without the trade-off of yield with the production of extractive from stage I, which can be used as a nutrient for the cultivation of microalgae in a biorefinery loop. A previous study also observed the reduction of solid residue (from the second step) and enhanced yield of bio-oil through sequential HTL compared to direct HTL due to enhanced mass transfer during higher temperature conditions in the former process. The fragility and porosity of the algal cell wall are increased by isolating polysaccharides, allowing for more physical interaction between water and lipids. This leads to improved extraction, even at lower temperatures (Miao et al., 2012).

Overall, these new insights were provided through comparative compounds and elemental analysis of bio-oil from direct vs two-stage HTL. The obtained results indicated a significant reduction in nitrogen heterocycle compounds in the two-stage bio-oil (Figure 4.7), which correlated to the removal of protein-degraded nitrogen products into the aqueous phase. This was confirmed by ammonium nitrogen and total nitrogen concentration of the stage I aqueous phase (Figure 4.5), showed substantial extraction of nitrogen in the initial stage. Extraction of nitrogen due to hydrolysis of protein and deamination of amino acids is reducing their availability to participate in cyclization and aromatization reactions during Stage II. Also, the initial stage aqueous phase has a large amount of total organic carbon (>20 mg/L at 220 °C) (Table 4.2), which suggested the extraction of organic carbon compounds due to dehydration and decarboxylation of saccharides (Fan et al., 2018).

Overall, the low temperature pretreatment can partition nitrogen into the aqueous phase while retaining carbon in solid residue I. The pretreatment strategy followed a dehydration and deamination mechanism with a decrease in both the H/C and N/C ratio of solid residue I (Figure 4.4). However, the nitrogen in the aqueous phase is majorly in its inorganic form, which can be recovered as a fertilizer, considering the closed-loop circular economy. Vadlamudi et al. (2024) also confirmed that the evolution and migration of nitrogen from chicken manure to the aqueous phase greatly reduced the Maillard reaction and the formation of N-heterocyclic compounds in the bio-oil (Vadlamudi et al., 2024).

From Figure 4.9, a decrease in the N/C and an increase in the H/C ratio were observed in the two-stage bio-oil. This was also confirmed by the bio-oil compound characterization (Figure 4.7), showed a decrease in N- and O-based heterocyclic compounds in two-stage HTL. This improves the quality of bio-oil, as evident with improved HHV (MJ/kg) of two-stage HTL bio-oil.

The N- and O-based compounds were decreased from 13.36% in direct HTL to 1.98% in two-stage HTL bio-oil. The formation of nitrogenous heterocyclic compounds resulted from the Maillard reaction between amino acids (from protein) and sugars (from carbohydrates) (Fan et al., 2018). The pyridines, pyrazines, pyrrole compounds, and their derivatives resulted from the Maillard reaction, showing a higher % area of such N-heterocyclic compounds in bio-oils from direct HTL. The partial removal of major sugars and nitrogen components from this biomass to the aqueous phase reduces the chances for the formation of ring heterocyclic compounds at higher temperatures (Fan et al., 2018; Vadlamudi et al., 2024).

Also, the low temperature of 300 °C in two-stage HTL for bio-oil production can be one of the reasons for the less formation of nitrogen and oxygen heterocyclic compounds. It is already reported that nitrogen in bio-oil produced at a higher temperature (350 °C) was higher than at a lower temperature (300 °C) when performed with model compounds lysine and lactose. This is corresponded with the high nitrogen concentration of the aqueous phase in stage I. The high nitrogen content in bio-oil at high temperature conditions is due to increased hydrolysis rate, which results in more Maillard products (N and O heterocyclic compounds) (Fan et al., 2018) in direct HTL compared to the two-stage HTL process.

4.4 Summary

A two-stage HTL was used to enhance the quality of the algal biofuel. In the first stage, a low-temperature treatment called solvolysis and hydrolysis extracted the proteins and carbohydrates components into aqueous phase I, while simultaneously concentrating the energy-dense algae solid residue I. By subjecting the algae to two different sets of pretreatment temperatures, 220 °C and 240 °C for 30 min, the N and O contents were effectively reduced in solid residue I with an insignificant difference of H/C and N/C of pretreated algae at both temperatures. A lower temperature of 220 °C was found to be suitable for hydrothermal pretreatment due to low energy investment in lower temperature conditions. The pretreated microalgae at 220 °C give the highest bio-oil yield at 300 °C. GC-MS confirmed the lower number of N-based compounds, i.e., reduction in fatty acid amides and heterocyclic compounds in bio-oil from

two-stage HTL. The hypothetical pathway suggested a reduction in the path toward Maillard reaction and amine formation when microalgae are subjected to two-stage HTL. The results from the two-stage HTL process significantly enhanced the bio-oil quality without the expense of reduced yield.

Chapter 5

Bio-oil as a promising product from co-liquefaction of dairy wastewater grown microalgae with dairy sludge: Study on synergistic effect and sustainable energy generation

Chapter 5. Bio-oil as a promising product from co-liquefaction of dairy wastewater grown microalgae with dairy sludge: Study on synergistic effect and sustainable energy generation.

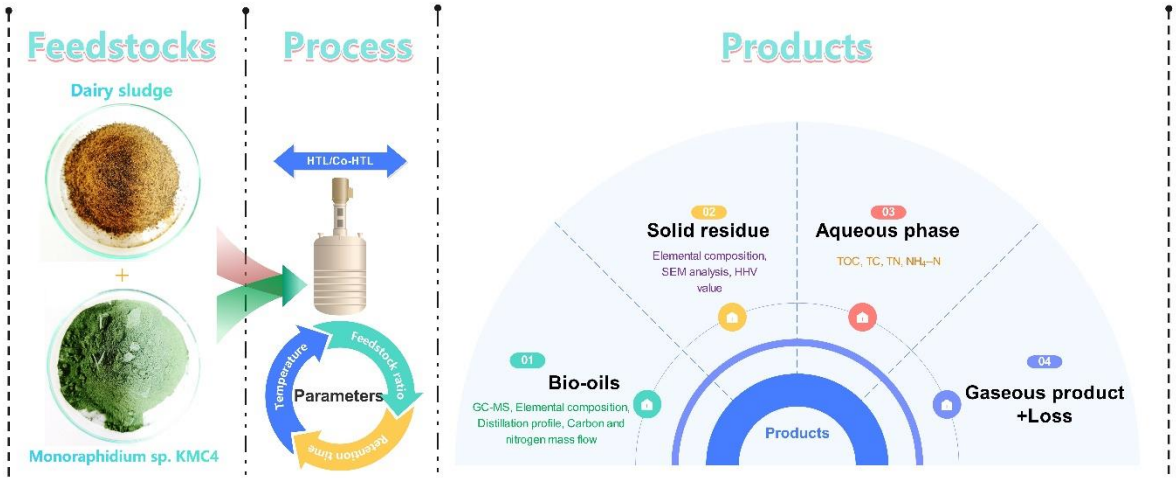

5.1 Background

Implementation of renewable energy production utilizing biomass would be an essential and sustainable approach to address this matter (Hossain et al., 2022). In recent years, microalgae are considered as potential feedstocks for biofuel production. Also, microalgae can be cultivated in dairy wastewater (which constitutes organic and inorganic nutrients for growth) to reduce the overall expense of biomass production process. However, the cultivation and harvesting part of microalgal biomass generation is expensive and poses a substantial barrier to commercial scale-up. The present microalgae-based research has commenced the optimization of co-feedstocks in an effort to increase the yield of bio-oil for achieving commercialization. Therefore, currently the investigation is focused on co-HTL of microalgae with other feedstock to enhance the bio-oil quantity and quality (Islam et al., 2022).

The dairy sludge, which is a common waste product from dairy industry, can be considered as feedstock for bio-oil due to its wide availability in all seasons. The waste-to-energy conversion process of dairy waste involves biological treatment which converts organic wastes into biogas using anaerobic fermentation. However, the conversion by microorganisms is partial and generates a secondary effluent. This secondary effluent can be further reused for some valuable product production to maximize its economic value and reduce environmental pollution.

Hydrothermal liquefaction of dairy sludge offers significant potential for recovering both energy and nutrients from high-moisture waste effluents. From previously reported studies, it has been observed that using more than one feedstock reduces the overall biofuel cost and increased bio-oil yield. Therefore, valorisation of algal biomass with dairy sludge for bio-oil will be a cost feasible and sustainable process.

As far as our literature comprehension states, the co-HTL studies has not been previously reported for these co-feedstocks. Also, the co-liquefaction effect using three parameters (synergistic, antagonistic and additive) was estimated after blending of two feedstocks to understand the interaction of molecules from both feedstocks to enhance the characteristics and yield of bio-oil. To develop an effective co-HTL approach, this research integrates the optimization of reaction parameters for bio-oil production from microalgae and dairy sludge. The primary objective of the process was to optimize conversion rates and distribution of co-HTL products through one-variable at a time (OVAT) optimization such as, temperature, feedstock ratio, and reaction time. The process derived bio-oil was characterized by techniques including elemental analysis, functional group analysis, and class of compounds classification via gas chromatography-mass spectrometry (GC–MS). The boiling point distributions of bio-oils were analyzed using thermogravimetric analysis to understand the proportions of petroleum fractions via thermal stability curve. Also, solid biochar (solid residue) and liquid by-product (aqueous phase) were characterized to determine their suitability for various applications.

5.2 Methodology

In this chapter, microalgae were co-fed with dairy sludge for bio-oil production. In this chapter, the dairy sludge was thoroughly characterized and selected for bio-oil production. An interaction between two different feedstocks: microalgae and dairy sludge was studied during co-HTL reactions. Single feedstock HTL reactions were performed along with co-feedstock HTL with different biomass ratio for achieving highest bio-oil yield. Boiling point distribution profile of bio-oils was observed along with compounds differentiations through GC-MS analysis.

5.3 Results and Discussion

5.3.1 Preliminary studies

5.3.1.1 Characterization of sludge collected from dairy wastewater

The proximate, elemental, and biochemical characteristics of all feedstocks are given in Table 5.1. The dairy sludge I collected after flocculator (at sludge thickener) consisted of higher volatile matter (50.21 ± 2.02 wt%) compared to that obtained after aeration tank (39.10 ± 1.23 wt%) and clarifier (30.21 ± 1.56 wt%). The organic matter corresponded to the anaerobic bacteria, oils, fats, and grease which was higher in sludge collected after flocculator. The ash content of dairy sludge III (56.14 ± 0.64 wt%) was found to be highest compared to other two sludges, which was related to presence of an excessive inorganic form of compounds in the former one. However, the volatile content of dairy sludge was lower than microalgae. The ultimate composition revealed higher carbon, hydrogen, and nitrogen in dairy sludge I compared to sludge II and III. The higher heating value of 16.23 ± 0.7 MJ Kg^{-1} was observed in dairy sludge I while lower values were noticed in sludge II and III. Therefore, the dairy sludge I was chosen for thermochemical conversion to bio-oil for co-HTL studies.

Table 5.1. Characteristics of microalgae and collected dairy sludge.

Components	KMC4	Dairy Sludge I	Dairy Sludge II	Dairy Sludge III
Proximate composition				
Moisture (wt%)	6.30±0.36	5.75 ± 0.65	5.05 ± 0.15	5.35 ± 0.17
Volatile matter (wt%)	71.50±0.18	50.21 ± 2.02	39.10 ± 1.23	30.21 ± 1.56
Fixed carbon (wt%)	13.80±0.30	8.90 ± 0.25	7.45 ± 0.15	8.3 ± 0.5
Ash (wt%)	8.40±0.12	35.14 ± 0.75	48.40 ± 0.49	56.14 ± 0.64
Ultimate composition				
C (wt%)	43.58±1	36 ± 0.93	31.10 ± 1.33	27.78 ± 1.11
H (wt%)	6.73±0.01	6.60 ± 0.14	6.30 ± 0.13	6.01 ± 0.12
N (wt%)	8.70±0.40	10.65 ± 0.08	8.30 ± 0.14	6.55 ± 0.18
S (wt%)	0	1.05 ± 0.06	1.42 ± 0.04	1.30 ± 0.1

O (wt%)*	32.59±0.20	46.1 ± 0.11	52.88 ± 0.1	58.36 ± 0.06
HHV (MJ Kg^{-1})	18.50	16.23 ± 0.7	14.7 ± 0.14	12.23 ± 0.7
Biochemical composition				
Carbohydrate (wt%)	28.73±1.60	–	–	–
Protein (wt%)	48.50±1.30	–	–	–
Lipid (wt%)	20.29±2.30	–	–	–

The XPS survey spectrum revealed the elemental composition of the dairy sludge surface by displaying characteristic binding energy peaks corresponded to specific elements (Figure 5.1). In this spectrum, prominent peaks were observed for carbon (C 1s), oxygen (O 1s), nitrogen (N 1s), and silicon (Si 2p). Other minor amounts of phosphorus and transition metals were present in the dairy sludge including zinc, cobalt, iron, and chromium (Figure 5.2).

Strong C 1s and O 1s peaks were expected, as dairy sludge is rich in organic matter such as fats, proteins, and carbohydrates, which contributed to high carbon and oxygen content. The characteristics peaks fitted in the C 1s spectrum were C–C (284.9 eV), C-O (285.5 eV), C=O (287.7 eV), and COOH (289.3 eV) (Moulder et al., 1992; Xiao et al., 2019). The major peak in the dairy sludge was C-C, which accounts for 62.31% of total carbon. Other major functionalities were 28.47% (C-O) and 8.16% (C=O). These peaks represented the presence of fats, carbohydrates and oil-based compounds. The N 1s belonged to nitrogen-containing compounds, likely originated from dairy-based proteins and chemicals added for floc formation in the tanks before sludge thickener sample collection point. The N 1s represented major peaks as protein-N (60.07%), amine-N (27.81%), and inorganic-N (12.10%), and the corresponded binding energies were 400.26 eV, 399.14 eV, and 401.95 eV, respectively (Guo et al., 2024; Xiao et al., 2019). Notably, the relative surface content of protein-N was significantly higher than that of other functionalities.

In O 1s spectra, the peaks at 530.4 eV and 532.39 eV were related to C=O and O-H/P=O, respectively (Moulder et al., 1992). Also, the 532.8 eV peak represented the existence of SiO_2 (Moulder et al., 1992; Zerga et al., 2024). Presence of hydroxyl and carbonyl group could represent polysaccharides availability in dairy sludge sample. The presence of silicates, silica and phosphate can be attributed to mineral content in the sludge and may came from soil and sand in the treatment plant. The Si 2p spectrum represented two characteristic peaks at 103.9

eV and 102.35 eV which confirmed the presence of silica in the form of silicon dioxide and silicates (Moulder et al., 1992).

From EDS analysis, presence of transition metals such as phosphorus, calcium, sodium, magnesium, zinc and iron were confirmed. Other minerals such as potassium, nickel, copper, chromium, cobalt, chlorine and manganese were found below 0.1 atomic wt% in dairy sludge (Figure 5.2). The transition metals- Zn, Fe, Co, and Cr are typically introduced through corrosion of metallic equipment, pipe wear, or as trace contaminants in water. Overall, this elemental profile reflected the complex composition of dairy sludge, influenced by biological system, industrial processes, and treatment chemicals used within the dairy effluent management system. The complex composition of dairy sludge was also confirmed by XRD and FTIR analysis.

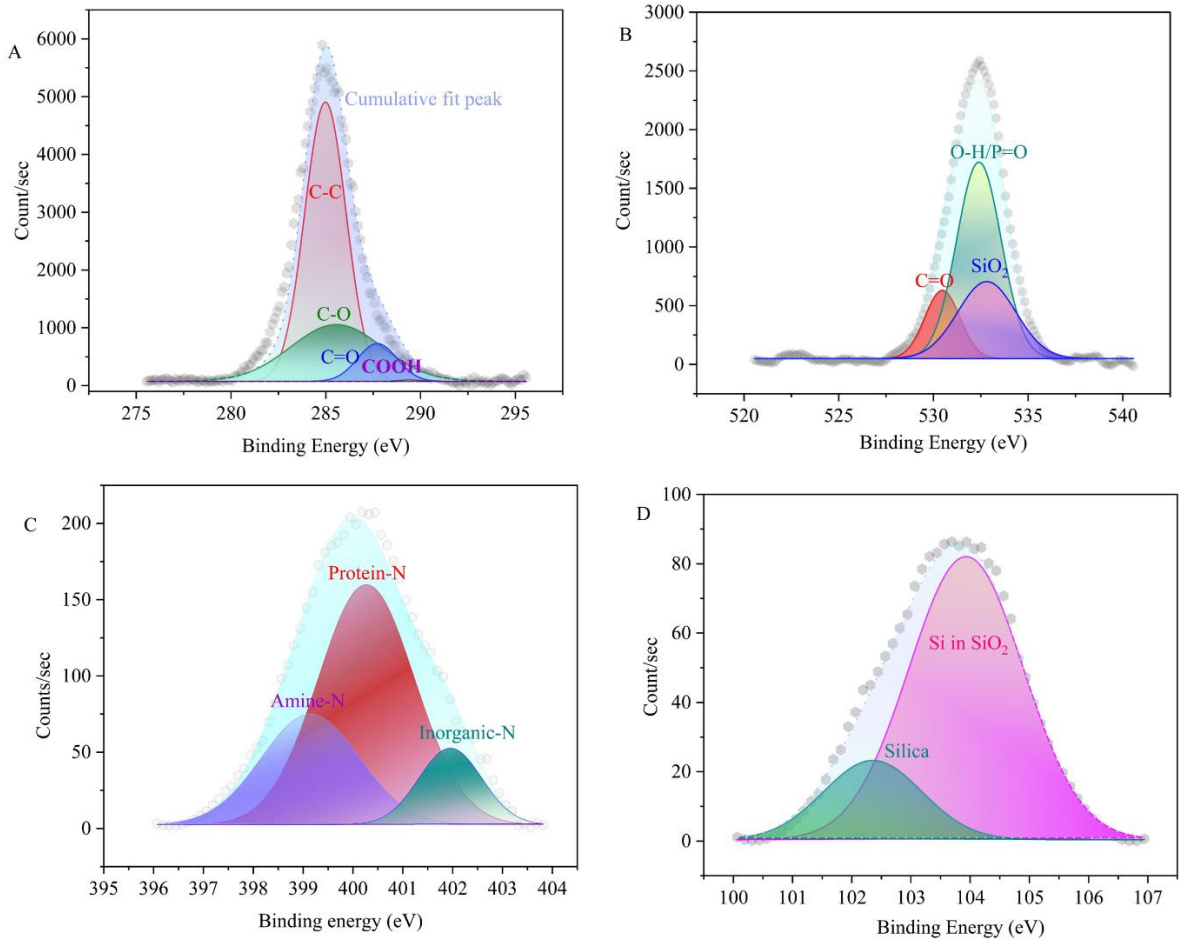

Figure 5.1. XPS analysis of dairy sludge, A) C 1s, B) O 1s, C)N 1s, D) Si 2p.

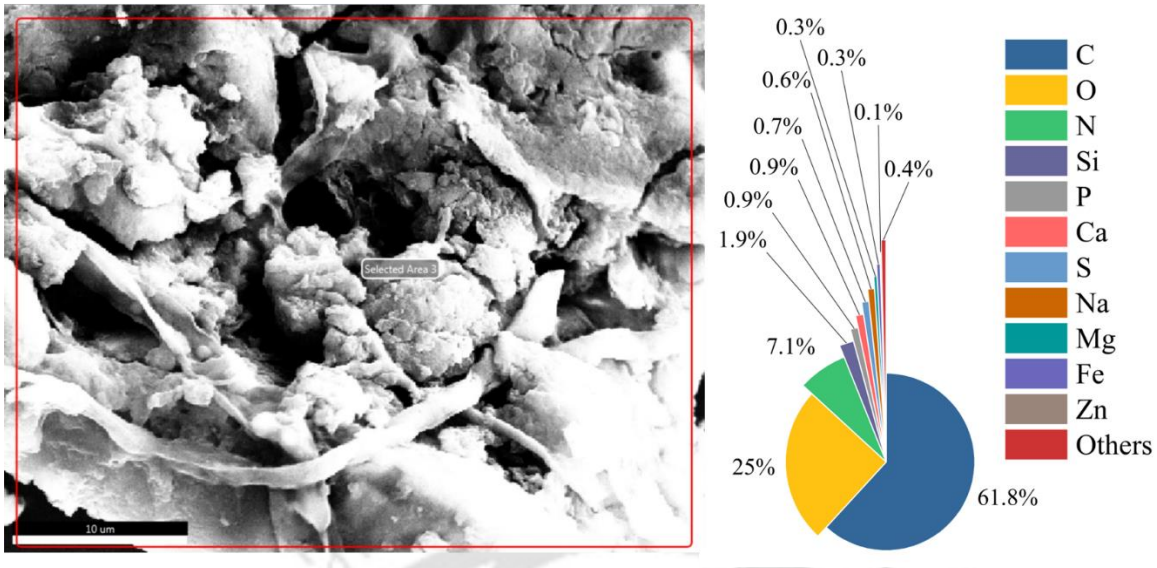

Figure 5.2. Atomic weight composition of microconstituent and macroconstituent of dairy sludge (The values were averaged after calculated from different area).

The XRD pattern of dairy sludge I disclosed the presence of multiple crystalline phases (Figure 5.3A). The dominant peaks corresponded to SiO_2 (α) and graphite (♣), suggested that silica and carbonaceous material were a major crystalline component in the sludge. Sludge has three noticeable peaks related to silica and silicates at 20.30° (*hkl*:100), 23.01° (*hkl*:101), and 50.26°, which is common in the sludge samples. The strong peak at 26.72° and 43.45° (*hkl*:102) were due to graphite and carbon, possibly from carbonaceous form of compounds present in the dairy sludge.

The ZnO and ZnO_2 (β) were noted by several peaks at 36.63° (*hkl*:101) and 68.30° (*hkl*:201) with low intensity, indicated its presence in trace amount. Peaks at 29.52° and 45.92° reflected the presence of calcite (Thriveni et al., 2014). The peak at 39.58° (*hkl*:008) is related to presence of calcium phosphate compounds like hydroxyapatite. Minor phases such as Fe_2O_3 (Φ) and CoO (π) were also detected, indicated their availability in small quantity. The Fe_2O_3 showed peaks at $2\theta = 47.45°$ (Pulungan et al., 2024) while cobalt oxide appeared at 42.5° (*hkl*:0014). These minor transition elements might be originated from machinery system in the dairy treatment plant, example like anaerobic digester. The relatively low intensity of these peaks suggested that these phases are present in small quantities.

Studies reported the effect of naturally occurring metal oxides (Fe_2O_3 and calcite) in biomass ash can provide heterogeneous catalytic effects without adding external catalysts (Chen et al.,

2017). Alkali metals such as Na, K and alkaline earth metals such as Ca, Mg (present in KMC4 and dairy sludge both) can act as in situ catalysts, enhancing the depolymerization of biomass, decarboxylation, and dehydration reactions. Presence of K^+ and Ca^{2+} can promote conversion of feedstock into oil-phase compounds. The relationship between bio-oil yield and Na^+ ion content is weak, and the same holds for the yields of biocrude oil and biochar in relation to K^+ ion content. They may reduce coke or char formation, directing more mass into the bio-oil phase (Satiada et al., 2024).

It is also reported that sodium and potassium (water soluble) were majorly transferred to the aqueous phase while magnesium, calcium, iron, zinc and chromium (less water soluble) concentrated in the solid fraction after HTL (Cheng et al., 2018; Lu et al., 2022). Fe_2O_3 present in the dairy sludge can act as a catalyst in HTL. It can enhance the yield of gaseous and bio-oil fractions while reducing char formation. It influences the decomposition of chain, hydrogenation, and cracking of long-chain hydrocarbons, thereby initiating polymerization, cyclization, and aromatization reactions (Fu et al., 2016).

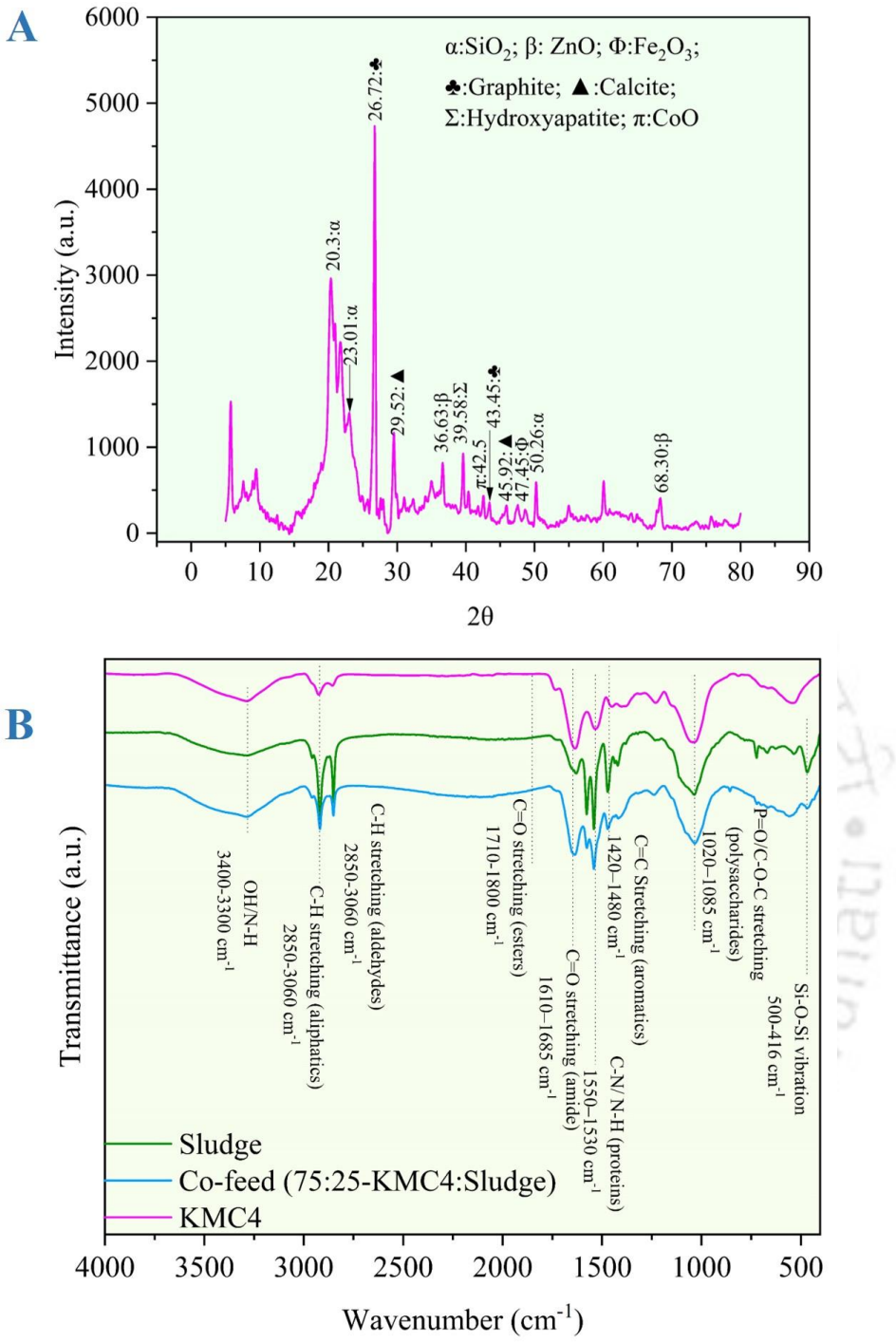

Figure 5.3. A) XRD plot of dairy sludge B) FTIR spectra of individual and co-feedstock.

The FTIR spectra of dairy sludge is almost similar to KMC4 algal biomass (Figure 5.3B). The peak between 3300-3400 cm^{-1} corresponded to the OH bending of acidic and alkaline compounds. This region also contributed to N–H ligand stretching. This confirmed the presence of carbohydrates, proteins, lipids (sterols and fatty acids), and nucleic acids in all

feedstocks. The C=O stretching at 1710-1800 cm^{-1} was associated with lipids, esters and carbonyl groups of chlorophyll pigments. While the C=O stretching between 1610-1685 cm^{-1} was linked with protein (amide I bands) and the C-N/N-H stretching between 1510-1530 cm^{-1} was related to protein (amide II band).

The P=O bond and C-O-C stretching between 1020-1085 cm^{-1} confirmed the availability of phospholipids and nucleic acid and carbohydrates. The sludge sample showed a Si-O-Si symmetric and asymmetric stretching vibration bending between 500-406 cm^{-1}, confirmed the presence of silica and silicates (Zerga et al., 2024). The microalgae biomass spectra do not report this vibration. The co-feed spectra showed a small peak at same wavelength, confirming the addition of a sludge sample with KMC4 algal biomass.

5.3.2 TGA analysis of feedstocks

The dairy sludge represented three phases of decomposition in the TGA profile (Figure 5.4). The removal of evaporation of free and bound moisture from dairy sludge caused a mass loss in the thermogravimetric profile from 50 °C to 180 °C, known as dehydration zone. The devolatilization zone involved the removal of volatile organic substances from the sludge sample, which has various boiling points. Lastly, above 600 °C, the char formation zone was observed due to decomposition of carbon bonds derived from inorganic substances or carbonate compounds. This stage is mainly associated with inorganic transformations and the stabilization of the remaining solid char.

Also, DTG spectra represented the decomposition profile of dairy sludge. Three distinct peaks were noticed from the DTG curve, indicated that the sludge mass loss can be categorized into three steps, which correlated to the release of moisture and the degradation of organic volatile components. The remaining mass will be considered as char after stage III. The peak between 650-700 °C can be due to carbonate decomposition (Merabtene et al., 2019) and silica phase transition. In KMC4, the moisture content from biomass was removed up to 140 °C. The mass loss of ~ 62–65 wt% was observed in devolatilization phase. In DTG, the degradation of carbohydrates and proteins was initiated from 150 °C and is followed by a temperature of 350 °C while the latter temperature was related with lipid breakdown.

KMC4 showed the steepest weight loss in stage II, indicated a higher content of volatile organic matter, whereas sludge decomposed more gradually due to its more stable matrix and possible

inorganic content. The Co-HTL blended feedstock showed an intermediate behavior, benefitted from the synergy between the two feedstocks.

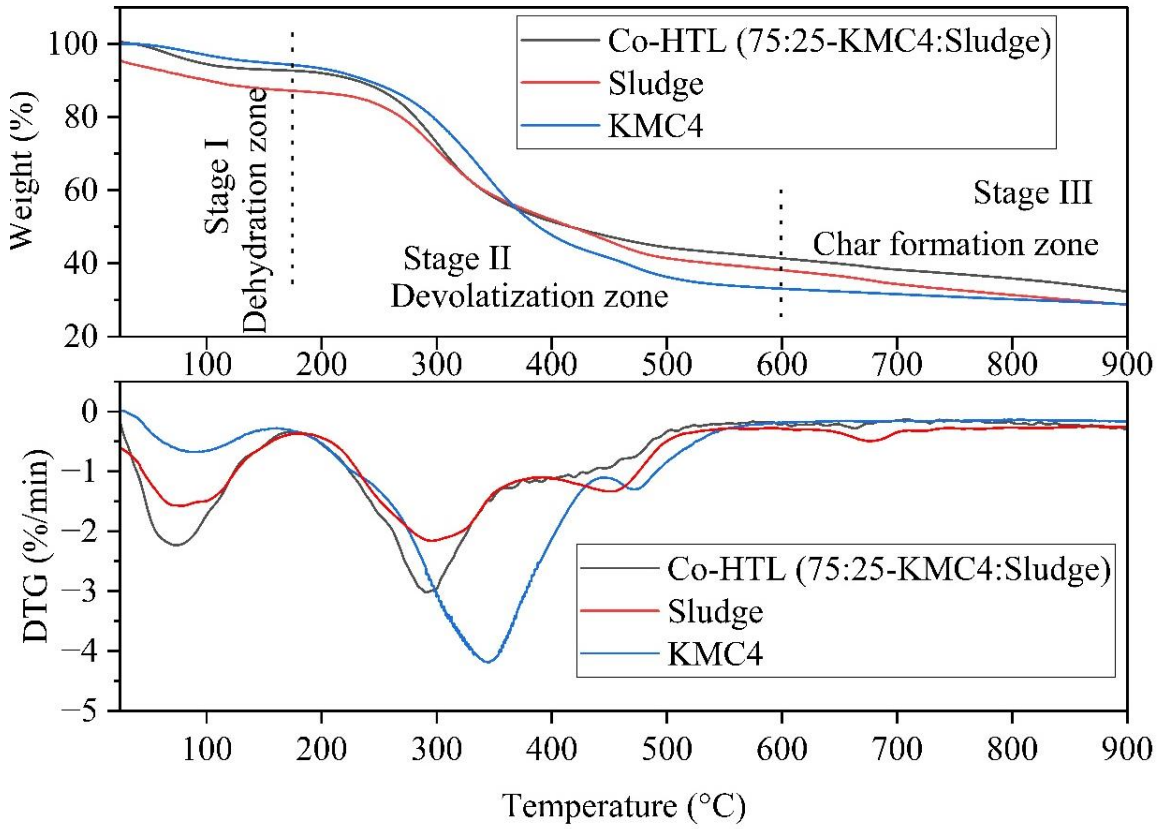

Figure 5.4. Thermogravimetric and Derivative thermogravimetry spectra of individual and blended feedstock.

5.3.3 Hydrothermal liquefaction of individual feedstocks

5.3.3.1 Bio-oil from *Monoraphidium* sp. KMC4

The product distribution from individual feedstocks was investigated for each feedstock individually before conducting the co-HTL studies. The details of bio-oil production from *Monoraphidium* sp. KMC4 grown on dairy wastewater explained in Chapter 4 (4.3.1.1). However, the key results are mentioned again here. Increasing the reaction temperature from 275 °C to 350 °C contributed to a notable increment in bio-oil production (20.31±1.5 wt% to 33.50±1.45 wt%).

Also, the duration of reaction time has a significant influence on the conversion of biomass, the products distribution, and their composition. The effect of retention time on the yield of bio-oil was analyzed at 350 °C. The bio-oil yield showed an increasing trend (27.42±1.12 to

33.50±1.45 wt%) when the retention time increased from 15 to 30 min. However, above 30 min, the yield started to decline. From this observation, it was noted that a 30 min retention time proved the sufficient conversion of biomass and resulted in the highest bio-oil yield. A bio-oil yield of 33.50 wt % was produced from HTL with an energy value of 34.14 MJ kg^{-1} at 350 °C and 30 min. This optimal condition resulted in 8.30 % of solid residue with conversion rate of 91.70 wt%.

5.3.4 Bio-oil from dairy wastewater sludge

The sample collected after flocculator (Sludge I) at the sludge thickener and aeration tank sludge (Sludge II) have higher volatile matter compared to after clarifier sample (Sludge III). The sludge samples collected from two locations namely, sludge thickener and after aerobic aeration tank, were analyzed for their potential for bio-oil production due to higher volatile matter of Sludge I and Sludge II compared to Sludge III. Dairy wastewater treatment via anaerobic digestion followed by sludge thickener resulted in the formation of fats, emulsifiers, floatation of grease, microbes and oily compounds, which were responsible for the organic matter load of sludge I.

The product distribution profile of Sludge I and Sludge II are depicted in Figure 5.5. On increasing the temperature from 275 °C to 350 °C, the bio-oil yield of sludge I was increased from 7.60±0.30 wt% to 18.16±0.32 wt% while the bio-oil yield of sludge II was also increased but was comparatively lower from sludge I (from 2.10±0.14 to 10.15±0.12 wt%). This lesser bio-oil produced from sludge II was because of lower volatile matter present in it (39.10 ± 1.23%) compared to sludge I (50.21 ± 2.02%). In both cases, the maximum bio-oil were formed at 350 °C. Nevertheless, the maximal bio-oil yield attained from sludge I (18.16±0.32 wt%) was 45.79 wt% less in comparison with *Monoraphidium* sp. KMC4 (bio-oil yield-33.50±1.45 %). This was attributed to the low volatile matter (50.21±2.08 wt%) present in the sludge I feedstock compared to KMC4 (71.50±0.18%). The bio-oil yield started to decrease after 350 °C, due to an increase in gaseous product formation or repolymerization to solid or aqueous phase at higher temperature.

Furthermore, the raise in reaction time from 30 min to 45 min during liquefaction of sludge I and sludge II has resulted in decreased bio-oil yield (sludge I- from 18.16±0.32 to 14.34±0.20 wt% and sludge II- from 10.15±0.14 to 7.01±0.18 wt%). The solid content was higher at lower temperature (275 °C) (51.21±1.30 wt%-sludge I and 61.40±1.13 wt%-sludge II) but decreased at 350 °C (37.30±1.74 wt%-sludge I and 46.30±1.44 wt%-sludge II). Moreover, the high ash content of sludge II (46.40±0.49 wt%) has resulted in higher solid residue at all reaction

temperatures which restricted the conversion percent within 36.5 wt% to 53.7 wt%. The % conversion of sludge I reached above 60 wt% which suggested its potential conversion to bio-oil. In comparison with previous research, the bio-oil yield obtained from dairy sludge I is less (18.16%) compared to the yield from sludge received from sewage wastewater (22 %) (Mishra and Mohanty, 2020) (Table 5.2).

Despite this, the high ash content of sludge posed a major obstacle that could impede the production of significant bio-oil yield. Therefore, additional research can be conducted to assess the interaction between co-feedstock to study the impact on the bio-oil yield in co-HTL or to interpret the potential for commercialization on an industrial level due to wide availability of sludge throughout the year.

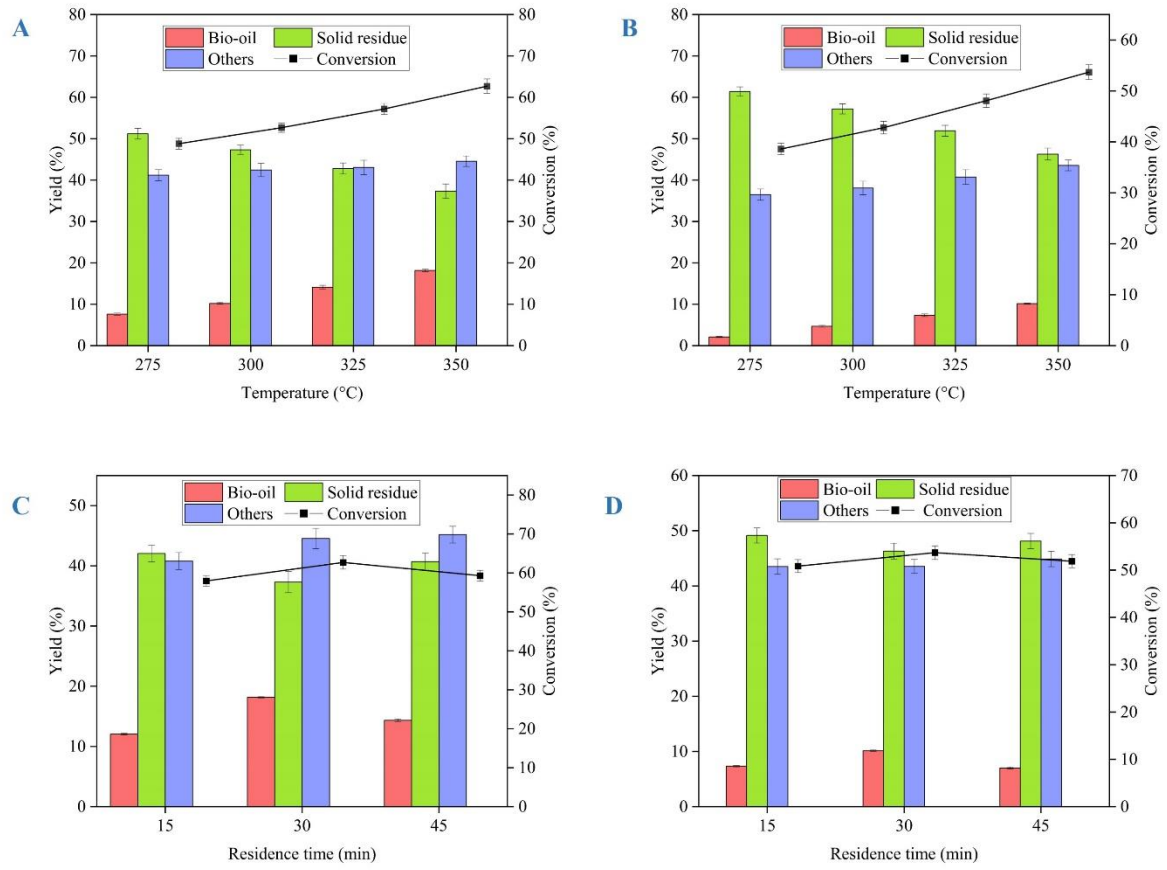

Figure 5.5. Effect of temperature and retention time on the products distribution (wt%) and conversion (%); (A) and (C) dairy sludge 1; (B) and (D) dairy sludge 2 (Others includes aqueous phase, gaseous product and losses).

Table 5.2. Bio-oil from individual microalgae, dairy-based feedstocks, or other co-feedstocks.

Feedstock	Bio-oil yield (%)	Reference
Microalgae feedstocks		
Chlorella	~22	(Xu et al., 2019)
Mixed-culture	20.5±0.3 (Light bio-oil) 7.5±0.4 (Heavy bio-oil)	(Audu et al., 2021)
Chlorella sorokiniana	43.03±0.01	(Bisht et al., 2022)
Monoraphidium sp. KMC4	33	(Mishra and Mohanty, 2020)
Monoraphidium sp. KMC4	33.50±1.45	This study
Dairy based feedstocks		
Dairy manure digestates	58-60 (acid addition) and 42-46 (alkali addition)	(Posmanik et al., 2018)
Dairy wastewater treated anaerobic digested sludge	18.16±0.32 (without any acid addition)	This Study
Co-feedstocks		
Domestic Sewage Sludge: Microalgal biomass (25:75)	39.38	(Mishra and Mohanty, 2020)
Swine Manure: Mixed algal biomass	35.7	(Chen et al., 2014)
Chlorella: Sewage Sludge (1:1)	26.8	(Xu et al., 2019)
Kitchen Wastewater Sludge: Chlorella sorokiniana	57.5 ± 0.22	(Bisht et al., 2022)
Monoraphidium sp. KMC4: Dairy Wastewater Treated Anaerobic Digestion Sludge (75:25)	32.94±1.21	This Study

5.3.5 Bio-oil from co-HTL of Monoraphidium sp. KMC4 and dairy sludge I

5.3.5.1 Effect of temperature

The current investigation has examined the impact of different reaction parameters on the co-HTL of *Monoraphidium* sp. KMC4 and dairy sludge, as illustrated in Figure 5.6. The co-HTL study was conducted using dairy sludge I as it showed higher bio-oil formation compared to other sludges. The initial investigation examined the impact of varying temperature values on the distribution of products using a feed ratio of 50:50 (wt%) (microalgae: dairy sludge I)

(Figure 5.6A). Increasing the reaction temperature from 275 °C to 350 °C has raised the bio-oil yield. An optimum temperature of 350 °C was identified for the co-HTL process, as it resulted in the attainment of a maximal bio-oil of 25.10±0.30 wt%. Contrastingly, the bio-oil yield was 25.07% lower than that was obtained by the HTL of *Monoraphidium* sp. KMC4 (33.5±1.45 wt%). This was owed to substantial variations in the volatile content in feedstocks used in this study (Table 5.1).

Consequently, using both feedstocks in ratio of 50:50 (KMC4: Dairy Sludge) led to a reduction of 12% in volatile matters with respect to KMC4 volatile matter, which consequently impeded the overall conversion of co-feedstock to bio-oil. An increase in temperature from 275 °C to 350 °C led to reduction in proportion of solid residue from 37.3±1.31 wt% to 20.03±1.74 wt%. It was proposed that the hydrolysis of biomass at low temperatures leads to high solid residue while high temperature corresponded to lower solid and high bio-oil yield.

When the reaction temperature increased close to the critical point, water dissociate into H^+ and OH^- ions, thereby resembling an acidic and basic catalyst. Following this, isomerization, depolymerization, and repolymerization reactions occurred due to a low dielectric constant, and the unstable intermediates were transformed into bio-oil. Despite the reduction in solid residue with increasing temperature for bio-oil production with a 50:50 (wt%) ratio of both feedstocks, the overall conversion was lower compared to individual KMC4 bio-oil conversion. The explanation in this case is that the feedstock composition, which was 50:50 (wt%), contained approximately 22.40% ash, which lowered the bio-oil yield.

Following this, a temperature rise led to a conversion of 79.97 wt% at 350 °C, which was 12.98% less than that obtained from microalgae conversion alone at 350 °C (91.70 wt% conversion). Still, in order to enhance the bio-oil yield and conversion rate while minimizing other products, the impact of various feedstock ratios on the co-liquefaction process was investigated.

5.3.5.2 Effect of feedstock ratio

The impact of various feedstock ratio of microalgae and dairy sludge I on the distribution of co-liquefaction products at the optimal temperature of 350 °C was examined. The maximum bio-oil yield of 32.94±1.21 wt% was observed at the 75:25 wt% (microalgae: dairy sludge I) feedstock ratio, in contrast to 50:50 wt% and 25:75 wt% ratios (Figure 5.6B). This was the result of a reduced ash content (12.36±2.12 wt%) and an increased volatile matter (68.24±1.31

wt%) in comparison to the 50:50 ratio co-feedstock (Ash-22.4±1.1 wt% and VM-62.92±0.91 wt%). Still, the bio-oil yield was observed to be almost similar as that obtained from individual KMC4 and 44.53% higher at the 75:25 wt% feedstock ratio in comparison to dairy sludge I alone.

At 75:25 wt% feedstock ratio, an increased bio-oil yield revealed a decreased solid residue of 15.3±1.25 wt% compared to 25:75 wt% (30.4±0.89 wt%) and 50:50 wt% (20.03±1.74 wt%). In the case of bio-oil from 25:75-KMC4: dairy sludge I, a substantial decline in bio-oil yield occurred due to the decreased organic matter content of co-feedstock, because of the addition of dairy sludge in a higher ratio.

Therefore, a feedstock ratio of 75:25 wt% (microalgae: dairy sludge I) was determined to be ideal for the co-liquefaction process, which achieved a maximal conversion of 84.7±1.25 wt% while produced a lower solid residue. Thus, it was determined that the selection of KMC4 and dairy sludge I as co-liquefaction feedstocks was feasible due to similar bio-oil yield. However, to study the influence of the reaction time on distribution of products and conversion percent, further experiments were conducted with consideration of optimum feedstock of 75:25 KMC4 and dairy sludge I with a temperature of 350 °C.

5.3.5.3 Effect of residence time

For obtaining maximum bio-oil yield, the HTL/co-HTL studies were performed for 30 min duration. However, due to the different feedstock compositions, residence time was also proposed as one of the critical reaction factors. Thus, at the ideal reaction temperature of 350 °C and 75:25 wt% ratio (microalgae: dairy sludge I), the impact of reaction time (15 min to 45 min) on product distribution was investigated (Figure 5.6C).

A positive trend in the bio-oil yield on increasing the reaction time from 15 min to 30 min was observed. The bio-oil yield was decreased (27.34±0.78 wt%) at 45 min of reaction time. A highest bio-oil yield of 32.94±1.21 wt% was achieved at an optimum time of 30 min. However, the solid yield (16.88±1.24 wt%) was increased on increasing the reaction time, which can be attributed to the repolymerization of bio-oil components into solid. The increase in retention time of 45 min decreased the conversion to 83.12±1.24 wt%.

In a previous work, co-HTL of microalgae and rice husk with a 50:50 ratio yielded maximum bio-oil at 300 °C and then reduced a bit to 33.10% at 350 °C. The bio-oil yield increased up to 60 min, after which it slightly declined with further increase in residence time. A 60 min

residence time was sufficient for the formation of oily compounds, whereas extending the duration beyond this optimal point led to recondensation or repolymerization of the bio-oil (Gai et al., 2015a). The results of the present investigation indicated that co-feedstocks can be used for investigating commercial bio-oil production via co-HTL. Additional research at a larger scale will be helpful in the investigation of the physicochemical properties of fractional distillate-derived biofuel fractions and their subsequent engine applications.

5.3.5.4 Co-liquefaction process effect

Co-liquefaction of two feedstocks was designed to enhance the yield and properties of bio-oil. Co-liquefaction effect (CE) on bio-oil yield was described as variation between the actual yield of mixed feedstock and the mass-fraction-averaged yield derived from the yields of individual feedstocks. Synergistic effect (SE) happens when the value is positive while the antagonistic effect (AE) occurs when negative, or the additive effect arise when the difference is zero. The below mention equation for calculating the co-liquefaction effect on bio-oil was adapted from Yang et al., 2019 (Yang et al., 2019).

$$Co - liquefaction\ effect = Y_{co-feed} - \sum Y_i \times x_i \quad [5.1]$$

where $Y_{co\text{-}feed}$ signifies the yield from co-liquefaction of two feedstocks, Y_i implies yield from single feedstock HTL, and x_i denotes the mass fraction of each feed within the blend. The synergistic effect (SE) signified the enhancement in bio-oil yield, which is the objective of co-HTL. Such synergy on yield of bio-oil attributed to favourable interaction between intermediates and secondary products formed during the reactions from both feedstocks. The magnitude of the synergistic impact was contingent upon the mixing ratio of diverse feedstock and the parameters of the HTL reaction, including temperature and residence duration. The KMC4 microalgae showed maximum bio-oil yield of 33.50±1.45 wt% while the dairy sludge formed only 18.16±0.32 wt% of bio-oil from individual HTL reactions. On performing the co-HTL at the ideal reaction temperature of 350 °C at 75:25 wt% ratio (Microalgae: dairy sludge I) for 30 min, 32.94±1.21 wt% bio-oil was achieved.

For evaluation of the co-liquefaction effect on the basis of yield using equation 5.1, it was observed that the co-liquefaction effect was positive after calculation, suggested the synergistic effect on using two feedstocks for bio-oil production. The transformation of more organic compound from the feedstocks into bio-oil might be the reason behind this phenomenon at this

loading ratio. For understanding the synergistic influence on characteristics and properties of bio-oil, the discussion is given in section 5.3.6.2.

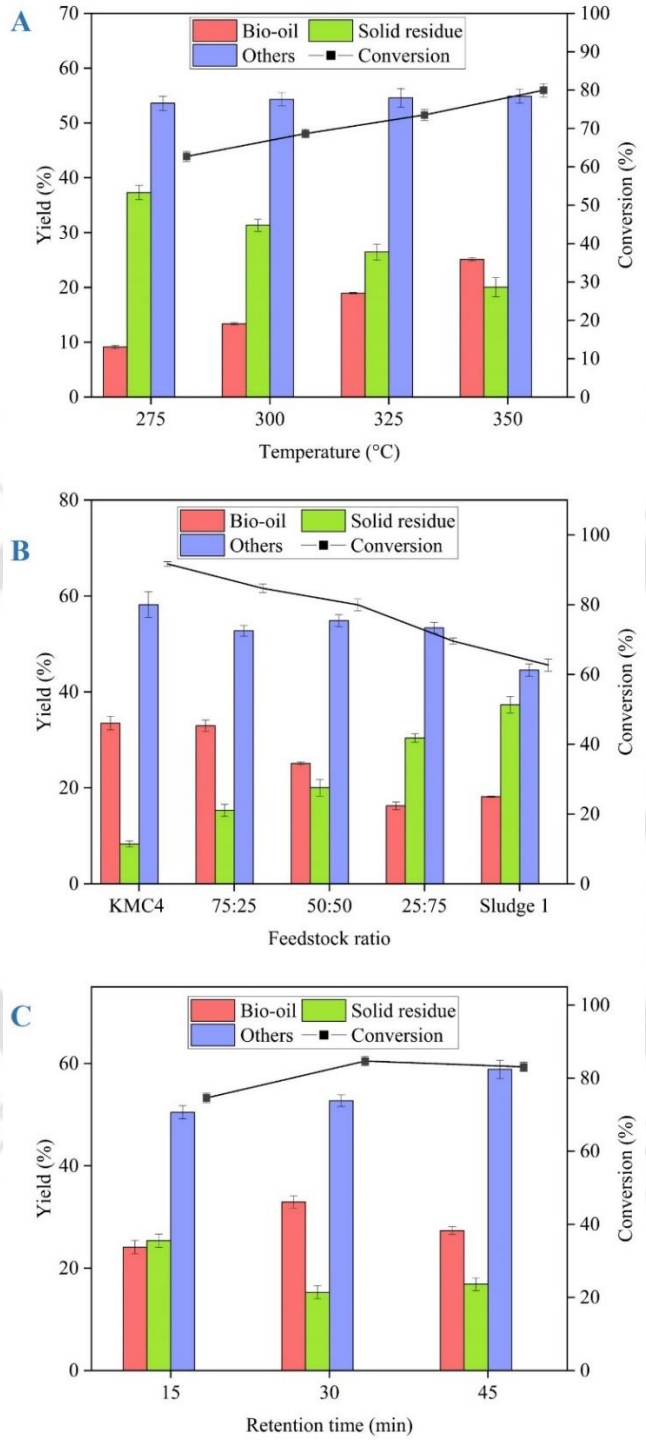

Figure 5.6. Effect of (a) temperature (50:50 wt% microalgae: dairy sludge I, 30 min); (b) blending ratio (at 350 °C, 30 min); and (c) time (at 350 °C, 75:25 wt% microalgae: dairy sludge I) on products distribution (wt%) and conversion (%) (Others includes aqueous phase, gaseous product and losses).

5.3.6 Bio-oil characterization

5.3.6.1 Elemental composition

All the bio-oil samples were composed of a major proportion of carbon (67.13% - 75.46%) and hydrogen (7.45% - 9.41%) (Table 5.3). The co-HTL bio-oil resulted in an increased atomic H/C (1.5 mol/mol) and decreased O/C (0.11 mol/mol) and N/C (0.03 mol/mol) ratio. A lower O/C and higher H/C in the co-HTL bio-oil were due to deoxygenation and dehydration reactions during the process. The sludge bio-oil constituted lowest atomic H/C (1.33 mol/mol) and highest O/C (0.2 mol/mol), and N/C (0.08 mol/mol) ratio which resulted in low energy density. However, the KMC4 bio-oil has almost a similar H/C (1.36 mol/mol) atomic ratio to sludge bio-oil. Contrarily, the N/C (0.05 mol/mol) and O/C (0.14 mol/mol) ratio of KMC4 bio-oil was lesser than sludge bio-oil. This has resulted in an intensification of the energy density of bio-oil.

This investigation demonstrated a pronounced reduction in nitrogen content during the co-HTL process. Deamination and decarboxylation reaction from nitrogenous compounds in the feedstock can be one of the reasons for reduction of nitrogen in bio-oil. A reduction in O/C and an increment in H/C gives higher HHV of co-HTL bio-oil. The comparative analysis between co-HTL bio-oil and petroleum crude showed a generally similar composition, with the primary differences being the elevated nitrogen and oxygen levels in the bio-oil. Therefore, catalytic upgrading of the bio-oil is suggested to enhance its quality and reduce these heteroatoms simultaneously (Mishra and Mohanty, 2020). Table 5.4 presents a structured benchmarking of co-hydrothermal liquefaction process against previous literature.

Table 5.3. Properties of bio-oils obtained from both HTL and co-HTL.

Properties[a]	KMC4	Dairy sludge	KMC4: dairy sludge	Commercial crude (Chaudhuri, 2016)
Bio-oil (%)	33.50 ± 1.45	18.16 ± 0.32	32.94 ± 1.21	–
C (%)	72.60± 0.75	67.13± 1.01	75.46 ± 0.81	85–90
H (%)	8.24± 0.07	7.45± 0.44	9.41 ± 0.65	10–14
N (%)	4.60± 0.72	6.86± 0.12	3.06 ± 0.07	<0.1–2.0
S (%)	0.87± 0.01	0.04 ± 0.04	0.15 ± 0.04	0.2-3
O[b] (%)	13.69	18.52	11.92	1-1.5
H/C (mol/mol)	1.36	1.33	1.50	-
O/C (mol/mol)	0.14	0.2	0.11	-
N/C (mol/mol)	0.05	0.08	0.03	-

N/O (mol/mol)	0.37	0.42	0.28	-
HHV (MJ Kg^{-1})	34.14	30.96	38.24	42–49
Energy Yield (%)	61.82	34.64	66.22	–

The CHNSO and bio-oil yield were analysed in terms of wt%.

The three Van Krevelen plots provided a comparative analysis of the elemental properties (in atomic ratios form) of bio-oils derived from KMC4, dairy sludge, and their co-hydrothermal liquefaction (Co-HTL) (Figure 5.7). These diagrams are critical for assessing fuel quality and understanding deoxygenation and denitrogenation trends. The top-left diagram plots the H/C vs. N/C atomic ratios, indicated a reduction in nitrogen content and an improvement in hydrogen content. The Co-HTL bio-oil (blue) showed the highest H/C and lowest N/C, suggested an increased amount of hydrogen and decreased amount of nitrogen which is favorable for fuel quality due to increased heating value and lower NOx emissions.

The dairy sludge bio-oil (brown) has higher N/C, indicated more nitrogenous compounds, which are common in protein-rich feedstocks such as sludge. The top-right diagram showed H/C vs O/C ratios to evaluate oxygen content reduction. The Co-HTL bio-oil appeared to have the best quality, with higher H/C and lower O/C ratios, reflected effective deoxygenation. The dairy sludge bio-oil showed the highest O/C, which reflected its lower degree of deoxygenation and consequently lower energy density and stability. The KMC4 bio-oil falls in between, showed moderate quality. The bottom diagram directly compared N/C vs O/C ratios.

The Co-HTL bio-oil was located at the lowest point for both ratios, clearly demonstrated effective simultaneous denitrogenation and deoxygenation. The linear trend line represented the trajectory of improvement from single-feed bio-oils toward the co-processed product. Overall, these plots collectively highlighted the synergistic benefits of co-liquefaction in improving the bio-oil quality by lowering heteroatom amount and increasing H/C ratio which is a key indicator of a more refined and energy-dense fuel.

Table 5.4. Literature comparison of the microalgae with other waste feedstock from co-HTL process.

Feedstock	Feedstock ratio	Bio-oil production conditions	Bio-oil Yield (%)	C (%)	H (%)	N (%)	O (%)	HHV (MJ/Kg)	References
Microalgae with faecal sludge	25% microalgae: 75% faecal sludge	300 °C for 60 min	38	69.19	9.63	2.81	18.37	33.83	(Islam et al., 2022)
Microalgae and peat	50:50 ratios	300 °C for 60 min	36.6	66.91	9.42	2.75	20.23	32	(Hossain et al., 2022)
Chlorella and sewage sludge	50:50 ratios	350 °C for 15 min	16.4	72.1	4.4	8.4	14.1	32.9	(Ellersdorfer, 2020)
Chlorella and food waste	50:50 ratios	350 °C for 15 min	17.1	71.2	3.9	8.7	15.8	32.4	(Ellersdorfer, 2020)
Chlorella and pharmaceutical sludge	1:1	320 °C for 60 min	40.58	73.82	8.80	5.79	9.61	35.99	(X. Zhang et al., 2022)
Microalgae and sewage sludge	1:1	340 °C for 30 min	~26	70.88	8.09	6.52	12.61	33.44	(Xu et al., 2019)
Monoraphidium sp. KMC4 and dairy sludge	75:25	350 °C for 30 min	32.94	75.46	9.41	3.06	11.92	38.24	Present work

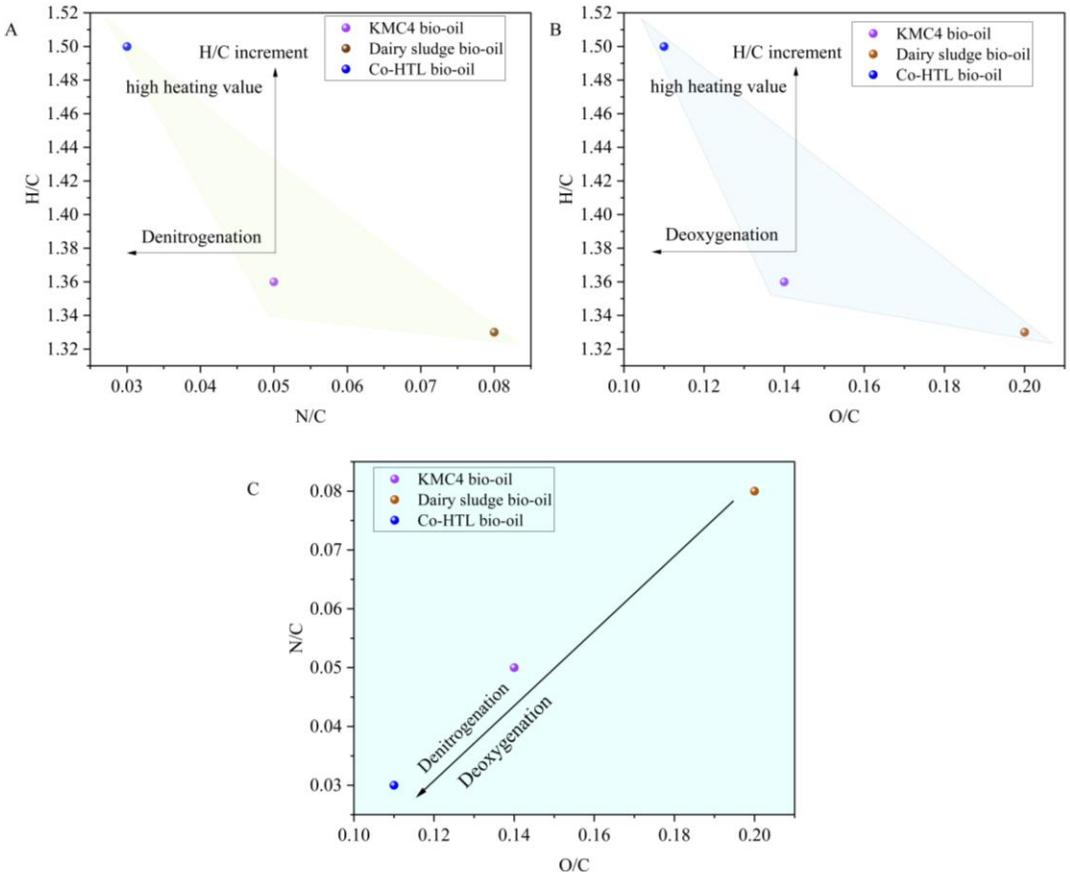

Figure 5.7. Van krevelan plots of KMC4, dairy sludge and co-feedstock bio-oil. (The atomic ratio is in mol/mol).

5.3.6.2 GC–MS analysis

The bio-oil obtained from co-HTL and individual feedstock of microalgae and dairy sludge were analyzed by GC–MS to determine major class of compounds (Figure 5.8). Identified compounds are depicted in Table A.2 in Appendix. Briefly, bio-oil obtained from KMC4 consisted of a mixture of classes including hydrocarbons (48.07%), esters (26.45%), and N and O-based compounds (13.36%). A lower fraction of phenols/their derivatives (6.48%), and other alcohols (2.55%) were reported. While bio-oil generated from dairy sludge constituted a major proportion of N and O-based compounds (40.76%) and hydrocarbons (27.83%). The esters (6.72%), alcohols (10.57%), and acids (11.77%) were also present in sludge bio-oil.

The presence of higher amounts of N and O compounds in dairy sludge bio-oil showed undesirable characteristics due to potential NOx emissions and instability. The amides, amines, nitriles, and N and O cyclic compounds, i.e., C═O and C–N functional group compounds, were categorized as N- and O-based compounds. The fatty acids was reacted with ammonium

(deamination of amino acids) to form aliphatic amine compounds namely, N-methylhexadecanamide, dodecanamide, N-3-methylbutyl-, dodecanamide, N-isobutyl-, hexadecanamide, myristamide, N-(3-methylbutyl)-,N,N-dimetylpalmitamide, octadecanamide, and myristamide, N-isobutyl-. Hexadecanamide is produced when ammonium-N reacts with hexadecenoic acid (Gai et al., 2015b; Liu et al., 2022).

The dairy sludge bio-oil produced only fatty acid amides or nitriles type of compounds from nitrogenous compounds present in it. However, the KMC4 and co-HTL bio-oil consists of both aliphatic amines and N- and O-based cyclic compounds. These cyclic compounds were formed due to a reaction between unstable or intermediates of lipid-protein or carbohydrate-protein breakdown products. This reaction is called as Maillard reaction, which is one of the major pathways happened in bio-oil formation from high protein microalgae. The lipids and fats present in dairy sludge under HTL conditions are converted to glycerol and fatty acids. Tetradecanoic acid and n-Hexadecanoic acid (~11.77%) were found in the bio-oil, which confirmed the presence of fats in the dairy sludge sample. However, the proportion of fatty acids reduced to 0.46% in co-HTL bio-oil. This can be due to a major shift in reaction mechanism using co-feedstock as only 25% of dairy sludge was added to 75% of KMC4 for bio-oil formation. The hydrocarbons were formed from the decarboxylation of fatty acid. The major hydrocarbons present in the dairy sludge bio-oil were dodecane, eicosane, heptadecane, hexadecane, pentadecane, 1-Nonadecene, 5β-cholest-3-ene, decane, and tetradecane (~18.14%).

The KMC4 bio-oil has the highest hydrocarbon content (~48%), contributed to better energy density. Hydrocarbons were significantly lower in the sludge bio-oil (~27%), reflected a more oxygenated, less energy-rich profile. The Co-HTL bio-oil exhibited the highest ester content (~48%), a class associated with improved fuel properties such as lubricity and volatility. This indicated synergistic esterification between KMC4 and sludge-derived intermediates. Also, the sludge bio-oil was also comprised of acids (~12%) and alcohols (~8%), both of which can lead to corrosiveness and poor storage stability. Their levels were significantly reduced in the Co-HTL bio-oil, highlighted an improvement in quality. The co-HTL bio-oil has reduced the aromatics, fatty acid amides, N and O based compounds, and alcohols. In this context, it can be elucidated that the co-HTL process might have favored the esters formation and reduced the Maillard reaction to form N and O cyclic compounds. The increase in ester compounds might be because of the conversion of fatty acid with alcohols to form methyl esters.

Interestingly, the proportion of ketone was increased in co-HTL. It has already been reported that glycerol separation from fatty acid during the process could be converted to ketones (Aljabri et al., 2022). The bio-oil also comprised of phenol and its derivatives in small amount which was derived from the degradation of carbohydrates-based compounds, suggested less toxic nature of bio-oil. The glucose and fructose sugar in microalgae are initially converted to furan-based intermediates and then to phenol through rearrangement (Gai et al., 2015b). Coming to the point of view of synergistic impact from co-liquefaction process based on properties and characteristics of bio-oil obtained, it was observed that calorific value and elemental properties were enhanced, supported that the co-liquefaction process have synergistic effect on bio-oil quality. The calorific value of bio-oil from co-feedstocks was increased along with the decrease in N and O-based compounds and increase in esters, confirmed by GC-MS.

Presence of Fe_2O_3 in the dairy sludge helps in deoxygenation reaction (Bian et al., 2017; de Caprariis et al., 2022) which has increased the H/C and decreased the O/C ratios of co-HTL bio-oil. The presence of CaO and Fe_2O_3 can facilitate esterification/transesterification via acid-base catalysis, which might have increased esters in co-feedstock bio-oil. Also, the reactions of alcohols and carboxylic acids forms esters that are catalyzed by acidic sites, which may come from mineral elements or acidic groups in the sludge (Widiarti et al., 2019). Iron consists of empty d-orbitals, which can increase the total number of active sites of the catalysts and Fe-Co also helps in deoxygenation and esterification reactions (Pulungan et al., 2024). A decrease in hydrocarbons in co-feed bio-oil compared to KMC4 bio-oil can be due to shifting of oxygen-retaining pathways (e.g., esterification, ketonization) rather than full deoxygenation to hydrocarbons. Also, N-rich compounds (from DS) may suppress deoxygenation by forming stable intermediates or reacting with acids, diverting pathways using CoO and Fe_2O_3 for promoting esterification reaction (Pulungan et al., 2024).

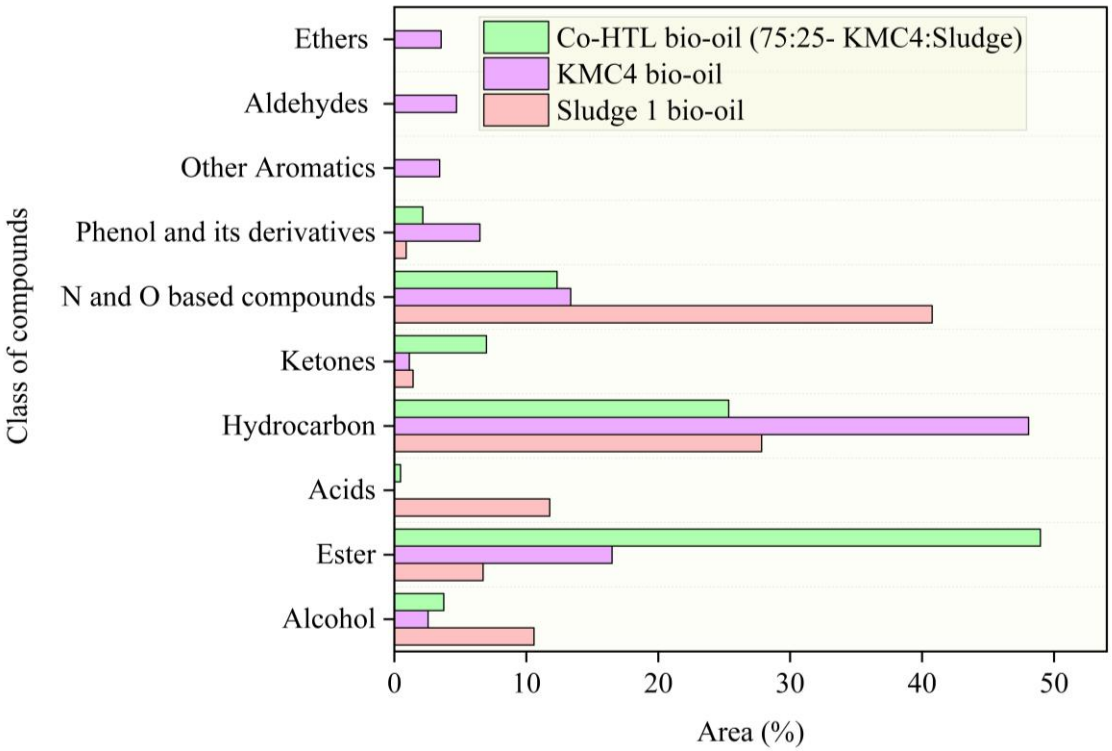

Figure 5.8. GC-MS of bio-oils from individual KMC4, dairy sludge and co-feedstock.

5.3.6.3 Probable Synergistic reactions in co-HTL studies

When microalgae KMC4 was co-fed with dairy sludge in co-HTL, a synergistic pathway emerged that explains the shift from nitrogen-rich heterocyclic and aromatic compounds toward long-chain esters. Under the high-temperature, subcritical water conditions of HTL, the lipids and proteins in KMC4 and the lipids in dairy sludge undergo extensive hydrolysis (Figure 5.9). This released free fatty acids (such as n-hexadecanoic acid from sludge (10.16%)) and alcohols during HTL, which act as precursors for esterification. At the same time, nitrogen-containing heterocycles and chlorinated aromatics from KMC4 peptide hydrolysis, such as triazole derivatives and chlorophenyl carbamates which are very unstable, producing small amines that partitioned into the aqueous phase or react with fatty acids to form aliphatic amides such as dodecanamide. So, a pool of free fatty acids, alcohols and N-species were available for secondary reactions. During HTL, free fatty acids reacted with alcohols forming long chain esters instead towards fatty acid amide and hydrocarbon formation.

Presence of cobalt oxide and Fe_2O_3 might have promoted ester formation (Pulungan et al., 2024; Wang et al., 2020). Hexadecanoic acid, hexadecyl ester (22.59%) and Octadecanoic acid, octadecyl ester (11.01%) forms of esters were found in co-HTL bio-oil. However, alcohols were formed from carbohydrate breakdown (sugar to alcohols), glycerol (from triglyceride

hydrolysis), or sludge borne fatty alcohols (e.g. 1-octadecanol and 1-dodecanol). This explained that both feedstocks supply fatty acid and alcohols for ester formation while catalytic ions present in sludge helps in ester formation. N-heterocyclic rings (triazoles, pyridazines) and aromatic heterocycles were susceptible to hydrolysis, ring opening, or cleavage under HTL conditions.

Ring opening yielded smaller amines or ammonia which partition to the water phase or form fatty amides. Some triazole/triazolone derivatives and chlorinated heteroaromatics listed in KMC4 bio-oil was not found in Co-HTL. Coming to the decrement in aromatics, aromatic rings can be partially hydrogenated or alkylated to form alkanes/alkylated cyclohexanes or be incorporated into larger aliphatic chains via alkylation. Aromatics such as 2,4-Di-tert-butylphenol and benzene derivatives show decreased proportion in Co-HTL which is consistent with hydrogenation/alkylation. This showed lower aromatic signal in co-HTL bio-oil.

Overall, the fatty acids or aliphatic compounds pathway to form fatty amide and aromatics diverged towards esters formation. Myristamide, N-methylhexadecanamide and Octadecanamide like molecules arranged themselves to form Octadecanoic acid, octadecyl ester. This reduction of heterocyclic N and long chain aliphatic amides towards ester and small chain fatty amide formation lowered N-heterocycle proportion in the co-HTL bio-oil fraction. Together, these transformations decreased the number of nitrogen-containing heterocycles and aromatic compounds in the bio-oil while simultaneously increased the yield of long-chain esters.

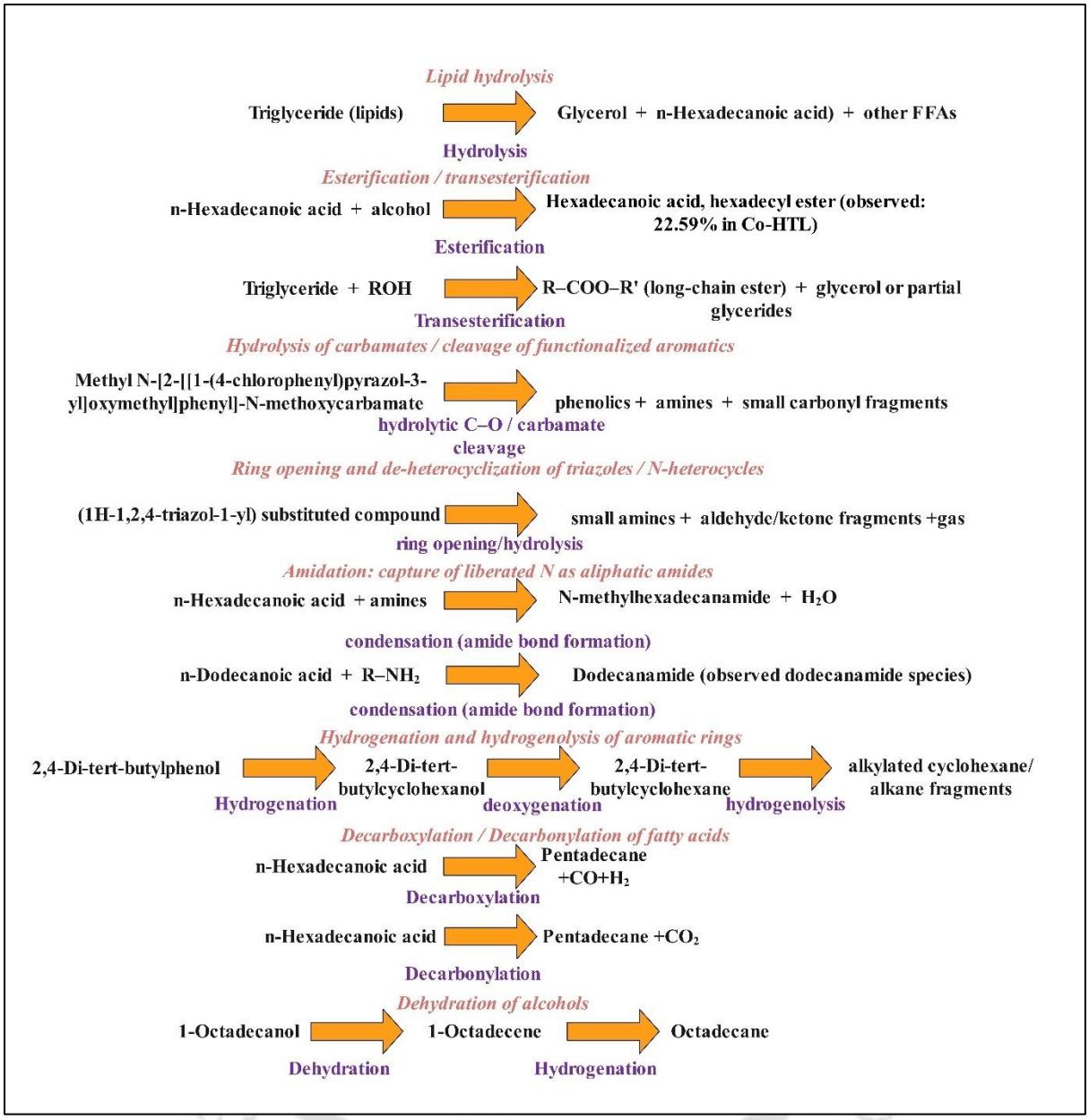

Figure 5.9. Probable reactions happened during co-liquefaction.

5.3.6.4 Boiling point distribution of bio-oils

The thermal stability of bio-oils was performed using TGA due to the presence of compounds with higher boiling points that cannot be detected by GC-MS analysis (Huang et al., 2018b). The boiling point distribution profiles of bio-oil from individual and co-feedstocks are presented in Figure 5.10. All bio-oils have shown distinct thermal stability profile with respect to the boiling points of product. Poor distillation distribution was observed in dairy sludge bio-oil. Only 31.56% of low boiling point compounds were recorded from dairy sludge bio-oil which will include products such as heavy naphtha (<193 °C), kerosene (193-271 °C), and gas

oil fractions (271-343 °C). A huge fraction of vac gas oil (52.82%) was observed with 15.62% of vac residue in dairy sludge bio-oil. The higher volatile content with lower ash amount in algae formed higher heavy naphtha (6.26%), kerosene (12.69%), and gas oil (35.34%) proportion.

On comparing the bio-oil from co-feedstock to individual KMC4, 43.42% was reported with products heavy naphtha and kerosene from the former one. Alkanes, aromatics, and alkenes represent heavy naphtha and kerosene fractions which were present in major proportion in KMC4 bio-oil. However, esters do not come under petroleum-derived naphtha or kerosene fractions. The esters were present in thermochemical based bio-oil products, they resemble compounds in naphtha-range fuels due to their volatility and moderate boiling points. Only 18.95% of heavy naphtha and kerosene distribution resulted from individual KMC4 bio-oil. An almost similar vac residue of 10.79% was observed in co-HTL bio-oil in comparison with individual KMC4 (11.37%) which was also lower than of dairy sludge (15.62%). The presence of high vac residue in dairy sludge bio-oil was due to presence of heavy compounds.

The co-HTL bio-oil (reaction with 75:25-KMC4: dairy sludge) had 66.33% light fractions (30–343 °C) which was higher than individual KMC4 (54.29%). Hence, a better boiling points distribution profile of compounds could be due to the availability of minerals in dairy sludge (Fe, Co) and microalgae (Al, K, Ca, Mg, etc.) that exhibited some catalytic properties during the co-HTL reaction, which enhanced the proportion of heavy naphtha and kerosene in contrast to microalgae fractions.

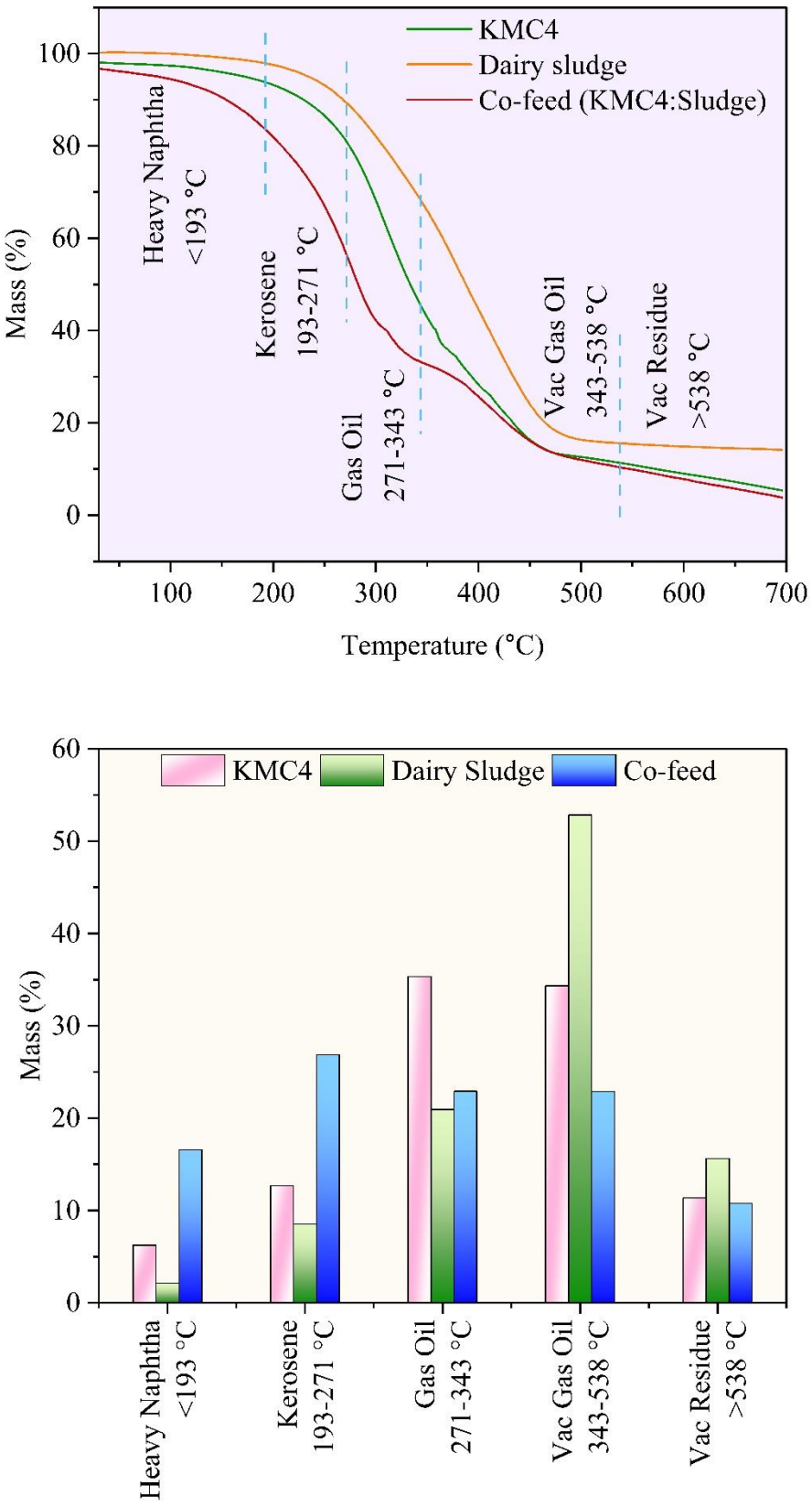

Figure 5.10. Thermal degradation curves and boiling point distribution of the bio-oils obtained by single feedstock HTL and co-HTL.

5.3.6.5 Functional groups analysis

The functional groups in the bio-oils were demonstrated using FTIR spectrums (Figure 5.11). The O–H and N–H stretching vibrations appeared in the 3100 cm^{-1}–3600 cm^{-1} region. The O–H stretch was commonly found in alcohols, carboxylic acids, and phenols, and appeared as a broad and strong peak due to hydrogen bonding, often spanning a wide range from around 3200 cm^{-1} to 3600 cm^{-1}. The N–H stretch was associated with amines or amides, sharper and narrower with medium intensity. The Amide II (N–H bend + C–N stretch) appeared between 1510 cm^{-1} –1580 cm^{-1} while Amide I (C=O stretch) was found between 1630 cm^{-1} –1690 cm^{-1}. The presence of long-chain aliphatic hydrocarbons was indicated by the broad and intense peaks between 3000 cm^{-1}–2800 cm^{-1} and 1460 cm^{-1}–1350 cm^{-1}, which were attributed to C–H stretching of CH_3 and CH_2 groups.

The aliphatic hydrocarbons, carboxylic acids, ketones, aldehydes, and esters presence in bio-oil were indicative of the carboxyl functional groups that are designated to the peak between 1800 cm^{-1}–1590 cm^{-1}. These peaks were more prominent in co-HTL bio-oil, suggested a higher content of saturated aliphatic compounds compared to KMC4 and dairy sludge bio-oil. Strong bands observed around 1260 cm^{-1} – 1000 cm^{-1} in all three samples, were associated with C–O stretching vibrations, likely from aliphatic esters, alcohols, or carboxylic acids. Dairy sludge and co-HTL bio-oil showed more intense peaks in this range, indicating a significant number of oxygenated functionalities. In the 900–700 cm^{-1} region, weak to moderate bands were detected, which can be assigned to aromatic C–H out-of-plane bending vibrations, signified the presence of substituted aromatic rings, which were prominent in KMC4 bio-oil.

Taken together, the fingerprint region highlighted subtle but significant structural differences in the three bio-oils. Co-HTL bio-oil appeared richer in oxygenated aliphatics, which can be due to presence of esters, ketones, and alcohols while KMC4 retained more aromatic characteristics, which can be related to presence of N and O-based compounds. These differences can be correlated with feedstock type or HTL processing conditions.

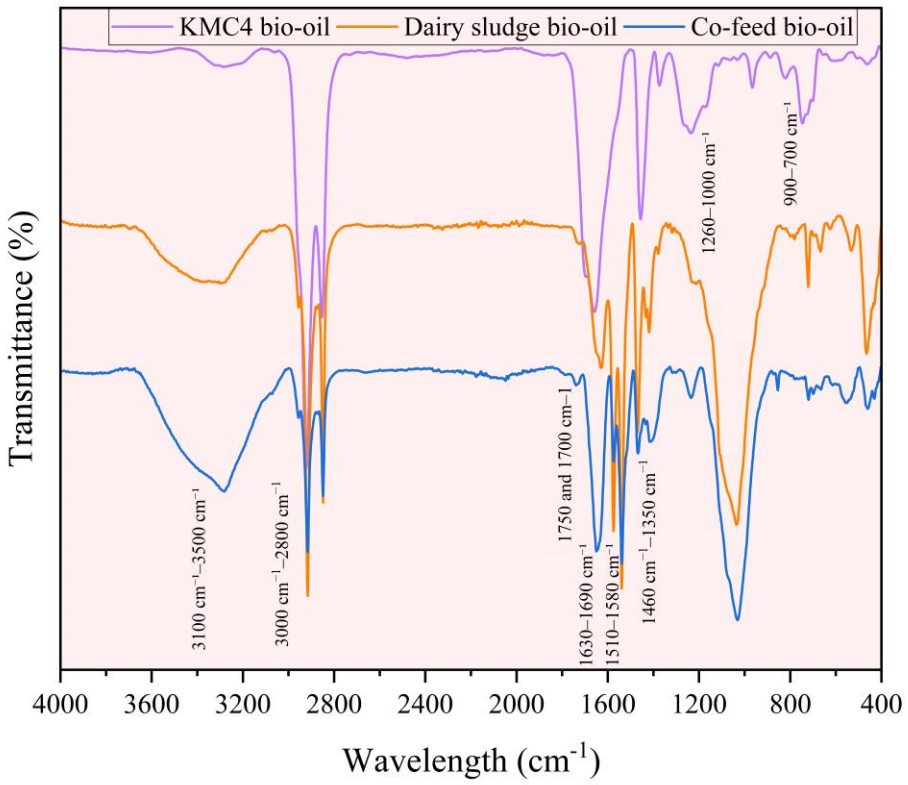

Figure 5.11. FTIR spectrums of bio-oils.

5.3.7 Aqueous phase and solid residue characterization

The liquid product and solid residue generated from HTL and co-HTL process were consist of nutrients and energy value which showed their potential towards reuse. The pH of aqueous phase ranged between mid-neutral to alkaline in all three optimum aqueous phase samples due to the presence of nitrogen via deamination and hydrolysis reactions. This can be confirmed by ammonium and total nitrogen in aqueous phase samples (Figure 5.12). The maximum ammonium-N (3.68 g/L) and total nitrogen (4.79 g/L) were found in KMC4 aqueous phase. The lowest concentration of ammonium-N (0.91 g/L) and total nitrogen (1.07) were reported in dairy sludge aqueous phase.

The total carbon (12.1 g/L) and organic carbon (9.9 g/L) were found to be highest in KMC4 aqueous phase sample. Moderate concentration of total organic carbon (8.11 g/L) and total carbon (10.73 g/L) were reported in the co-HTL aqueous phase while the lowest were observed from dairy sludge (total organic carbon (3.21 g/L) and total carbon (3.50 g/L)). The aqueous

phase can be used for microalgal cultivation, anaerobic fermentation, and reuse during HTL (SundarRajan et al., 2021; Taghipour et al., 2021; Watson et al., 2020).

The solid residue from HTL and co-HTL process solid residue have comparable elemental value and energy density (Table 5.5). The solids produced from HTL of dairy sludge (11.04 MJ/kg) have lower HHV value compared to KMC4 (17.64 MJ/kg) and co-HTL process (14.73 MJ/kg). The carbon content of KMC4 solid residue (46.74%) was comparably higher than that of dairy sludge (22.33%). While the nitrogen content of solid residue (5.24%) from dairy sludge was higher compared to solid residue from KMC4 (3.12%) and co-feed (4.01%). The solid residue or biochar can be also used in other applications such as adsorption (Ponnusamy et al., 2020), wastewater treatment (Law et al., 2022; Ponnusamy et al., 2020), catalyst for energy generation (Wang et al., 2021), and in anaerobic digestion as a carbon supplement and buffer (Chen et al., 2018; Ponnusamy et al., 2020).

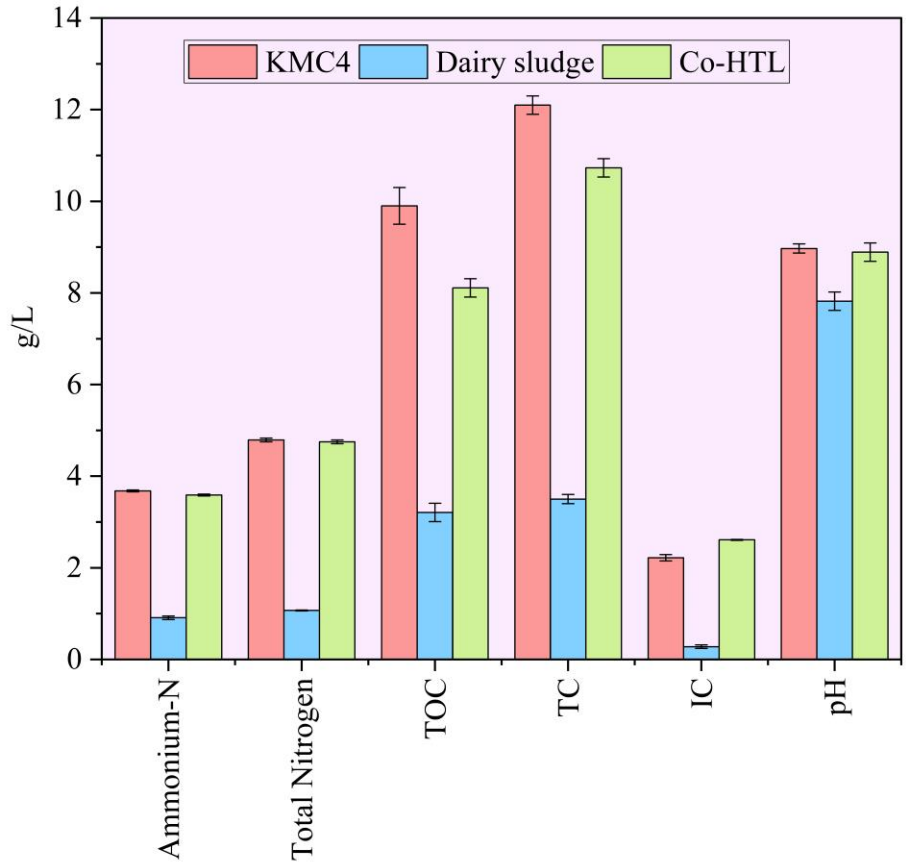

Figure 5.12. Aqueous phase characterization obtained from both individual HTL and co-HTL process. TOC represents total organic carbon, TC represents total carbon, and IC represents inorganic carbon of the aqueous phase.

Table 5.5. Elemental Composition of solid residue obtained from individual and co-HTL process. The CHNS was estimated on wt% basis.

Solid Residue	C (%)	H (%)	N (%)	S (%)	HHV (MJ/kg)
KMC4	46.74	6.34	3.12	0.17	17.64
Dairy Sludge	22.33	7.53	5.24	0.76	11.04
Co-feed	33.12	7.13	4.01	0.36	14.73

5.4 Summary

Microalgae as a renewable feedstock is receiving an attention for bio-oil production using HTL. Still, the feedstock accessibility throughout the year is a challenge. To assure the regular supply of feedstock and through waste to bioenergy approach, this investigation demonstrated the feasibility of the co-HTL of dairy wastewater treatment derived sludge and microalgae as a feedstock for bio-oil generation. It was found that the combination of microalgae and dairy sludge in a ratio of 75:25 produced bio-oil with 32.94 wt% yield compared to other combinations with a calorific value of 38.24 MJ kg^{-1}. Microalgae yielded higher bio-oil (33.50%) than dairy sludge (18.16%) at 350 °C for 30 min. The Co-HTL bio-oil showed the highest H/C (1.5 mol/mol) and lowest N/C (0.03 mol/mol), suggesting it possesses higher amount of hydrogen and a reduced amount of nitrogen which has resulted in increased heating value. The Co-HTL bio-oil appeared to have the best quality, with higher H/C (1.5 mol/mol) and lower O/C (0.11 mol/mol) ratios, indicated effective deoxygenation and dehydration reactions. The bio-oil derived by co-HTL of co-feedstocks exhibited improved quality, characterized by decreased levels of N-heterocyclic compounds, aromatics, and increased esters with better calorific value. The co-liquefaction process showed synergistic effect on the basis of quantity and quality. The thermal stability from TGA proved that a better boiling points distribution profile of compounds in bio-oil from co-HTL of dairy sludge and microalgae (25:75), consisted of higher amount of heavy naphtha and kerosene fractions. This bio-oil can be further refined through upgradation system for its use as aviation fuel. The bio-oil characterization confirmed that co-HTL process of dairy sludge and microalgae is a promising feedstock for bioenergy production.

Chapter 6

Non-catalytic and catalytic co-pyrolysis of microalgae and dairy sludge: An ex-situ fed batch process using H-ZSM-5 towards sustainable biofuel production

Chapter 6. Non-catalytic and catalytic co-pyrolysis of microalgae and dairy sludge: An ex-situ fed batch process using HZSM-5 towards sustainable biofuel production.

Graphical abstract of Chapter 6

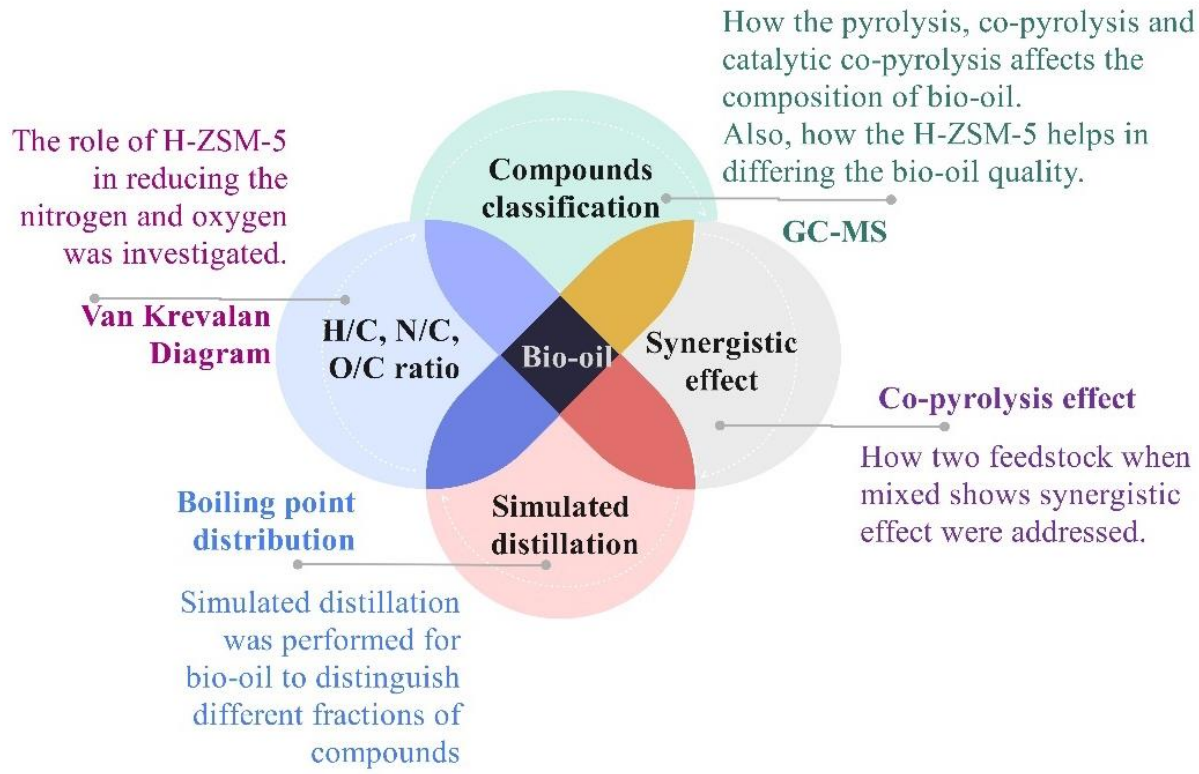

6.1 Background

Combining the dairy sludge with microalgae offers an alternative solution to individual feedstock utilization. The co-pyrolysis method takes advantage of the complementary characteristics of both feedstocks, presenting a promising strategy to enhance bio-oil quality and yield, while also lowering production costs by utilizing low-cost feedstock. Co-pyrolysis, the simultaneous thermal decomposition of two or more feedstocks, has emerged as a promising technique for improving both the yield and quality of bio-oil (Mustapha and Isa, 2024). In particular, the combined pyrolysis of microalgae with different biomass types has demonstrated considerable potential to enhance the properties and output of bio-oil (Khodaparasti et al., 2023; Wang et al., 2016).

Researchers are using the co-pyrolysis process to enhance production of value-added products and economic efficiency. Synergistic and antagonist effects between microalgae and sewage sludge were observed after co-pyrolysis of both feedstocks at optimized conditions. The positive synergistic effect was observed in favour of gas formation and showed a negative effect on bio-oil yield (Khodaparasti et al., 2023). It was observed that co-pyrolysis was better than individual pyrolysis of sludge due to better heat value of microalgae addition (Wang et al., 2016). Blending these two biomass types can offset their individual drawbacks and improve overall process efficiency. Nonetheless, obtaining optimal yields and desirable product quality from this mixture is complex and requires catalytic interventions to steer the reaction pathways toward valuable liquid fuels.

The achievement of optimal yield and quality from co-pyrolysis is still a challenge and requires a catalytic approach. In previous literature, H-ZSM-5 catalyst increased the reaction rates and diminished the gas formation during the pyrolysis of sewage sludge (Zaker et al., 2021). Also, the catalyst showed strong performance in increasing the aromatization and deoxygenation but showed a lesser effect in terms of denitrogenation reactions. It was also noticed that the bio-oil yield decreased in a catalytic process compared to non-catalytic pyrolysis (Mustapha et al., 2021). The ZSM-5 possesses distinctive characteristics, including medium pore size, robust acid sites, and a high silica-alumina ratio, which enhance its catalytic activity for cracking and aromatization (Thangalazhy-Gopakumar et al., 2012). Using the catalyst with multifunctional qualities could lead to progress in better quality bio-oil, leading towards sustainable and efficient conversion. Consequently, this study was conducted on the pyrolysis of microalgae and dairy sludge utilizing the H-ZSM-5 catalyst for better quality fuel production. Also, the target of this study is to understand the co-pyrolysis and catalytic effect in terms of yield and quality by assessing the three factors: synergistic, antagonistic, or additive. These factors will allow this investigation to understand if there is any interaction between molecules from both feedstocks to enhance the bio-oil characteristics and yield.

6.2 Methodology

In this chapter, microalgae was co-fed with dairy sludge for bio-oil production from pyrolysis. An interaction between two different feedstocks: microalgae and dairy sludge was studied during co-pyrolysis reactions. The effect of H-ZSM-5 in changing the profile of bio-oil was investigated via GC-MS analysis. Boiling point distribution of bio-oils was observed along with compounds differentiations through GC-MS analysis.

6.3 Result and Discussion

6.3.1 Fresh Catalyst characterization

The XRD diffraction peaks of fresh catalyst showed a similar peak pattern zeolite database samples. The five main peaks centred at 2θ= 8.02°, 8.89°, 23.21°, 24°, and 24.4°, corresponded to JCPDS card No. 00-44-0002 for mutinaite (a zeolite), which confirmed the MFI structure of the H-ZSM-5 (Figure 6.1). The ammonia TPD (Temperature Programmed Desorption of Ammonia) profiles illustrate the presence of weak and strong acidic sites. The Fresh H-ZSM-5 (red curve) exhibits wo prominent peaks: a lower-temperature peak around 250 °C representing weak acid sites (547.57 µmol/g) (Brønsted or Lewis sites on the surface) and a well-defined high-temperature peak centered near 500°C representing strong Brønsted acid sites (280.67 µmol/g) within the zeolite pores (Figure 6.2).

In scanning electron microscopy, fresh H-ZSM-5 showed well-defined crystalline morphology, which was a characteristic of the catalyst framework (Figure 6.3A). It was revealed that catalyst particles exhibited the characteristic coffin-shaped/prismatic morphology of MFI zeolite. Occasional aggregation of smaller crystallites into larger clusters was observed. The clear faceting and absence of an amorphous phase indicated a high degree of crystallinity in fresh catalyst.

SAED pattern showed sharp, well-defined diffraction spots and planes in fresh catalyst, confirmed the high crystallinity and ordered planes of the MFI framework (Figure 6.3B). Overall, SEM and diffraction planes of fresh H-ZSM-5 showed well-defined rectangular and square-shaped crystals with smooth surfaces and crystalline planes, confirmed the integrity of the catalyst. Also, the elemental distribution confirmed the well dispersion of silicon, almunium and oxygen over the catalyst (Figure 6.3C).

The XPS spectra of pristine and crystalline H-ZSM-5 exhibited the characteristic surface chemical states of the zeolite (Figure 6.3D). A prominent peak in the Si 2p region, located about 103.28 eV, corresponded to silicon within the silica (SiO_2) framework. This peak also indicated the presence of O-Si-O/Si-O-Al bonds inside the siliceous framework. The presence of silicates was confirmed by binding energy peak at 104.5 eV. The O 1s spectrum exhibited a substantial contribution from lattice oxygen in metal oxide (like Al-O bond) and silicon dioxide at 531.07 eV and 532.86 eV, respectively. The Al 2p deconvoluted spectra revealed three distinct peaks, which showed the different forms of bonds with aluminum species. The small peak at 73.4 eV corresponded to Al species while a peak at 74.65 eV was indicative of

framework tetrahedral Al within the zeolite structure as $A1_2SiO_5$, sillimanite, which was also seen in the XRD plot (Moulder et al., 1992). The peak at 75.45 eV referred to AlO(OH) form of H-ZSM-5, which confirmed its presence from XRD spectra (2θ=14°, 22.28° and 37.62°).

The thermal degradation curves showed a slight weight loss of around 6-10 %, attributed to moisture loss from room temperature to 200 °C in an inert atmosphere (Figure 6.4). Above this, the catalyst was considered stable up to a temperature of 800 °C. This confirmed the excellent thermal stability of pristine H-ZSM-5. The initial weight loss below ~150 °C is attributed to the removal of physically adsorbed water and a minor weight loss at higher temperatures associated with dehydroxylation of Brønsted acid sites. While the absence of significant mass loss at elevated temperatures confirmed that the H-ZSM-5 is stable and free of organic residues.

The nitrogen adsorption-desorption isotherms of fresh H-ZSM-5 was a combination of type I and type IV (Figure 6.5) with an inflection point starting around $P/P_0 = 0.48$, which represents the presence of intercrystalline mesopores (Sang et al., 2017). The surface area of pristine H-ZSM-5 catalyst was 278.42 m^2/g, revealed an accessible active surface for adsorption and catalytic activity. The nitrogen adsorption analysis revealed a micropore volume of 0.11 cm^3/g, confirmed the formation of a microporous network characteristic of the MFI structure of H-ZSM-5 (Table 6.1). This revealed that the internal channels were well accessible for efficient contact between pyrolytic vapors and catalytic sites. This increases the probability of secondary reactions like dehydration and aromatization.

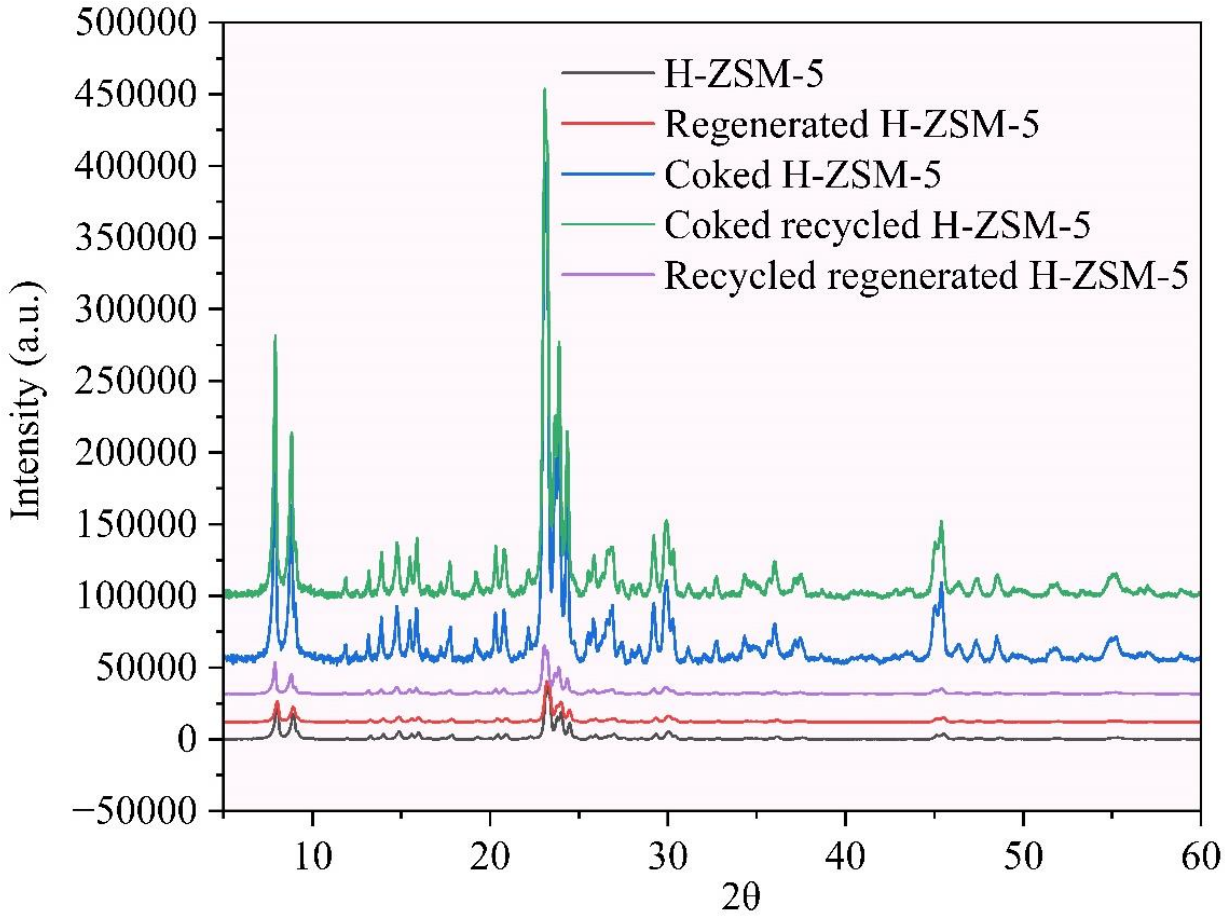

Figure 6.1. XRD pattern of H-ZSM, regenerated and coked catalyst.

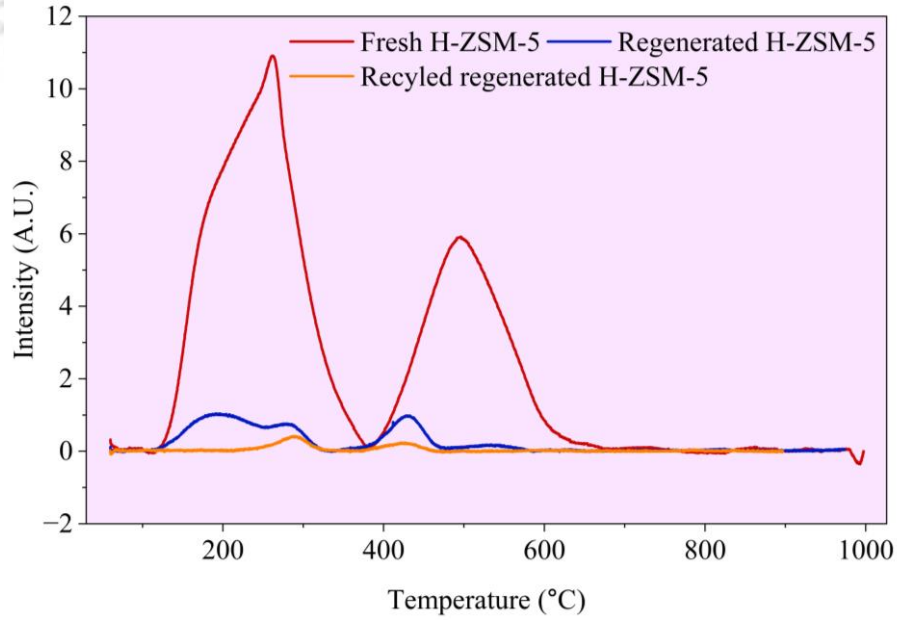

Figure 6.2. Ammonia TPD profile of fresh and regenerated H-ZSM-5.

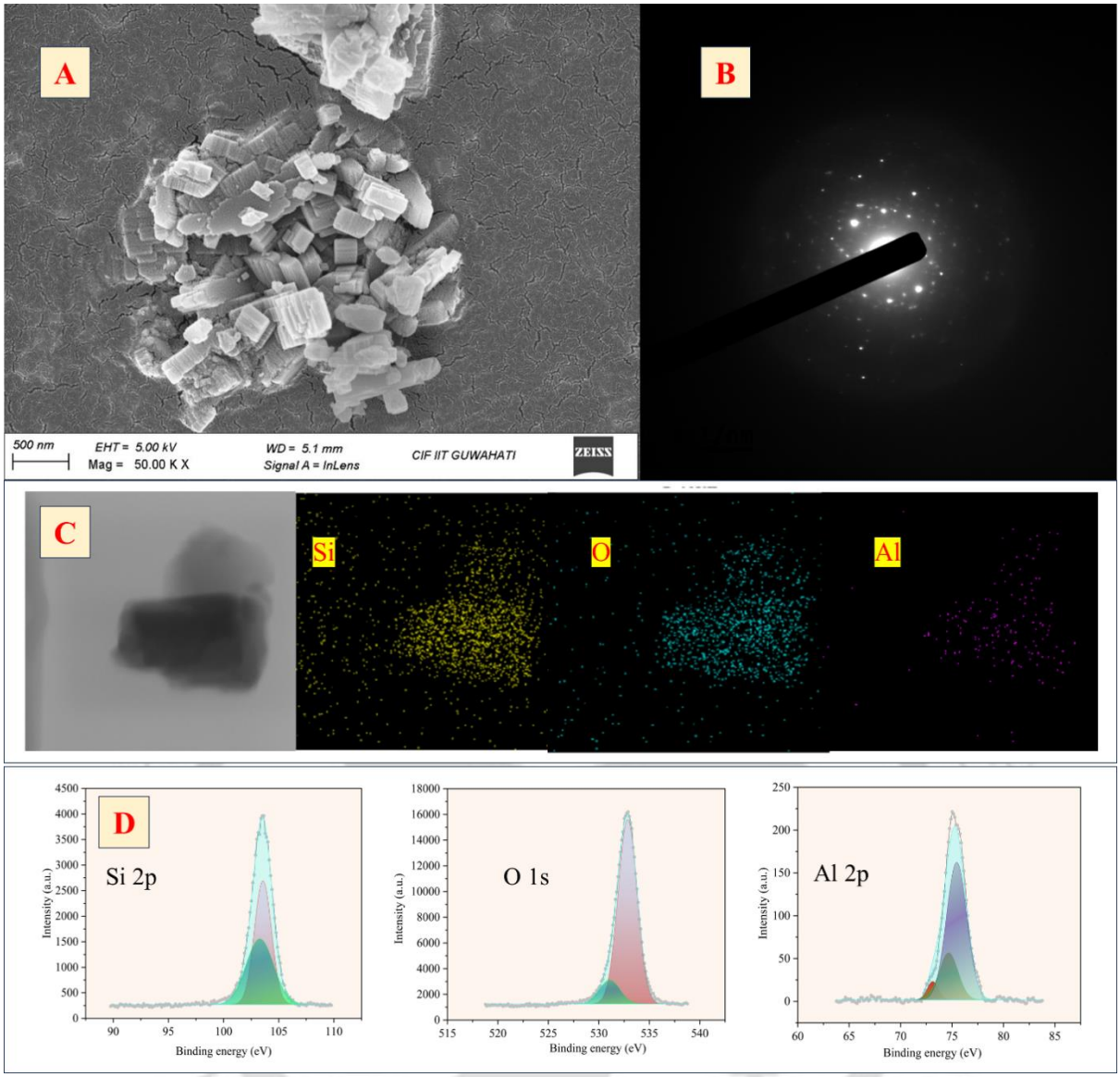

Figure 6.3. Fresh catalyst A) Surface topography; B) SAED pattern; C) Elemental distribution; D) XPS spectra.

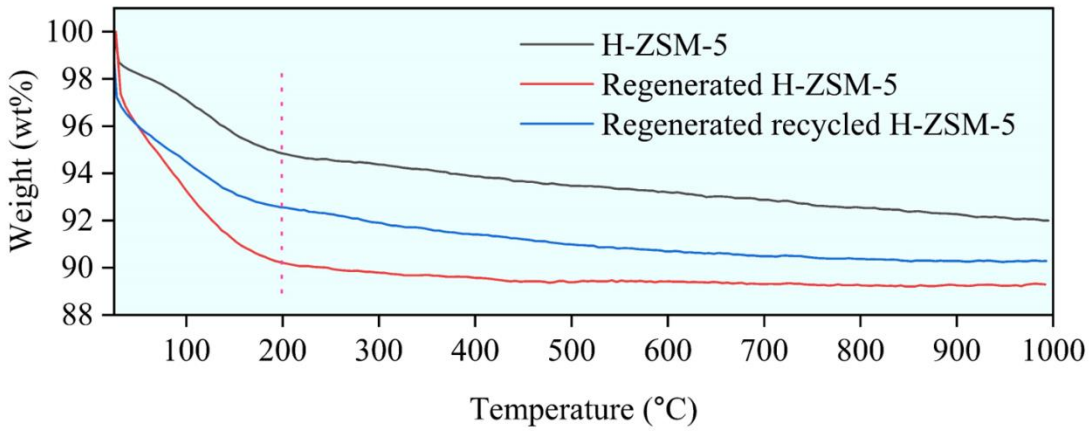

Figure 6.4. Thermal stability of fresh and regenerated H-ZSM-5.

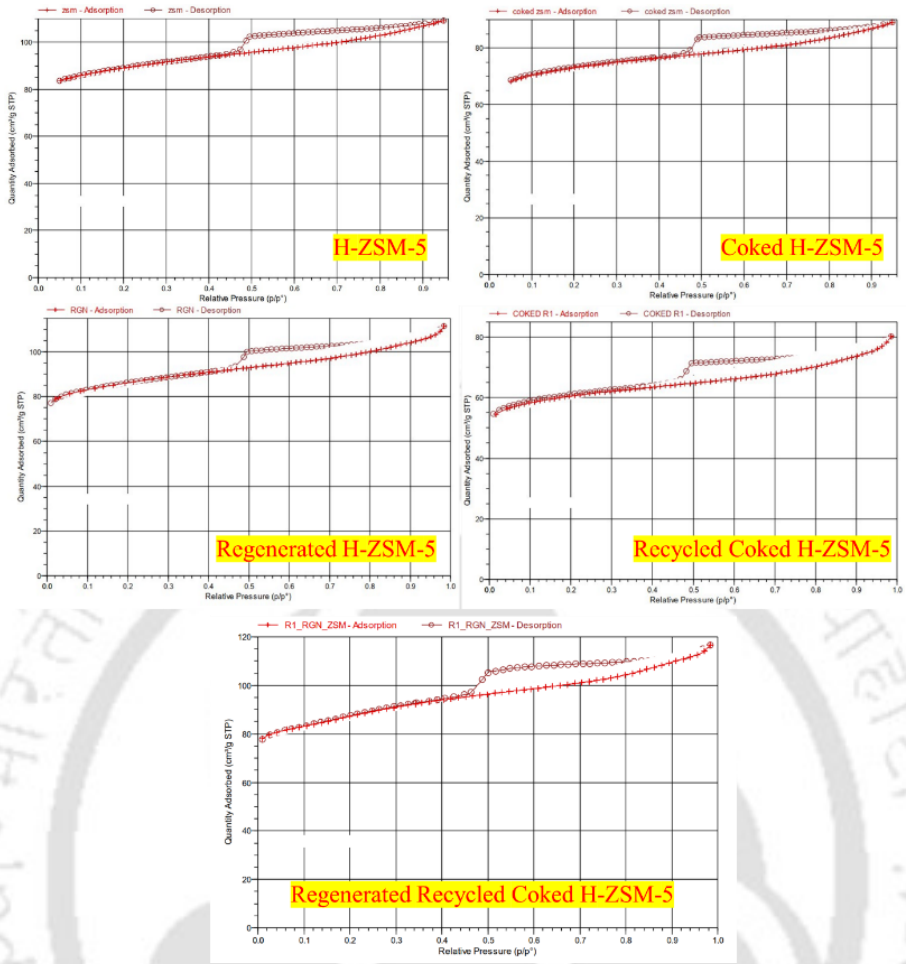

Figure 6.5. Adsorption and desorption profile of fresh, regenerated, coked, recycled coked H-ZSM-5.

Table 6.1. Textural parameters of fresh and spent H-ZSM-5.

Name	BET Surface Area (m^2/g)	Micropore volume (cm^3/g)	Pore Size (nm)	Mesopore volume (cm^3/g)	Micropore Surface Area (m^2/g)	Mesopore Surface Area (m^2/g)
Calcined H-ZSM-5	278.42	0.11	3.4	0.05	211.14	142.3
Coked H-ZSM-5	228.02	0.08	3.3	0.04	172.71	115.75
Regenerated H-ZSM-5	266.02	0.1	3.44	0.05	199.5	132.66
Coked catalyst recycled	188.43	0.07	3.39	0.03	143.44	96.04
Regenerated recycled (R1) H-ZSM-5	274.1	0.09	3.37	0.02	181.12	93.59

Overall, the structural, morphological, and thermal properties of pristine H-ZSM-5 provided additional bulk, morphological, and thermal information that complemented and extended the surface chemical insights gained from XPS analysis. The phase peaks confirmed highly crystalline H-ZSM-5 with a pure MFI framework and the absence of any additional peaks associated with impurity phases or amorphous carbon. SEM micrographs showed the typical coffin-shaped morphology and well-defined crystal edges, indicated good crystallization and structural integrity. The SAED pattern further corroborated the crystalline nature of the zeolite by showing well-ordered diffraction spots. The surface and micropore volume revealed the microporous framework for efficient diffusion of reactants and products and contributing to significant catalytic activity. The thermal stability revealed that H-ZSM-5 is stable and free of organic residues at high temperature. Together, these approaches confirmed that the pristine H-ZSM-5 possesses a highly crystalline, thermally stable MFI structure with well-defined morphology, which was completely in agreement with the surface chemical state observed by XPS.

6.3.2 Products yield

6.3.2.1 Pyrolysis and co-pyrolysis of KMC4 and dairy sludge

Temperature directly influenced the product distribution in pyrolysis. This study encompassed experiments conducted at distinct reaction temperatures, spanning the range of 500 °C-600 °C, with a residence time of 60 min and 120 min. The pyrolytic liquid generated during co-pyrolysis was due to the rapid breakdown and depolymerization of the biomass and sludge. According to the findings of this investigation, an increase in the pyrolysis temperature led to a greater oil yield till 550 °C from both the individual feedstocks. An upward trajectory in bio-oil yield became evident, escalated from 17.61 wt% to 24.23 wt% as the temperature was raised from 500 °C to 550 °C for KMC4 algal biomass (Figure 6.6A).

While 19.06 wt% of bio-oil was obtained at 550 °C from dairy sludge feedstock. However, beyond 550 °C, a declined trend in bio-oil production was reported, likely attributed to the transformation of organic compounds into non-condensable gases from both the feedstocks. The gas yield increased from 14.05 wt% to 28.52 wt% as the temperature increased from 550 °C to 600 °C in the case of KMC4 biomass. While the non-condensable gas yield increased to 32.54 wt% at 600 °C with dairy sludge. At higher temperatures, the secondary reactions of vapors to gases become more prominent. The solid residue yield reduced from 68.34% to

53.25% for KMC4, while it diminished from 62.25% to 52.23% for dairy sludge at temperature from 500 °C to 600 °C.

The product distribution from individual feedstocks was also investigated by changing heating rate and reaction time. Increasing the heating rate and reaction time did not enhance the bio-oil production from both the feedstocks. By changing the heating rate from 20 °C min^{-1} to 40 °C min^{-1}, a decrease in bio-oil yield (24.23% to 20.12%-KMC4 and 19.06% to 14.32%-dairy sludge) was observed from both feedstocks (Figure 6.6B). It was observed that the higher heating rate of 40 °C min^{-1} increased the gaseous product formation compared to 20 °C min^{-1} for both individual feedstocks. A high heating rate in pyrolysis enhanced gas yield by rapidly breaking down biomass into lighter molecules, favoring devolatilization and cracking reactions, especially when combined with high temperatures, which forces more organic matter into the gaseous phase.

By changing the reaction time from 60 min to 120 min, a significant change in bio-oil (24.23% to 19.46% for KMC4 and 19.06% to 14.98% for dairy sludge) was observed (Figure 6.6C). The longer biomass stays at a high temperature, the more secondary cracking of volatiles occurs. When the vapor residence time was higher, the volatile species generated during thermal decomposition remained longer in the hot reaction zone (Aravind et al., 2020). This extended exposure promoted secondary reactions such as cracking of the volatile intermediates. These reactions converted condensable vapors into gaseous products, thereby increased the gas yield. In contrast, when the vapor residence time is shorter, the volatile products are quickly swept away from the reaction zone before significant secondary reactions can occur, resulting in higher liquid yield and comparatively less char and gas products.

The co-pyrolytic study of co-feed at the optimized condition of 550 °C, 20 °C min^{-1} heating rate for 60 min. A 28.42 wt% bio-oil was recovered from pyrolysis of co-feedstock (KMC: sludge-75:25), with 50 wt% solid residues left in the reactor. The non-condensable gas was found to be 21.58 wt% at these optimized conditions. Increasing the sludge for blending for co-pyrolysis enhanced the solid biochar formation along with decreased bio-oil yield (Figure 6.6D). This is due to reduced volatiles fraction in increasing the dairy sludge with microalgae.

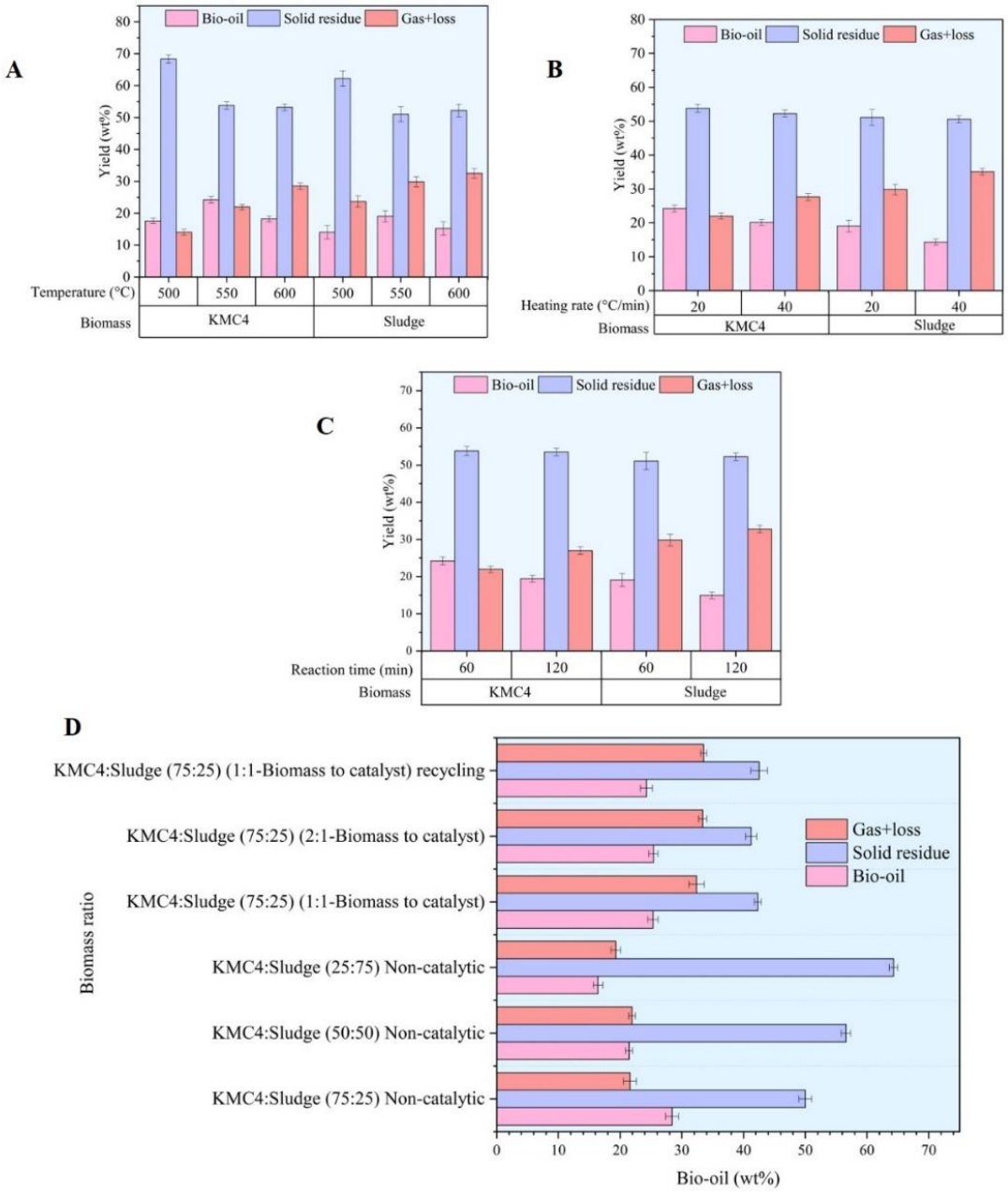

Figure 6.6. Product distribution of individual feedstocks A) temperature at fixed 20 °C/min heating rate and 60 min, respectively; B) heating rate at fixed temperature and time of 550 °C and 60 min, respectively; reaction time at fixed temperature and heating rate of 550 °C and 20 °C/min, respectively. D) co-feedstocks at 550 °C, 20 °C/min, and 60 min, respectively, under non-catalytic, catalytic, and recycling experiments.

6.3.2.2 Catalytic co-pyrolysis of KMC4 and dairy sludge

The bar chart shows the effect of catalytic and non-catalytic pyrolysis of the co-feedstock KMC4:dairy sludge (75:25) on product distribution (bio-oil, solid residue, and gas/loss fractions). In the non-catalytic run, the bio-oil of 28.42% was observed along with a higher fraction of solid residues (Figure 6.6D). Upon introducing catalysts at a 1:1 biomass-to-catalyst ratio, a notable decrement in bio-oil yield was observed (25.32%), coupled with reduced solid residue (42.3%) and enhanced gas fraction (32.38%), which reflected enhanced breakdown of macromolecules towards gas formation.

Reducing the catalyst loading to a 2:1 (biomass-to-catalyst ratio) showed approximately similar yield (25.39%) of bio-oil, with a reduced char formation (41.23%), with enhanced gas formation (33.38%), likely due to secondary cracking. Interestingly, under recycling catalyst conditions (KMC4: dairy sludge (75:25) (2:1-biomass to catalyst)), a minor decrease in bio-oil yield (24.25%) was observed compared to the fresh catalyst run, suggesting a minor reduction in efficiency of a reused catalyst. Overall, the results demonstrated that catalytic HTL reduced bio-oil yield while lowering solid residues compared to non-catalytic runs, with the 2:1 biomass to catalyst loading showed the most efficient conversion, while a catalyst recycling still retained considerable activity but with slightly diminished efficiency.

6.3.2.4 Co-pyrolysis process effect on bio-oil yield

The effect of co-pyrolysis process on bio-oil yield was examined by comparing the theoretically calculated value to an experimental one [Equation 6.1]. The linear calculation was done according to a previous reported equation in a recent investigation (Qi et al., 2018).

$$Calculated\ yield\ (\%) = y_1 * m_1 + y_2 * m_2 \qquad [6.1]$$

where y_1 and y_2 were the bio-oil yields from individual pyrolysis of microalgae and dairy sludge, respectively, while m_1 and m_2 were the mass fractions used in co-pyrolysis experiment. The difference between the experiment and calculated yield defines whether the reaction is synergistic, antagonistic, and additive. Synergistic effect (SE) happens when the value is positive while the antagonistic effect (AE) occurs when it is negative, and the additive effect arises when the difference is zero (Yang et al., 2019). The significant impact relied on the mixing ratio of feedstocks and reaction parameters.

The pyrolytic bio-oil from KMC4 microalgae (24.23%) was higher compared to that from dairy sludge (19.06%). On performing co-pyrolysis at 550 °C using 75:25 wt% ratio (Microalgae: Dairy Sludge) for 60 min, 28.42% bio-oil yield was achieved. Using the calculated yield from equation 6.1, it was observed that co-pyrolysis effect was positive as the experimental value is more than calculated one. This stated the synergistic effect on using two feedstocks together for co-pyrolysis.

The interactions in co-feed were also seen in DTG curve with the major shift and degradation in co-feed decomposition profile between 250 °C to 550 °C (Chapter 5). The shift in degradation from co-feed to more organic compounds into bio-oil was a reason for this phenomenon at this loading ratio. To understand the synergy between two feedstocks towards bio-oil compositional changes, the discussion is reported under 6.3.4.

6.3.3 Spent and Regenerated Catalysts Characterization

The coked H-ZSM-5 referred to a catalyst which was obtained from catalytic co-pyrolysis carried out at optimum conditions (550 °C, 20 °C/min, and 60 min). However, coked recycled H-ZSM-5 was a catalyst obtained from catalytic co-pyrolysis at above mentioned conditions using the recycled catalyst. The regenerated H-ZSM-5 was used in the recycling experiment. While recycled regenerated H-ZSM-5 was a catalyst obtained after regeneration from a recycling experiment.

The XRD characterization of spent, regenerated, and recycled catalyst showed a similar peak pattern of zeolite mentioned above in section of fresh catalyst properties, confirmed the MFI structure of the H-ZSM-5. The amorphous and crystalline carbonaceous phase in the spent coked catalyst was confirmed by searching for carbon and graphite peaks. The graphite peak in coked catalyst at 7.92°, 15.88°, 23.86°, 32.1°, 44.42° corresponded to graphite card reader 01-074-2328. The amorphous carbon peak was also reported in spent coked and recycled coked catalyst, distinguished at 2θ= 17.74°, 20.34°, 26.6°, and 26.9° with Card No.: 01-073-5048. The presence of amorphous and graphitic carbon peaks represented the formation of coke in spent catalyst while the characteristics peaks in regenerated H-ZSM-5 confirmed the integrity of the phases after regeneration (Figure 6.1).

After the first regeneration (blue curve), there is a loss in signal intensity dropping from 547.57 µmol/g to 143.91 µmol/g for weak active sites, indicating that the vast majority of original acid sites are no longer available for ammonia adsorption. While, a strong active site decreased from

280.67 µmol/g to 74.146 µmol/g. Active sites are highly decreased in the recycled regenerated catalyst (orange curve), which reflects a loss of catalytic acidity. The irreversible dealumination of the zeolite framework or the poisoning of active sites by inorganic minerals can be one of the reasons for decreased intensity of weak and strong active sites.

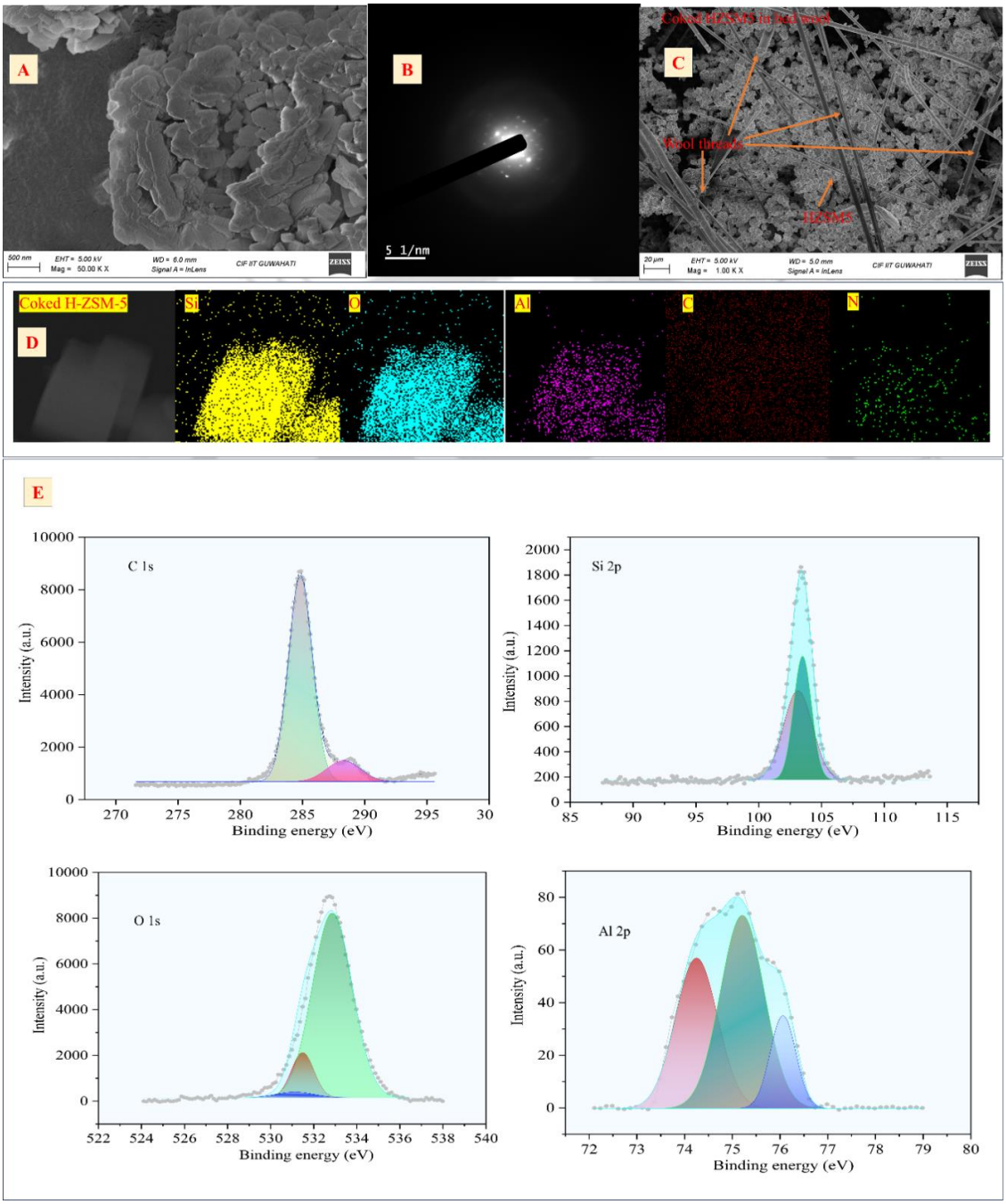

Figure 6.7. A) Surface topography of Spent Catalyst; B) SAED pattern of Spent Catalyst; C) Surface topography of wool support for Catalyst; D) Elemental distribution of Spent Catalyst; E) XPS spectra of Spent Catalyst.

The coked (Figure 6.7A) and recycled coked H-ZSM-5 (Figure 6.8) appeared to have amorphous patches at the edges of structure, which look blurred and less sharp in SEM micrographs. The coking accumulation in spent catalyst reduced the external surface area and blocked pore openings, which has led to catalyst deactivation. And, diffraction spots and planes become less intensed or blurred due to the presence of amorphous carbon deposits in spent coked catalyst (Figure 6.7B). An additional diffuse ring appeared that is a characteristic of amorphous phases (coke).

SAED showed sharp, well-defined diffraction spots and planes in regenerated catalyst, confirming the high crystallinity and ordered planes of the MFI framework. After coke removal, clear diffraction spots reappeared, that confirmed the recovery of crystallinity in the regenerated catalyst (Figure 6.9). However, the regenerated catalyst after recycling catalytic co-pyrolysis showed reappearance of spots, but with lower sharpness and intensity compared to fresh/regenerated catalysts, as evident from the SAED pattern.

Along with the catalyst micrographs, the microscopy visual of wool was studied after catalytic reactions (Figure 6.7C). The wool substrate manifested as elongated, silky fibrous strands (designated as wool threads), created a three-dimensional framework. The H-ZSM-5 crystals were distinctly observable as aggregated micro and nano-sized particles exhibited prismatic to coffin-shaped morphology, uniformly dispersed and affixed to the wool fibers. Post-reaction, the zeolite crystals displayed a coarser surface roughness, signifying coke accumulation on the exterior crystal surfaces and within interparticle gaps. The close interaction between the wool fibers and H-ZSM-5 particles forms a high-surface-area composite bed that improves catalyst distribution and reduces pressure loss during pyrolysis. This verifies that the wool served as an efficient support and physical carrier for H-ZSM-5, enabled uniform catalyst distribution and offered pathways for vapor transport.

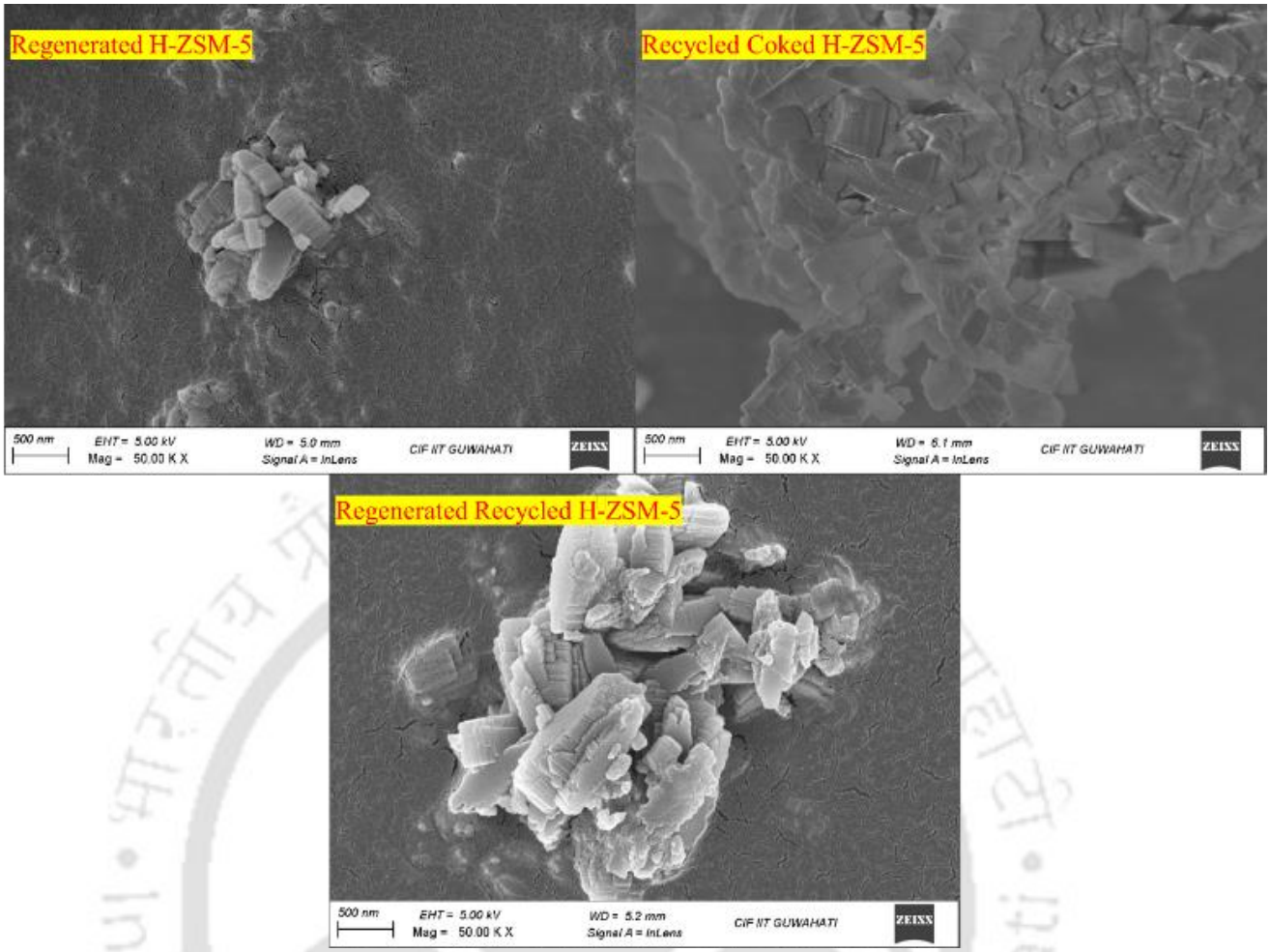

Figure 6.8. Surface micrographs of regenerated, recycled coked and regenerated recycle coked catalyst.

The coke deposit was observed at the edges of spent catalyst that looked blurred at the edges or corners of spent catalyst in elemental mapping. The carbon deposition was confirmed by electronic image and mapping (Figure 6.7D). The surface of spent catalyst was covered with some amount of carbon species, which led to deactivation of zeolite. The formation of near-graphitic carbonaceous deposits on the external surface is attributed to the accumulation of coke precursors that could not undergo continuous reaction because of the non-uniform internal metal distribution. Products diffusing out of the micropores were re-adsorbed on the external surface of the catalyst, which contains a high density of acid sites. This environment promoted successive oligomerization, cyclization, and dehydrogenation to aromatics, followed by condensation to polycyclic aromatics, ultimately leading to the development of near-graphitic carbonaceous deposits (Sang et al., 2017).

Overall, the micrographs and SAED pattern revealed the coke deposition in a spent catalyst is attributed to the cracking reactions that happened between vapors and a catalyst during catalytic co-pyrolysis.

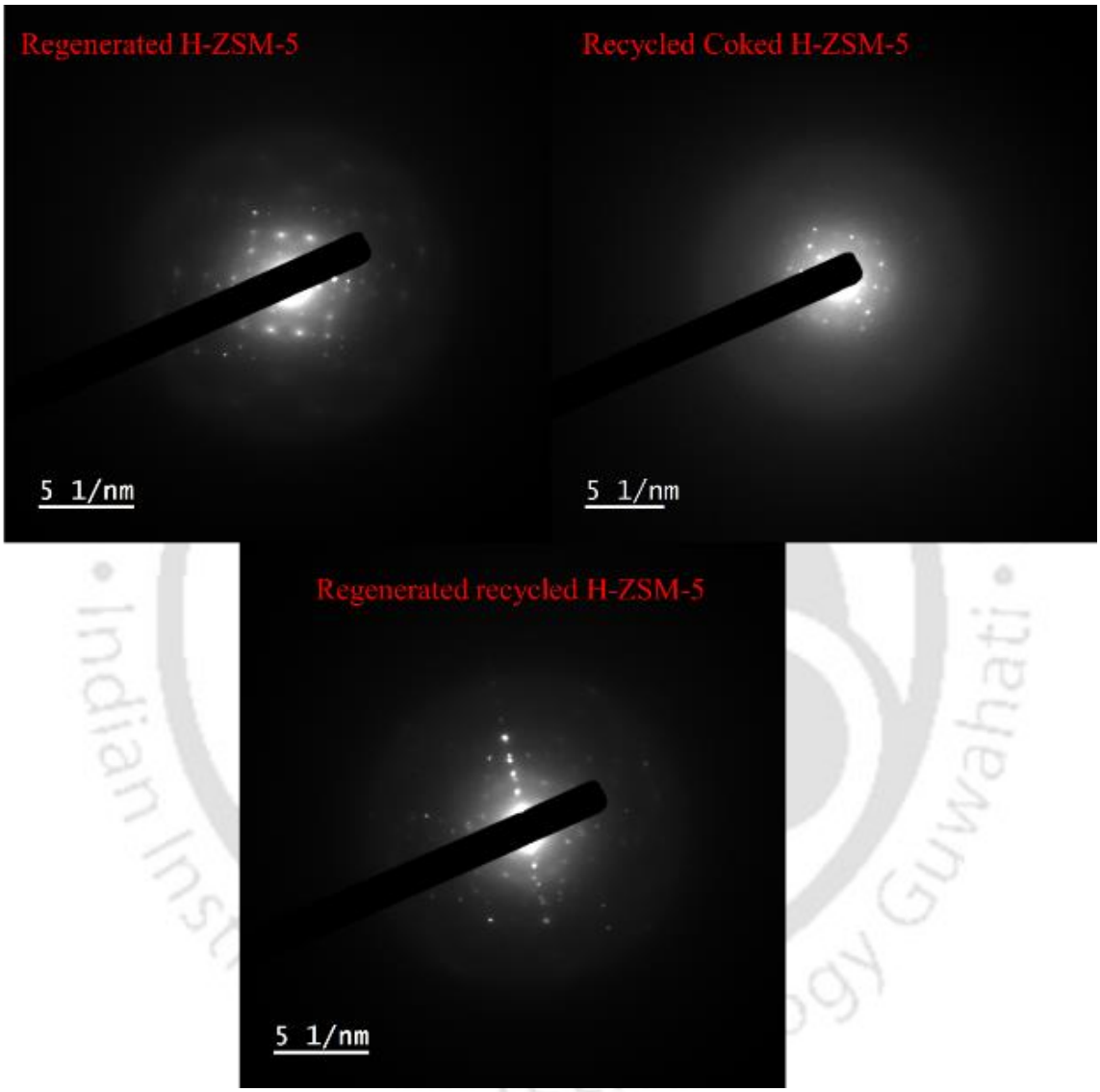

Figure 6.9. SAED diffraction pattern of regenerated, recycled coked and regenerated recycle coked catalyst.

Following catalytic utilization and coke accumulation, the C 1s spectrum of the coked catalyst (Figure 6.7E) exhibited new characteristics, including a prominent C–C/C–H peak (≈284.82 eV) and a shoulder at 288.30 eV attributed to C=O groups, confirmed the existence of carbonaceous deposits and oxygenated coke precursors on the zeolite surface (Moulder et al., 1992). In the Si 2p region of the coked sample, the principal framework peak persists, albeit

seen with a shift in peak binding energy at main peak at 103.1 eV, signified the presence of Si-O-Al bond. While the secondary peak at 103.4 eV, attributed to O-Si-O bond. The O 1s area exhibited supplementary contributions from adsorbed oxygenated species (C=O) in addition to lattice oxygen (metal oxide) at 531.4 eV (Moulder et al., 1992). The peak at 532.8 eV corresponded to O-Si-O bond.

The Al 2p deconvoluted envelope undergoes alterations: the principal Al peak is displaced, appeared at 74.2 as oxides form like Al-O in zeolite (Moulder et al., 1992). While, presence of aluminium hydroxide oxide, AlO(OH) at 75.2 eV was confirmed from peaks in XRD spectra of coked catalyst (2θ=14° (card number: 00-049-0133)). However, around 76.05 eV is attributed to extra-framework Al species, such as $Al(OH)_3$ (2θ=24.71°and 45.07°, 26.83°, 28.40°, and 45.31°). Collectively, these alterations suggested that coking results in the accumulation of oxygenated substances.

The O 1s region also revealed an extra component at higher binding energy attributable to oxygenated functional groups within the coke. Overall, the XPS analysis confirmed that while the zeolite framework remains structurally intact after reaction, carbonaceous deposits accumulated on the surface and alter the electronic environment of aluminium sites.

Additionally, ZSM-5 catalyst had strong acidic sites, and some nitrogenous functional groups were easily adsorbed onto the acidic sites to form coke (Thangalazhy-Gopakumar et al., 2012). The N 1s deconvoluted spectra represented five important peaks. It provided insights into the nitrogen environment and possible nitrogen interactions after catalytic reactions onto the catalyst (Figure 6.10). The peak at 397.5 eV, 399.7 eV, 400.5 eV, 401.8 eV and 403.6 represented pyridinic-, pyrrolic-N, pyridinic N-H, pyridinic N-O (Lazar et al., 2019) and azide group (Moulder et al., 1992; O'Donoghue et al., 2016), respectively, on the surface of coked catalyst. The presence of multiple nitrogen environments indicated that nitrogen from the feedstock retained in the catalyst during reaction, contributed to catalyst deactivation. The XPS spectra showed clear differences in the surface chemistry of H-ZSM-5 between fresh and spent coked catalyst.

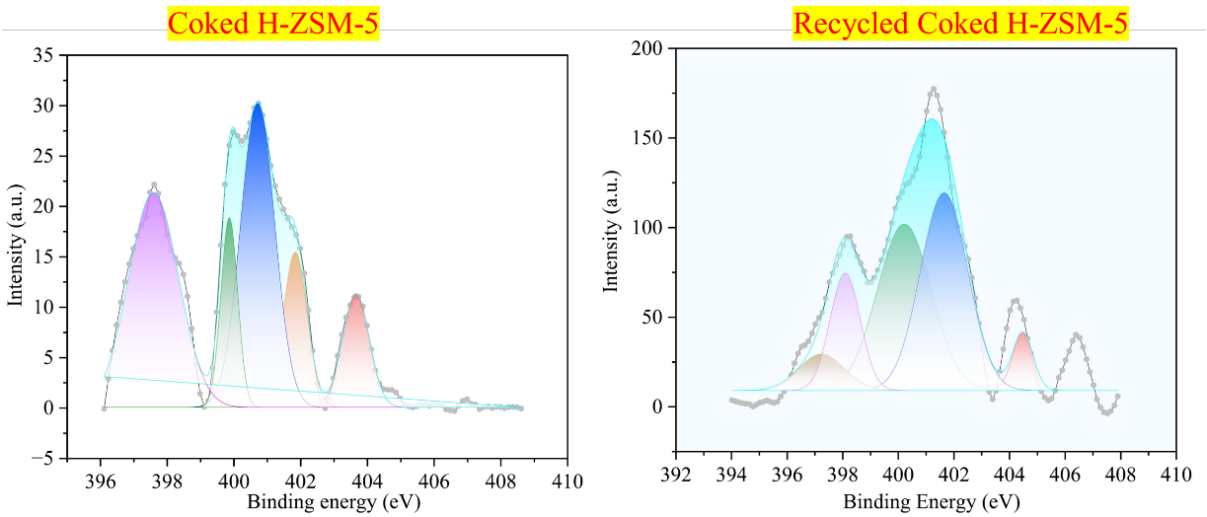

Figure 6.10. N 1s deconvolution spectra of coked and recycled coked H-ZSM-5.

The regenerated H-ZSM-5 exhibited prominent silicon dioxide bond peaks in the Si 2p and O 1s spectra, while the Al 2p region continued to display framework Al at around 74–75 eV, signifying that regeneration predominantly reinstates the original zeolite structure (Figure 6.11). The regenerated recycled H-ZSM-5 exhibited the same characteristics, albeit with a minor displacement in the Al 2p region, indicative of partial dealumination and the creation of $Al(OH)_x$ species with each successive regeneration.

The spectra of recycled coked H-ZSM-5 exhibited notable alterations: in the C 1s region, prominent peaks associated with C–C/C–H (284.6 eV) and C=O (287.82 eV) affirmed the accumulation of carbonaceous coke and oxygenated species; in the O 1s region, lattice oxygen peaks observed at 532.92 eV for O-Si-O bond, while new oxygen-containing groups (C=O) emerged at 531.5 eV, signifying surface saturation by coke. The Al 2p region exhibited peaks at 73.4 eV, 74.9 eV, and 75.5 eV which referred to a shift in aluminum, Al-O-Si bond, and AlO(OH) (Motamedi and Cadien, 2014). These alterations indicated that although regeneration can reinstate the original surface states and but coking gradually altered the zeolite surface due to carbonaceous deposits, oxygenated species, and extraframework aluminum, potentially reducing its catalytic efficacy.

The TGA-DTG profile of the spent catalysts were shown in Figure 6.12. The combustion behaviour from TGA-DTG graphs revealed the presence of coke on the surface of a catalyst. The first DTG peak referred to volatile matter and small molecular weight amorphous carbon loss, while another DTG peak at high temperature corresponded to near-graphite or high

molecular weight carbonaceous species. The DTG peak at high temperature showed that the species were difficult to combust, which is attributed to heavy coke.

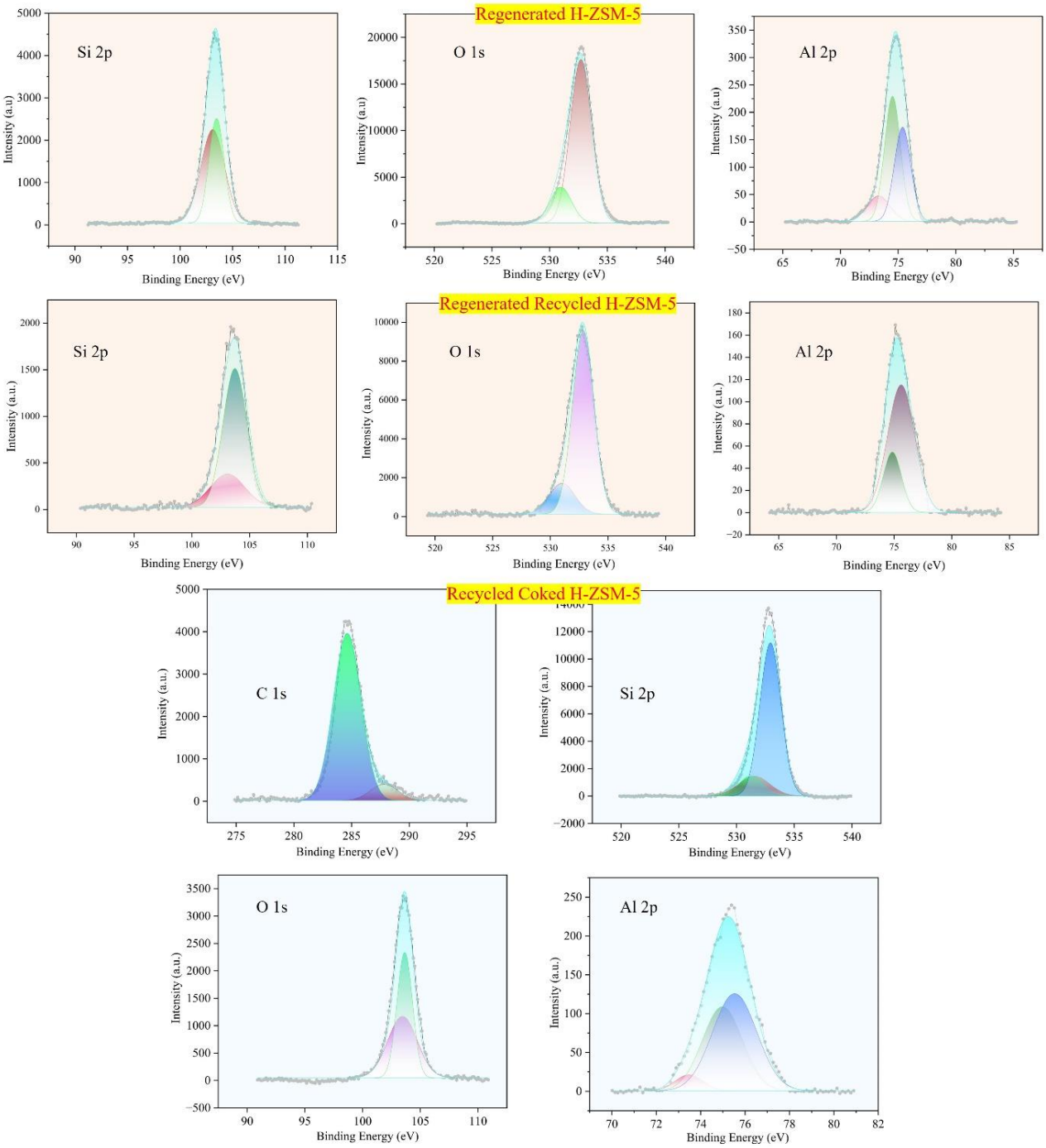

Figure 6.11. XPS spectrum of regenerated, recycled coked and regenerated recycle coked catalyst.

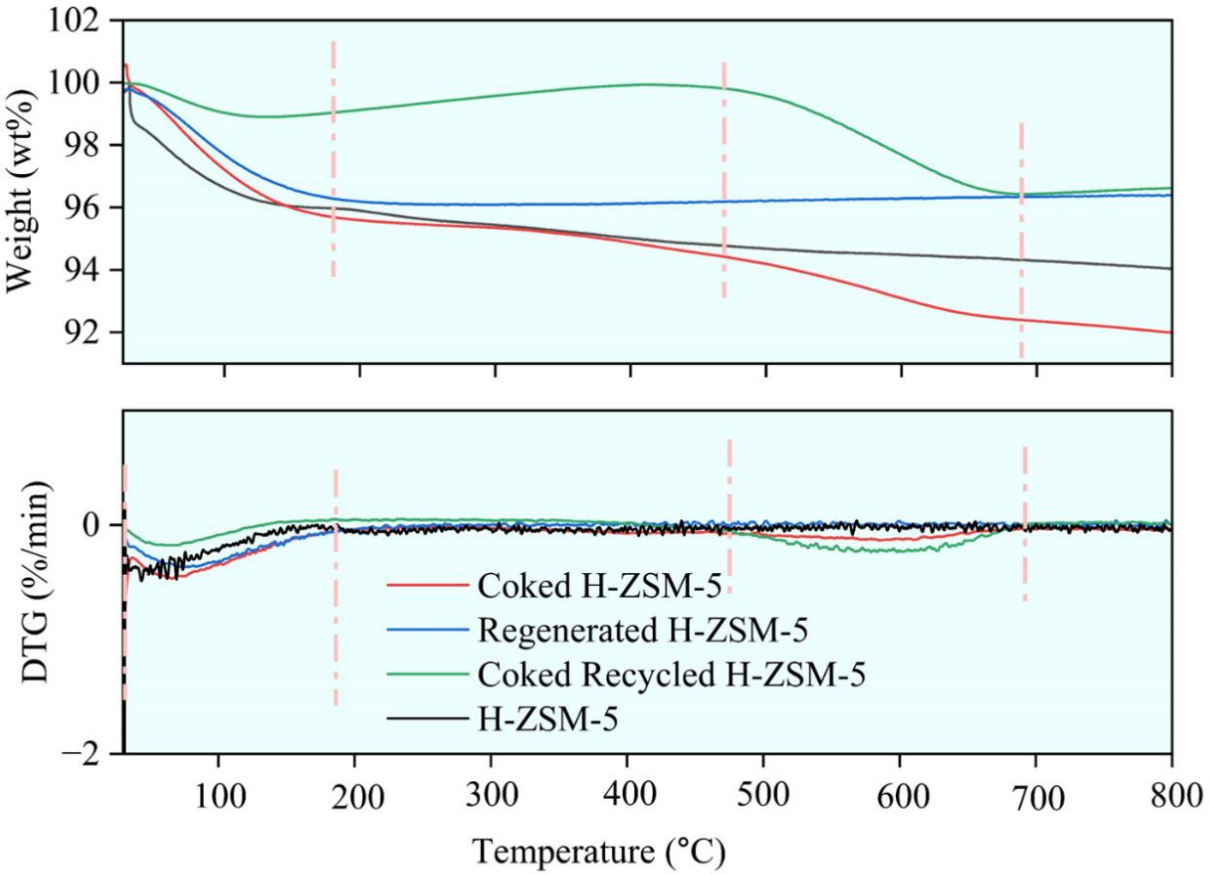

Figure 6.12. Combustion behaviour of spent catalyst in Thermogravimetric analyser.

For coked catalyst from the catalytic co-pyrolysis and recycling experiment, the isotherms showed a decrease in both micropore and mesopore volume (Figure 6.5). This confirmed the deposition of coke in the micropores and intercrystalline mesopores. The surface area of coked catalyst is given in Table 6.1. It assumed that coke accumulates within the channels of H-ZSM-5, partially occupying and blocking the pore space, thereby reducing the available micro and mesoporous surface area and volume. About a 27% decrease in micropore volume was observed in a coked catalyst compared to a fresh one. Since H-ZSM-5 is a microporous zeolite whose mesopores arise from the aggregation of small crystals, this suggests that coke formation was more pronounced on the external surface than within the micropores (Sang et al., 2017). Similarly, recycled coked catalyst observed same decrement in micropore volume of 30% compared to the regenerated catalyst. The pore size gives clearer distinction between coking on external and inside pore of catalyst.

Coming to point of coked catalyst from catalytic co-pyrolysis conditions: 550°, 20 °C min^{-1} and 60 min, the pore size reduced (3.3 nm) compared to a fresh catalyst (3.4 nm). This indicates

that coke deposits happened inside these micropores and partially fill or block the channels, which decreases the pore size of the spent catalyst. When observing the pore size of recycled coked catalyst at same conditions, it was decreased (3.39 nm) compared to regenerated catalyst (3.44 nm). This confirmed that major amount of coke was formed on the external surface, not near or at mouth of micropores. It was also observed that the surface area of regenerated catalyst after recycling (regenerated recycled H-ZSM-5) was lesser than fresh and first regenerated one for recycling. The adsorption and desorption isotherm of regenerated catalyst after recycling is similar of regenerated one for recycling.

6.3.4 Bio-oil characterization

6.3.4.1 Elemental composition

All bio-oil samples contained predominantly carbon (51.12–67.56 wt%) and hydrogen (8.06–10.1 wt%). The KMC4 bio-oil exhibited the highest atomic H/C ratio (1.89 mol/mol) together with O/C (0.5 mol/mol) and N/C (0.1 mol/mol) ratios (Table 6.2). Comparatively, the dairy sludge has a lower H/C ratio (1.72 mol/mol), O/C (0.22 mol/mol), and N/C (0.07 mol/mol) ratios, suggested the presence of less oxygenated and nitrogenated compounds. For the co-pyrolysis process, the H/C ratio (1.76 mol/mol) got increased with an increase in O/C (0.23 mol/mol), however with no change in N/C ratio (0.07 mol/mol). Coming to catalytic co-pyrolysis process, the H/C ratio (1.79 mol/mol) got increased with a decrease in O/C (0.19 mol/mol) and N/C ratio (0.06 mol/mol). This indicated effective deoxygenation, deamination, decarboxylation, and dehydration during the process, resulting in an increased energy density. Table 6.3 presents a structured benchmarking of catalytic and non-catalytic process against previous literature.

Table 6.2. Properties of bio-oils obtained from single pyrolysis, non-catalytic, and catalytic co-pyrolysis.

Properties	KMC4	Dairy sludge	Co-PY	Catalytic co-PY	Catalytic co-PY recycle	Commercial Crude (Chaudhuri, 2016)
C (%)	51.12± 0.34	65.56± 0.07	64.97 ± 0.66	67.56± 0.16	62.37± 0.41	85–90
H (%)	8.06± 0.04	9.4± 0.24	9.52 ± 0.15	10.1± 0.06	9.17± 0.3	10–14
N (%)	6.5± 0.15	5.6± 0.55	5.6 ± 0.47	5.1± 0.07	5.3± 0.11	<0.1–2.0
S (%)	-	-	-	-	-	0.2-3

O^b (%)	34.32	19.44	19.91	17.24	23.16	1-1.5
H/C (mol/mol)	1.89	1.72	1.76	1.79	1.76	-
O/C (mol/mol)	0.5	0.22	0.23	0.19	0.27	-
N/C (mol/mol)	0.1	0.07	0.07	0.06	0.07	-
N/O (mol/mol)	0.21	0.33	0.32	0.33	0.26	-
HHV (MJ Kg^{-1})	23.12	25.96	27.36	30.23	30.05	42–49

The Van Krevelen diagrams present a comparative analysis of the elemental composition of bio-oils which shifts with different pyrolysis conditions (Figure 6.13). The abundance of nitrogen and oxygen element in KMC4 confirmed that bio-oil has highest O/C and N/C ratio as shown in H/C vs O/C and H/C vs N/C plots. The dairy sludge bio-oil has lower O/C, N/C, and H/C compared to KMC4. Non-catalytic co-pyrolysis moves the data point leftwards, as shown in N/C vs O/C plot, indicated partial deoxygenation and denitrogenation from synergistic cracking between the KMC4 and the dairy sludge components. This reaction decreased the O/C ratio of single feedstock pyrolytic bio-oil as compared to co-pyrolytic bio-oil.

KMC4 and dairy sludge bio-oils contained the most nitrogenous species, however co-pyrolysis (72:25-KMC4: dairy sludge) without a catalyst lowered the N/C ratio slightly due to dilution and cracking. When H-ZSM-5 was introduced in co-pyrolysis, the O/C and N/C ratio dropped further while H/C rose slightly, showing that the catalyst has effectively performed deoxygenation, denitrogenation (conversion of nitrogen-containing compounds into light N-gases or amines in solid biochar), and dehydration, resulted in a higher heating value. H-ZSM-5 actively performed denitrogenation, which produces a bio-oil with much lower nitrogen content and thus improved stability. The catalytic co-pyrolysis with H-ZSM-5 reflected the progressive removal of heteroatoms. However, the recycling experiment with regenerated H-ZSM-5 showed increased O/C and N/C and a lower H/C ratio, showed reduced efficiency of the catalyst.

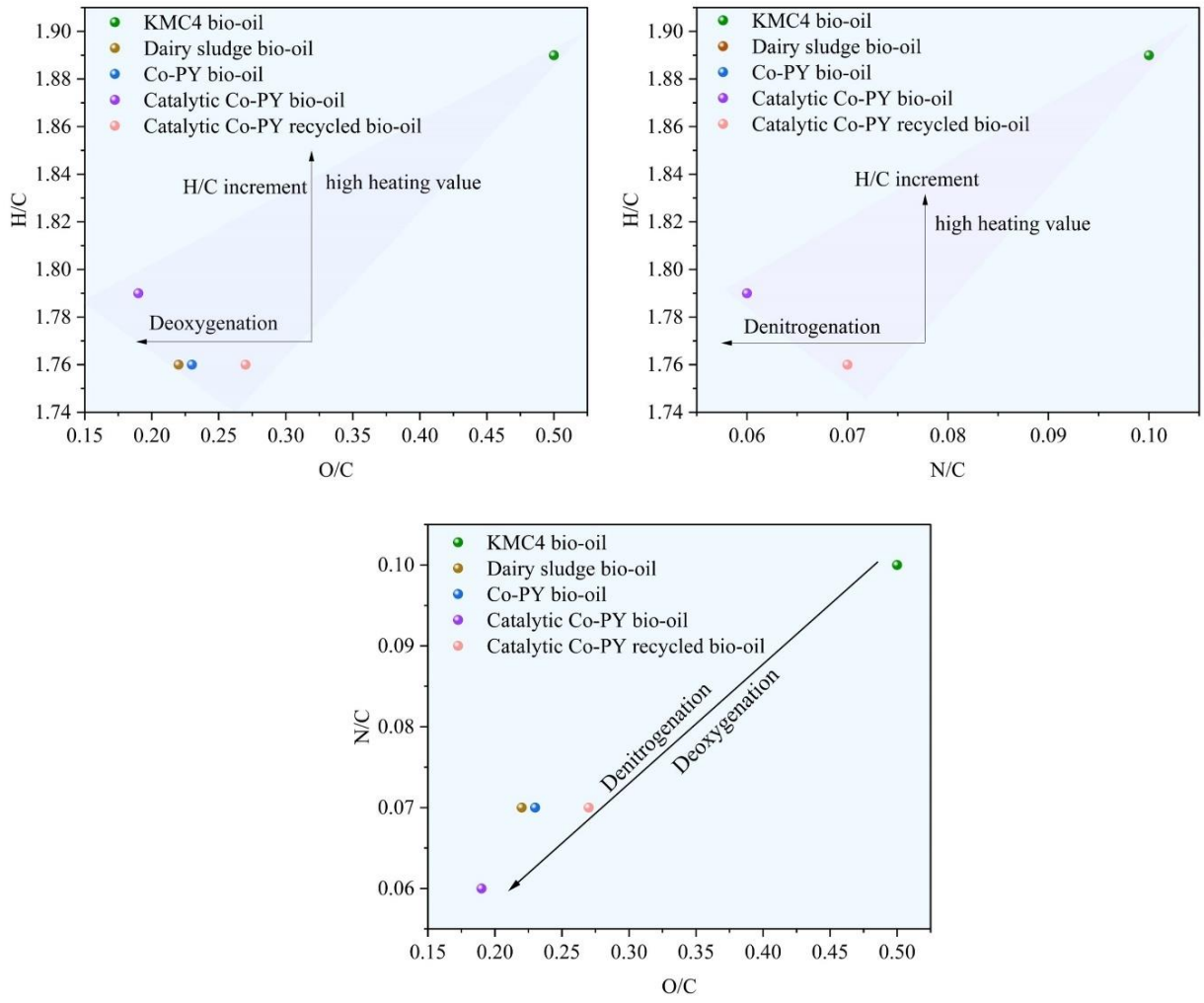

Figure 6.13. Van Krevelen plots of KMC4, dairy sludge, Co-pyrolysis, catalytic co-pyrolysis, and recycled bio-oil. (The unit of all elements is presented in mol/mol).

Table 6.3. Literature comparison of the non-catalytic and catalytic co-pyrolysis work with previous studies.

Feedstock	Feedstock ratio	Conditions	Bio-oil Yield (%)	C (%)	H (%)	N (%)	O (%)	HHV (MJ/Kg)	References
Sewage Sludge and Microalgae *Chlorella Vulgaris*	Microalgae /sludge= 0.82)	520 °C for 30 min	32.93	52.35	7.81	7.14	32.16	23.14	(Khodaparasti et al., 2023)

Chlorella vulgaris residue (CVR) and Sewage Sludge (SS)	80:20-microalgae residue:SS	539.33 °C for 23 min	47	-	-	-	-	-	(Kumar et al., 2024)
Isochrysis sp. and Sewage Sludge	Sludge: *Isochrysis* - 1:2	500 °C	34.90	-	-	-	-	36.908	(Wang et al., 2016)
Chlorella sp.	-	550 °C with HZSM-5	41.9	-	-	-	-	-	(Shirazi et al., 2020)
Chlorella sp.	-	550 °C	62	-	-	-	-	-	(Shirazi et al., 2020)
Nannochloropsis sp. residue	-	HZSM-5 catalyst- to-material of 1/1 at 400 °C	19.7	65.21	9.83	5.43	19.53	32.2	(Pan et al., 2010)
Nannochloropsis sp. residue	-	400 °C	47.6	56.13	7.13	5.34	30.09	24.4	(Pan et al., 2010)
Chlorella vulgaris	-	500 °C for 30 min	52.7	51.4	10.4	12.4	24.8	18.6	(Thangalazhy-Gopakumar et al., 2012)
Microalgae and Sewage Sludge	Biomass blend ratio of 1:1	500 °C, biomass to HZSM-5 catalyst ratio of 2:1	24	74.81	9.77	7.11	6.57	36.46	(Mustapha and Isa, 2024)
Microalgae and Sewage Sludge	Biomass blend ratio of 1:1	500 °C	22	71.53	9.42	7.48	11.57	34.82	(Mustapha and Isa, 2024)

Monorap hidium sp. KMC4 and Dairy sludge	75:25, algae to dairy sludge	550 °C, 20 °C/min, 60 min and 2:1 biomass to catalyst	25.39	67.56	10.10	5.10	17.24	30.23	Our Study

6.3.4.2 GC–MS analysis

The pyrolysis of microalgae KMC4 yielded a product mixture primarily composed of nitrogen-containing (amines, amides, nitriles, and pyridines) (39.84%), hydrocarbons (14.72%), and esters (15.25%) (Table A.3 in Appendix), directly indicative of the algal biomass high protein and lipid content (Figure 6.14A). A moderate quantity of oxygenated compounds, including ketones (6.44%), alcohols (5.38%), and O-cyclic compounds (3.20%) is detected as a result of carbohydrate and pigment breakdown. Low amount of aldehyde and acids were reported from algal biomass pyrolytic bio-oil. Aromatic compounds were also found in less quantity (3.63%). As algal biomass comprised of major hemicellulose type compounds, the aromatics were found to be lower, which were found to be highest from cellulose in a previous study (Wang et al., 2014).

However, dairy sludge produces a markedly distinct spectrum, characterized by a significantly higher proportion of aromatics (50.95%) and hydrocarbons (18.34%) with a considerably less nitrogenous products (17.98%). It can be concluded that dairy sludge constituents contain more cellulose-based carbohydrates that break down to form naptha-based aromatics. Dairy sludge and KMC4 pyrolytic bio-oil have a very distinct spectrum of nitrogenous compounds, as some compounds are found very high in the former one while lower in the later one. The reduced nitrogenous compounds reported from GC-MS was aligned with low nitrogen content of bio-oil from dairy sludge (5.6%) compared with KMC4 (6.5%). The sludge can comprised of a higher concentration of carbohydrates, lipids, and humic compounds, coupled with a moderate protein content, which promotes decarboxylation and aromatization rather than amination reactions during thermal cracking.

When non-catalytic co-pyrolysis of the two feedstocks was performed in a ratio of 75:25-KMC4: dairy sludge, the resultant product distribution demonstrated distinct synergy between the two feedstocks in compound chemistry. The proportion of nitrogen-based species (32.97%) in bio-oil significantly diminished in comparison to individual microalgae. This change was

due to the interactions between fragments derived from algal proteins and intermediates derived from sludge lipids, which facilitate transesterification, decarboxylation, and dehydration reactions, resulted in the production of more stable esters and hydrocarbons while inhibited the formation of nitrogen heterocycles. The effect of co-pyrolysis synergistically enhanced and changed the bio-oil chemistry, observed with increased the calorific value. The introduction of H-ZSM-5 during the co-pyrolysis of KMC4 and dairy sludge significantly altered the product spectrum in comparison to the non-catalytic process. The acidity and shape-selective micropores and mesopores of the zeolite expedited secondary reactions of the vapors when they pass through a catalyst bed within the reactor. Substantial nitrogenerated, oxygenated molecules and aromatics were decreased along with an enhanced hydrocarbons proportion in catalytic pyrolytic bio-oil. The atmosphere in catalytic co-pyrolysis was subjected to cracking, dehydration, decarboxylation, denitrogenation and decarbonylation while yielding more hydrocarbons, resulted in the release of high amount of gases product (discussed in production distribution section) compared to bio-oil.

Additionally, ZSM-5 catalyst had strong acidic sites, and some nitrogenous functional groups were easily adsorbed to the acidic sites, confirmed by XPS and EDS (Thangalazhy-Gopakumar et al., 2012), decreased formation of N-containing compounds in bio-oil (Zhang et al., 2022). Nitrogen-containing compounds originating from algal proteins undergo deamination and denitrogenation to form gases or lower chain molecules prior to cyclization into stable heterocycles, significantly reduced the yield of N-heterocyclic compounds in the bio-oil. Also, this catalyst is able to increase the formation and degradation of HCN and decomposition of NH_3 to N_2 and H_2, showed some nitriles and amides in higher proportion in catalytic bio-oil (Torri et al., 2013).

Interestingly, more esters were also reported in catalytic co-pyrolytic bio-oil. Unsaturated intermediates and carboxylic acids from the mixed feedstock undergo esterification in the presence of ZSM-5 (Omar et al., 2018) within the pores, led to a heightened proportion of esters in the condensable fraction. The catalyst enhanced the vapors from a nitrogen- and oxygen-rich mixture into a hydrocarbon and esters-rich product with reduced heteroatom content and increased energy density, illustrated its dual function in cracking, deoxygenation, dehydration and esterification reactions during catalytic co-pyrolysis.

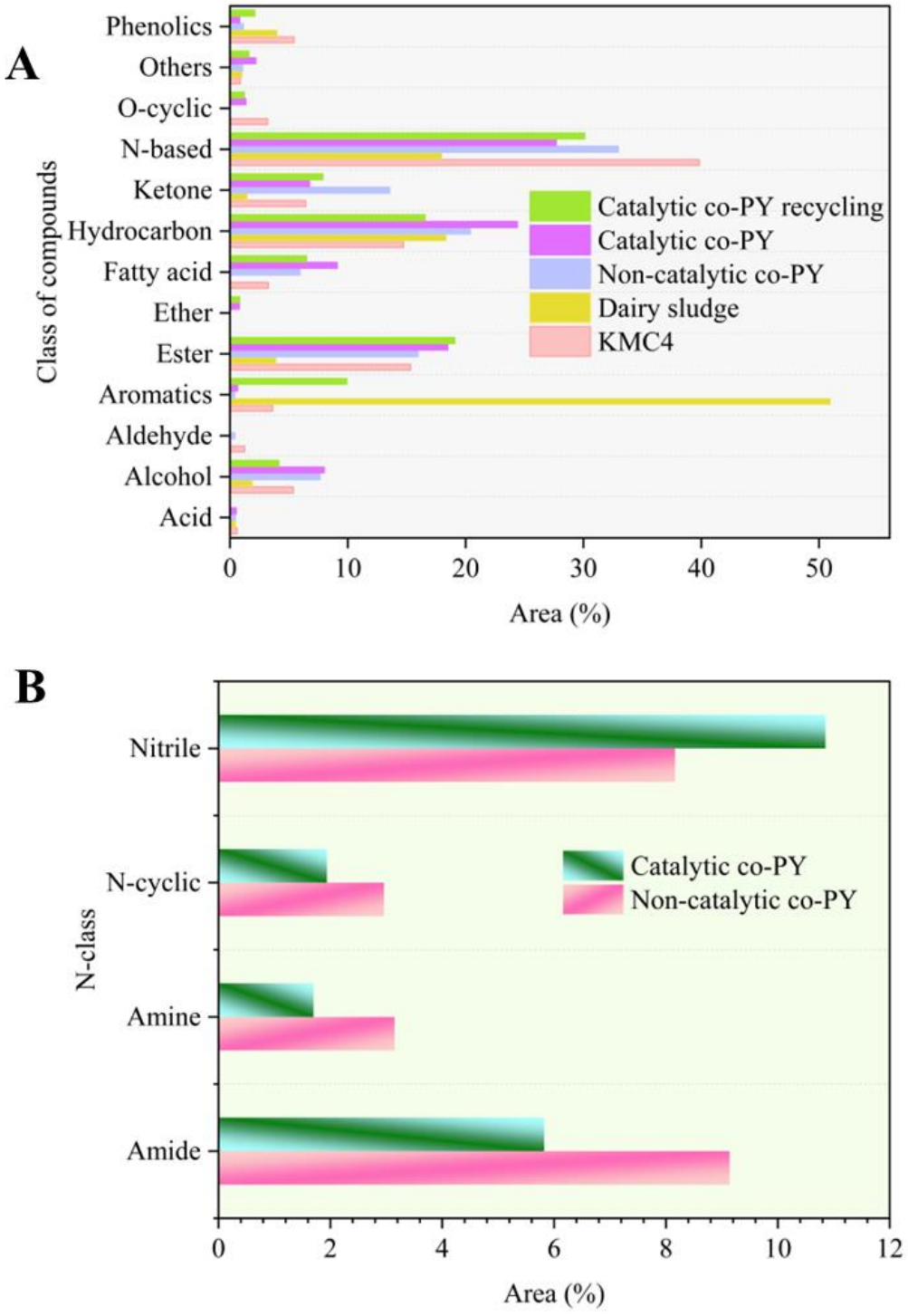

Figure 6.14. A) GC-MS of bio-oil obtained from individual, non-catalytic, catalytic, and recycle catalytic co-pyrolysis; B) Change in N-based compounds from non-catalytic to catalytic co-pyrolytic bio-oil.

6.3.4.3 Probable major reactions during catalytic co-pyrolysis

Debiagi et al. (2017) find that the heat stability of various components of algal biomass varies. The initial mass loss pertains to the degradation of carbohydrates, while the subsequent loss commences at approximately 300 °C, indicating protein fragmentation. Protein pyrolysis is a complex, multiphase, and multistep process. Initial depolymerization and degradation resulted in low molecular weight intermediate product species and gas (Debiagi et al., 2017). The sequential pyrolysis of these intermediary species yields nitrogen-containing amides, pyrroles, pyridines, and diketopiperazines (Shen et al., 2024), along with other gaseous and tar compounds. The cleavage of C-C/C-N bonds and ring condensation are the primary mechanisms leading to the formation of imines and pyrroline derivatives during the process, resulting in the generation of NO_x gases. (Liu et al., 2021). The pyrolysis of amino acids follows decarboxylation, R-group removal, dehydration, and deamination reactions.

The carbohydrates are first degraded into anhydrosugars and furfurals. Subsequent reactions such as decarbonylation, deoxygenation, dehydration, cracking, and rearrangement were followed to produce oxygenated compounds, including aldehydes, ketones, acids, phenols, and alcohols. Certain light oxygenates and olefins are generated and subsequently cyclized to produce oxygenated aromatic hydrocarbons. The pyrolysis of lipids involves the decomposition of fatty acids by a complex series of processes, including cracking, decarbonylation, aromatization, isomerization, and various other transformations. This intricate sequence of reactions produces acids, alcohols, ketones, and aldehydes (Shen et al., 2024).

The catalytic bio-oil had a high content of hydrocarbon compared to the non-catalytic one due to the strong deoxygenation effect of zeolite. Upon H-ZSM-5 introduction in co-pyrolysis, the O/C and N/C ratio decreases while H/C rises slightly, showing the effect of deoxygenation and denitrogenation. H-ZSM-5 provides strong acid sites that promote cracking of long-chain amides and nitriles. Amide and nitrile groups undergo C–N bond cleavage, producing smaller hydrocarbons and forming gases.

Hexadecanenitrile, octadecanamide, tetradecanamide, 2-propen-1-amine, N,N-bis(1-methylethyl)-, hexadecanamide, dodecanenitrile, benzenepropanenitrile, and 9H-pyrido[3,4-b]indole were decreased from non-catalytic to catalytic pyrolytic bio-oil. Like, hexadecanamide and hexadecanenitrile can be cracked into hydrocarbons like 2-hexadecene, 3,7,11,15-tetramethyl-, [R-[R*,R*-(E)]]- and 1-pentadecene and gaseous compounds.

Hexadecanenitrile, octadecanamide, and tetradecanamide decreased from non-catalytic to catalytic process while hexadecanamide and dodecanenitrile were not found, suggesting acid-catalyzed cracking, deamination, and decarboxylation reactions during catalytic co-pyrolysis (Table A.3 in Appendix).

The selective micropores of H-ZSM-5 may have favored the transformation of compounds like benzenepropanenitrile into aromatic hydrocarbons. The N-functional groups are stripped off, while the carbon skeleton rearranges into benzene or polyaromatics. This lowers the detected nitrogen species in the bio-oil fraction. Benzenepropanenitrile can break down to benzene, dodecyl-, and benzene, decyl- and gaseous product, which are found in catalytic bio-oil. Also, when H-ZSM-5 was incorporated, an increase in nitriles and a decrease in amides and nitrogen heterocycles were observed. H-ZSM-5 is endowed with robust acid sites that facilitate the deamination, dehydration, and decarboxylation of protein-derived intermediates, including amino acids and amides. When the dehydration reaction was more pronounced with H-ZSM-5, nitriles were formed from amides (Zhang et al., 2022), as seen in GC-MS results of catalytic pyrolytic bio-oil (Figure 6.14B and Figure 6.15).

Compounds like methyl stearate, pentadecanoic acid, 14-methyl-, methyl ester, tridecanoic acid, 12-methyl-, methyl ester, octadecanoic acid, 2-(2-hydroxyethoxy)ethyl ester, acetic acid, 3,7,11,15-tetramethyl-hexadecyl ester, heptadecanoic acid, methyl ester were decreased in the catalytic experiment, but l-(+)-ascorbic acid 2,6-dihexadecanoate was increased (Table A.3 in Appendix). Compounds like methyl stearate, methyl pentadecanoate, and methyl tridecanoate are simple esters. On incorporating H-ZSM-5, their ester groups are easily attacked at the acid sites, leading to decarboxylation/deoxygenation/cracking, forming CO_2, H_2O, and hydrocarbons. It was also observed in a study that esters increased due to the inhibiting effect of esters to form acids at high pyrolytic temperature (Zhang et al., 2022).

Fatty acids like n-Hexadecanoic acid and 3-tetradecanynoic acid were not found in catalytic pyrolytic bio-oil. This might be due to H-ZSM-5 acid sites that promoted the removal of the –COOH group in fatty acids. This leads to CO_2 and water release and formation of hydrocarbons (Arumugam et al., 2021) like 2-hexadecene, 3,7,11,15-tetramethyl. However, l-(+)-Ascorbic acid 2,6-dihexadecanoate reported in higher amount in catalytic bio-oil, is a diester of ascorbic acid with two long-chain fatty acids. It has multiple ester linkages and is not a simple straight-chain ester. In non-catalytic pyrolysis, it may decompose along with other oxygenates. Under catalytic conditions, one thing may had happenned is that it doesn't crack as easily as small

esters because of the steric hindrance in H-ZSM-5 pores. When larger molecules or compounds try to access or leave zeolite porous channels, it is difficult to catalyse a reaction due to the limited space and dimension of the pores, which hinders catalytic activity.

Also, it is interesting to notice that heavier hydrocarbons formed in catalytic pyrolysis. H-ZSM-5 acid sites do not just crack bonds but also catalyze oligomerization/polymerization of olefins (Quann et al., 1988). Larger intermediates or long-chain radicals trapped in pores may undergo condensation or recombination instead of cracking, shows hindrance in micropores and this favors heavy alkanes/alkenes. Also, on acidic zeolites, hydrogen transfer stabilizes carbocations, which can terminate radical cracking sequences prematurely. Instead of fully cracking, intermediates can be capped as saturated or branched heavy hydrocarbons.

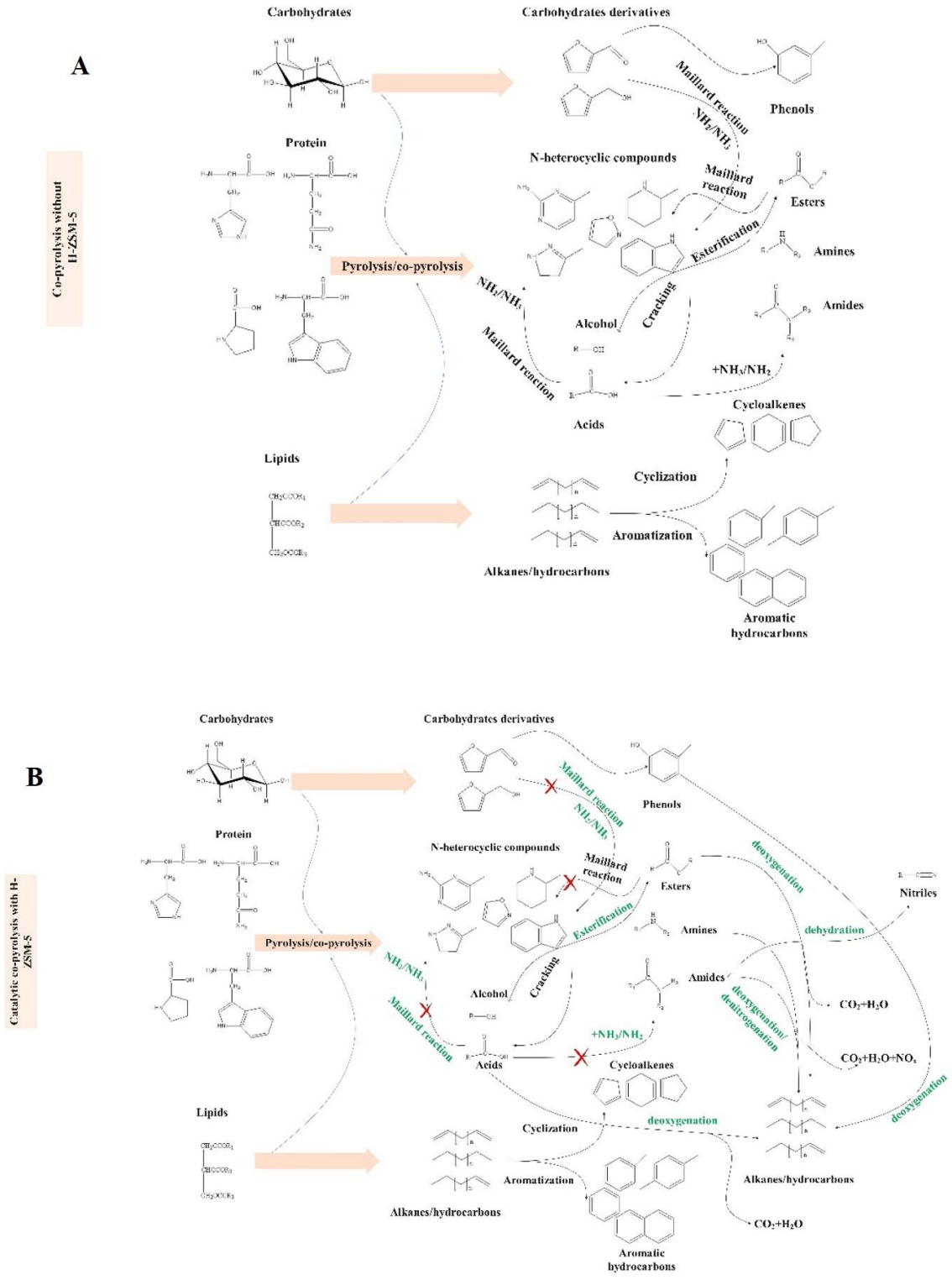

Figure 6.15. Probable mechanism in non-catalytic and catalytic co-pyrolysis.

6.3.4.4 Boiling point distribution

Figure 6.16 illustrates the boiling point distribution (BPD) of bio-oil derived from both individual, co-feedstocks, without and with catalyst, and recycled catalytic process. All bio-oils showed unique distillation profile concerning the boiling points of the products. Poor BPD was noted in dairy sludge pyrolytic bio-oil, with a high proportion of gas oil (20.55%) and vacuum gas oil (44.27%). The dairy sludge bio-oil consisted of 29.64% of low-boiling-point compounds, which encompasses products such as heavy naphtha (<193 °C), petroleum (193-271 °C), and gas oil fractions (271-343 °C). The proportion of heavy naphtha (17.94%) and kerosene fractions (36.09%) was higher in algal bio-oil due to the reduced ash content and higher volatile content irrespective of less bio-oil formation. Alkanes, aromatics, and alkenes are classified under heavy naphtha and kerosene fractions which are present in major proportion in KMC4 bio-oil.

On mixing these two feedstocks for co-pyrolysis, it was observed that the proportion of heavy naphtha was decreased to 8.91% with the high proportion of kerosene and gas oil fractions. An increase in heavy naphtha (11.37%) and gas oil (36.56%) fraction was observed in catalytic pyrolysis bio-oil, which referred to an increased hydrocarbons, fatty acids, and esters. A lower vac residue of 9.6% was observed in co-pyrolysis bio-oil in comparison with individual KMC4 (16.48%), which resembled to low presence of heavy compounds. While in catalytic co-pyrolysis, a decrease in 53.23% of vac residue was observed compared with the non-catalytic process. From this observation, it was found that H-ZSM-5 was able to reduce the amount of heavy boiling point compounds.

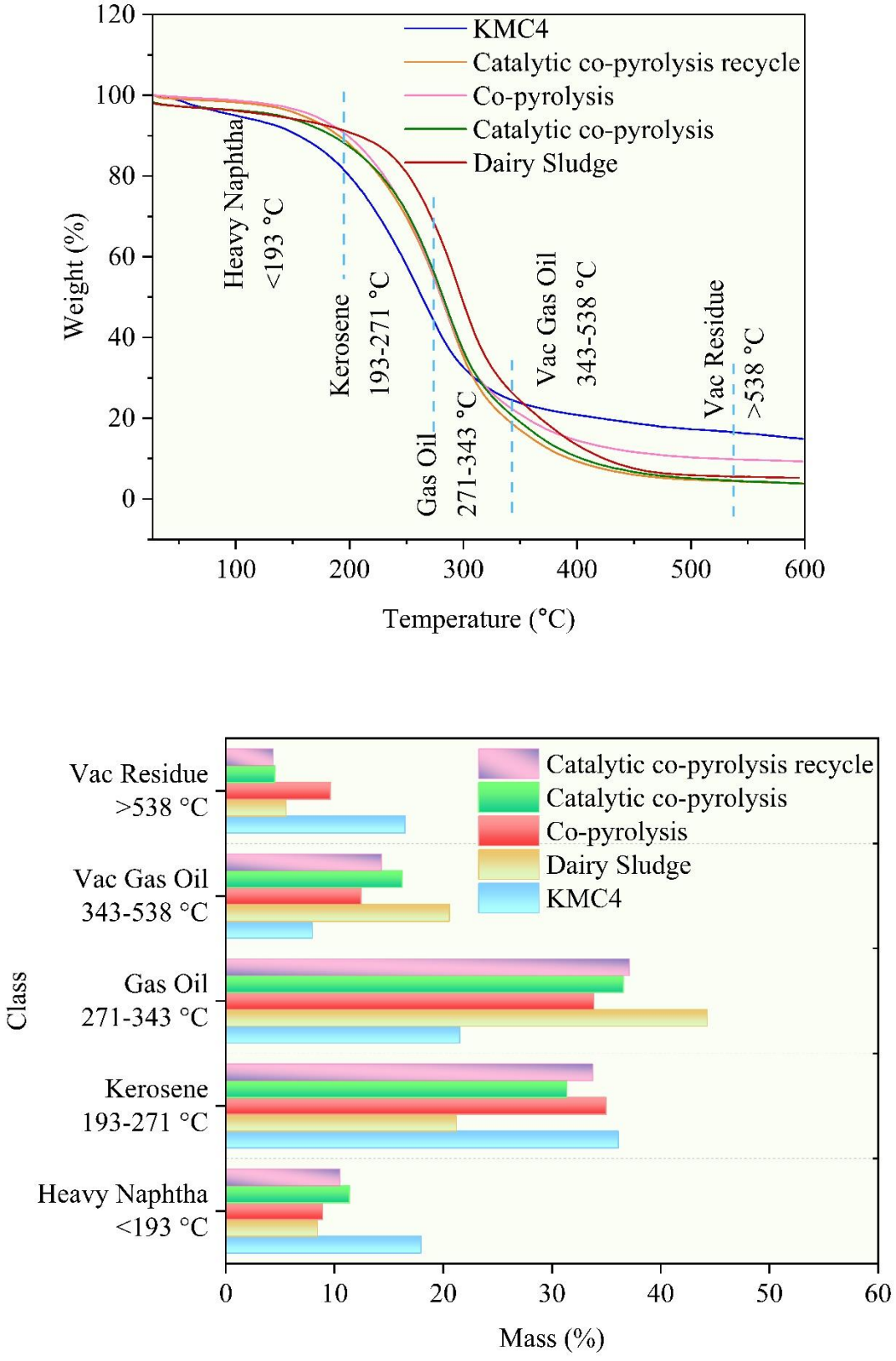

Figure 6.16. Boiling point distribution of pyrolytic bio-oils.

6.3.4.5 FTIR spectrum

FTIR spectrum were used to illustrate the bio-oils functional groups (Figure 6.17). In 3100 cm^{-1}- 3600 cm^{-1} range, the stretching vibrations of O-H and N-H molecules were observed. Hydrogen bonding caused the O-H stretch, which was prevalent in alcohols, carboxylic acids, and phenols, to show as a broad and powerful peak, typically spanning a large range from approximately 3200 cm^{-1} to 3600 cm^{-1}. The N-H stretch belonged to amines or amides, exhibited a sharper, narrower profile with medium intensity. The Amide II band (N-H bending and C-N stretching) was observed between 1510 cm^{-1} and 1580 cm^{-1} whereas the Amide I band (C=O stretching) was detected between 1630 cm^{-1} and 1690 cm^{-1}.

The existence of long-chain aliphatic hydrocarbons was evidenced by the peaks observed between 3000 cm^{-1} and 2800 cm^{-1}, as well as between 1460 cm^{-1} and 1350 cm^{-1}, corresponded to C-H stretching of CH_3 and CH_2 groups. The presence of aliphatic hydrocarbons, carboxylic acids, ketones, aldehydes, and esters in bio-oil indicated the existence of carboxyl functional groups associated with the peak between 1800 cm^{-1} and 1590 cm^{-1}.

Prominent bands detected between 1260 cm^{-1} and 1000 cm^{-1} in all bio-oils are attributed to C–O stretching vibrations, presumably originating from aliphatic esters, alcohols, or carboxylic acids. In the 900 cm^{-1}- 700 cm^{-1} range, bands were attributable to aromatic C-H out-of-plane bending vibrations. The FTIR spectra displayed similar transmittance pattern, indicating the presence of comparable functional groups. The similar pattern suggested the primary chemical nature of the bio-oil and confirmed the functional group distribution. However, the variation in bio-oil classes of compounds were distinguished on the basis of GC-MS.

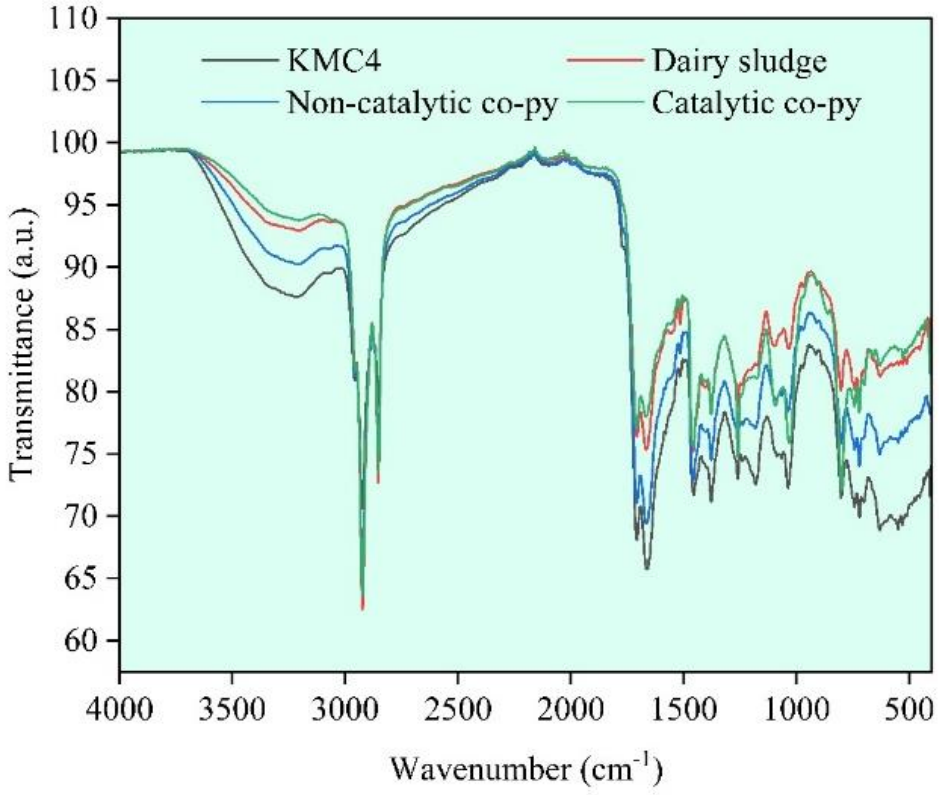

Figure 6.17. Functional group analysis of pyrolytic bio-oils.

6.4 Summary

The bio-oil produced from co-pyrolysis holds a considerable potential as an alternative to conventional fossil fuels. Co-pyrolysis process of microalgae and dairy sludge was conducted to produce liquid fuel. The maximum yield of co-pyrolysis bio-oil was obtained from algae and dairy sludge at 550 °C and 60 min. The study revealed the synergistic effect between two feedstocks on bio-oil yield and quality for co-pyrolysis. The influence of catalyst H-ZSM-5 on the increased nitriles from the catalytic cracking of bio-oils was observed. With catalyst, the bio-oil yield was improved with less nitrogenous compounds and aromatics, which were prominent in microalgae and dairy sludge bio-oil, respectively. The O/C and N/C ratio dropped in catalytic bio-oil while H/C raised slightly, showed that the catalyst has effectively performed deoxygenation, denitrogenation and dehydration, resulted in a higher heating value of product. The reaction pathways suggested that H-ZSM-5 increased the nitriles from dehydration of amides and followed denitrogenation reaction to reduce the formation of lower cyclic compounds. The boiling point distribution profile of catalytic bio-oil showed a lower proportion of vac residue. The structural, texture, and thermal properties of fresh catalyst reveal

its well-defined crystalline morphology. While the coked spent catalyst revealed coke deposition as confirmed from XPS, TGA, elemental mapping, and BET analysis. This investigation highlighted the effect of H-ZSM-5 towards enhancing the quality of bio-oil which can be further upgraded towards biofuel production.

Chapter 7
Conclusions, Social Impact and Future Prospect

Chapter 7. Conclusions, Social Impact and Future Prospects

This section presents the key conclusions drawn from the research undertaken in this thesis and offers recommendations for future investigations that can further expand upon the findings and framework established in this study. In this research work, research gaps were presented in the co-processing of waste dairy sludge with microalgae towards bio-oil production, together with the aim of reducing nitrogen content in bio-oil via a two-stage HTL process. Identifying important feedstocks for producing value-added products is crucial in thermochemical conversion processes. This study investigated the potential of Monoraphidium sp. KMC4 towards bioremediation potential for simulated synthetic dairy wastewater. For two stage-HTL process, microalgae was pretreated at lower temperature for bio-oil production with lower heteroatoms content, by increasing the H/C and decreasing the N/C of solid I from the first stage. The nitrogen, organic carbon and inorganic carbon were recovered in the aqueous phase of stage I. The effect of first stage on the bio-oil composition obtained from second stage is of much interest to thermochemical conversion processes due to its better quality. Together with microalgae, another waste derived from dairy industry i.e. dairy sludge was co-processed for bio-oil production from two widely used technologies, hydrothermal liquefaction and pyrolysis for liquid fuel production. From co-HTL and co-pyrolysis process, the purpose is to understand the synergistic interaction between two feedstocks along with reduced nitrogen. Distillation profile revealed better boiling point compounds in bio-oil from co-HTL of dairy sludge and microalgae (25:75) with enhanced heavy naphtha and kerosene fractions. In catalytic co-pyrolysis of dairy sludge and microalgae, the aim was to reduce the nitrogen of bio-oil by incorporating H-ZSM-5 and to study the synergistic interactions between those feedstocks.

7.1. Conclusions

❖ *Monoraphidium* sp. KMC4 was cultivated mixotrophically for simultaneous treatment of dairy wastewater and biomass production. The KMC4 was cultivated with varying chemical oxygen demand concentrations of simulated synthetic dairy wastewater.

❖ *Monoraphidium* sp. KMC4 outperformed in 50% strength with biomass concentration of 1.47 g L^{-1}. A significant change in biomass of 3.69 g L^{-1} was achieved after maintaining the pH of algal culture.

❖ The nutrient consumption promoted microalgal growth in the form of biomass productivity (122 mg L^{-1} day^{-1}), accumulation of carbohydrate (28.73±1.6 wt%), protein (48.50±1.3 wt%), and lipid (20.29±2.3 wt%).

❖ This strain showed efficacious performance in treating simulated synthetic dairy wastewater obtaining biomass for bio-oil production due to a significant volatile matter content and higher heating value.

❖ The biomass demonstrated satisfactory thermal degradation behavior which revealed its feasibility as feedstock for thermochemical conversion to bio-oil.

❖ The bio-oil generated from direct high-temperature and two-stage hydrothermal liquefaction was compared for its elemental quality and yield.

❖ A bio-oil yield of 33.50% was achieved via direct HTL, with high N/C (0.05 mol/mol), H/C (1.36 mol/mol), and O/C (0.11 mol/mol) ratios.

❖ The implementation of two-stage hydrothermal liquefaction was applied to increase the H/C and to decrease the N/C of the feedstock, to increase the H/C and to decrease the N/C and the O/C of bio-oil. This resulted in better bio-oil quality by the prior extraction of carbohydrates and protein components from algae biomass at lower pretreatment temperatures.

❖ Initially, at a lower temperature (140 °C), a nominal decrease in the nitrogen content during pretreatment from microalgae feedstock was noted, while a significant reduction in nitrogen amount was observed at higher pretreatment temperatures (>200 °C). There was a 76.47% decrement in the N/C ratio from algae feedstock to solid residue I at 240 °C, which was almost 2.5 times higher than that at a lower pretreatment temperature.

❖ The TOC and total nitrogen of the aqueous phase were increased from 1.6 g L^{-1} to 22.21 g L^{-1} and 1.15 to 6.81 g L^{-1} when the temperature was increased from 140 °C to 240 °C due to more hydrolysis of algae biomass at extreme temperatures in stage I of two-stage HTL.

❖ Overall, the low temperature pretreatment partitioned the nitrogen into the aqueous phase while retained carbon in solid residue I.

❖ The bio-oil from direct HTL had a significant number of nitrogen-based compounds (13.36%), i.e., amides, amines, and heterocyclic forms, while it was reduced to 1.98% in the two-stage hydrothermal liquefaction process. A reduction of 38% nitrogen in bio-oil was observed from direct HTL compared to two-stage HTL through elemental analysis.

❖ The total bio-oil yield from two-stage HTL of KMC4 microalgae was 36.67 wt% (combining first- and second-stage bio-oil) under stage I conditions of 220 °C and 30 min, and stage II conditions of 300 °C and 30 min.

❖ The hypothetical pathway suggested a reduction in the path toward Maillard reaction and amine formation when microalgae are subjected to two-stage HTL. The results from the two-stage HTL process significantly enhanced the bio-oil quality without the expense of reduced yield.

❖ The waste-to-energy conversion process offers significant potential for dairy sludge for bio-oil production, which contains a good amount of volatile matter, can be used as key starting components via co-HTL process.

❖ Co-hydrothermal liquefaction (Co-HTL) of algal biomass with dairy sludge for generating bio-oil production reduces the dependence of liquid fuel production from microalgae due to easy availability of waste dairy sludge, reduces the overall expense of biomass production process.

❖ Microalgae yielded higher bio-oil (33.50%) than dairy sludge (18.16%). Similar bio-oil yield of 32.94 wt% was observed for co-HTL of 75:25 ratio (algae to dairy sludge) with a heating value of 38.24 MJ kg^{-1}, highest compared to other feedstock ratios (50:50 and 25:75).

❖ The co-liquefaction process showed synergistic effect on the basis of quality and quality.

❖ The co-HTL bio-oil resulted in an increased atomic H/C and decreased O/C and N/C ratio. A lower O/C and higher H/C in the co-HTL bio-oil was observed due to deoxygenation and dehydration reactions.

❖ The bio-oil derived by co-HTL of co-feedstocks exhibited improved quality, characterized by decreased levels of N-heterocyclic, aromatics, and increased esters.

❖ The thermal stability profile suggested that a better boiling point compounds in bio-oil was observed from co-HTL of dairy sludge and microalgae (25:75) with enhanced heavy naphtha and kerosene fractions.

❖ The study also observed that dairy sludge as feedstock alone does not show significant bio-oil yield and quality. From the approach of effective conversion of co-feedstock to valuable products, the co-HTL derived bio-oil can be used as an alternative in bioenergy sector after upgradation studies.

❖ The bio-oil quality from co-processing of dairy wastewater-grown microalgae and dairy sludge in co-pyrolysis was compared to the co-HTL.

❖ Similarly, in co-pyrolysis, synergistic effects between protein- and lipid-rich microalgal biomass and dairy sludge was observed.

❖ In absence of a catalyst, the bio-oil yield was improved with less nitrogenous compounds and aromatics, which were prominent in microalgae and dairy sludge bio-oil, respectively.

❖ The introduction of H-ZSM-5 modified the product distribution, leading to decreased nitrogen-containing compounds, more hydrocarbons and esters. Reaction pathway suggested that H-ZSM-5 increased the nitriles from dehydration of amides and reduced cyclic nitrogenated compounds by denitrogenation reaction.

❖ The coked spent catalyst revealed coke deposition and partial alteration.

❖ H-ZSM-5 promoted the deoxygenation, decarboxylation, and dehydration reactions as observed from better H/C and lower O/C ratio of bio-oil.

❖ Boiling point distribution of catalytic pyrolytic bio-oil showed an increase in heavy naphtha and gas oil fraction, which referred to an increased hydrocarbons, fatty acid, and esters.

❖ Looking at the required product yield from both thermochemical processes, the HTL and co-HTL process resulted in more bio-oil compared to co-pyrolysis and catalytic co-pyrolysis process.

❖ Similarly, bio-oil from HTL and co-HTL achieved better energy density and properties compared to co-pyrolysis and catalytic co-pyrolysis process.

❖ When comparing the different HTL process, DHTL, SHTL, and co-HTL, SHTL process obtained better bio-oil quality without the expense of more reduced yield (Figure 7.1).

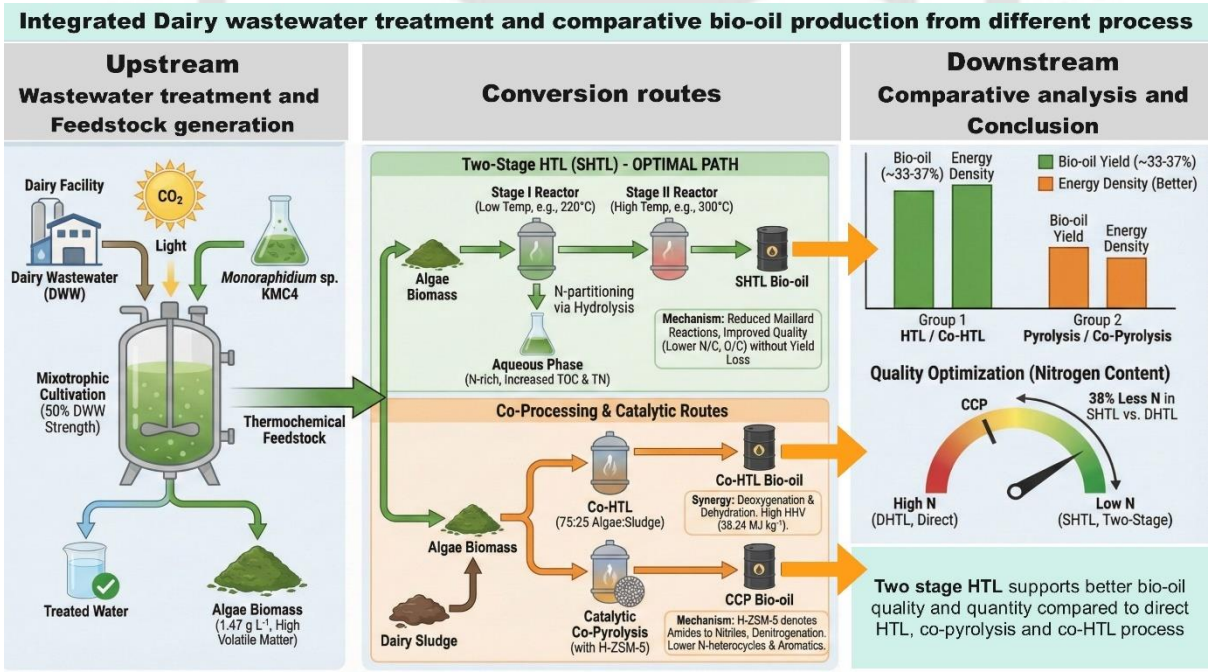

Figure 7.1. Conclusion of integrated wastewater treatment and biofuel production.

7.2 SWOT analysis and social impact for production of biofuel

Worldwide, countries are striving to tackle environmental challenges, including global warming and climate change, as well as the depletion of fossil fuel supplies. Moreover, nations seek to achieve net-zero carbon emissions amid the current and escalating global energy crises. Consequently, various biomass including microalgae as alternative sustainable feedstocks are being investigated for bioenergy production.

Several countries globally recognize the advantages of biofuel generation and are actively promoting their bioenergy programs. This evolution has primarily been propelled by policies promoting biofuel utilization and production, motivated by its capacity to enhance energy security and mitigate greenhouse gas emissions in critical sectors. A SWOT analysis delineates the principal aspects affecting the future advancement of worldwide biofuel production using thermochemical conversion methods.

Some recommendations from the SWOT analysis are provided in Figure 7.1 includes:

1. There is a potential for nutrient recycling towards an anaerobic digestion process and microalgae cultivation to reduce the overall cost of the SHTL and DHTL process.

2. Also, the SHTL process offers a path to derive important platform chemicals from the first-stage aqueous phase.

3. The co-HTL and co-pyrolysis process offers industrial symbiosis between dairy plants and an algal cultivation system. It gives a potential road towards a decentralized waste-to-energy path at dairy facilities.

4. Focus on generating third-generation feedstocks and using waste sludge to avoid fuel vs food problems.

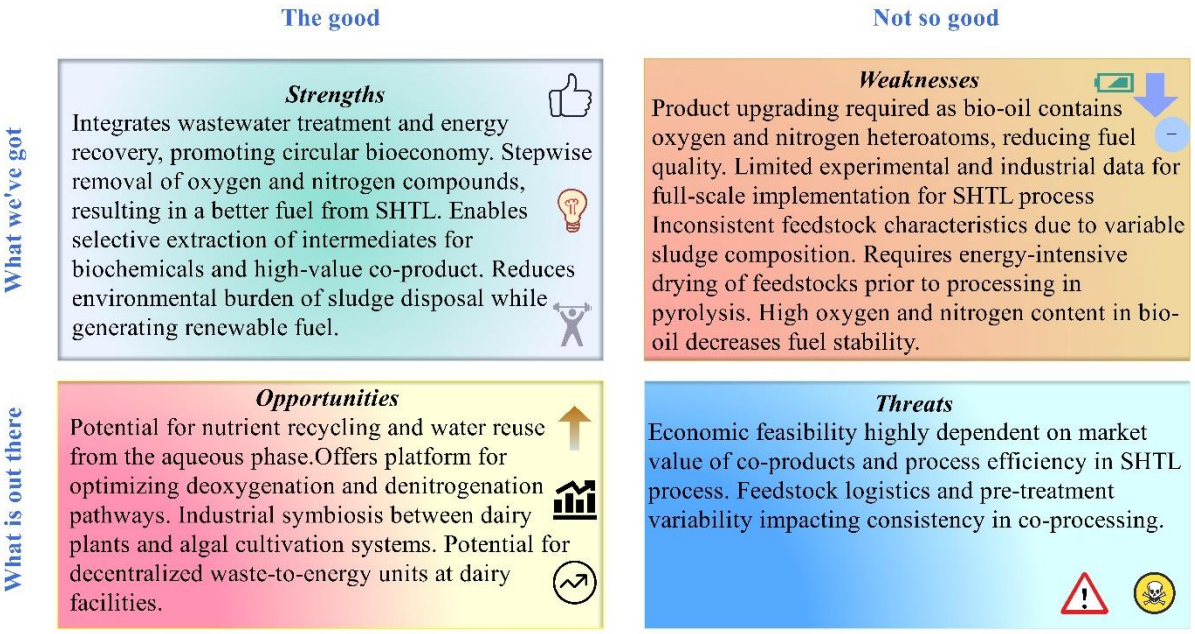

Figure 7.2. SWOT analysis of integrated wastewater treatment and biofuel production.

Figure 7.3. Sustainable development goals addressed by this research work.

The social impact of this research is strongly aligned with the United Nations Sustainable Development Goals (SDGs), as it addresses critical societal challenges while promoting sustainable and positive change across multiple sectors. The work presented in this thesis makes a meaningful contribution to key global priorities, particularly SDG 7 (Affordable and Clean Energy) by advancing sustainable energy solutions, and SDG 13 (Climate Action) through its emphasis on reducing environmental impact and supporting climate mitigation efforts (Figure 7.2).

7.3 Future Perspective

- The identification and cultivation of microalgal strains with varied compositions, high growth rates, and environmental robustness are essential for feedstock exploration. This entails examining genetic alterations and growing methodologies to enhance biomass productivity and quality.
- The effect of different algal macromolecular composition on bio-oil yield and quality from two-stage HTL process remains the future work to understand the correlation between feedstock composition, process conditions and product distribution.
- Development of continuous-flow reactors and process optimization for two-stage HTL process to enhance process efficiency and scalability for industrial applications.
- Improving performance predictability across various algal biomasses and operational conditions is essential, alongside the development of reliable continuous HTL reactor systems that enable flexible recovery of high-value co-products.
- Aqueous phase utilization towards microalgae cultivation to maximize value from by-products.
- The bio-oil can be refined through upgradation system for its use as aviation fuel after blending. The raw and upgraded bio-oil needs comprehensive refinery-compatibility analyses for comparison studies.
- Efforts should focus on understanding and mitigating challenges related to reactor design and catalytic upgradation. To enhance the microalgae conversion process, adopting bio-based catalysts is recommended, as they offer a more cost-effective and sustainable alternative to expensive synthetic catalysts.
- Comparative Life cycle assessment (LCA) of each thermochemical conversion process and carbon footprint analysis to ensure environmental sustainability of the integrated process. While the thesis demonstrates laboratory-scale technical feasibility of the integrated wastewater-to-bio-oil route, a rigorous techno-economic assessment and detailed scale-up design, including energy integration, water-recycle strategy, and catalyst-regeneration economics is required.

Appendix

Table A.1. Comparison between compounds present in bio-oil produced from both direct (DHTL) and two-stage (SHTL) hydrothermal liquefaction.

Area (%)		Compounds Name
DHTL	SHTL	
0.18	0.00	Methyl N-[2-[[1-(4-chlorophenyl)pyrazol-3-yl]oxymethyl]phenyl]-N-methoxycarbamate
2.76	0.00	(1RS,2RS;1RS,2SR)-1-(4-chlorophenoxy)-3,3-dimethyl-1-(1H-1,2,4-triazol-1-yl)butan-2-ol
0.02	0.00	(1RS,2RS;1RS,2SR)-1-(biphenyl-4-yloxy)-3,3-dimethyl-1-(1H-1,2,4-triazol-1-yl)butan-2-ol
0.00	0.12	(2,2,6-Trimethylbicyclo[4.1.0]hept-1-yl)-methanol
0.48	0.00	(2RS)-N,N-diethyl-2-(1-naphthyloxy)propanamide
0.00	0.36	(6-Hydroxymethyl-2,3- dimethylphenyl)methanol
0.00	0.42	(R)-9-[(S)-2- (Hydroxymethyl)pyrroli din-1-yl]-3-methyl-3,4- dihydro-2Hbenzo[b][1,4,5]oxathiazepine 1,1-dioxide
0.02	0.00	(R)-Cyano(4-fluoro-3-phenoxyphenyl)methyl (1R,3R)-3-(2,2-dichloroethen-1-yl)-2,2-dimethylcyclopropane-1-carboxylate
0.37	0.00	(RS)-1-(4-chlorophenoxy)-3,3-dimethyl-1-(1H-1,2,4-triazol-1-yl)butan-2-one
0.66	0.00	(RS)-1-(4-chlorophenyl)-4,4-dimethyl-3-(1H-1,2,4-triazol-1-ylmethyl)pentan-3-ol
0.06	0.00	(RS)-α-cyano-3-phenoxybenzyl 2,2,3,3-tetramethylcyclopropanecarboxylate
0.05	0.00	(Z)-2-chloro-1-(2,4-dichlorophenyl)vinyl diethyl phosphate
0.18	0.00	(Z)-2-tert-butylimino-3-isopropyl-5-phenyl-1,3,5-thiadiazinan-4-one
0.06	0.00	β-2,2,6,6-Tetramethyl-4-piperidylaminocrotonic acid, ethyl ester
0.17	0.00	.beta.-d-Lyxofuranoside, O-nonyl-
0.35	0.00	{(RS)-2-[3-(4-chlorophenyl)propyl]-2,4,4-trimethyl-1,3-oxazolidin-3-yl}(imidazol-1-yl)methanone fumarate (2:1)
0.00	0.59	1-(2-Hydroxyethyl)-1,2,5,5-tetramethyl-cisdecalin(1R,2S,4as,8as)
0.60	0.00	1,2-Benzenedicarboxylic acid, bis(2-methylpropyl) ester
0.99	0.00	1,2-Benzenedicarboxylic acid, butyl octyl ester
0.06	0.00	1,3-Propanediol, ethyl tetracosyl ether
0.02	0.00	1-[[2-(2,4-dichlorophenyl)-4-propyl-1,3-dioxolan-2-yl]methyl]-1,2,4-triazole
0.12	0.00	11-Methyldodecanol
0.34	0.00	1-Decanol, 2-hexyl-
0.08	0.00	1-Decene
0.00	1.47	1-Dodecanol, 3,7,11-trimethyl
1.46	0.00	1-Dodecene
1.06	0.00	1-Heptacosanol
10.38	0.00	1-Nonadecene
0.02	0.00	1-Octanol, 2-butyl-
0.42	0.00	2,4-Dimethyldodecane
6.48	0.60	2,4-Di-tert-butylphenol
0.83	0.00	2,6,10-Trimethyltridecane

0.26	0.00	2-Bromotetradecane
0.02	0.00	2-cyano-N-[(ethylamino)carbonyl]-2-(methoxyimino)acetamide
0.15	0.00	2-Hexadecene, 3,7,11,15-tetramethyl-, [R-[R*,R*-(E)]]-
0.17	0.00	2-Isopropyl-5-methyl-1-heptanol
0.32	0.00	2-Methyl-2-(methylthio)propanal O-[(methylamino)carbonyl]oxime
0.94	0.00	2-Methylpentacosane
0.14	0.00	2-tert-butyl-5-(4-tert-butylbenzylthio)-4-chloropyridazin-3(2H)-one
0.60	0.00	3,7,11,15-Tetramethylhexadec-2-ene
0.52	0.00	3-Ethyl-2,6,10-trimethylundecane
0.00	0.56	3-Phenylindole
0.00	0.43	4-(1'-Pyperidinocarbonylpropyl)-2-methylpyridine
0.00	2.96	4,2-Cresotic acid, 6-methoxy-, bimol. ester, methyl ester, 4,6- dimethoxy-o-toluate
0.42	0.00	4-Amino-3,5,6-trichloro-2-pyridinecarboxylic acid
0.51	0.00	4-amino-6-tert-butyl-4,5-dihydro-3-methylthio-1,2,4-triazin-5-one
0.02	0.00	4-Heptanone, 2-methyl-
0.09	0.00	4-nitrophenyl 2,4,6-trichlorophenyl ether
0.02	0.00	4-Piperidinone, 2,2,6,6-tetramethyl-
0.66	0.00	4-Piperidinone, 2,2,6,6-tetramethyl-, oxime
0.26	0.00	5,5-Dibutylnonane
0.65	0.00	5,5-Diethylpentadecane
0.37	0.00	6,6-Dimethyl-cyclooct-4-enone
0.75	0.00	7,9-Di-tert-butyl-1-oxaspiro(4,5)deca-6,9-diene-2,8-dione
0.00	0.68	7-Hexadecenal
0.00	0.39	7-Tetradecene
0.00	0.09	9-Hydroxy-7-nonanal
2.89	2.96	9-Octadecene, (E)-
0.00	0.42	9-Octadecenoic acid (Z)-, phenylmethyl ester
0.00	2.33	Acetic acid, 3,7,11,15-tetramethyl-hexadecyl ester
0.62	0.00	Arachidamide, N-3-methylbutyl-
0.26	0.00	Arachidamide, N-butyl-
0.23	0.00	Arachidamide, N-ethyl-
3.23	10.60	Benzene, 1,3-bis(1,1- dimethylethyl)-
0.00	0.62	Benzeneacetic acid, 4-tridecyl ester
1.60	0.00	butyl (2,4-dichlorophenoxy)acetate
0.14	0.00	Carbonic acid, decyl hexadecyl ester
0.00	1.12	Carbonic acid, decyl undecyl ester
0.00	3.65	Carbonic acid, eicosyl vinyl ester
0.00	1.62	Carbonic acid, tridecyl vinyl ester
0.17	0.00	Cyclohexane, 1,2,3-trimethyl-, (1.alpha.,2.beta.,3.alpha.)-
0.00	0.33	Cyclooctanamine
0.23	0.00	Cyclopropanemethanol, 2,2-dimethyl-3-(2-methyl-1-propenyl)-
0.08	1.94	Decane, 2,3,5,8- tetramethyl
0.00	0.66	Decane, 2,4,6- trimethyl
1.57	0.00	Di Methyl Phthalate
0.85	0.00	Di(2-ethylhexyl) phthalate
1.59	0.00	Dibutyl phthalate
0.05	0.00	Dichloroacetic acid, nonyl ester

0.49	0.00	Didecyl phthalate
0.05	0.00	Diethyl 2-[(dimethoxyphosphorothioyl)sulfanyl]butanedioate
0.34	6.44	Dodecane, 2,6,10- trimethyl
1.68	0.00	Dodecane, 2,6,11-trimethyl-
0.15	0.00	Dodecane, 2-methyl-6-propyl-
0.11	0.00	Dodecane, 4-methyl-
0.46	0.00	Dotriacontyl isopropyl ether
3.83	0.00	E-14-Hexadecenal
16.50	0.00	Eicosane
0.00	1.34	Eicosyl isopropyl ether
0.00	0.47	Furane-2-carboxaldehyde, 5-yl)hydrazone
0.11	0.00	Glutaric acid, 2-ethylhexyl 3,7-dimethyloctyl ester
0.14	0.00	Heptadecanal
1.45	0.00	Heptadecane
0.63	0.00	Heptadecane, 3-methyl-
0.25	0.00	Heptadecane, 4-methyl-
0.08	0.00	Heptadecane, 7-methyl-
0.09	0.00	Heptadecane, 8-methyl-
0.00	0.55	Heptane, 2,4,6- trimethyl
2.16	0.00	Hexacosyl nonyl ether
0.34	0.00	Hexadecanamide
4.14	15.13	Hexadecane
0.00	1.15	Hexadecane, 1-chloro-
0.11	0.00	Hexadecane, 1-iodo-
0.17	4.77	Hexadecane, 2,6,10,14-tetramethyl
7.96	0.00	Hexadecanoic acid, methyl ester
0.26	0.00	Hexadecyl nonyl ether
0.00	0.95	Hexane, 2,3,4 trimethyl
0.17	0.00	isopropyl (E,E)-(RS)-11-methoxy-3,7,11-trimethyldodeca-2,4-dienoate
0.12	0.00	Isopropyl octadecyl ether
0.00	4.20	Methoxyacetic acid, 2-pentadecyl ester
0.00	0.75	Methoxyacetic acid, 2-tetradecyl ester
0.00	7.30	Methoxyacetic acid, 3-tridecyl ester
0.00	0.26	Methoxyacetic acid, 4-tetradecyl ester
0.00	1.51	Methoxyacetic acid, 4-tridecyl ester
0.00	0.24	Methoxyacetic acid, tridecyl ester
0.09	0.00	Methyl (E)-3-(dimethoxyphosphinothioyloxy)-2-methylacrylate
0.02	0.00	Methyl N-(4-chloro-2-methylphenoxy)carbamate
0.03	0.00	N,N-dimethyl-1,2,3-trithian-5-ylamine
0.09	0.00	N-[(6-chloro-3-pyridyl)methyl]-N'-cyano-N-methylacetamidine
0.94	0.00	N-butoxymethyl-2-chloro-2',6'-diethylacetanilide
0.00	5.95	n-Heptadecanol-1
0.14	0.00	N-maleic acid 2,2,6,6-Tetramethyl,-4-piperidylmonoamide
0.34	0.00	n-Nonadecanol-1
0.00	4.90	Nonadecane
0.02	0.00	Nonane, 5-methyl-5-propyl-
0.20	0.00	Nonyl tetracosyl ether
0.02	0.00	O,O-diethyl O-(4-oxo-1,2,3-benzotriazin-3(4H)-yl) phosphate

0.06	0.00	O-2-diethylamino-6-methylpyrimidin-4-yl O,O-dimethyl phosphorothioate
0.89	0.00	O-6-chloro-3-phenylpyridazin-4-yl S-octyl thiocarbonate
0.14	0.00	Octadecane, 4-methyl-
0.74	0.00	Octadecane, 5-methyl-
0.00	0.66	Octadecanoic acid, 2- oxo-, methyl ester
0.00	1.88	Octane, 1,1'- sulfonylbis
0.03	0.00	Octane, 3,3-dimethyl-
0.00	0.16	Oxalic acid, allyl hexadecyl ester
0.00	0.10	Oxalic acid, allyl pentadecyl ester
0.00	0.92	Oxirane, decyl-
0.14	0.00	Pentadecane
0.28	0.00	Pentadecane, 2,6,10-trimethyl-
0.18	0.00	Pentadecane, 4-methyl-
0.00	0.24	Piperidine, 3-isopropyl-
0.31	0.00	Prohydrojasmon-1
0.43	0.00	Prohydrojasmon-2
0.29	0.00	rac-(1R,2S,4S)-1-methyl-4-(1-methylethyl)-2-((2-methylphenyl)methoxy)-7-oxabicyclo[2.2.1]heptane
2.25	0.00	S-(6-chloro-3-pyridinylmethyl) O,O-diethyl phosphorodithioate
0.09	0.00	S-[(tert-Butylsulfanyl)methyl] O,O-diethyl phosphorodithioate
0.18	0.00	S-2-methylpiperidinocarbonylmethyl O,O-dipropyl phosphorodithioate
0.00	0.29	Sulfurous acid, 2-propyltridecyl ester
0.00	0.45	Sulfurous acid, hexyl pentadecyl ester
0.28	0.00	Sulfurous acid, octadecyl pentyl ester
0.71	2.37	Tetradecane
0.00	0.04	Tetradecane, 1-chloro-
0.00	1.21	Tetradecane, 2,6,10- trimethyl
0.37	0.00	Tetradecane, 3-methyl-
0.03	0.00	Tetradecane, 4-methyl-
0.28	0.00	trans-2-Dodecen-1-ol
0.00	0.75	Trichloroacetic acid, pentadecyl ester
0.03	0.00	Tridecane, 2-methyl-
0.03	0.00	Tridecane, 3-methylene-

Table A.2. GC-MS of bio-oils from HTL and co-HTL process.

Bio-oil Area%			Compounds name
KMC4	Sludge	Co-HTL	
0.18	0	0	Methyl N-[2-[[1-(4-chlorophenyl)pyrazol-3-yl]oxymethyl]phenyl]-N-methoxycarbamate
2.76	0	0	(1RS,2RS;1RS,2SR)-1-(4-chlorophenoxy)-3,3-dimethyl-1-(1H-1,2,4-triazol-1-yl)butan-2-ol
0.02	0	0	(1RS,2RS;1RS,2SR)-1-(biphenyl-4-yloxy)-3,3-dimethyl-1-(1H-1,2,4-triazol-1-yl)butan-2-ol
0	0.86	0	(2E)-3,7,11,15-tetramethyl-2-hexadecene
0.48	0	0	(2RS)-N,N-diethyl-2-(1-naphthyloxy)propanamide
0.02	0	0	(R)-Cyano(4-fluoro-3-phenoxyphenyl)methyl (1R,3R)-3-(2,2-dichloroethen-1-yl)-2,2-dimethylcyclopropane-1-carboxylate
0.37	0	0	(RS)-1-(4-chlorophenoxy)-3,3-dimethyl-1-(1H-1,2,4-triazol-1-yl)butan-2-one
0.66	0	0	(RS)-1-(4-chlorophenyl)-4,4-dimethyl-3-(1H-1,2,4-triazol-1-ylmethyl)pentan-3-ol
0.06	0	0	(RS)-α-cyano-3-phenoxybenzyl 2,2,3,3-tetramethylcyclopropanecarboxylate
0.05	0	0	(Z)-2-chloro-1-(2,4-dichlorophenyl)vinyl diethyl phosphate
0.18	0	0	(Z)-2-tert-butylimino-3-isopropyl-5-phenyl-1,3,5-thiadiazinan-4-one
0.17	0	0	beta.-d-Lyxofuranoside, O-nonyl-
0.06	0	0	β-2,2,6,6-Tetramethyl-4-piperidylaminocrotonic acid, ethyl ester
0.35	0	0	{(RS)-2-[3-(4-chlorophenyl)propyl]-2,4,4-trimethyl-1,3-oxazolidin-3-yl}(imidazol-1-yl)methanone fumarate (2:1)
0.6	0.84	0	1,2-benzenedicarboxylic acid, bis(2-methylpropyl) ester
0.99	0	0	1,2-benzenedicarboxylic acid, butyl octyl ester
0	0	0.70	1,2-octadecanediol
0	0	1.86	1,3-propanediamine,N1,N1'-(methylenedi-4,1 phenylene)bis[N1-methyl-
0.06	0	0	1,3-propanediol, ethyl tetracosyl ether
0.02	0	0	1-[[2-(2,4-dichlorophenyl)-4-propyl-1,3-dioxolan-2-yl]methyl]-1,2,4-triazole
0.12	0	0	11-methyldodecanol
0	0	0.76	1-buten-3-yne, 1-chloro-, (E)-
0.34	0	0.63	1-decanol, 2-hexyl-
0.08	0	0	1-decene
0	1.28	0	1-dodecanol
1.46	0	0	1-dodecene
0	0	0.47	1'E-dehydrojuvabi-3'-ol
1.06	0	0	1-heptacosanol
0	1.04	0	1-heptadecene
0	2.37	0	1-Methylbutyl hexadecanoate
10.38	1.73	0	1-nonadecene
0	2.92	0	1-octadecanol
0.02	0	0	1-Octanol, 2-butyl-
0	1.08	0	1-tridecanol
0	0	0.90	2-(2,4-dichloro-6-nitrophenoxy)ethanol
0.42	0	0	2,4-dimethyldodecane

6.48	0	0	2,4-Di-tert-butylphenol
0	0	0.45	2,4-Di-tert-butylthiophenol
0.83	0	0	2,6,10-trimethyltridecane
0	0	1.28	2,6-Naphthalenedione, octahydro-1,1,8a-trimethyl-, cis-
0	0	1.14	2-[4-Cyclohexylbutanoylamino]-3-chloro-1,4-naphthoquinone
0	0	0.47	2-amino-2,3-dimethylbutanoic acid
0.26	0	0	2-bromotetradecane
0.02	0	0	2-cyano-N-[(ethylamino)carbonyl]-2-(methoxyimino)acetamide
0.15	0	11.12	2-hexadecene, 3,7,11,15-tetramethyl-, [R-[R*,R*-(E)]]-
0.17	0	0	2-isopropyl-5-methyl-1-heptanol
0.32	0	0	2-methyl-2-(methylthio)propanal O-[(methylamino)carbonyl]oxime
0.94	0	0	2-methylpentacosane
0	1.42	0	2-pentadecanone, 6,10,14-trimethyl-
0.14	0	0	2-tert-butyl-5-(4-tert-butylbenzylthio)-4-chloropyridazin-3(2H)-one
0.6	0	0	3,7,11,15-tetramethylhexadec-2-ene
0.52	0	0	3-ethyl-2,6,10-trimethylundecane
0	0.90	0	3-heptadecene, (Z)-
0	0	1.06	4,4,6-trimethyl-cyclohex-2-en-1-ol
0.42	0	0	4-amino-3,5,6-trichloro-2-pyridinecarboxylic acid
0.51	0	0	4-amino-6-tert-butyl-4,5-dihydro-3-methylthio-1,2,4-triazin-5-one
0.02	0	0	4-heptanone, 2-methyl-
0.09	0	0	4-nitrophenyl 2,4,6-trichlorophenyl ether
0.02	0	0	4-piperidinone, 2,2,6,6-tetramethyl-
0.66	0	0	4-piperidinone, 2,2,6,6-tetramethyl-, oxime
0.26	0	0	5,5-dibutylnonane
0.65	0	0	5,5-diethylpentadecane
0	1.01	0	5.α-ergost-8(14)-ene
0	2.98	0	5.β-cholest-3-ene
0	2.75	0	5.β-cholestan-3.α-ol, trifluoroacetate
0.37	0	0	6,6-dimethyl-cyclooct-4-enone
0.75	0	0	7,9-di-tert-butyl-1-oxaspiro(4,5)deca-6,9-diene-2,8-dione
0	0	3.56	8,8,9-trimethyl-deca-3,5-diene-2,7-dione
0	1.56	0	9,19-cyclolanostan-3-ol, acetate, (3β)-
0	0	0.54	9-octadecenamide
2.89	0	0	9-octadecene, (E)-
0.62	0	0	Arachidamide, N-3-methylbutyl-
0.26	0	0	Arachidamide, N-butyl-
0.23	0	0	Arachidamide, N-ethyl-
3.23	0	0	Benzene, 1,3-bis(1,1- dimethylethyl)-
1.6	0	0	Butyl (2,4-dichlorophenoxy)acetate
0.14	0	0	Carbonic acid, decyl hexadecyl ester
0	1.07	0.43	Cholest-2-ene
0	1.44	0	Cholest-4-ene
0	0.98	0	Cholest-5-en-3-ol (3β)-
0	1.38	0	Cholest-5-ene
0.17	0	0	Cyclohexane, 1,2,3-trimethyl-, (1α,2β,3α)-

0.23	0	0	Cyclopropanemethanol, 2,2-dimethyl-3-(2-methyl-1-propenyl)-
0	1.74	5.91	Decane
0.08	0	0	Decane, 2,3,5,8- tetramethyl
1.57	0	0	Di Methyle Phthalate
0.85	0	0	Di(2-ethylhexyl) phthalate
1.59	0	0	Dibutyl phthalate
0.05	0	0	Dichloroacetic acid, nonyl ester
0.49	0	0	Didecyl phthalate
0.05	0	0	Diethyl 2-[(dimethoxyphosphorothioyl)sulfanyl]butanedioate
0	0.95	0	Docosane
0	2.60	4.17	Dodecanamide, N-3-methylbutyl-
0	5.97	1.20	Dodecanamide, N-isobutyl-
0	2.08	0	Dodecane
0.34	0	0	Dodecane, 2,6,10- trimethyl
1.68	0	0	Dodecane, 2,6,11-trimethyl-
0.15	0	0	Dodecane, 2-methyl-6-propyl-
0.11	0	0	Dodecane, 4-methyl-
0.46	0	0	Dotriacontyl isopropyl ether
3.83	0	0	E-14-Hexadecenal
16.5	1.38	0	Eicosane
0	0	2.14	Ethanone, 1-[2,3-dihydro-6-hydroxy-2-(1-hydroxy-1-methylethyl)-4-methoxy-7-benzofuranyl]-, (+)-
0	0	0.58	Fumaric acid, monoamide, N-(3-chlorolphenyl)-, butyl ester
0.11	0	0	Glutaric acid, 2-ethylhexyl 3,7-dimethyloctyl ester
0.14	0	0	Heptadecanal
1.45	2.42	0	Heptadecane
0.63	0	0	Heptadecane, 3-methyl-
0.25	0	0	Heptadecane, 4-methyl-
0.08	0	0	Heptadecane, 7-methyl-
0.09	0	0	Heptadecane, 8-methyl-
0	1.62	0	Heptadecanenitrile
2.16	0	0	Hexacosyl nonyl ether
0.34	4.79	0	Hexadecanamide
4.14	1.60	0	Hexadecane
0.11	0	0	Hexadecane, 1-iodo-
0.17	0	0	Hexadecane, 2,6,10,14-tetramethyl
0	0.97	0	Hexadecanoic acid, 1-methylethyl ester
0	0	22.59	Hexadecanoic acid, hexadecyl ester
7.96	1.32	0	Hexadecanoic acid, methyl ester
0	0	0.60	Hexadecanoic acid, tetradecyl ester
0	0	13.62	Hexadecanoic acid, tetradecyl ester
0.26	0	0	Hexadecyl nonyl ether
0.17	0	0	Isopropyl (E,E)-(RS)-11-methoxy-3,7,11-trimethyldodeca-2,4-dienoate
0.12	0	0	Isopropyl octadecyl ether
0.09	0	0	Methyl (E)-3-(dimethoxyphosphinothioyloxy)-2-methylacrylate
0	0	0.57	Methyl 16-hydroxy-hexadecanoate
0.02	0	0	Methyl N-(4-chloro-2-methylphenoxy)carbamate

0	1.23	0	Methyl stearate
0	3.84	0	Myristamide, N-(3-methylbutyl)-
0	0	0.64	Myristamide, N-butyl-
0	2.11	0	Myristamide, N-ethyl-
0	2.15	0	Myristamide, N-isobutyl-
0	0.89	0	Myristamide, N-methyl-
0	3.77	0	N ,N-dimetylpalmitamide
0	0	0.53	N,N'-Bis(2-pyrrolidinoethyl)terephthalamide
0.03	0	0	N,N-dimethyl-1,2,3-trithian-5-ylamine
0	0	0.81	N,N-dimethyloctadecanamide
0.09	0	0	N-[(6-chloro-3-pyridyl)methyl]-N'-cyano-N-methylacetamidine
0.94	0	0	N-butoxymethyl-2-chloro-2',6'-diethylacetanilide
0	10.19	0	n-Hexadecanoic acid
0.14	0	0	N-maleic acid 2,2,6,6-Tetramethyl,-4-piperidylmonoamide
0	10.45	0.47	N-methylhexadecanamide
0.34	0	0	n-Nonadecanol-1
0.02	0	0	Nonane, 5-methyl-5-propyl-
0.2	0	0	Nonyl tetracosyl ether
0.02	0	0	O,O-diethyl O-(4-oxo-1,2,3-benzotriazin-3(4H)-yl) phosphate
0.06	0	0	O-2-diethylamino-6-methylpyrimidin-4-yl O,O-dimethyl phosphorothioate
0.89	0	0	O-6-chloro-3-phenylpyridazin-4-yl S-octyl thiocarbonate
0	2.57	0	Octadecanamide
0	0	1.71	Octadecane, 3-ethyl-5-(2-ethylbutyl)-
0.14	0	0	Octadecane, 4-methyl-
0.74	0	0	Octadecane, 5-methyl-
0	0	11.01	Octadecanoic acid, octadecyl ester
0.03	0	0	Octane, 3,3-dimethyl-
0.14	0	0	Pentadecane
0	1.67	0	Pentadecane
0	0	5.42	Pentadecane, 2,6,10,13-tetramethyl-
0.28	0	0	Pentadecane, 2,6,10-trimethyl-
0.18	0	0	Pentadecane, 4-methyl-
0	0.90	0.60	Phenol, 2,4-bis(1,1-dimethylethyl)-
0	0	1.11	Phenol, 2,4-dichloro-6-nitro-
0.31	0	0	Prohydrojasmon-1
0.43	0	0	Prohydrojasmon-2
0	0	0.97	Pyrimidin-2,4-dione, 1,2,3,4-tetrahydro-5-methyl-1-[[2-hydroxymethyl-3-dimethylamino]tetrahydrofur-5-yl-, hydrochloride
0.29	0	0	rac-(1R,2S,4S)-1-methyl-4-(1-methylethyl)-2-((2-methylphenyl)methoxy)-7-oxabicyclo[2.2.1]heptane
2.25	0	0	S-(6-chloro-3-pyridinylmethyl) O,O-diethyl phosphorodithioate
0.09	0	0	S-[(tert-Butylsulfanyl)methyl] O,O-diethyl phosphorodithioate
0.18	0	0	S-2-methylpiperidinocarbonylmethyl O,O-dipropyl phosphorodithioate
0	1.05	0	Squalene
0.28	0	0	Sulfurous acid, octadecyl pentyl ester
0.71	2.53	0	Tetradecane

0.37	0	0	Tetradecane, 3-methyl-
0.03	0	0	Tetradecane, 4-methyl-
0	1.58	0	Tetradecanoic acid
0.28	0	0	trans-2-Dodecen-1-ol
0.03	0	0	Tridecane, 2-methyl-
0.03	0	0	Tridecane, 3-methylene-

Table A.3. Compounds present in non-catalytic and catalytic pyrolytic bio-oils.

Compounds Name	KMC4	Dairy sludge	Non-catalytic co-PY	Catalytic co-PY	Catalytic co-PY recycle
(1S,4R,6S)-1-methyl-4-(prop-1-en-2-yl)-7-oxabicycloheptan-2-one	0	0	0.42	0	0
(2-Methyl-3-biphenylyl)methanol	0	0.23	0	0	0
(2R)-2,5,7,8-tetramethyl-2-[(4R, 8R)-4, 12-trimethyltridecyl]-3,4-dihydro-2H-1-benzopyran-6-ol	0	0.23	0	0.2	0
(3-Methyl-2-pent-2-enylcyclopent-2-enylideneaminooxy)acetic acid, methyl ester	0.25	0	0	0	0
(3R,3aS,8aR)-6,8a-dimethyl-3-(propan-2-yl)-2,3,4,5,8,8a-hexahydroazulen-3a(1H)-ol	0	0	0.23	0	0
(5S,6aR,10aS)-5-Propyldecahydrodipyrrolo[1,2-a:1',2'-c]pyrimidine	0	0.23	0	0	0
(Acridin-9-ylamino)-acetic acid	0	0.31	0	0	0
(E,Z,Z)-2,4,7-Tridecatrienal	0.43	0	0	0	0
(R)-(-)-(Z)-14-Methyl-8-hexadecen-1-ol	0	0	0	0	0.33
[1,1'-Biphenyl]-2-amine	0.25	0	0	0	0
1(2H)-Naphthalenone, octahydro-4-hydroxy-, trans-	1.81	0	0	0	0
1-(2-Methoxy-3-pyrazinyl)-1-ethanone	0.22	0	0	0	0
1-(4-Amino-furazan-3-yl)-5-(4-methyl-piperazin-1-ylmethyl)-1H-[1,2,3]triazole-4-carboxylic acid ethyl ester	0.49	0	0	0	0
1,1,6-trimethyl-3-methylene-2-(3,6,9,13-tetramethyl-6-ethenye-10,14-dimethylene-pentadec-4-enyl)cyclohexane	0	0.22	0	0	0
1,1':3',1"-Terphenyl, 5'-phenyl-	0	0.35	0	0	0
1,1'-Biphenyl, 2,4'-dimethyl-	0	0.28	0	0	0
1,1'-Biphenyl, 2-methyl-	0	0.33	0	0	0
1,1'-Biphenyl, 4-methyl-	0	0.58	0	0	0
1,2-Benzenedicarboxylic acid, bis(2-methylpropyl) ester	0.43	0	0	0.41	0
1,2-Dihexylcyclopropene	0	0	0	0	0.25
1,2-dihydroacenaphthylene	0	0.3	0	0	0
1,2-Oxathiane, 6-dodecyl-, 2,2-dioxide	0.21	0	0	0.32	0.4
1,3-Benzenedicarboxylic acid, bis(2-ethylhexyl) ester	0	0	0	0.25	0
1,3-dimethyl-2-phenyl-naphthalene	0	0.31	0	0	0
1,3-Dioxolane, 2,2-dimethyl-4-[(tetradecyloxy)methyl]-	0	0	0	0	0.28
1,4:3,6-Dianhydro-.alpha.-d-glucopyranose	1.81	0	0	0	0.37
1,4-Methanonaphthalene, 1,4-dihydro-	0	2.38	0	0	0

1,4-Methanonaphthalene,1,4-dihydro-9-((1-methylethylidene)-	0	0.3	0	0	0
1,7-Dimethyl-4-(1-methylethyl)cyclodecane	0.4	0	0	0	0
1,8-Diazabicyclo[5.4.0]undec-7-en-11-one	0.34	0	0	0	0
1-.beta.-d-Ribofuranosyl-1,2,4-triazole-3-carboxylic acid	0.48	0	0	0	0
10-Heptadecen-8-ynoic acid, methyl ester, (E)-	0.47	0	0	0	0
10-Methyl-dodecanoic acid, pyrrolidide	0	0	0	0.28	0
12-Hydroxy-octadecanoic acid, octyl ester	0	0	0	0.23	0
12-Tricosanone	0	0.25	0	0	0
13-Octadecenal, (Z)-	0	0	0.3	0	0
13-Pentacosanone	0	0	0	0.23	0
14-Heptacosanone	0	0	0.24	0	0
14-Methyl-heptadecanoic acid, pyrrolidide	0	0	0	0	0.49
16-Hentriacontanone	0	0	0.95	0.95	0.29
16-Nitrobicyclo[10.4.0]hexadecan-1-ol-13-one	0	0	0	0.3	0
17.alfa.,21.beta.-28,30-Bisnorhopane	0	0.45	0	0	0.23
1-Aziridinedecanoic acid, 2,2-dimethyl-.iota.-oxo-, ethyl ester	0	0	0	0	0.49
1-Decanol, 2-hexyl-	0	0	0	0	0.46
1-Dodecanol	0	0	0.65	0	0
1-Dodecanol, 3,7,11-trimethyl-	0.73	0.27	0	0.2	0
1-Dodecene	0.24	0	0	0	0
1-Eicosene	0	0.45	0	0.41	0.35
1-Heneicosyl formate	0	0	0	0.2	0
1-Heptacosanol	0.92	0	0.32	0.32	0.29
1-Heptadecene	0.68	0	0	0	0
1-Heptene, 2-isohexyl-6-methyl-		0	0.34	0	0
1-Hexadecanol	0.27	0	0	0	0
1-Hexadecanol, 3,7,11,15-tetramethyl-	0.26	0	0	0	0
1H-Imidazole, 5-octanoyl-	0.46	0	0	0	0.86
1H-Inden-1-one, 2,3,3a,4,7,7a-hexahydro-, cis-	0.41	0	0	0	0
1H-Indene, 1,1,3-trimethyl-	0	0.68	0	0	0
1H-Indene, 1,3-dimethyl-	0	0.76	0	0	0
1H-Indene, 2,3-dihydro-1,2-dimethyl-	0	1.03	0	0	0
1H-Indene, 2,3-dihydro-5-methyl-	0	0.4	0	0	0
1H-Indole, 1,2,3,5,7-pentamethyl-	0.25	0	0	0	0
1H-Indole, 2,3-dimethyl-	0	0.55	0	0	0
1H-Isoindole-1,3(2H)-dione, 2-(oxiranylmethyl)-	0.62	0	0	0	0
1H-Isoindole-1,3(2H)-dione, 2-methyl-	1.07	0	0.34	0	0.74
1H-Isoindole-1,3(2H)-dione, N-ethyl-	0.44	0	0	0	0

1-Hydroxy-4,4-dimethylcyclohexanecarbonitrile	0.23	0	0	0	0
1-Isopropyl-1H-indole	0	0.29	0	0	0
1-Naphthalenemethanamine	0	1.02	0	0	0
1-Nonadecene	1.32	0	3.6	0.85	3.75
1-Octanol, 2,2-dimethyl-	0.41	0	0	0	0
1-Octanone, 1-(2-furanyl)-	0	0	0	0.31	0
1-Pentadecene	0.59	0	0	0.26	0.42
1-Phenanthrenecarboselenoic acid, 1,2,3,4,4a,4b,5,6,10,10a-decahydro-1,4a-dimethyl-7-(1-methylethyl)-, Se-phenyl ester, [1R-(1.	0	0.27	0	0	0
1-phenylethan-1-one	0.58	0	0	0	0
1-Propanol, 3-(1-octadecenyloxy)-	0	0	0	0.21	0
1-Tetradecanol	0.2	0	1.05	0	0.72
1-Tetradecene	0.42	0	0.56	0	0.48
1-Undecene, 11,11-diethoxy-	0	0	0	0.2	0.26
2-(1,5-Dimethyl-hexyl)-cyclobutanone	0	0	0	0	0.27
2(1H)-Naphthalenone, octahydro-4a,5-dimethyl-3-(1-methylethyl)-, (3.alpha.,4a.beta.,5.beta.,8a.alpha.)-	0.2	0	0	0	0
2-(1H-Benzo[g]indol-3-yl)-1-methylethylamine	0	0.46	0	0	0
2(3H)-Furanone, dihydro-5-tetradecyl-	0.31	0	0	0	0
2(4H)-Benzofuranone, 5,6,7,7a-tetrahydro-4,4,7a-trimethyl-	0.5	0	0	0	0
2,2-Dimethyl-3-(2-methylprop-1-enyl)cyclopropane-1-carboxylic acid	0	0	0	0	0.38
2,2-Dimethylbutanedioic acid	0	0	0.33	0	0
2,3,4-Trifluorobenzoic acid, pentadecyl ester	0.24	0	0	0	0
2,3,7-Trimethylindole	0	0.69	0	0	0
2,4-Dimethoxyamphetamine	0	0	0	0.37	0.21
2,4-Imidazolidinedione, 3-butyl-	0	0	0.22	0	0
2-Acetoxy-1,1,10-trimethyl-6,9-epidioxydecalin	0	0	0	0.23	0
2-Butenamide, N,2,3-trimethyl-	0.2	0	0	0	0
2-Cyclopenten-1-one, 2-methyl-3-pentyl-	0	0	0	0	0.21
2-Cyclopenten-1-one, 2-pentyl-	0	0	0.8	0.38	0
2-Diethoxymethyl-3-methyl-butan-1-ol	0	0	0.22	0	0
2-Ethyl-2,3-dihydro-1H-indene	0	0.25	0	0	0
2-Heptacosanone	0	0	0	0	0.31
2-Hexadecene, 3,7,11,15-tetramethyl-, [R-[R*,R*-(E)]]-	1.67	0.47	0.84	1.3	1.77
2-Hexyldodecyl butyrate	0	0.44	0	0	0
2-Hydroxy-1,2,5,5,6,7exo-hexamethyl-4-oxo-3-oxabicyclo[4.1.0]heptane	0	0	0	0.27	0

2-Hydroxy-3,5,5-trimethyl-cyclohex-2-enone	0.58	0	0	0	0
2-Isopropyl-5-methyl-6-oxabicyclo[3.1.0]hexane-1-carboxaldehyde	0.27	0	0	0	0
2-Methyl-6-propylpyridine	1.05	0	0	0	0
2-methyltetracosane	0.35	0	0	0	0
2-Naphthalenamine, 1,2,3,4-tetrahydro-N-methyl-1-(2-methyl-1-propenyl)-, trans-	0	0.21	0	0	0
2-Nonadecanone	0.24	0	1.99	0	0
2-Pentacosanone	0	0	0	0	0.79
2-Pentadecanone, 6,10,14-trimethyl-	0	0	0.37	0	1.05
2-Phthalimidoethyl 1-pyrrolidinecarbodithioate	0.49	0	0	0	0
2-Propen-1-amine, N,N-bis(1-methylethyl)-	1.47	0.23	1.04	0.92	0
2-Tridecanone	0.3	0	0	0	0.24
3-(2-Methyl-propenyl)-1H-indene	0.22	0	0	0	0
3,11-Diazabicyclo[4.4.1]undecan-4-one, 11-methyl-	0	0	0.22	0	0
3,3,5,5-Tetramethylcyclohexanol	0	0	0	0	0.51
3,6-Diisopropylpiperazin-2,5-dione	0.47	0	0	0	0
3-Diethylamino-1-(3-nitro-phenyl)-pyrrolidine-2,5-dione	0.23	0	0	0	0
3-Heptanol, 6-methyl-	0.61	0	0	0	0
3-Heptylthiophene	0	0	0	0	0.35
3-Hexen-1-ol, 2,5-dimethyl-, formate,(Z)-	0.21	0	0	0	0
3-Methyl-2-(3,7,11-trimethyldodecyl) furan	0.25	0	0	0	0
3-Methyl-2-(3,7,11-trimethyldodecyl)thiophene	0.23	0	0	0	0.4
3-Methyl-4-(phenylthio)-2-prop-2-enyl-2,5-dihydrothiophene 1,1-dioxide	0	0	0	0	0.41
3-Methylcarbazole	0	0.35	0	0	0
3-n-Hexadecylthiophene	0.27	0.26	0	0.5	0
3-Octanol	0	0	0	0.42	0
3-Oxabicyclo[3.3.0]octan-2-one, 7-methylene-4,4-dimethyl-	0	0	0.27	0	0
3-Phenylpropanoic acid, dodec-9-ynyl ester	0.49	0	0	0	0
3-Tetradecanynoic acid	0	0	0.37	0	0
4,4,6-Trimethyl-cyclohex-2-en-1-ol	0	0	0	0	0.38
4.alpha.,5-Cyclo-A-homo-5.alpha.-cholestan-6-one	0	0	0.44	0	0
4.alpha.,5-Cyclo-A-homo-5.alpha.-cholestan-6-one	0	0	0	0.5	0
4a-Methyl-1-methylene-1,2,3,4,4a,9,10,10a-octahydrophenanthrene	0	0		0.28	

4beta,5,6,12-Tetrahydrochrysene	0	0.44	0	0	0
4-Cyanobenzoic acid, 6-ethyl-3-octyl ester	1.26	0	0	0	0
4-Ethylbiphenyl	0	0.59	0	0	0
4H-Benz[de]anthracene, 5,6-dihydro-	0	0.28	0	0	0
4-Isopropylcyclohexanone	0	0	0	0	0.92
4-Methyl-2-(3,7,11-Trimethyldodecyl) thiophene	0	0	0	0.29	0
4-Methylheptanamide, N,N-dimethyl-	0	0	0	0.37	0
4-Phenylbut-3-ene-1-yne	0	0.39	0	0	0
4-Piperidinone, 2,2,6,6-tetramethyl-	1.65	0.91	0.68	0.6	0.38
5-(2-Propenylidene)-10,11-dihydro-5H-dibenzo[a,d]cycloheptene	0	0.26	0	0	0
5,10-Diethoxy-2,3,7,8-tetrahydro-1H,6H-dipyrrolo[1,2-a:1',2'-d]pyrazine	0.82	0	0	0.47	0
5,6-Dihydrochrysene	0	0.41	0	0	0
5,6-Epoxy-6-methyl-2-heptanone	0	0	0	0.2	0
5,8-Decadien-2-one, 5,9-dimethyl-, (E)-	0	0	0.77	0	0
5,8-Dimethyl-1,2,3,4-tetrahydro-1-naphthol	0	0.26	0	0	0
5,9-Dimethyl-2-(1-methylethyl)cyclodecane-1,4-dione	0.26	0	0	0	0
5-.alpha.-Androst-2-en-17-.beta.-ol, 17-methyl-	0	0	0.3	0.26	0
5.alpha.-Ergost-8(14)-ene	0	0.27	0.67	0	0
5-.beta.-cholestan-3.alpha.-ol, formate	0	0.28	0	0	0
5.beta.-Podocarpa-8,11,13-trien-16-oic acid, methyl ester	0	0.23	0.52	0.27	0.22
5-Benzyl-acenaphthylene	0	0.47	0	0	0
5-Chloropentanoic acid, 2-chlorophenyl ester	0.37	0	0	0	0
5H-Indeno[1,2-b]pyridine	0	0.46	0	0.33	0
5-Phenylvaleric acid	0.27	0	0	0	0
5-Pregnene, 3-acetoxy-20-[(N-acetyl-4-methylpyrrolidin-2-yl)carbonyl]-	0.49	0	0	0	0
5β-Cholestane	0	0	0	0.24	0
6,11-Undecadiene, 1-acetoxy-3,7-dimethyl-	0.38	0	0	0	0
6-Dodecanol acetate	0	0	0	0	1.14
6-Heptadecyne, 1-chloro-	0.22	0	0	0	0
6-Octadecenoic acid, methyl ester, (Z)-	0.3	0	0	0	0
7,12-Dihydro-2-methylbenz[a]anthracene	0	0.69	0	0	0
7b-Phenyl-2a,7b-dihydro-3H-cyclobuta[a]indene	0	0.25	0	0	0
7-ethyl-1,4-dimethylazulene	0	0.36	0	0	0
7-Octen-2-ol, 2,6-dimethyl-	0.21	0	0	0	0
7-Tridecanone, oxime	0	0	0.63	0	0

9,10[1',2']-Benzenoanthracene, 9,10-dihydro-	0	0.21	0	0	0
9,10-Dimethylanthracene	0	0	0	0.26	0
9,19-Cyclolanostan-3-ol, acetate, (3.beta.)-	0	0	0	0.34	0.5
9-Heptadecanone	0	0	0.81	0.49	0
9H-Pyrido[3,4-b]indole	1	0	0.4	0.26	0.44
9-Octadecenamide, (Z)-	1	0	0	0.81	0.79
9-Octadecenoic acid, (E)-	1.14	0	0	0	0
9-Octadecenoic acid, 1,2,3-propanetriyl ester, (E,E,E)-	0.2	0	0	0	0
9-Tricosene, (Z)-	0	0.3	0.24	0.62	0
Acetamide, N-(3-methylphenyl)-2-phenyl-	0.41	0	0	0	0
Acetic acid, 3,7,11,15-tetramethyl-hexadecyl ester	0	0	0.59	0.34	0.69
Acetic acid, 3-hydroxy-7-isopropenyl-1,4a-dimethyl-2,3,4,4a,5,6,7,8-octahydronaphthalen-2-yl ester	0	0	0	0.29	0
Anthracene	0	0.41	0	0.39	0
Anthracene, 2-ethyl-	0	0.25	0	0	0
Anthracene, 2-methyl-	0	0	0	0.4	0
Anthracene, 9-(2-propenyl)-	0	0.38	0	0	0
Azepan-2-one	0	0.69	0	0	0
Aziridine, 1,2-diisopropyl-3-methyl-, trans-	0.23	0	0.49	0	0
Bacteriochlorophyll-c-stearyl	0	0	0	0	0.23
Barbituric acid, 5-allyl-5-(2-hydroxyallyl)-	0	0	0	0	0.28
Benz(a)anthracene, 12-ethyl-7-methyl-	0	0.23	0	0	0
Benz[a]anthracene, 7,12-dimethyl-	0	0.31	0	0	0
Benz[a]anthracene, 7-methyl-	0	0.3	0	0	0
Benzenamine, N,4-dimethyl-	0	0	0.48	0	0
Benzene, (2,3-dimethyldecyl)-	0	0	0.28	0	0
Benzene, (2-methyl-1-butenyl)-	0	0.23	0	0	0
Benzene, 1,1'-(1,2-ethenediyl)bis[2-methyl-	0	0.22	0	0	0
Benzene, 1,1'-(1,3-propanediyl)bis-	0.32	0.45	0	0	0.22
Benzene, 1,2-bis(9-borabicyclo[3.3.1]non-9-yloxymethyl)-	0	0	0	0.26	0
Benzene, 1-isocyano-2-methyl-	0.35	0	0	0	0
Benzene, 1-tert-butyl-4-cyclopropylmethyl-	0.45	0	0	0	0
Benzene, decyl-	0	0	0	0.2	0
Benzene, dodecyl-	0	0	0	0.21	0.24
Benzenepropanenitrile	1.4	0	0.4	0.32	1.05
Benzofuro[3.2-d]pyrimidin-4(3H)-one	0.73	0	0.21	0	0.3
Benzoic acid, 2,5-dimethyl-, (2,4-dimethylphenyl)methyl ester	0	0	0	0.2	0

Benzoic acid, diphenylmethyl ester	0	0.67	0	0	0
Benzonitrile, 2,4,6-trimethyl-	1.46	0	0	0	0
Benzonitrile, 4-(1-methylethyl)-	0	0	0	0.46	0
Benzothiazole, 2-phenyl-	0	0.43	0	0	0
Benzyl nitrile	0	0	0	0	0.28
Bicyclo[3.1.0]hexan-3-ol, 4-methylene-1-(1-methylethyl)-, [1S-(1.alpha.,3.beta.,5.alpha.)]-	0	0	0.23		0.43
Bicyclo[4.4.1]undeca-1,3,5,7,9-pentaene	0	0.71	0	0	0
Biphenyl	0.28	0.45	0	0	0
Bis(2-ethylhexyl) phthalate	0.39	0.3	0.4	0.51	0.46
Bis(dodecanamido)methane	0	0	0.31	0	0
Bufa-20,22-dienolide, 3-(acetyloxy)-14,15-epoxy-16-hydroxy-, (3.beta.,5.beta.,15.beta.,16.beta.)-	0	0	0.61	0	0
Butan-2-one, 4-(2,2-dimethyltetrahydrofuran-3-yl)-, semicarbazone	0	0	0	0	0.21
Cetene	0	0	0	0	0.3
Cholest-14-ene, (5.alpha.)-	0	0.4	0	0	0
Cholest-24-ene, (5.alpha.,20.xi.)-	0	0.26	0	0	0
Cholest-2-ene	0	0.31	0	0.9	0.52
Cholest-3-ene, (5.beta.)-	0		0.85		0.76
Cholest-4-ene	0	0.92	0.35	1.05	0.24
Cholest-7-ene, (5.alpha.,14.beta.)-	0	0	0.73	0	0
Cholestan-3-ol, (3.alpha.,5.beta.)-	0	0	0.35	0.2	0.29
Cyclohexanecarboxaldehyde, 3,3-dimethyl-5-oxo-	0.3	0	0	0	0
Cyclohexanepropanol, .alpha.,2,2,6-tetramethyl-	0.29	0	0	0	0
Cyclohexene, 4-(1,5-dimethyl-1,4-hexadienyl)-1-methyl-	0	0.27	0	0	0
Cycloprop[a]indene, 1,1a,6,6a-tetrahydro-	0	0.59	0	0	0
Cyclopropane, 1-methyl-1-(2-methylpropyl)-2-nonyl-	0	0	0	0	0.22
Cyclotetradecane	0	0	0.32	0	0
Decane, 1,1'-oxybis-	0.38	0	0	0	0
Decane, 1-iodo-	0.22	0	0	0	0
Decanoic acid, 3-methyl-	0	0	0	0.36	0
Decanoic acid, pyrrolidide	0	0	0.38	0	0
Dibenz(a,h)anthracene, 7,14-dihydro-	0	0.25	0	0	0
Dibutyl phthalate	0.23	0	0	0.56	0
Diethyl Phthalate	0.43	0	0	0	0
Docosanamide	0	0	1.29	0	0
Dodecane	0	0.24	0.55	0	0.56
Dodecane, 2,6,10-trimethyl-	0	0	0	0	0.24

Dodecane, 2-methyl-	0	0	0.25	0	0
Dodecane, 4-methyl-	0.49	0	0	0	0
Dodecanenitrile	0.61	0	0.49	0	0.25
Dodecanoic acid	0	0	0	0	0.22
Dodecanoic acid, methyl ester	0	0	0.24	0	0
Dotriacontane	0.27	0.37	0	0	0
Eicosane	1.07	1.31	2.41	1.79	2.43
Eicosanoic acid, 2-hydroxyethyl ester	0.4	0	0	0	0
Ethanone, 1-[2-methyl-5-(1-methylethenyl)cyclopentyl]-, (1.alpha.,2.alpha.,5.beta.)-	0.42	0	0	0.2	0
Ethyl 14-methyl-hexadecanoate	0	0	0	1.07	0
Ethyl 2,2-dimethyl-3-(2-methylprop-1-enyl)cyclopropane-1-carboxylate	0	0.27	0	0	0
Ethyl 3α,7α,12α-trihydroxy-5β-cholan-24-oate	0	0	0	0	0.43
Ethyl 5-amino-1-methylpyrazole-4-carboxylate	0.24	0	0	0	0
Fucose, 2,3,4,5-tetraacetate, L-	0	0	0	0.21	0
Glycine, N-butoxycarbonyl-, ethyl ester	0	0	0	0.44	0
Heptadecane	0	1.13	0	0.66	0
Heptadecanenitrile	0.49	2.08	1.58	1.75	1.43
Heptadecanoic acid, 16-methyl-, methyl ester	0.21	0	0	0	0.3
Heptadecanoic acid, methyl ester	0	0	0.54	0.41	0.66
Hexacontane	0	0	0.36	0	0.89
Hexadecanamide	1.35	0.43	0.75		1.04
Hexadecane	0	0.81	1.6		1.04
Hexadecanenitrile	1.6	0	3.36	2.95	0.96
Hexadecanoic acid, 15-methyl-, methyl ester	0	0	0.41	0	0.7
Hexadecanoic acid, 2-hydroxyethyl ester	0	0	0	0	0.6
Hexadecanoic acid, methyl ester	0	0	0.22	0	0
Hexanohydrazide, 2-butyl-2-hydroxy-N2-(3-phenylpropenylideno)-	0	0.42	0	0	0
Hexanoic acid, morpholide	0	0	0.34	0.53	0.27
Hexatriacontane	0	0.35	0	0	0
Indeno[2,1-a]indene, 5,10-dihydro-	0	0.47	0	0	0
Indole	0	0	0	0	0.21
Indolizine	0.8	0	0	0	0
Indoxazene, 3-undecyl-	0	0	0.54	0.41	0
i-Propyl 11,12-methylene-octadecanoate	0	0	0.26	0	0
Isoheptadecanol	0	0	0.24	0	0
Isoindole-1,3-dione	0.63	0	0	0	0
Isoxazole, 5-chloro-3-(2-phenylethyl)-	0.24	0	0	0	0

l-(+)-Ascorbic acid 2,6-dihexadecanoate	5.05	0	1.81	3.47	0.46
L-Arginine, N2-[(phenylmethoxy)carbonyl]-	0	0	0.33	0	0
L-Glutamine, N2-[(phenylmethoxy)carbonyl]-	0	0	0.67	0	0
Lithocholic acid, methyl ester, methyl ether	0	0	0	0.57	0.57
m-[4-Phenyl-1-piperazinyl]phenol	0.26	0	0	0	0
Methanone, (4-methylphenyl)phenyl-	0.28	0	0	0	0
Methoxycarbonyl isothiocyanate	0	0	0.77	0	0
Methyl 13-methyltetradecanoate	0	0	0	0.27	0
Methyl 18-methylnonadecanoate	0	0	0.33	0.31	0.22
Methyl 3-methyl-pentadecanoate	0	0	0	0.37	0
Methyl stearate	0	0.22	1.54	1.14	1.16
Methyl tetradecanoate	0	0	0	0.33	0.31
N,N'-Dibutylidene-hydrazine	0.36	0	0	0	0.63
N,N-Diethyloctadecanamide	0	0	0	0	0
N,N-Dimethyldecanamide	0.3	0	0.34	0	0
N,N-Dimethyldodecanamide	0.22	0	0	0.53	0
Naphthalene, 1,2,3,4-tetrahydro-1,1,6-trimethyl-	0.25	0	0	0	0
Naphthalene, 1,2,3,4-tetramethyl-	0	0.69	0	0	0
Naphthalene, 1,3-dimethyl-	0	2.62		0.24	0
Naphthalene, 1,4,6-trimethyl-	0	0	0	0.2	0
Naphthalene, 1,4-dimethyl-	0	0	0	0.49	0
Naphthalene, 1,5-dimethyl-	0.42	1.61	0	0	0
Naphthalene, 1,6,7-trimethyl-	0	0.98	0.23	0	0
Naphthalene, 1,6-dimethyl-4-(1-methylethyl)-	0	0.23	0	0	0
Naphthalene, 1,8-dimethyl-	0	0.67	0	0	0
Naphthalene, 1-ethyl-	0	0	0.2	0	0
Naphthalene, 1-methyl-7-(1-methylethyl)-	0	0.79	0	0	0
Naphthalene, 1-phenyl-	0	0.43	0	0	0
Naphthalene, 1-propyl-	0	0.62	0	0	0
Naphthalene, 2,3,6-trimethyl-	0	1.92	1.08	0	0
Naphthalene, 2,3-dimethyl-	0	0.81	0	0	0
Naphthalene, 2,6-dimethyl-	0	0	0.48	0	0
Naphthalene, 2-methyl-	0.29	0	0.76	0	0
Naphthalene, 2-phenyl-	0.35	0.59	0.22	0	0
Naphthalene, decahydro-1,1,4a-trimethyl-6-methylene-5-(3-methylene-4-pentenyl)-, [4aS-(4a.alpha.,5.alpha.,8a.beta.)]-	0	0.32	0	0	0
N-Decanoylmorpholine	0	0	0.36	0	0.31
n-Hexadecanoic acid	0	0	3.5	0	3.88

N-Methyl-6-[4-methylphenyl]-1,2,4,5-tetrazinamine	0	0	0.39	0	
N-Methyldodecanamide	0.62	0.29	0.67	1.12	0.62
N-n-Butylphthalimide	0.55	0	0	0	0
n-Nonadecanol-1	0	0	0	0.25	0
N-n-Propylphthalimide	0.28	0	0	0	0
n-Octyl guanidine	0	0	0.21	0	0
Nonadecanamide	0	0	0	0.28	1.12
Nonadecanenitrile	0.41	0	0.44	1.27	0.55
Nonane, 5-methyl-5-propyl-	0	0	0.23	0	0
Nopyl acetate	0	0	0	0	0.25
Norharmane, N-methyl-	0	0	0.22	0	0
n-Pentadecanol	0	0	1.9	0.8	1.85
Octacosanol	0	0	0	0	0.44
Octadecan-4-one	0	0	0.37	0.58	0.25
Octadecanamide	0.25	0.25	2.21	0.97	1.75
Octadecanamide, N-butyl-	0	0	0.48	0	0
Octadecane	0	0	0	0	0.3
Octadecane, 3-ethyl-5-(2-ethylbutyl)-	0	0	0	0.82	0
Octadecanenitrile	0	0	0.76	2.19	1.47
Octadecanoic acid	0.37	0	0	4.12	1.46
Octadecanoic acid, 10-oxo-, methyl ester	0	0	0.3	0	0
Octadecanoic acid, 17-methyl-, methyl ester	0	0	0	0.55	0
Octadecanoic acid, 2-(2-hydroxyethoxy)ethyl ester	0	0	0.7	0	0
Octadecanoic acid, 2-methylpropyl ester	0	0	0	0	0.25
Octadecanoic acid, 2-propenyl ester	0.37	0.21	0	0	0
Octanamide, N,N-dimethyl-	0	0.26	0	0	0.36
o-Dodecylphenol	0	0	0.29	0	0
Oleanitrile	1.29	0	0.41	0.48	0
Oleic Acid	0.83	0	0	0	0.36
Oleylamine	0	0.23	0	0	0
Oxalic acid, 2-phenylethyl tetradecyl ester	0	0	0.28	0	0.25
Oxalic acid, 2-phenylethyl tetradecyl ester	0	0	0	0	0
Oxalic acid, hexadecyl 2-phenylethyl ester	0	0	0.37	0	0
Oxirane, hexadecyl-		0	0	0.4	0
p-Cresol	1.2	0.21	0	0.76	0.59
p-Decylphenol	0	0	0.27	0	0
Pentadecane	0.48	0	0	0	0
Pentadecane, 1-methoxy-13-methyl-	0	0.22	0	0	0
Pentadecane, 2,6,10,14-tetramethyl-	0.26	0.31	0	0	0
Pentadecanenitrile	0	0	0	0.2	0

Pentadecanenitrile, 15-bromo-	0.25	0	0	0	0
Pentadecanoic acid, 14-methyl-, methyl ester	0	0	1.39	0.67	0.47
Pentadecanoic acid, methyl ester	0	0	0.44	0	0.22
Perylene	0	0.33	0	0	0
Phenanthrene	0	0.42	0	0	0
Phenanthrene, 1-methyl-	0	0.83	0	0	0
Phenanthrene, 2,3,5-trimethyl-	0	0.43	0.43	0	0
Phenanthrene, 2,5-dimethyl-	0	0.6	0	0	0
Phenanthrene, 3,4,5,6-tetramethyl-	0	0.47	0	0	0
Phenanthrene, 4,5-dimethyl-	0	0.4	0	0	0
Phenanthrene, 4,5-dimethyl-	0	0	0.5	0	0
Phenol, 2,4-dimethyl-	0.84	0	0	0	0
Phenol, 2,5-dimethyl-	0	0	0	0.2	0
Phenol, 2-methyl-	0.25	0.53	0	0	0
Phenol, 3,4-dimethyl-	0	0.23	0	0	0
Phenol, 3-methyl-	0.4	1.7	0	0	0
Phenol, 4-ethyl-	1.41	0	0	0.49	0
Phenol, 4-ethyl-2-methoxy-	0	0	0.26	0	0
Phenylhydrazine, 3-isopropoxy-	0.23	0	0	0	0
Phthalic acid, 2-cyclohexylethyl butyl ester	0.64	0	0	0	0
Phytol, acetate	0.99	0	0.29	0.56	1.01
Piperazine-3,5-dione, 1-tetradecanoyl-	0.29	0	0	0	0
Piperidin-4-one, 1-ethyl-2,3-dimethyl-	0.79	0	0	0	0
Propanol-1, 2-methyl-2-(.alpha.-naphthyl)-	0.2	0	0	0	0
Pyrene, 1,3-dimethyl-	0	0.32	0	0	0
Pyrene, 1-methyl-	0	0.56	0	0	0
Pyrene, 4,5,9,10-tetrahydro-	0	0.32	0	0	0
Pyrimido[1,2-a]azepine, 2,3,4,6,7,8,9,10-octahydro-	0.39	0	0	0	0
Pyrrolidine, 1-(1-pentenyl)-	0.4	0	0	0	0
Pyrrolo[1,2-a]pyrazine-1,4-dione, hexahydro-3-(2-methylpropyl)-	1.01	0	0	0	0
Quinoline	0	1.22	0	0	0
Quinoline, 2,4-dimethyl-, 1-oxide	0.31	0	0	0	0
Semioxamazide	0	0	0.24	0	0
Stigmasta-4,22-diene	0	0.28	1.07	1.09	0.28
Stigmastane	0	0.41	0.21	0	0.2
Succinic acid, 2-decyl octadecyl ester	0	0	0	0	0.29
Succinic acid, monoamide, N-methyl-N-phenyl, tetradecyl ester	0	0	0	0	0.22
Tetracosane	0	0	0.3	1.37	1.18
Tetracyclo[5.3.0.0<2,6>.0<3,10>]deca-4,8-diene	0	1.2	0	0	0

Tetradecanamide	0.7	0	1.39	1.21	1.9
Tetradecane	0.33	0	0	0	0.36
Tetradecanenitrile	0.39	0.76	0.72	1.03	0.71
Tetradecanoic acid	0.4	0	0	0	0
Tetrapentacontane	0	1.12	0	0.67	0.84
trans-2-Decen-1-ol, pentafluoropropionate	0.21	0	0	0	0
trans-2-Dodecenoic acid	0	0	0	0	0.47
Tridecane, 3-methylene-	0.59	0	0	0	0
Tridecanoic acid, 12-methyl-, methyl ester	0	0	0.82	0	0
Tridecanoic acid, pyrrolidide	0	0	0.51	0	0
Triphenylene, 1-methyl-	0	0.22	0	0	0
Undecanenitrile	0	0	0	0.2	0
Undecanenitrile, 11-mercapto-	0	0	0	0	0.34
Z,Z-4,16-Octadecadien-1-ol acetate	0	0	0.54	0.39	0

REFERENCES

Abnisa, F., Wan Daud, W.M.A., 2014. A review on co-pyrolysis of biomass: An optional technique to obtain a high-grade pyrolysis oil. Energy Convers. Manag. 87, 71–85. https://doi.org/10.1016/j.enconman.2014.07.007

Agarwalla, A., Mishra, S., Mohanty, K., 2022. Treatment and recycle of harvested microalgal effluent using powdered activated carbon for reducing water footprint and enhancing biofuel production under a biorefinery model. Bioresour. Technol. 360, 127598. https://doi.org/10.1016/j.biortech.2022.127598

Alalam, S., Ben-Souilah, F., Lessard, M.H., Chamberland, J., Perreault, V., Pouliot, Y., Labrie, S., Doyen, A., 2021. Characterization of Chemical and Bacterial Compositions of Dairy Wastewaters. Dairy 2, 179–190. https://doi.org/10.3390/dairy2020016

Aljabri, H., Das, P., Khan, S., AbdulQuadir, M., Thaher, M., Hawari, A.H., Al-Shamary, N.M., 2022. A study to investigate the energy recovery potential from different macromolecules of a low-lipid marine Tetraselmis sp. biomass through HTL process. Renew. Energy 189, 78–89. https://doi.org/10.1016/j.renene.2022.02.100

Anastasakis, K., Biller, P., Madsen, R.B., Glasius, M., Johannsen, I., 2018. Continuous Hydrothermal Liquefaction of Biomass in a Novel Pilot Plant with Heat Recovery and Hydraulic Oscillation. Energies 11, 1–23. https://doi.org/10.3390/en11102695

Anastasakis, K., Ross, A.B., Jones, J.M., 2011. Pyrolysis behaviour of the main carbohydrates of brown macro-algae. Fuel 90, 598–607. https://doi.org/10.1016/j.fuel.2010.09.023

Annavelink, B., Chaves, L.G., van Ree, R., Gursel, I.V., 2022. IEA Bioenergy Task 42 Biorefining in a circular economy: Global biorefinery status report 2022, IEA Bioenergy.

APHA, 1998. Standard methods for the examination of water and wastewater, 20th edition. Am. Public Heal. Assoc. Washington, DC, USA. https://doi.org/10.2105/SMWW.2882.216

Aravind, S., Kumar, P.S., Kumar, N.S., Siddarth, N., 2020. Conversion of green algal biomass into bioenergy by pyrolysis. A review. Environ. Chem. Lett. 18, 829–849. https://doi.org/10.1007/s10311-020-00990-2

Arif, M., Li, Y., El-Dalatony, M.M., Zhang, C., Li, X., Salama, E.S., 2021. A complete characterization of microalgal biomass through FTIR/TGA/CHNS analysis: An approach for biofuel generation and nutrients removal. Renew. Energy 163, 1973–1982. https://doi.org/10.1016/j.renene.2020.10.066

Arora, K., Kaur, P., Kumar, P., Singh, A., Patel, S.K.S., Li, X., Yang, Y.H., Bhatia, S.K., Kulshrestha, S., 2021. Valorization of Wastewater Resources Into Biofuel and Value-Added Products Using Microalgal System. Front. Energy Res. 9, 1–25. https://doi.org/10.3389/fenrg.2021.646571

Arumugam, M., Goh, C.K., Zainal, Z., Triwahyono, S., Lee, A.F., Wilson, K., Taufiq-yap, Y.H., 2021. Hierarchical hzsm-5 for catalytic cracking of oleic acid to biofuels. Nanomaterials 11, 1–11. https://doi.org/10.3390/nano11030747

Asghari, F.S., Yoshida, H., 2006. Acid-catalyzed production of 5-hydroxymethyl furfural from D-fructose in subcritical water. Ind. Eng. Chem. Res. 45, 2163–2173. https://doi.org/10.1021/ie051088y

Audu, M., Wang, H., Arellano, D., Cheng, F., Dehghanizadeh, M., Jarvis, J.M., Yan, J., Brewer, C.E., Jena, U., 2021. Ash-pretreatment and hydrothermal liquefaction of filamentous algae grown on dairy wastewater. Algal Res. 57, 102282. https://doi.org/10.1016/j.algal.2021.102282

Ayub, H.M.U., Ahmed, A., Lam, S.S., Lee, J., Show, P.L., Park, Y.K., 2022. Sustainable valorization of algae biomass via thermochemical processing route: An overview. Bioresour. Technol. https://doi.org/10.1016/j.biortech.2021.126399

Aziz, S.Q., Ali, S.M., 2017. Characterization of municipal and dairy wastewaters with 30 quality parameters and potential wastewater treatment by biological trickling filters. Int. J. Green Energy 14, 1156–1162. https://doi.org/10.1080/15435075.2017.1370594

Balasubramanian, R., Sircar, A., Sivakumar, P., Anbarasu, K., 2018. Production of biodiesel from dairy wastewater sludge: A laboratory and pilot scale study. Egypt. J. Pet. 27, 939–943. https://doi.org/10.1016/j.ejpe.2018.02.002

Bhardwaj, A., Singh, J., Chaman, S., 2018. Molecular characterization of native dairy wastewater degrading microbes isolated from dairy industry effluent. Nat. Environ. Pollut. Technol. 17, 517–523.

Bhatia, S.K., Mehariya, S., Bhatia, R.K., Kumar, M., Pugazhendhi, A., Awasthi, M.K., Atabani, A.E., Kumar, G., Kim, W., Seo, S.O., Yang, Y.H., 2021. Wastewater based microalgal biorefinery for bioenergy production: Progress and challenges. Sci. Total Environ. https://doi.org/10.1016/j.scitotenv.2020.141599

Bian, J., Zhang, Q., Zhang, P., Feng, L., Li, C., 2017. Supported Fe2O3 nanoparticles for catalytic upgrading of microalgae hydrothermal liquefaction derived bio-oil. Catal. Today 293–294, 159–166. https://doi.org/10.1016/j.cattod.2017.02.008

Biller, P., Ross, A.B., 2011. Potential yields and properties of oil from the hydrothermal liquefaction of microalgae with different biochemical content. Bioresour. Technol. 102, 215–225. https://doi.org/10.1016/j.biortech.2010.06.028

Bisht, B., Gururani, P., Pandey, S., Kumar Jaiswal, K., Kumar, S., Vlaskin, M.S., Verma, M., Kim, H., Kumar, V., 2022. Multi-stage hydrothermal liquefaction modeling of sludge and microalgae biomass to increase bio-oil yield. Fuel 328, 125253. https://doi.org/10.1016/j.fuel.2022.125253

Bondurant, L.C., Obeid, W., Hatcher, P.G., 2023. Two-step hydrothermal liquefaction of Scenedesmus/Desmodesmus algae for the production of hydrocarbon-based fuels. Org. Geochem. 182, 104637. https://doi.org/10.1016/j.orggeochem.2023.104637

Borges, F.C., Xie, Q., Min, M., Muniz, L.A.Ô.R., Farenzena, M., Trierweiler, J.O., Chen, P., Ruan, R., 2014. Fast microwave-assisted pyrolysis of microalgae using microwave absorbent and HZSM-5 catalyst. Bioresour. Technol. 166, 518–526. https://doi.org/10.1016/j.biortech.2014.05.100

Brar, A., Kumar, M., Pareek, N., 2019. Comparative appraisal of biomass production, remediation, and bioenergy generation potential of microalgae in dairy wastewater. Front. Microbiol. 10, 1–12. https://doi.org/10.3389/fmicb.2019.00678

Brindhadevi, K., Anto, S., Rene, E.R., Sekar, M., Mathimani, T., Thuy Lan Chi, N., Pugazhendhi, A., 2021. Effect of reaction temperature on the conversion of algal biomass to bio-oil and biochar through pyrolysis and hydrothermal liquefaction. Fuel 285. https://doi.org/10.1016/j.fuel.2020.119106

Brunner, G., 2014. Reactions in Hydrothermal and Supercritical Water, Supercritical Fluid Science and Technology. https://doi.org/10.1016/B978-0-444-59413-6.00005-4

Campanella, A., Harold, M.P., 2012. Fast pyrolysis of microalgae in a falling solids reactor: Effects of process variables and zeolite catalysts. Biomass and Bioenergy 46, 218–232. https://doi.org/10.1016/j.biombioe.2012.08.023

Castello, D., Pedersen, T.H., Rosendahl, L.A., 2018. Continuous hydrothermal liquefaction of biomass: A critical review. Energies 11. https://doi.org/10.3390/en11113165

Central Pollution Control Board, 1986, 1986. General Standards for Discharge of Environmental Pollutants. Environ. Rules 2, 545–560.

Chaiwong, K., Kiatsiriroat, T., Vorayos, N., Thararax, C., 2013. Study of bio-oil and bio-char production from algae by slow pyrolysis. Biomass and Bioenergy 56, 600–606. https://doi.org/10.1016/j.biombioe.2013.05.035

Chakraborty, M., Miao, C., McDonald, A., Chen, S., 2012. Concomitant extraction of bio-oil and value added polysaccharides from Chlorella sorokiniana using a unique sequential hydrothermal extraction technology. Fuel 95, 63–70. https://doi.org/10.1016/j.fuel.2011.10.055

Chandra, R., Pradhan, S., Patel, A., Ghosh, U.K., 2021. An approach for dairy wastewater remediation using mixture of microalgae and biodiesel production for sustainable transportation. J. Environ. Manage. 297, 113210. https://doi.org/10.1016/j.jenvman.2021.113210

Chaudhuri, U.R., 2016. Fundamentals of Petroleum and Petrochemical Engineering. Fundam. Pet. Petrochemical Eng. https://doi.org/10.1201/b10486

Chen, Jie, Zhang, J., Pan, W., An, G., Deng, Y., Li, Y., Hu, Y., Xiao, Y., Liu, T., Leng, S., Chen, Jiefeng, Li, J., Peng, H., Leng, L., Zhou, W., 2022. A novel strategy to simultaneously enhance bio-oil yield and nutrient recovery in sequential hydrothermal liquefaction of high protein microalgae. Energy Convers. Manag. 255. https://doi.org/10.1016/j.enconman.2022.115330

Chen, W.T., Qian, W., Zhang, Y., Mazur, Z., Kuo, C.T., Scheppe, K., Schideman, L.C., Sharma, B.K., 2017. Effect of ash on hydrothermal liquefaction of high-ash content algal biomass. Algal Res. 25, 297–306. https://doi.org/10.1016/j.algal.2017.05.010

Chen, W.T., Zhang, Y., Zhang, J., Schideman, L., Yu, G., Zhang, P., Minarick, M., 2014. Co-liquefaction of swine manure and mixed-culture algal biomass from a wastewater

treatment system to produce bio-crude oil. Appl. Energy 128, 209–216. https://doi.org/10.1016/j.apenergy.2014.04.068

Chen, X., Li, Z., He, N., Zheng, Y., Li, H., Wang, H., Wang, Y., Lu, Y., Li, Q., Peng, Y., 2018. Nitrogen and phosphorus removal from anaerobically digested wastewater by microalgae cultured in a novel membrane photobioreactor. Biotechnol. Biofuels 11, 190. https://doi.org/10.1186/s13068-018-1190-0

Cheng, C.L., Lo, Y.C., Huang, K. Lou, Nagarajan, D., Chen, C.Y., Lee, D.J., Chang, J.S., 2022. Effect of pH on biomass production and carbohydrate accumulation of Chlorella vulgaris JSC-6 under autotrophic, mixotrophic, and photoheterotrophic cultivation. Bioresour. Technol. 351, 127021. https://doi.org/10.1016/j.biortech.2022.127021

Cheng, F., Cui, Z., Chen, L., Jarvis, J., Paz, N., Schaub, T., Nirmalakhandan, N., Brewer, C.E., 2017. Hydrothermal liquefaction of high- and low-lipid algae: Bio-crude oil chemistry. Appl. Energy 206, 278–292. https://doi.org/10.1016/j.apenergy.2017.08.105

Cheng, F., Cui, Z., Mallick, K., Nirmalakhandan, N., Brewer, C.E., 2018. Hydrothermal liquefaction of high- and low-lipid algae: Mass and energy balances. Bioresour. Technol. 258, 158–167. https://doi.org/10.1016/j.biortech.2018.02.100

Cheng, F., Mallick, K., Henkanatte Gedara, S.M., Jarvis, J.M., Schaub, T., Jena, U., Nirmalakhandan, N., Brewer, C.E., 2019. Hydrothermal liquefaction of Galdieria sulphuraria grown on municipal wastewater. Bioresour. Technol. 292, 121884. https://doi.org/10.1016/j.biortech.2019.121884

Chokshi, K., Pancha, I., Ghosh, A., Mishra, S., 2016. Microalgal biomass generation by phycoremediation of dairy industry wastewater: An integrated approach towards sustainable biofuel production. Bioresour. Technol. 221, 455–460. https://doi.org/10.1016/j.biortech.2016.09.070

Collard, F.-X., Wijeyekoon, S., Bennett, P., 2023. Commercial status of direct thermochemical liquefaction technologies. IEA Bioenergy Task 34.

Cui, Z., Greene, J.M., Cheng, F., Quinn, J.C., Jena, U., Brewer, C.E., 2020. Co-hydrothermal liquefaction of wastewater-grown algae and crude glycerol: A novel strategy of bio-crude oil-aqueous separation and techno-economic analysis for bio-crude oil recovery and upgrading. Algal Res. 51, 102077. https://doi.org/10.1016/j.algal.2020.102077

da Silva, T.L., Moniz, P., Silva, C., Reis, A., 2021. The role of heterotrophic microalgae in waste conversion to biofuels and bioproducts. Processes 9, 1–24. https://doi.org/10.3390/pr9071090

Danalewich, J.R., Papagiannis, T.G., Belyea, R.L., Tumbleson, M.E., Raskin, L., 1998. Characterization of dairy waste streams, current treatment practices, and potential for biological nutrient removal. Water Res. 32, 3555–3568. https://doi.org/10.1016/S0043-1354(98)00160-2

Dandamudi, K.P.R., Murdock, T., Lammers, P.J., Deng, S., Fini, E.H., 2021. Production of functionalized carbon from synergistic hydrothermal liquefaction of microalgae and swine manure. Resour. Conserv. Recycl. 170, 105564. https://doi.org/10.1016/j.resconrec.2021.105564

Daneshvar, E., Zarrinmehr, M.J., Koutra, E., Kornaros, M., Farhadian, O., Bhatnagar, A., 2019. Sequential cultivation of microalgae in raw and recycled dairy wastewater: Microalgal growth, wastewater treatment and biochemical composition. Bioresour. Technol. 273, 556–564. https://doi.org/10.1016/j.biortech.2018.11.059

de Andrade, F.P., De Farias Silva, C.E., dos Santos, J., Ribeiro, T.R.M., Medeiros, J.A., do Nascimento, M.A.A., Santos, G.K.S., dos Santos Carneiro, W., Almeida, R.M.R.G., de Oliveira, A.M.M., Feijó, F.M., da Silva Costa, M.M., de Andrade Lima, G.S., Ribeiro-Júnior, K.A.L., Tonholo, J., 2023. Dairy wastewater treatment by Tetradesmus sp. in open system: molecular identification and the effect of light intensity and organic load in the process. Energy, Ecol. Environ. 8, 356–369. https://doi.org/10.1007/s40974-023-00278-5

de Caprariis, B., Damizia, M., Tai, L., De Filippis, P., 2022. Hydrothermal Liquefaction of Biomass using Waste Material as Catalyst: Effect on the Bio-crude Yield and Quality. Chem. Eng. Trans. 92, 607–612. https://doi.org/10.3303/CET2292102

de Morais, M.G., Costa, J.A.V., 2007. Biofixation of carbon dioxide by Spirulina sp. and Scenedesmus obliquus cultivated in a three-stage serial tubular photobioreactor. J. Biotechnol. 129, 439–445. https://doi.org/10.1016/j.jbiotec.2007.01.009

Debiagi, P.E.A., Trinchera, M., Frassoldati, A., Faravelli, T., Vinu, R., Ranzi, E., 2017. Algae characterization and multistep pyrolysis mechanism. J. Anal. Appl. Pyrolysis 128, 423–436. https://doi.org/10.1016/j.jaap.2017.08.007

Demirbas, M.F., 2009. Biorefineries for biofuel upgrading: A critical review. Appl. Energy 86, S151–S161. https://doi.org/10.1016/j.apenergy.2009.04.043

Denton, F., Halsnæs, K., Akimoto, K., Burch, S., Morejon, C.D., Farias, F., Jupesta, J., Shareef, A., Schweizer-Ries, P., Teng, F., Zusman, E., Castaneda, A., Larsen, M.A.D., Some, S., 2022. Accelerating the transition in the context of sustainable development. In Climate Change 2022: Mitigation of Climate Change, the Working Group III contribution. https://doi.org/https://doi.org/10.1017/9781009157926

Department of Biotechnology MoS&T GOI, 2021. ANNUAL REPORT 2021-21. https://doi.org/https://dbtindia.gov.in/sites/default/files/Final%20English%20Annual%20Report%202021.pdf

Deshavath, N.N., Goud, V. V., Veeranki, V.D., 2021. Liquefaction of lignocellulosic biomass through biochemical conversion pathway: A strategic approach to achieve an industrial titer of bioethanol. Fuel 287. https://doi.org/10.1016/j.fuel.2020.119545

Divya Kuravi, S., Venkata Mohan, S., 2022. Mixotrophic cultivation of Monoraphidium sp. In dairy wastewater using Flat-Panel photobioreactor and photosynthetic performance. Bioresour. Technol. 348, 126671. https://doi.org/10.1016/j.biortech.2021.126671

Divya Kuravi, S., Venkata Mohan, S., 2021. Mixotrophic cultivation of isolated Messastrum gracile SVMIICT7: Photosynthetic response and product profiling. Bioresour. Technol. 341, 125798. https://doi.org/10.1016/j.biortech.2021.125798

Dong, X., Chen, Z., Xue, S., Zhang, J., Zhou, J., Liu, Y., Xu, Y., Liu, Z., 2013. Catalytic pyrolysis of microalga Chlorella pyrenoidosa for production of ethylene, propylene and butene. RSC Adv. 3, 25780–25787. https://doi.org/10.1039/c3ra43850c

Du, Z., Ma, X., Li, Y., Chen, P., Liu, Y., Lin, X., Lei, H., Ruan, R., 2013. Production of aromatic hydrocarbons by catalytic pyrolysis of microalgae with zeolites: Catalyst screening in a pyroprobe. Bioresour. Technol. 139, 397–401. https://doi.org/10.1016/j.biortech.2013.04.053

Dubois, M., Gilles, K.A., Hamilton, J.K., Rebers, P.A., Smith, F., 1956. Colorimetric Method for Determination of Sugars and Related Substances.

Ebadian, M., McMillan, J.D., Saddler, J. (John) N., Dyk, S. van, 2019. Commercializing Conventional and Advanced Transport Biofuels from Biomass and other Renewable

Feedstocks, Implementation Agendas: 2018-2019 Update Compare and Contrast Transport Biofuels Policies. IEA Bioenergy Task 39 256.

Ekka, B., Mieriņa, I., Juhna, T., Turks, M., Kokina, K., 2022. Quantification of different fatty acids in raw dairy wastewater. Clean. Eng. Technol. 7, 1–6. https://doi.org/10.1016/j.clet.2022.100430

Ellersdorfer, M., 2020. Hydrothermal co-liquefaction of chlorella vulgaris with food processing residues, green waste and sewage sludge. Biomass and Bioenergy 142, 105796. https://doi.org/10.1016/j.biombioe.2020.105796

Fan, Y., Hornung, U., Dahmen, N., Kruse, A., 2018. Hydrothermal liquefaction of protein-containing biomass: study of model compounds for Maillard reactions. Biomass Convers. Biorefinery 8, 909–923. https://doi.org/10.1007/s13399-018-0340-8

Fan, Y., Prestigiacomo, C., Gong, M., Tietz, T., Hornung, U., Dahmen, N., 2022. Comparative investigation on the value-added products obtained from continuous and batch hydrothermal liquefaction of sewage sludge. Front. Environ. Sci. 10, 1–13. https://doi.org/10.3389/fenvs.2022.996353

Faried, M., Samer, M., Abdelsalam, E., Yousef, R.S., Attia, Y.A., Ali, A.S., 2017. Biodiesel production from microalgae: Processes, technologies and recent advancements. Renew. Sustain. Energy Rev. 79, 893–913. https://doi.org/10.1016/j.rser.2017.05.199

Fu, Y., Guo, Y., Zhang, K., 2016. Effect of Three Different Catalysts (KCl, CaO, and Fe2O3) on the Reactivity and Mechanism of Low-Rank Coal Pyrolysis. Energy and Fuels 30, 2428–2433. https://doi.org/10.1021/acs.energyfuels.5b02720

Gai, C., Li, Y., Peng, N., Fan, A., Liu, Z., 2015a. Co-liquefaction of microalgae and lignocellulosic biomass in subcritical water. Bioresour. Technol. 185, 240–245. https://doi.org/10.1016/j.biortech.2015.03.015

Gai, C., Zhang, Y., Chen, W., Dong, Y., 2014. Energy and nutrient recovery efficiencies in biocrude oil produced via hydrothermal liquefaction of Chlorella pyrenoidosa. RSC Adv. 16958–16967. https://doi.org/10.1039/c3ra46607h

Gai, C., Zhang, Y., Chen, W.T., Zhang, P., Dong, Y., 2015b. An investigation of reaction pathways of hydrothermal liquefaction using Chlorella pyrenoidosa and Spirulina platensis. Energy Convers. Manag. 96, 330–339.

https://doi.org/10.1016/j.enconman.2015.02.056

Gao, K., 2021. Approaches and involved principles to control pH/pCO2 stability in algal cultures. J. Appl. Phycol. 33, 3497–3505. https://doi.org/10.1007/s10811-021-02585-y

Garcha, S., Verma, N., Brar, S.K., 2016. Isolation, characterization and identification of microorganisms from unorganized dairy sector wastewater and sludge samples and evaluation of their biodegradability. Water Resour. Ind. 16, 19–28. https://doi.org/10.1016/j.wri.2016.10.002

Garcia Alba, L., Torri, C., Samorì, C., Van Der Spek, J., Fabbri, D., Kersten, S.R.A., Brilman, D.W.F., 2012. Hydrothermal treatment (HTT) of microalgae: Evaluation of the process as conversion method in an algae biorefinery concept. Energy and Fuels 26, 642–657. https://doi.org/10.1021/ef201415s

Gatamaneni Loganathan, B., Orsat, V., Lefsrud, M., Wu, B. Sen, 2020. A comprehensive study on the effect of light quality imparted by light-emitting diodes (LEDs) on the physiological and biochemical properties of the microalgal consortia of Chlorella variabilis and Scenedesmus obliquus cultivated in dairy wastewater. Bioprocess Biosyst. Eng. 43, 1445–1455. https://doi.org/10.1007/s00449-020-02338-0

Gebremedhin, M., Mishra, S., Mohanty, K., 2018. Augmentation of native microalgae based biofuel production through statistical optimization of campus sewage wastewater as low-cost growth media. J. Environ. Chem. Eng. 6, 6623–6632. https://doi.org/10.1016/j.jece.2018.08.061

GOI, 2023. Government of India Ministry of Statistics and Programme Implementation National Statistical Office https://www.mospi.gov.in/. Mospi.

Gong, X., Zhang, B., Zhang, Y., Huang, Y., Xu, M., 2014. Investigation on pyrolysis of low lipid microalgae chlorella vulgaris and dunaliella salina. Energy and Fuels 28, 95–103. https://doi.org/10.1021/ef401500z

Gu et al., 2020a. Comparative techno-economic analysis of algal biofuel production via hydrothermal liquefaction: One stage versus two stages. Appl. Energy 259, 114115. https://doi.org/10.1016/j.apenergy.2019.114115

Gu, Martinez-Fernandez, J.S., Pang, N., Fu, X., Chen, S., 2020b. Recent development of hydrothermal liquefaction for algal biorefinery. Renew. Sustain. Energy Rev.

https://doi.org/10.1016/j.rser.2020.109707

Guo, S., Wu, Y., Wang, Z., Yin, X., 2024. Effect of electrolytic zero-valent iron activated sodium hypochlorite on sludge dewatering performance. Water Sci. Technol. 89, 989–1002. https://doi.org/10.2166/wst.2024.037

Gupta, S., Pawar, S.B., Pandey, R.A., 2019. Current practices and challenges in using microalgae for treatment of nutrient rich wastewater from agro-based industries. Sci. Total Environ. https://doi.org/10.1016/j.scitotenv.2019.06.115

He, S., Zhao, M., Wang, J., Cheng, Z., Yan, B., Chen, G., 2020. Hydrothermal liquefaction of low-lipid algae Nannochloropsis sp . and Sargassum sp .: Effect of feedstock composition and temperature. Sci. Total Environ. 712, 135677. https://doi.org/10.1016/j.scitotenv.2019.135677

He, Z., Xu, D., Liu, L., Wang, Y., Wang, S., Guo, Y., Jing, Z., 2018. Product characterization of multi-temperature steps of hydrothermal liquefaction of Chlorella microalgae. Algal Res. 33, 8–15. https://doi.org/10.1016/j.algal.2018.04.013

Hemalatha, M., Sravan, J.S., Min, B., Venkata Mohan, S., 2019. Microalgae-biorefinery with cascading resource recovery design associated to dairy wastewater treatment. Bioresour. Technol. 284, 424–429. https://doi.org/10.1016/j.biortech.2019.03.106

Hietala, D.C., Godwin, C.M., Cardinale, B.J., Savage, P.E., 2019. The independent and coupled effects of feedstock characteristics and reaction conditions on biocrude production by hydrothermal liquefaction. Appl. Energy 235, 714–728. https://doi.org/10.1016/j.apenergy.2018.10.120

Hietala, D.C., Savage, P.E., 2021. A molecular, elemental, and multiphase kinetic model for the hydrothermal liquefaction of microalgae. Chem. Eng. J. 407, 127007. https://doi.org/10.1016/j.cej.2020.127007

Ho, D.P., Ngo, H.H., Guo, W., 2014. A mini review on renewable sources for biofuel. Bioresour. Technol. 169, 742–749. https://doi.org/10.1016/j.biortech.2014.07.022

Hossain, M.R., Khalekuzzaman, M., Bin Kabir, S., Islam, M.B., Bari, Q.H., 2022. Production of light oil-prone biocrude through co-hydrothermal liquefaction of wastewater-grown microalgae and peat. J. Anal. Appl. Pyrolysis 161, 105423. https://doi.org/10.1016/j.jaap.2021.105423

Hu, Y., Gong, M., Feng, S., Xu, C. (Charles), Bassi, A., 2019. A review of recent developments of pre-treatment technologies and hydrothermal liquefaction of microalgae for bio-crude oil production. Renew. Sustain. Energy Rev. 101, 476–492. https://doi.org/10.1016/j.rser.2018.11.037

Huang, P.P., Yang, R.F., Qiu, T.Q., Fan, X.D., 2013. Solubility of fatty acids in subcritical water. J. Supercrit. Fluids 81, 221–225. https://doi.org/10.1016/j.supflu.2013.06.009

Huang, Z., Wufuer, A., Wang, Y., Dai, L., 2018a. Hydrothermal liquefaction of pretreated low-lipid microalgae for the production of bio-oil with low heteroatom content. Process Biochem. 69, 136–143. https://doi.org/10.1016/j.procbio.2018.03.018

Huang, Z., Wufuer, A., Wang, Y., Dai, L., 2018b. Hydrothermal liquefaction of pretreated low-lipid microalgae for the production of bio-oil with low heteroatom content. Process Biochem. 69, 136–143. https://doi.org/10.1016/j.procbio.2018.03.018

Huck, W., 2023. Transforming our world: the 2030 Agenda for Sustainable Development. Sustain. Dev. Goals. https://doi.org/10.5040/9781509934058.0025

IEA Bioenergy, 2018. Success Stories of Advanced Biofuels for Transport - RELIANCE CATALYTIC HYDROTHERMAL LIQUEFACTION.

Islam, M.B., Khalekuzzaman, M., Kabir, S. Bin, Hossain, M.R., Alam, M.A., 2022. Substituting microalgal biomass with faecal sludge for high-quality biocrude production through co-liquefaction: A sustainable biorefinery approach. Fuel Process. Technol. 225, 107063. https://doi.org/10.1016/j.fuproc.2021.107063

Jamal F, 2023. Accelerating Biodiesel Blending in India. New Delhi: The Energy and Resources Institute.

Jazrawi, C., Biller, P., He, Y., Montoya, A., Ross, A.B., Maschmeyer, T., Haynes, B.S., 2015. Two-stage hydrothermal liquefaction of a high-protein microalga. Algal Res. 8, 15–22. https://doi.org/10.1016/j.algal.2014.12.010

Jena, U., Das, K.C., 2011. Comparative evaluation of thermochemical liquefaction and pyrolysis for bio-oil production from microalgae. Energy and Fuels 25, 5472–5482. https://doi.org/10.1021/ef201373m

Jensen, C.U., Rodriguez Guerrero, J.K., Karatzos, S., Olofsson, G., Iversen, S.B., 2017. Fundamentals of Hydrofaction^{TM}: Renewable crude oil from woody biomass. Biomass

Convers. Biorefinery 7, 495–509. https://doi.org/10.1007/s13399-017-0248-8

Keszei, E., 2012. Phase Equilibria, Handbook of Crystal Growth. https://doi.org/10.1007/978-3-642-19864-9

Khodaparasti, M.S., Khorasani, R., Tavakoli, O., Khodadadi, A.A., 2023. Optimal Co-pyrolysis of municipal sewage sludge and microalgae Chlorella Vulgaris: Products characterization, synergistic effects, mechanism, and reaction pathways. J. Clean. Prod. 390, 135991. https://doi.org/10.1016/j.jclepro.2023.135991

Kim, H.S., Park, W.K., Lee, B., Seon, G., Suh, W.I., Moon, M., Chang, Y.K., 2019. Optimization of heterotrophic cultivation of Chlorella sp. HS2 using screening, statistical assessment, and validation. Sci. Rep. 9, 1–13. https://doi.org/10.1038/s41598-019-55854-9

Kiran, B., Venkata Mohan, S., 2022. Phycoremediation potential of Tetradesmus sp. SVMIICT4 in treating dairy wastewater using Flat-Panel photobioreactor. Bioresour. Technol. 345. https://doi.org/10.1016/j.biortech.2021.126446

Kiran, B., Venkata Mohan, S., 2021. Photosynthetic transients in Chlorella sorokiniana during phycoremediation of dairy wastewater under distinct light intensities. Bioresour. Technol. 340. https://doi.org/10.1016/j.biortech.2021.125593

Kothari, R., Pathak, V. V., Kumar, V., Singh, D.P., 2012. Experimental study for growth potential of unicellular alga Chlorella pyrenoidosa on dairy waste water: An integrated approach for treatment and biofuel production. Bioresour. Technol. 116, 466–470. https://doi.org/10.1016/j.biortech.2012.03.121

Kothari, R., Prasad, R., Kumar, V., Singh, D.P., 2013. Production of biodiesel from microalgae Chlamydomonas polypyrenoideum grown on dairy industry wastewater. Bioresour. Technol. 144, 499–503. https://doi.org/10.1016/j.biortech.2013.06.116

Krishnan, R.Y., Manikandan, S., Subbaiya, R., Kim, W., Karmegam, N., Govarthanan, M., 2022. Advanced thermochemical conversion of algal biomass to liquid and gaseous biofuels: A comprehensive review of recent advances. Sustain. Energy Technol. Assessments 52, 102211. https://doi.org/10.1016/j.seta.2022.102211

Kruse, A., Dinjus, E., 2007. Hot compressed water as reaction medium and reactant. Properties and synthesis reactions. J. Supercrit. Fluids 39, 362–380.

https://doi.org/10.1016/j.supflu.2006.03.016

Kumar, A., Jamro, I.A., Wang, J., Ullah, A., Kumari, L., Cui, B., Tao, J., Guo, D., Yan, B., Aborisade, M.A., Oba, B.T., Nkinahamira, F., Ndagijimana, P., Laghari, A.A., Rong, H., Chen, G., 2024. Co-pyrolysis of microalgae residue and sewage sludge: An in-depth characterization of kinetics, drivers, and gas-oil-char behaviors. J. Anal. Appl. Pyrolysis 179, 106438. https://doi.org/10.1016/j.jaap.2024.106438

Kumar, A.K., Sharma, S., Shah, E., Parikh, B.S., Patel, A., Dixit, G., Gupta, S., Divecha, J.M., 2019. Cultivation of Ascochloris sp. ADW007-enriched microalga in raw dairy wastewater for enhanced biomass and lipid productivity. Int. J. Environ. Sci. Technol. 16, 943–954. https://doi.org/10.1007/s13762-018-1712-0

Kuppens, T., Cornelissen, T., Carleer, R., Yperman, J., Schreurs, S., Jans, M., Thewys, T., 2010. Economic assessment of flash co-pyrolysis of short rotation coppice and biopolymer waste streams. J. Environ. Manage. 91, 2736–2747. https://doi.org/10.1016/j.jenvman.2010.07.022

Kuravi, D., Venkata Mohan, S., 2022. Mixotrophic cultivation of Monoraphidium sp. In dairy wastewater using Flat-Panel photobioreactor and photosynthetic performance. Bioresour. Technol. 348, 126671. https://doi.org/10.1016/j.biortech.2021.126671

Kusmayadi, A., Huang, C.Y., Kit Leong, Y., Lu, P.H., Yen, H.W., Lee, D.J., Chang, J.S., 2023. Integration of microalgae cultivation and anaerobic co-digestion with dairy wastewater to enhance bioenergy and biochemicals production. Bioresour. Technol. 376, 128858. https://doi.org/10.1016/j.biortech.2023.128858

Lam, T.P., Lee, T.-M., Chen, C.-Y., Chang, J.-S., 2018. Strategies to control biological contaminants during microalgal cultivation in open ponds. Bioresour. Technol. 252, 180–187. https://doi.org/10.1016/j.biortech.2017.12.088

Lavanya, M., Meenakshisundaram, A., Renganathan, S., Chinnasamy, S., Lewis, D.M., Nallasivam, J., Bhaskar, S., 2016. Hydrothermal liquefaction of freshwater and marine algal biomass: A novel approach to produce distillate fuel fractions through blending and co-processing of biocrude with petrocrude. Bioresour. Technol. 203, 228–235. https://doi.org/10.1016/j.biortech.2015.12.013

Law, X.N., Cheah, W.Y., Chew, K.W., Ibrahim, M.F., Park, Y.K., Ho, S.H., Show, P.L.,

2022. Microalgal-based biochar in wastewater remediation: Its synthesis, characterization and applications. Environ. Res. 204. https://doi.org/10.1016/j.envres.2021.111966

Lazar, P., Mach, R., Otyepka, M., 2019. Spectroscopic Fingerprints of Graphitic, Pyrrolic, Pyridinic, and Chemisorbed Nitrogen in N-Doped Graphene. J. Phys. Chem. C 123, 10695–10702. https://doi.org/10.1021/acs.jpcc.9b02163

Lee, X.J., Ong, H.C., Gan, Y.Y., Chen, W.H., Mahlia, T.M.I., 2020. State of art review on conventional and advanced pyrolysis of macroalgae and microalgae for biochar, bio-oil and bio-syngas production. Energy Convers. Manag. 210, 112707. https://doi.org/10.1016/j.enconman.2020.112707

Li, F., Srivatsa, S.C., Bhattacharya, S., 2019. A review on catalytic pyrolysis of microalgae to high-quality bio-oil with low oxygeneous and nitrogenous compounds. Renew. Sustain. Energy Rev. 108, 481–497. https://doi.org/10.1016/j.rser.2019.03.026

Li, H., Liu, Z., Zhang, Y., Li, B., Lu, H., Duan, N., Liu, M., Zhu, Z., Si, B., 2014. Conversion efficiency and oil quality of low-lipid high-protein and high-lipid low-protein microalgae via hydrothermal liquefaction. Bioresour. Technol. 154, 322–329. https://doi.org/10.1016/j.biortech.2013.12.074

Li, P., Chen, X., Wang, X., Shao, J., Lin, G., Yang, H., Yang, Q., Chen, H., 2017. Catalytic Upgrading of Fast Pyrolysis Products with Fe-, Zr-, and Co-Modified Zeolites Based on Pyrolyzer-GC/MS Analysis. Energy and Fuels 31, 3979–3986. https://doi.org/10.1021/acs.energyfuels.6b03105

Lin, Y., Song, G., Ling, H., Ge, J., Ping, W., 2021. Isolation of a high-ammonium-tolerant Monoraphidium sp. and evaluation of its potential for biodiesel production. Process Biochem. 111, 297–304. https://doi.org/10.1016/j.procbio.2021.11.010

Liu, H., Chen, Y., Yang, H., Hu, J., Wang, X., Chen, H., 2022. Evolution pathway of nitrogen in hydrothermal liquefaction polygeneration of Spirulina as the typical high-protein microalgae. Algal Res. 66, 102759. https://doi.org/10.1016/j.algal.2022.102759

Liu, J., Zhao, W., Yang, S., Hu, B., Xu, M., Ma, S., Lu, Q., 2021. Formation mechanism of NO x precursors during the pyrolysis of 2 , 5-diketopiperazine based on experimental and theoretical study. Sci. Total Environ. 801, 149663.

https://doi.org/10.1016/j.scitotenv.2021.149663

López Barreiro, D., Zamalloa, C., Boon, N., Vyverman, W., Ronsse, F., Brilman, W., Prins, W., 2013. Influence of strain-specific parameters on hydrothermal liquefaction of microalgae. Bioresour. Technol. 146, 463–471. https://doi.org/10.1016/j.biortech.2013.07.123

Lowry, O.H., Rosebrough, N.J., Farr, A.L., Randall, R.J., 1951. PROTEIN MEASUREMENT WITH THE FOLIN PHENOL REAGENT*.

Lu, J., Watson, J., Liu, Z., Wu, Y., 2022. Elemental migration and transformation during hydrothermal liquefaction of biomass. J. Hazard. Mater. 423, 126961. https://doi.org/10.1016/j.jhazmat.2021.126961

Lu, W., Wang, Z., Wang, X., Yuan, Z., 2015. Cultivation of Chlorella sp. using raw diary wastewater for nutrient removal and biodiesel production: Characteristics comparison of indoor bench-scale and outdoor pilot-scale cultures. Bioresour. Technol. 192, 382–388. https://doi.org/10.1016/j.biortech.2015.05.094

Maddi, B., Viamajala, S., Varanasi, S., 2011. Comparative study of pyrolysis of algal biomass from natural lake blooms with lignocellulosic biomass. Bioresour. Technol. 102, 11018–11026. https://doi.org/10.1016/j.biortech.2011.09.055

Magyar, T., Németh, B., Tamás, J., Nagy, P.T., 2024. Improvement of N and P ratio for enhanced biomass productivity and sustainable cultivation of Chlorella vulgaris microalgae. Heliyon 10. https://doi.org/10.1016/j.heliyon.2023.e23238

Mahata, C., Mishra, S., Dhar, S., Ray, S., Mohanty, K., Das, D., 2023. Utilization of dark fermentation effluent for algal cultivation in a modified airlift photobioreactor for biomass and biocrude production. J. Environ. Manage. 330, 117121. https://doi.org/10.1016/j.jenvman.2022.117121

Markou, G., Georgakakis, D., 2011. Cultivation of filamentous cyanobacteria (blue-green algae) in agro-industrial wastes and wastewaters: A review. Appl. Energy 88, 3389–3401. https://doi.org/10.1016/j.apenergy.2010.12.042

Mathanker, A., Das, S., Pudasainee, D., Khan, M., Kumar, A., Gupta, R., 2021. A review of hydrothermal liquefaction of biomass for biofuels production with a special focus on the effect of process parameters, co-solvents and extraction solvents. Energies.

https://doi.org/10.3390/en14164916

Mathimani, T., Baldinelli, A., Rajendran, K., Prabakar, D., Matheswaran, M., Pieter van Leeuwen, R., Pugazhendhi, A., 2019. Review on cultivation and thermochemical conversion of microalgae to fuels and chemicals: Process evaluation and knowledge gaps. J. Clean. Prod. 208, 1053–1064. https://doi.org/10.1016/j.jclepro.2018.10.096

Melo, J.M., Telles, T.S., Ribeiro, M.R., de Carvalho Junior, O., Andrade, D.S., 2022. Chlorella sorokiniana as bioremediator of wastewater: Nutrient removal, biomass production, and potential profit. Bioresour. Technol. Reports 17, 100933. https://doi.org/10.1016/j.biteb.2021.100933

Merabtene, M., Kacimi, L., Clastres, P., 2019. Elaboration of geopolymer binders from poor kaolin and dam sludge waste. Heliyon 5, e01938. https://doi.org/10.1016/j.heliyon.2019.e01938

Miao, C., Chakraborty, M., Chen, S., 2012. Impact of reaction conditions on the simultaneous production of polysaccharides and bio-oil from heterotrophically grown Chlorella sorokiniana by a unique sequential hydrothermal liquefaction process. Bioresour. Technol. 110, 617–627. https://doi.org/10.1016/j.biortech.2012.01.047

Miao, X., Wu, Q., 2004. High yield bio-oil production from fast pyrolysis by metabolic controlling of Chlorella protothecoides. J. Biotechnol. 110, 85–93. https://doi.org/10.1016/j.jbiotec.2004.01.013

Minowa, T., Inoue, S., Hanaoka, T., Matsumura, Y., 2004. Hydrothermal Reaction of Glucose and Glycine as Model Compounds of Biomass 798, 794–798.

Mishra, S., Mohanty, K., 2020. Co-HTL of domestic sewage sludge and wastewater treatment derived microalgal biomass – An integrated biorefinery approach for sustainable biocrude production. Energy Convers. Manag. 204. https://doi.org/10.1016/j.enconman.2019.112312

Mishra, S., Mohanty, K., 2019. Comprehensive characterization of microalgal isolates and lipid-extracted biomass as zero-waste bioenergy feedstock: An integrated bioremediation and biorefinery approach. Bioresour. Technol. 273, 177–184. https://doi.org/10.1016/j.biortech.2018.11.012

Moazezi, M.R., Bayat, H., Tavakoli, O., Hallajisani, A., 2022. Hydrothermal liquefaction of

Chlorella vulgaris and catalytic upgrading of product: Effect of process parameter on bio-oil yield and thermodynamics modeling. Fuel 318, 123595. https://doi.org/10.1016/j.fuel.2022.123595

Mohanty, S.S., Mohanty, K., 2023a. Valorization of Chlorella thermophila biomass cultivated in dairy wastewater for biopesticide production against bacterial rice blight: a circular biorefinery approach. BMC Plant Biol. 23, 1–14. https://doi.org/10.1186/s12870-023-04579-z

Mohanty, S.S., Mohanty, K., 2023b. Production of a wide spectrum biopesticide from Monoraphidium sp. KMC4 grown in simulated dairy wastewater. Bioresour. Technol. 128815. https://doi.org/10.1016/j.biortech.2023.128815

Mohsenpour, S.F., Hennige, S., Willoughby, N., Adeloye, A., Gutierrez, T., 2021. Integrating micro-algae into wastewater treatment: A review. Sci. Total Environ. 752, 142168. https://doi.org/10.1016/j.scitotenv.2020.142168

Möller, M., Nilges, P., Harnisch, F., Schröder, U., 2011. Subcritical water as reaction environment: Fundamentals of hydrothermal biomass transformation. ChemSusChem 4, 566–579. https://doi.org/10.1002/cssc.201000341

Moser, L., Penke, C., Batteiger, V., 2021. An in-depth process model for FUEL production via hydrothermal liquefaction and catalytic hydrotreating. Processes 9. https://doi.org/10.3390/pr9071172

Motamedi, P., Cadien, K., 2014. XPS analysis of AlN thin films deposited by plasma enhanced atomic layer deposition. Appl. Surf. Sci. 315, 104–109. https://doi.org/10.1016/j.apsusc.2014.07.105

Moulder, J.F., Stickle, W.F., Sobol, P.E., Bomben, K.D., 1992. Handbook of X-ray photoelectron spectroscopy, Perkin-Elmer Corporation. https://doi.org/10.1002/0470014229.ch22

Mustapha, S.I., Isa, Y.M., 2024. Co-pyrolysis of microalgae and sewage sludge over ZnO/MgO/CeO2/HZSM-5 catalyst for energy and water treatment application. J. Environ. Chem. Eng. 12, 114955. https://doi.org/10.1016/j.jece.2024.114955

Mustapha, S.I., Rawat, I., Bux, F., Isa, Y.M., 2021. Catalytic pyrolysis of nutrient-stressed Scenedesmus obliquus microalgae for high-quality bio-oil production. Renew. Energy

179, 2036–2047. https://doi.org/10.1016/j.renene.2021.08.043

Naaz, F., Bhattacharya, A., Pant, K.K., Malik, A., 2019. Investigations on energy efficiency of biomethane/biocrude production from pilot scale wastewater grown algal biomass. Appl. Energy 254. https://doi.org/10.1016/j.apenergy.2019.113656

Najafabadi, M., Jalilian, F., Vossoughi, M., Pazuki, G., 2015. Effect of various carbon sources on biomass and lipid production of Chlorella vulgaris during nutrient sufficient and nitrogen starvation conditions. Bioresour. Technol. 180, 311–317. https://doi.org/10.1016/j.biortech.2014.12.076

Nelson, M., Zhu, L., Thiel, A., Wu, Y., Guan, M., Minty, J., Wang, H.Y., Lin, X.N., 2013. Microbial utilization of aqueous co-products from hydrothermal liquefaction of microalgae Nannochloropsis oculata. Bioresour. Technol. 136, 522–528. https://doi.org/10.1016/j.biortech.2013.03.074

Niu, Q., Du, X., Li, K., Ghysels, S., Lu, Q., Prins, W., Ronsse, F., 2024. Coke formation and mineral accumulation on HZSM-5/Al2O3 catalysts during in-situ catalytic fast pyrolysis of microalgae over multiple regeneration cycles. J. Anal. Appl. Pyrolysis 182, 106701. https://doi.org/10.1016/j.jaap.2024.106701

Nugroho, Y.K., Zhu, L., 2019. An integration of algal biofuel production planning, scheduling, and order-based inventory distribution control systems. Biofuels, Bioprod. Biorefining 13, 920–935. https://doi.org/10.1002/bbb.1982

O'Donoghue, C.S.J.N., Fomo, G., Nyokong, T., 2016. Electrode Modification Using Alkyne Manganese Phthalocyanine and Click Chemistry for Electrocatalysis. Electroanalysis 28, 3019–3027. https://doi.org/10.1002/elan.201600379

Obeid, R., Lewis, D.M., Smith, N., Hall, T., van Eyk, P., 2020. Reaction kinetics and characterisation of species in renewable crude from hydrothermal liquefaction of monomers to represent organic fractions of biomass feedstocks. Chem. Eng. J. 389, 124397. https://doi.org/10.1016/j.cej.2020.124397

Obeid, R., Smith, N., Lewis, D.M., Hall, T., van Eyk, P., 2021. A kinetic model for the hydrothermal liquefaction of microalgae, sewage sludge and pine wood with product characterisation of renewable crude. Chem. Eng. J. 428, 131228. https://doi.org/10.1016/j.cej.2021.131228

Ocampo, E., Beltrán, V. V., Gómez, E.A., Ríos, L.A., Ocampo, D., 2023. Hydrothermal liquefaction process: Review and trends. Curr. Res. Green Sustain. Chem. 7, 100382. https://doi.org/10.1016/j.crgsc.2023.100382

Omar, B.M., Bita, M., Louafi, I., Djouadi, A., 2018. Esterification process catalyzed by ZSM-5 zeolite synthesized via modified hydrothermal method. MethodsX 5, 277–282. https://doi.org/10.1016/j.mex.2018.03.004

Osman, A.I., Chen, L., Yang, M., Msigwa, G., Farghali, M., Fawzy, S., Rooney, D.W., Yap, P.S., 2023. Cost, environmental impact, and resilience of renewable energy under a changing climate: a review. Environ. Chem. Lett. 21, 741–764. https://doi.org/10.1007/s10311-022-01532-8

Pan, P., Hu, C., Yang, W., Li, Y., Dong, L., Zhu, L., Tong, D., Qing, R., Fan, Y., 2010. The direct pyrolysis and catalytic pyrolysis of Nannochloropsis sp. residue for renewable bio-oils. Bioresour. Technol. 101, 4593–4599. https://doi.org/10.1016/j.biortech.2010.01.070

Pandey, A., Srivastava, S., Kumar, S., 2019. Sequential optimization of essential nutrients addition in simulated dairy effluent for improved Scenedesmus sp ASK22 growth, lipid production and nutrients removal. Biomass and Bioenergy 128, 105319. https://doi.org/10.1016/j.biombioe.2019.105319

Pang, N., Bergeron, A.D., Gu, X., Fu, X., Dong, T., Yao, Y., Chen, S., 2020. Recycling of Nutrients from Dairy Wastewater by Extremophilic Microalgae with High Ammonia Tolerance. Environ. Sci. Technol. 54, 15366–15375. https://doi.org/10.1021/acs.est.0c02833

Patel, A.K., Joun, J., Sim, S.J., 2020. A sustainable mixotrophic microalgae cultivation from dairy wastes for carbon credit, bioremediation and lucrative biofuels. Bioresour. Technol. 313. https://doi.org/10.1016/j.biortech.2020.123681

Peng, X., Ma, X., Lin, Y., Guo, Z., Hu, S., Ning, X., Cao, Y., Zhang, Y., 2015. Co-pyrolysis between microalgae and textile dyeing sludge by TG-FTIR: Kinetics and products. Energy Convers. Manag. 100, 391–402. https://doi.org/10.1016/j.enconman.2015.05.025

Penhaul Smith, J.K., Hughes, A.D., McEvoy, L., Day, J.G., 2020. Tailoring of the biochemical profiles of microalgae by employing mixotrophic cultivation. Bioresour.

Technol. Reports 9, 100321. https://doi.org/10.1016/j.biteb.2019.100321

Peterson, A.A., Vogel, F., Lachance, R.P., Fröling, M., Antal, M.J., Tester, J.W., 2008. Thermochemical biofuel production in hydrothermal media: A review of sub- and supercritical water technologies. Energy Environ. Sci. 1, 32–65. https://doi.org/10.1039/b810100k

Ponnusamy, V.K., Nagappan, S., Bhosale, R.R., Lay, C.H., Duc Nguyen, D., Pugazhendhi, A., Chang, S.W., Kumar, G., 2020. Review on sustainable production of biochar through hydrothermal liquefaction: Physico-chemical properties and applications. Bioresour. Technol. 310, 123414. https://doi.org/10.1016/j.biortech.2020.123414

Posadas, E., Alcántara, C., García-Encina, P.A., Gouveia, L., Guieysse, B., Norvill, Z., Acién, F.G., Markou, G., Congestri, R., Koreiviene, J., Muñoz, R., 2017. Microalgae cultivation in wastewater, in: Microalgae-Based Biofuels and Bioproducts. Elsevier, pp. 67–91. https://doi.org/10.1016/B978-0-08-101023-5.00003-0

Posmanik, R., Martinez, C.M., Cantero-Tubilla, B., Cantero, D.A., Sills, D.L., Cocero, M.J., Tester, J.W., 2018. Acid and Alkali Catalyzed Hydrothermal Liquefaction of Dairy Manure Digestate and Food Waste. ACS Sustain. Chem. Eng. 6, 2724–2732. https://doi.org/10.1021/acssuschemeng.7b04359

Prestigiacomo, C., Costa, P., Pinto, F., Schiavo, B., Siragusa, A., Scialdone, O., Galia, A., 2019. Sewage sludge as cheap alternative to microalgae as feedstock of catalytic hydrothermal liquefaction processes. J. Supercrit. Fluids 143, 251–258. https://doi.org/10.1016/j.supflu.2018.08.019

Pritchard, D.W., Hurd, C.L., Beardall, J., Hepburn, C.D., 2015. Restricted use of nitrate and a strong preference for ammonium reflects the nitrogen ecophysiology of a light-limited red alga. J. Phycol. 51, 277–287. https://doi.org/10.1111/jpy.12272

Pulungan, A.N., Goei, R., Kembaren, A., Nurfajriani, N., Sihombing, J.L., Gea, S., Wong, H.R., Hasibuan, M.I., Rahayu, R., Tok, A.I.Y., 2024. Two stages upgrading of bio-oil through esterification and hydrodeoxygenation reactions using Fe2O3-CoO supported catalyst. Biomass Convers. Biorefinery 14, 20655–20664. https://doi.org/10.1007/s13399-023-04237-2

Qasim, W., Mane, A. V., 2013. Characterization and treatment of selected food industrial

effluents by coagulation and adsorption techniques. Water Resour. Ind. 4, 1–12. https://doi.org/10.1016/j.wri.2013.09.005

Qi, P., Chang, G., Wang, H., Zhang, X., Guo, Q., 2018. Production of aromatic hydrocarbons by catalytic co-pyrolysis of microalgae and polypropylene using HZSM-5. J. Anal. Appl. Pyrolysis 136, 178–185. https://doi.org/10.1016/j.jaap.2018.10.007

Qin, L., Wang, Z., Sun, Y., Shu, Q., Feng, P., Zhu, L., Xu, J., Yuan, Z., 2016. Microalgae consortia cultivation in dairy wastewater to improve the potential of nutrient removal and biodiesel feedstock production. Environ. Sci. Pollut. Res. 23, 8379–8387. https://doi.org/10.1007/s11356-015-6004-3

Quann, R.J., Green, L.A., Tabak, S.A., Krambeck, F.J., 1988. Chemistry of olefin oligomerization over zsm-5 catalyst. Ind. Eng. Chem. Res. 27, 565–570. https://doi.org/10.1021/ie00076a006

Rahman, N.A.A., Fermoso, J., Sanna, A., 2018. Effect of Li-LSX-zeolite on the in-situ catalytic deoxygenation and denitrogenation of Isochrysis sp. microalgae pyrolysis vapours. Fuel Process. Technol. 173, 253–261. https://doi.org/10.1016/j.fuproc.2018.01.020

Ramírez-Romero, A., Martin, M., Boyer, A., Bolzoni, R., Matricon, L., Sassi, J.F., Steyer, J.P., Delrue, F., 2023. Microalgae adaptation as a strategy to recycle the aqueous phase from hydrothermal liquefaction. Bioresour. Technol. 371, 128631. https://doi.org/10.1016/j.biortech.2023.128631

Ratha, S.K., Renuka, N., Abunama, T., Rawat, I., Bux, F., 2022. Hydrothermal liquefaction of algal feedstocks: The effect of biomass characteristics and extraction solvents. Renew. Sustain. Energy Rev. 156, 111973. https://doi.org/10.1016/j.rser.2021.111973

Ravi Kiran, B., Singh, P., Kuravi, S.D., Mohanty, K., Venkata Mohan, S., 2024. Modulating cultivation regimes of Messastrum gracile SVMIICT7 for biomass productivity integrated with resource recovery via hydrothermal liquefaction. J. Environ. Manage. 356, 120458. https://doi.org/10.1016/j.jenvman.2024.120458

Ravi Kiran, B., Venkata Mohan, S., 2022. Phycoremediation potential of Tetradesmus sp. SVMIICT4 in treating dairy wastewater using Flat-Panel photobioreactor. Bioresour. Technol. 345, 126446. https://doi.org/10.1016/j.biortech.2021.126446

Ravichandran, S.R., Venkatachalam, C.D., Sengottian, M., Sekar, S., Kandasamy, S., Ramasamy Subramanian, K.P., Purushothaman, K., Lavanya Chandrasekaran, A., Narayanan, M., 2022. A review on hydrothermal liquefaction of algal biomass on process parameters, purification and applications. Fuel 313. https://doi.org/10.1016/j.fuel.2021.122679

Razzak, S.A., Khan, M., Irfan, F., Shah, M.A., Nawaz, A., Hossain, M.M., 2024. Catalytic co-pyrolysis and kinetic study of microalgae biomass with solid waste feedstock for sustainable biofuel production. J. Anal. Appl. Pyrolysis 183, 106755. https://doi.org/10.1016/j.jaap.2024.106755

Ronsse, F., van Hecke, S., Dickinson, D., Prins, W., 2013. Production and characterization of slow pyrolysis biochar: Influence of feedstock type and pyrolysis conditions. GCB Bioenergy 5, 104–115. https://doi.org/10.1111/gcbb.12018

Sahoo, A., Saini, K., Jindal, M., Bhaskar, T., Pant, K.K., 2021. Co-Hydrothermal Liquefaction of algal and lignocellulosic biomass: Status and perspectives. Bioresour. Technol. https://doi.org/10.1016/j.biortech.2021.125948

Sánchez-Bayo, A., Megía Hervás, I., Rodríguez, R., Morales, V., Bautista, L.F., Vicente, G., 2021. Biocrude from nannochloropsis gaditana by hydrothermal liquefaction: An experimental design approach. Appl. Sci. 11. https://doi.org/10.3390/app11104337

Sang, Y., Xing, A., Wang, C., Han, Z., Wu, Y., 2017. Near-graphite coke deposit on nano-HZSM-5 aggregates for methanol to propylene and butylene reaction. Catalysts 7. https://doi.org/10.3390/catal7060171

Sangon, S., Ratanavaraha, S., Ngamprasertsith, S., Prasassarakich, P., 2006. Coal liquefaction using supercritical toluene-tetralin mixture in a semi-continuous reactor. Fuel Process. Technol. 87, 201–207. https://doi.org/10.1016/j.fuproc.2005.07.007

Sanz-Luque, E., Chamizo-Ampudia, A., Llamas, A., Galvan, A., Fernandez, E., 2015. Understanding nitrate assimilation and its regulation in microalgae. Front. Plant Sci. 6. https://doi.org/10.3389/fpls.2015.00899

Satiada, G.B.D.A., Carpio, R.B., Guerrero, G.A.M., Detras, M.C.M., Bambase, M.E., 2024. Influence of alkali catalysts on product yield and Si-containing products from hydrothermal liquefaction of corn stover. Heliyon 10, e37520.

https://doi.org/10.1016/j.heliyon.2024.e37520

Sato, N., Quitain, A.T., Kang, K., Daimon, H., Fujie, K., 2004. Reaction kinetics of amino acid decomposition in high-temperature and high-pressure water. Ind. Eng. Chem. Res. 43, 3217–3222. https://doi.org/10.1021/ie020733n

Sawalha, H., Al-Jabari, M., Zahdeh, N., Aburayyan, D., Jbour, M., Abufarah, H., 2022. Characterization of wastewater from dairy industry in Palestine and its adsorption on biowaste. Desalin. Water Treat. 275, 278–283. https://doi.org/10.5004/dwt.2022.28744

Shakya, R., Adhikari, S., Mahadevan, R., Shanmugam, S.R., Nam, H., Hassan, E.B., Dempster, T.A., 2017. Influence of biochemical composition during hydrothermal liquefaction of algae on product yields and fuel properties. Bioresour. Technol. 243, 1112–1120. https://doi.org/10.1016/j.biortech.2017.07.046

Shen, W., He, S., Mu, M., Cao, B., Wang, S., Naqvi, S.R., Hanelt, D., Abomohra, A., 2024. A comprehensive review on the intricate processes involved in algae pyrolysis mechanism and possible migration of undesirable chemical elements. J. Anal. Appl. Pyrolysis 177, 106365. https://doi.org/10.1016/j.jaap.2024.106365

Shia, Y.P., Yu, B.Y., 2023. Development of a rigorous and generalized model on the hydrothermal liquefaction (HTL) process for bio-oil production. Process Saf. Environ. Prot. 171, 541–554. https://doi.org/10.1016/j.psep.2023.01.046

Shirazi, Y., Viamajala, S., Varanasi, S., 2020. In situ and Ex situ Catalytic Pyrolysis of Microalgae and Integration With Pyrolytic Fractionation. Front. Chem. 8, 1–12. https://doi.org/10.3389/fchem.2020.00786

Singh, P., Mohanty, K., 2025. Bio-Oil Production via Two-Stage and Direct Hydrothermal Liquefaction Process from High-Protein Monoraphidium sp . KMC4 : A Comparative Study of Both Processes and an Insight into the Reaction Pathway. Energy and Fuels 39, 10109–10720. https://doi.org/10.1021/acs.energyfuels.5c01061

Singh, P., Venkata Mohan, S., Mohanty, K., 2023. Dairy wastewater treatment using Monoraphidium sp. KMC4 and its potential as hydrothermal liquefaction feedstock. Bioresour. Technol. 376, 128877. https://doi.org/10.1016/j.biortech.2023.128877

Skoneczny, S., Tabiś, B., 2015. The method for steady states determination in tubular biofilm reactors. Chem. Eng. Sci. 137, 178–187. https://doi.org/10.1016/J.CES.2015.06.024

Smith, R.T., Bangert, K., Wilkinson, S.J., Gilmour, D.J., 2015. Synergistic carbon metabolism in a fast growing mixotrophic freshwater microalgal species Micractinium inermum. Biomass and Bioenergy 82, 73–86. https://doi.org/10.1016/j.biombioe.2015.04.023

Song, W., Guo, M., 2012. Quality variations of poultry litter biochar generated at different pyrolysis temperatures. J. Anal. Appl. Pyrolysis 94, 138–145. https://doi.org/10.1016/j.jaap.2011.11.018

SPRERI CENTRE OF EXCELLENCE, 2023. Annual Report 2022-23.

SundarRajan, P., Gopinath, K.P., Arun, J., GracePavithra, K., Adithya Joseph, A., Manasa, S., 2021. Insights into valuing the aqueous phase derived from hydrothermal liquefaction. Renew. Sustain. Energy Rev. https://doi.org/10.1016/j.rser.2021.111019

Suparmaniam, U., Lam, M.K., Uemura, Y., Lim, J.W., Lee, K.T., Shuit, S.H., 2019. Insights into the microalgae cultivation technology and harvesting process for biofuel production: A review. Renew. Sustain. Energy Rev. 115, 109361. https://doi.org/10.1016/j.rser.2019.109361

Swain, P., Tiwari, A., Pandey, A., 2020. Enhanced lipid production in Tetraselmis sp. by two stage process optimization using simulated dairy wastewater as feedstock. Biomass and Bioenergy 139, 105643. https://doi.org/10.1016/j.biombioe.2020.105643

Swetha, A., ShriVigneshwar, S., Gopinath, K.P., Sivaramakrishnan, R., Shanmuganathan, R., Arun, J., 2021. Review on hydrothermal liquefaction aqueous phase as a valuable resource for biofuels, bio-hydrogen and valuable bio-chemicals recovery. Chemosphere 283. https://doi.org/10.1016/j.chemosphere.2021.131248

Taghipour, A., Hornung, U., Ramirez, J.A., Brown, R.J., Rainey, T.J., 2021. Aqueous phase recycling in catalytic hydrothermal liquefaction for algal biomass and the effect on elemental accumulation and energy efficiency. J. Clean. Prod. 289. https://doi.org/10.1016/j.jclepro.2020.125582

Tan, X.B., Lam, M.K., Uemura, Y., Lim, J.W., Wong, C.Y., Lee, K.T., 2018. Cultivation of microalgae for biodiesel production: A review on upstream and downstream processing. Chinese J. Chem. Eng. 26, 17–30. https://doi.org/10.1016/j.cjche.2017.08.010

Tang, Z., Chen, W., Chen, Y., Hu, J., Yang, H., Chen, H., 2021. Preparation of low-nitrogen

and high-quality bio-oil from microalgae catalytic pyrolysis with zeolites and activated carbon. J. Anal. Appl. Pyrolysis 159, 105182. https://doi.org/10.1016/j.jaap.2021.105182

Thangalazhy-Gopakumar, S., Adhikari, S., Chattanathan, S.A., Gupta, R.B., 2012. Catalytic pyrolysis of green algae for hydrocarbon production using H +ZSM-5 catalyst. Bioresour. Technol. 118, 150–157. https://doi.org/10.1016/j.biortech.2012.05.080

Thriveni, T., Nam, S.Y., Ahn, J.W., Um, N. Il, 2014. Enhancement of arsenic removal efficiency from mining waste water by accelerated carbonation. IMPC 2014 - 27th Int. Miner. Process. Congr.

Ting, H., Haifeng, L., Shanshan, M., Zhang, Y., Zhidan, L., Na, D., 2017. Progress in microalgae cultivation photobioreactors and applications in wastewater treatment: A review. Int. J. Agric. Biol. Eng. 10, 1–29. https://doi.org/10.3965/j.ijabe.20171001.2705

Toor, S.S., Rosendahl, L., Rudolf, A., 2011. Hydrothermal liquefaction of biomass: A review of subcritical water technologies. Energy 36, 2328–2342. https://doi.org/10.1016/j.energy.2011.03.013

Torri, C., Fabbri, D., Garcia-Alba, L., Brilman, D.W.F., 2013. Upgrading of oils derived from hydrothermal treatment of microalgae by catalytic cracking over H-ZSM-5: A comparative Py-GC-MS study. J. Anal. Appl. Pyrolysis 101, 28–34. https://doi.org/10.1016/j.jaap.2013.03.001

Uematsu, M., Frank, E.U., 1980. Static Dielectric Constant of Water and Steam. J. Phys. Chem. Ref. Data 9, 1291–1306. https://doi.org/10.1063/1.555632

Usami, R., Fujii, K., Fushimi, C., 2020. Improvement of Bio-Oil and Nitrogen Recovery from Microalgae Using Two-Stage Hydrothermal Liquefaction with Solid Carbon and HCl Acid Catalysis. ACS Omega 5, 6684–6696. https://doi.org/10.1021/acsomega.9b04468

Vadlamudi, D.P., Pecchi, M., Sudibyo, H., Tester, J.W., 2024. Direct and Two-Stage Hydrothermal Liquefaction of Chicken Manure: Impact of Reaction Parameters on Biocrude Oil Upgradation. ACS Sustain. Chem. Eng. 12, 4300–4313. https://doi.org/10.1021/acssuschemeng.3c08579

Verheyen, V., Cruickshank, A., Wild, K., Heaven, M.W., McGee, R., Watkins, M., Nash, D.,

2011. Characterization of organic particulates present in milk factory process waters used for reuse along with aerobically digested effluent wastewater. Bioresour. Technol. 102, 2118–2125. https://doi.org/10.1016/j.biortech.2010.08.053

Vieira Costa, J.A., Cruz, C.G., Centeno da Rosa, A.P., 2021. Insights into the technology utilized to cultivate microalgae in dairy effluents. Biocatal. Agric. Biotechnol. 35, 102106. https://doi.org/10.1016/j.bcab.2021.102106

Vo, T.K., Kim, S.S., Ly, H.V., Lee, E.Y., Lee, C.G., Kim, J., 2017. A general reaction network and kinetic model of the hydrothermal liquefaction of microalgae Tetraselmis sp. Bioresour. Technol. 241, 610–619. https://doi.org/10.1016/j.biortech.2017.05.186

Vuppaladadiyam, A.K., Liu, H., Zhao, M., Soomro, A.F., Memon, M.Z., Dupont, V., 2019. Thermogravimetric and kinetic analysis to discern synergy during the co-pyrolysis of microalgae and swine manure digestate. Biotechnol. Biofuels 12, 1–18. https://doi.org/10.1186/s13068-019-1488-6

Wang, B., He, Z., Zhang, B., Duan, Y., 2021. Study on hydrothermal liquefaction of spirulina platensis using biochar based catalysts to produce bio-oil. Energy 230, 120733. https://doi.org/10.1016/j.energy.2021.120733

Wang, B., Lan, C.Q., Horsman, M., 2012. Closed photobioreactors for production of microalgal biomasses. Biotechnol. Adv. 30, 904–912. https://doi.org/10.1016/j.biotechadv.2012.01.019

Wang, J., Yu, H., Wei, Z., Li, Q., Xuan, W., Wei, Y., 2020. Additive-Mediated Selective Oxidation of Alcohols to Esters via Synergistic Effect Using Single Cation Cobalt Catalyst Stabilized with Inorganic Ligand. Research 2020. https://doi.org/10.34133/2020/3875920

Wang, K., Brown, R.C., 2013. Catalytic pyrolysis of microalgae for production of aromatics and ammonia. Green Chem. 15, 675–681. https://doi.org/10.1039/c3gc00031a

Wang, K., Johnston, P.A., Brown, R.C., 2015. Comparison of in-situ and ex-situ catalytic pyrolysis in a micro-reactor system. Bioresour. Technol. 173, 124–131. https://doi.org/10.1016/j.biortech.2014.09.097

Wang, K., Kim, K.H., Brown, R.C., 2014. Catalytic pyrolysis of individual components of lignocellulosic biomass. Green Chem. 16, 727–735. https://doi.org/10.1039/c3gc41288a

Wang, X., Zhao, B., Yang, X., 2016. Co-pyrolysis of microalgae and sewage sludge: Biocrude assessment and char yield prediction. Energy Convers. Manag. 117, 326–334. https://doi.org/10.1016/j.enconman.2016.03.013

Watanabe, M., Aizawa, Y., Iida, T., Aida, T.M., Levy, C., Sue, K., Inomata, H., 2005. Glucose reactions with acid and base catalysts in hot compressed water at 473 K. Carbohydr. Res. 340, 1925–1930. https://doi.org/10.1016/j.carres.2005.06.017

Watson, J., Wang, T., Si, B., Chen, W.T., Aierzhati, A., Zhang, Y., 2020. Valorization of hydrothermal liquefaction aqueous phase: pathways towards commercial viability. Prog. Energy Combust. Sci. https://doi.org/10.1016/j.pecs.2019.100819

Widiarti, N., Ni'mah, Y.L., Bahruji, H., Prasetyoko, D., 2019. Development of CaO from natural calcite as a heterogeneous base catalyst in the formation of biodiesel: Review. J. Renew. Mater. 7, 915–939. https://doi.org/10.32604/jrm.2019.07183

Wu, X., Cen, Q., Addy, M., Zheng, H., Luo, S., Liu, Y., Cheng, Y., Zhou, W., Chen, P., Ruan, R., 2019. A novel algal biofilm photobioreactor for efficient hog manure wastewater utilization and treatment. Bioresour. Technol. 292, 121925. https://doi.org/10.1016/j.biortech.2019.121925

Wu, Z., Yang, W., Li, Y., Yang, B., 2018. Co-pyrolysis behavior of microalgae biomass and low-quality coal: Products distributions, char-surface morphology, and synergistic effects. Bioresour. Technol. 255, 238–245. https://doi.org/10.1016/j.biortech.2018.01.141

Xia, C., Pathy, A., Paramasivan, B., Ganeshan, P., Dhamodharan, K., Juneja, A., Kumar, D., Brindhadevi, K., Kim, S.H., Rajendran, K., 2022. Comparative study of pyrolysis and hydrothermal liquefaction of microalgal species: Analysis of product yields with reaction temperature. Fuel 311, 121932. https://doi.org/10.1016/j.fuel.2021.121932

Xiao, X., Fang, P., Huang, J.H., Tang, Z.J., Chen, X.B., Wu, H.W., Cen, C.P., Tang, Z.X., 2019. Mechanistic study on NO reduction by sludge reburning in a pilot scale cement precalciner with different CO2 concentrations. RSC Adv. 9, 22863–22874. https://doi.org/10.1039/c9ra04065j

Xiaogang, H., Jalalah, M., Jingyuan, W., Zheng, Y., Li, X., Salama, E.S., 2022. Microalgal growth coupled with wastewater treatment in open and closed systems for advanced

biofuel generation. Biomass Convers. Biorefinery 12, 1939–1958. https://doi.org/10.1007/s13399-020-01061-w

Xu, D., Wang, Y., Lin, G., Guo, S., Wang, S., Wu, Z., 2019. Co-hydrothermal liquefaction of microalgae and sewage sludge in subcritical water: Ash effects on bio-oil production. Renew. Energy 138, 1143–1151. https://doi.org/10.1016/j.renene.2019.02.020

Yabalak, E., Akay, S., Kayan, B., Gizir, A.M., Yang, Y., 2023. Solubility and Decomposition of Organic Compounds in Subcritical Water. Molecules 28. https://doi.org/10.3390/molecules28031000

Yang, C., Li, R., Zhang, B., Qiu, Q., Wang, B., Yang, H., Ding, Y., Wang, C., 2019. Pyrolysis of microalgae: A critical review. Fuel Process. Technol. 186, 53–72. https://doi.org/10.1016/j.fuproc.2018.12.012

Yang, C., Wu, J., Deng, Z., Zhang, B., Cui, C., Ding, Y., 2017. A Comparison of Energy Consumption in Hydrothermal Liquefaction and Pyrolysis of Microalgae. Trends Renew. Energy 3, 76–85. https://doi.org/10.17737/tre.2017.3.1.0013

Yang, He, Q. (Sophia), Yang, L., 2019. A review on hydrothermal co-liquefaction of biomass. Appl. Energy 250, 926–945. https://doi.org/10.1016/j.apenergy.2019.05.033

Yen, H.-W., Hu, I.-C., Chen, C.-Y., Nagarajan, D., Chang, J.-S., 2019. Design of photobioreactors for algal cultivation, in: Biofuels from Algae. Elsevier, pp. 225–256. https://doi.org/10.1016/B978-0-444-64192-2.00010-X

Yin, S., Dolan, R., Harris, M., Tan, Z., 2010. Subcritical hydrothermal liquefaction of cattle manure to bio-oil : Effects of conversion parameters on bio-oil yield and characterization of bio-oil. Bioresour. Technol. 101, 3657–3664. https://doi.org/10.1016/j.biortech.2009.12.058

Yin, S., Shao, Y., Bao, T., Zhu, J., 2023. Review on Nitrogen Transformation during Microalgae Thermochemical Liquefaction: Recent Advances and Future Perspectives. Energy and Fuels 37, 1525–1544. https://doi.org/10.1021/acs.energyfuels.2c03300

Yu, K.L., Lau, B.F., Show, P.L., Ong, H.C., Ling, T.C., Chen, W.H., Ng, E.P., Chang, J.S., 2017. Recent developments on algal biochar production and characterization. Bioresour. Technol. https://doi.org/10.1016/j.biortech.2017.08.009

Yue, Y., Kastner, J.R., Mani, S., 2018. Two-Stage Hydrothermal Liquefaction of Sweet

Sorghum Biomass - Part II: Production of Upgraded Biocrude Oil. Energy and Fuels 32, 7620–7629. https://doi.org/10.1021/acs.energyfuels.8b00669

Zaker, A., Chen, Z., Zaheer-Uddin, M., 2021. Catalytic pyrolysis of sewage sludge with HZSM5 and sludge-derived activated char: A comparative study using TGA-MS and artificial neural networks. J. Environ. Chem. Eng. 9, 105891. https://doi.org/10.1016/j.jece.2021.105891

Zerga, A.Y., Tahir, M., Bouguerra, M.D.E., Alias, H., 2024. Studying the productivity of sewage sludge (SS) components for photocatalytic CO2 transformation to CO and methane. J. Umm Al-Qura Univ. Appl. Sci. https://doi.org/10.1007/s43994-024-00185-3

Zhang, B., He, Z., Chen, H., Kandasamy, S., Xu, Z., Hu, X., Guo, H., 2018. Effect of acidic, neutral and alkaline conditions on product distribution and biocrude oil chemistry from hydrothermal liquefaction of microalgae. Bioresour. Technol. 270, 129–137. https://doi.org/10.1016/j.biortech.2018.08.129

Zhang, Liu, J., Li, D., Yang, Z., Wang, X., Lin, R., 2022. Research on the thermochemical conversion utilization of nitrogen-rich microalgae: Two-step catalytic pyrolysis of Nannochloropsis sp over ZSM-5. Energy Convers. Manag. 258, 115475. https://doi.org/10.1016/j.enconman.2022.115475

Zhang, X., Zhan, L., Lin, M., Zeng, Y., Li, R., Wu, Y., 2022. Production of acid-free bio-oil through improved co-HTL of sludge and microalgae: Experiment and life cycle assessment. J. Clean. Prod. 379, 134668. https://doi.org/10.1016/j.jclepro.2022.134668

Zhang, Y., Su, H., Zhong, Y., Zhang, C., Shen, Z., Sang, W., Yan, G., Zhou, X., 2012. The effect of bacterial contamination on the heterotrophic cultivation of Chlorella pyrenoidosa in wastewater from the production of soybean products. Water Res. 46, 5509–5516. https://doi.org/10.1016/j.watres.2012.07.025

List of Publications and Conference Presentations

List of Publications

From Thesis

Peer-reviewed Journals

❖ Pooja Singh and Kaustubha Mohanty. "Ex-situ Catalytic Co-pyrolysis of Microalgae and Dairy Sludge using H-ZSM-5 towards Bio-oil Production". **Journal of Analytical and Applied Pyrolysis** (2026): 107744

❖ Pooja Singh and Kaustubha Mohanty. "Bio-oil as a promising product from co-liquefaction of dairy wastewater grown microalgae with dairy sludge: Study on synergistic effect and sustainable energy generation". **Renewable Energy** (2026): 125574

❖ Pooja Singh and Kaustubha Mohanty. "Bio-Oil Production via Two-Stage and Direct Hydrothermal Liquefaction Process from High-Protein *Monoraphidium* sp. KMC4: A Comparative Study of Both Processes and an Insight into the Reaction Pathway". **Energy & Fuels** (2025): 10465-10478.

❖ Pooja Singh, Satya Sundar Mohanty, and Kaustubha Mohanty. "Comprehensive assessment of microalgal-based treatment processes for dairy wastewater". **Frontiers in Bioengineering and Biotechnology**, 12 (2024): 1425933.

❖ Pooja Singh, S. Venkata Mohan, and Kaustubha Mohanty. "Dairy wastewater treatment using *Monoraphidium* sp. KMC4 and its potential as hydrothermal liquefaction feedstock". **Bioresource Technology**, 376 (2023): 128877.

Book Chapters

❖ Pooja Singh, Suchetna Kushwah, and Kaustubha Mohanty. "Hydrothermal Liquefaction of Wet Algal Biomass to Bio-Oil and Other Value-Added Products". **Algal Biomass for Sustainable Clean Fuels and Biochemicals Production**, American Chemical Society (2026), 121-150.

❖ Pooja Singh and Kaustubha Mohanty. "Non-catalytic and catalytic microalgae pyrolysis: Product characterization and economic perspective". Advances in Algal Research, Springer Nature Singapore (2026), 433-452.

Other Publications

Boda Ravi Kiran, **Pooja Singh**, S. Venkata Mohan, Kaustubha Mohanty (2024). Bio-oil production from dairy wastewater treated *Messastrum gracile* SVMIICT7 biomass. Journal of Environmental Management, 356, 120458.

- Satya Sundar Mohanty, **Pooja Singh**, Shwetha Nistala, Kaustubha Mohanty (2024). A critical review on the environmental fate and removal technologies of herbicides: An emerging concern in India. Journal of Hazardous Materials Advances, 100496.
- **Pooja Singh**, Kaustubha Mohanty and Amit Bhatnagar. Harnessing Raw Dairy Wastewater for Microalgal Bioproduct Synthesis along with Bioremediation: A Circular Bioeconomy Approach. (Prepared).

Presentation in International/National Conferences

❖Bio-oil Production via co-HTL of Microalgae and Dairy Sludge: A study on synergistic effect and bioenergy generation. Advances in Algal Research, Rajagiri school of Social Sciences, Kochi & IIT Guwahati, 2025.

❖Treatment of dairy wastewater using *Monoraphidium* sp. KMC4 and subsequent thermochemical conversion of the biomass to biofuels. 3 -Min thesis Presentation, Research and Industrial Conclave-Synergy'2025, IIT Guwahati.

❖A comparative study of bio-oil production via two-stage and direct hydrothermal liquefaction process from microalgae grown on dairy wastewater. PYROASIA 2024 at IIT Guwahati.

❖Dairy wastewater treatment and production of polyhydroxybutyrate from *Monoraphidium* sp. KMC4 and Scenedesmus microalgae and their consortium. Advances in Algal Research. JNTU Hyderabad & IIT Guwahati, 2024.

❖An integrated approach towards microalgal biomass production on dairy wastewater with its potential for bio-oil production in a biorefinery manner. Emerging trends in water technology, LUT Finland, 2024.

❖Hydrothermal liquefaction of *Monoraphidium* sp. KMC4 grown on dairy wastewater for biocrude production. Advances in Algal Research, IIT Guwahati, 2023.

❖Hydrothermal liquefaction of high protein and high ash microalgae grown on dairy wastewater. The 1st International Conference on the Practical Zero Emissions & The 2nd Workshop on Water Sustainability & Green Technology 2023, Vietnam.

❖Hydrothermal liquefaction of microalgae grown on dairy wastewater for bio-oil production. Research and Industrial Conclave-Integration'23, IIT Guwahati.

❖An integrated approach towards dairy wastewater treatment using *Monoraphidium* sp. KMC4 with high value algal biomass production for biocrude production. International Conference on Biotechnology, Sustainable Bioresources and Bioeconomy 2022 jointly organized by IIT Guwahati and the Biotech Research Society India at IIT Guwahati, India.